LITHOSPHERIC ELECTRICAL CONDUCTIVITY STRUCTURE ACROSS SOUTHERN SCOTLAND AND NORTHERN ENGLAND

T.HARINARAYANA

Doctor of Philosophy
University of Edinburgh
1987

To my Mother

DECLARATION

I hereby declare that the work presented in this thesis is my own, unless otherwise stated in the text and that the thesis has been composed by myself.

T.HARINARAYANA

ABSTRACT

Magnetotelluric soundings in the range (100-0.01Hz.) have been carried out along a 140 km. profile across S.Scotland and N.England. Following discussion of the steps taken to reduce cultural noise in the response functions, the results for 13 stations along the traverse are presented. Since the study of dimensionality parameters supports 1-D modelling, rotationally invariant resistivity-depth data have been subjected to two 1-D inversion schemes and the different parameters of the model derived have been examined using the Most squares approach. Two dimensional numerical modelling has also been carried out considering both the present data and those of earlier induction studies along the profile.

The resulting geoelectrical model confirms the existence of a crustal conducting layer (10-50 Ohm.m.) as found in earlier induction studies. Results of this study show additionally that- a) the conductor rises to a depth of nearly 3.5 km. about 20km. south of the SUF i.e., near the axis of the Eskdalemuir magnetic variation anomaly b) the conductor is at a depth of about 8-10 km. in region of the Weardale granite in N. England, c) there is a marked resistivity-depth variation below S.Scotland and d) the surface resistivity along the profile decreases from NW to SE and corresponds well to the Ordovician, the Silurian and the Carboniferous sediments. The geophysical interpretation of the model has been discussed in association with the results of earlier induction studies, seismic and gravity studies and the various tectonic models of the Iapetus suture zone. Based on the present study and comparison with electric structures of other tectonic regions, a hypothetical tectonic model has been proposed for this study region. It comprises a resistive triangular wedge surrounded by a conducting layer which is incorporated as a signature for the presence of a subducting plate in an island arc environment.

In addition to these field investigations, several computational analyses have also been undertaken. The main studies were - a) procedures to reduce noise from the recorded data using digital filtering techniques and b) determination of the distortion of telluric field measurements due to a conducting hill using a conformal mapping method. Digital filters have been discussed with special reference to persistent noise signals, eg. power lines, electrical fences etc. Delay line filtering, notch filtering and the maximum entropy method have been applied to both synthetic and field data and the results are discussed. The effect of a two-dimensional conducting hill on the telluric fields measured on a horizontal surface has been studied using the Schwartz-Christoffel conformal transformation technique. The

results indicated that the distortion depends strongly on the inclination, height of the hill and depth to the basement. The distortion of apparent resistivity values computed from MT field measurements has also been discussed.

In addition, some consideration has been given to – a) the processing of the data in the time domain using adaptive filters, b) the application of joint inversion of DC–AMT data to resolve shallow structures in N.England and c) the distortion effects of near surface inhomogeneities in N.England.

These various studies are presented in 7 chapters with 3 Appendices and the results are discussed in chapter–8, where the conclusions and suggestions for further work are also presented.

ACKNOWLEDGEMENTS

I would like to express my sincere thanks to DR. Rosemary Hutton, my supervisor for the initial impetus for the project and encouragement. I am deeply indebted to her for continuing support and help throughout the preparation of this thesis.

I gratefully acknowledge for the discussions with Dr. Bruce Hobbs and for the facilities provided at the Department of Geophysics by Prof. Ken Creer. I wish to thank the Association of Commonwealth Universities for the financial support provided for this project.

I am grateful to Roger Hill for providing his 2D inversion software package and help rendered during its execution. I am thankful to Dr. Bernard Mckerrow and Dr. G.Panda for useful discussions in using adaptive filters. I wish to thank Tugrul Genc and Dr. Roger Hipkin for providing their interactive 2D gravity modelling program and for their suggestions during execution. I would like to express my sincere thanks to colleagues at Leeds University for permitting me to use D.C. resistivity data collected by their M.Sc. students.

I am pleased to extend my warm thanks to Stephen Ray, Philip Jones, Ian Livingstone and Alex Jackson for their assistance and help in the field work at various times. The permission given by the land owners to establish MT stations in their farms is also acknowledged. In the induction group, I enjoyed the companionship and discussions with Sergio Fontes, G.Dawes and conversations with M.Meju.

I am grateful to Dr. V. Shanmugasundaram and Mrs. Claire Wilson for comments made on the manuscript for better presentation. Last, but not least, to my wife, Vijaya for her help in typing parts of this thesis and support in various other ways.

TABLE OF CONTENTS

Declaration

Abstract

Acknowledgements

Table of contents

List of Figures

List of tables

CHAPTER 1 INTRODUCTION 1

1.1 Scope and objectives of the project 1

1.2 General 1

1.3 General geology and tectonic setting of the study region 2

1.3.1 The geology 3

1.3.2 Tectonic setting 7

1.4 Earlier geophysical studies 8

1.5 Contents of this thesis 16

CHAPTER 2 THEORY 17

2.1 Introduction 17

2.2 Field relationships 18

2.3 Induction in different media 23

2.3.1 The one dimensional case 23

2.3.1.1 Uniform half space 23

2.3.1.2 Layered medium 29

2.3.2 The two dimensional case 30

2.3.3 The three dimensional case 33

CHAPTER 3 INTRUMENTATION AND DATA ACQUISITION 34

3.1 Introduction 34

3.2 Instrumentation 35

3.2.1 The S.P.A.M. system 35

3.2.1.1 The analogue unit 36

3.2.1.2 The computer unit 43

3.2.2 The long period (Band-4) magnetotelluric system 43

3.2.3 The long period (Band-5) magnetotelluric system 46

3.3 Survey logistics 46

3.3.1 The field procedure 46
3.3.2 The in-field processing of the short period (AMT/MT) data 49
3.3.3 Data transcription 54
3.3.4 Station location 54
CHAPTER 4 DATA PROCESSING 59
4.1 Introduction 59
4.2 Frequency domain analysis 60
4.2.1 Estimation of the impedance tensor 60
4.2.2 The Coherence function 62
4.2.3 Apparent resistivity and phase 63
4.2.4 Directionality and dimensionality indicators 64
4.2.4.1 Directionality parameter 64
4.2.4.2 Dimensionality parameter 65
4.2.5 Single station geomagnetic transfer functions 79
4.2.6 Field polarization 80
4.3 Processing of field data 86
4.3.1 Event selection 86
4.3.2 Event analysis and averaging 89
4.3.3 Processing of long period (Band 5) data 92
4.4 Time domain processing 92
4.4.1 Introduction 92
CHAPTER 5 NOISE AND ERROR DURING FIELD MEASUREMENTS 108
5.1 Processing of noisy data using digital filtering techniques and additional data selection criteria 108
5.1.1 Field examples of noisy data in S.Scotland 108
5.1.1.1 A laboratory study of the hypothetical spike source 116
5.2 Distortion of telluric field measurement near hill using conformal mapping methods 119

CHAPTER 6 ONE DIMENSIONAL MODELLING RESULTS 122
6.1 Introduction 122
6.2 The qualitative study 125
6.2.1 The approximate inversion 128
6.3 The inversion procedures 129

6.3.1 Modified Montecarlo-Hedgehog inversion 129
6.3.2 The Linearised inversion 138
6.3.3 1-D models for the individual stations 140
6.4 The joint inversion of the D.C and MT measurements 162
6.5 Modelling of long period data 175
6.6 Summary 177
CHAPTER 7 TWO DIMENSIONAL MODELLING RESULTS 186
7.1 Introduction 186
7.2 The effect of near surface inhomogeneities and the edge effect 189
7.3 The effect of lateral inhomogeneities 194
7.3.1 Forward two dimensional modelling 197
7.3.2 The two dimensional inversion scheme 201
7.3.3 Modelling results 204
CHAPTER 8 DISCUSSION OF THE 1D AND 2D MODELLING RESULTS 215
8.1 Comparison of the resistivity model with geology 215
8.2 Comparison of the 2-D resistivity model with models derived from earlier induction studies 221
8.3 Comparison of the electrical resistivity model with other geophysical models 226
8.3.1 Seismic investigations: 226
8.4 Reasons for high electrical conductivity and tectonic implications 230
8.4.1 Reasons for high electrical conductivity 230
8.4.2 Tectonic implications: 230
8.5 Conclusions and suggestions for further work 237
8.5.1 Conclusions 237
8.5.2 Suggestions for further work 238

I APPENDIX-A 240
II APPENDIX-B 251
III APPENDIX-C 280
REFERENCES 299

LIST OF FIGURES

FIG.NO	Page No.
1.1 General geology of the study region.	5
1.2 Locations of earlier magnetotelluric stations.	11
1.3 The locations of deep DC resistivity soundings.	14
3.1 Block diagram showing the AMT/MT data acquisition system	38
3.2 A schematic block diagram for the pre-amplifier unit.	40
3.3 The response curves for the analogue unit	42
3.4 A schematic block diagram for the Band-4 MT system.	45
3.5 A schematic block diagram for the Band-5 MT system.	48
3.6 The flow chart of in-field processing	51
3.7 An example of in-field data results from WHI station	53
3.8 The station location map showing the AMT/MT stations.	56
4.1 The rotational properties of the impedance elements	68
4.2 Dimensionality weights and consistency checks	73
4.3 a-m Dimensionality indicators for all the field stations.	75-78
4.4 An example of the induction vectors.	82
4.5 An example of the telluric and magnetic polarization.	85
4.6 A typical time series data recorded at WHI station (No. 508).	88
4.7 A flow diagram for the data processing	91
4.8 a-m Response functions obtained from processing.	94-106
5.1 Signals recorded at various noisy stations.	110-115
5.2 Electric field (mV/km.) data recorded by SPAM in the lab.	118
5.3 A smoothed surface topography along the study traverse.	121
6.1 Magnetotelluric invariant apparent resistivity and phase	127
6.2-4 Bostick transformation of apparent resistivity and phase.	131-135
6.5 a-m One dimensional inversion of invariant functions	142-154
6.6-9 Compilation of one dimensional modelling results.	159-166
6.10 Joint inversion of results of MT and DC data	171-174
6.11 Comparison of the models obtained from DC, MT and Bore hole.	176
6.12 Results of Montecarlo and linearised invers	179-182
6.13 A schematic diagram based on the 1-D modelling results.	184
7.1 Models considered for forward computation.	191
7.2 Error in the response functions at Northumberland Basin.	193
7.3 Error in the response functions at Weardale Granite.	196
7.4 The final two-dimensional geo-electric model.	206

7.5 a-i Observed and computed E- and H- response functions. 208-212
8.1 The 2-D electrical model 217
8.2 A schematic diagram showing shallow structure 220
8.3 Results of earlier induction studies. 223-224
8.4 Results of NEC and WINCH profiles. 228
8.5 Summary of the tectonic models. 232
8.6 A speculative model. 235-236
A1 A block diagram showing the application of adaptive filters 242
A2. The error between the assumed and computed output sequences 245
A3 The error between the assumed and computed output sequences 248
A4. Comparision of assumed and computed impulse response functions 250

LIST OF TABLES

3.1 List of MT field stations. 58
6.1 Error between the computed and observed response functions. 156
6.2 Locations of MT, DC and B.H. near Rookhope. 168
6.3 Details of joint inversion results 174
7.1 An example of the grid sizes used in 2D modelling 199
7.2 List of stations considered in 2D modelling 202
7.3 List of blocks and their resistivities 203

CHAPTER 1

INTRODUCTION

1.1. Scope and objectives of the project

In recent years, several geological and geophysical investigations have been carried out in Southern Uplands and Northern England to obtain information on the crustal structure. This part of Britain has enjoyed a particularly rich share of such investigations owing to its association with the ancient tectonic history. Amongst the geophysical techniques, the 'magnetotelluric' (MT) is known as one of the most effective technique to probe the earth to great depths. This method gives information on the distribution of 'electrical conductivity' below the earth's surface from observations made on the surface. Electrical conductivity is an important physical parameter which is a function of the composition and physical state of a material. By understanding the variation of conductivity in the earth, structural parameters, composition of the rocks etc., may be deduced.

In this project, the magnetotelluric method was used to study the geoelectrical crustal structure on a regional scale to obtain the conductivity parameter both at shallow as well as at deeper levels. The main objectives of the project were- a) magnetotelluric investigations along a 140 km. traverse across Southern Scotland and Northern England to determine the geoelectrical crustal structure and b) interpretation of the structure in terms of the geology and tectonic setting of the region using the results of the present study and those of earlier induction studies.

1.2. General

The magnetotelluric method depends on the natural electromagnetic fields originating from the interaction of the ionosphere and magnetosphere and from world wide thunderstorm activity. Due to these phenomena the Earth's static magnetic field is disturbed, resulting in varying magnetic fields whose amplitudes can range from about 100 nT for periods of 1 hour or 1 day to as small as 0.01 nT at 10-1000 Hz. frequency. These varying magnetic fields

induce in the earth electric (popularly known as 'telluric') currents whose characteristics depend directly on the earth's electrical structure.

From observations of the varying magnetic fields, large scale horizontal inhomogeneities in the electrical conductivity structure can be derived by identifying the anomalous part of the variation field - a method known as 'Geomagnetic deep sounding' (GDS). Similarly, by studying the simultaneously recorded telluric field variations at two different locations one can map the lateral variations of the conductivity at surface to subsurface levels - a method known as the 'telluric current method'. Both the GDS and telluric current methods, however, are largely qualitative. The magnetotelluric method, which involves the observation of both magnetic and telluric field variations at a location, is superior to them in that quantitative estimations of conductivity and depth parameters of the earth structure can be obtained.

Among other geophysical techniques for probing the earth to deep crustal levels, deep seismic techniques are well established. In recent years, however, MT has been becoming increasingly popular. With regard to cost, MT studies are 5 to 10 times cheaper than seismic investigations. While the structural information derived from seismics is generally accepted as reliable, especially in oil exploration, magnetotelluric field investigations are known to be advantageous in some special situations; for example, at places where sediments are covered by thick volcanic rocks. The combined use of seismic reflection and MT techniques has recently been recommended by Jones (1987).

1.3. General geology and tectonic setting of the study region

In the following, the main features of the geology and tectonics of the study region are summarised, a more detailed account being given of the immediate surroundings of the traverse which extends in the NW_SE direction across Northern England and Southern Scotland. This summary is derived largely from Greig(1971), Eastwood (1971) and Harris et al (1979).

1.3.1. The geology

The greater part of the study region is covered by Ordovician, Silurian –of Lower Palaeozoic period– and Carboniferous sediments (Fig. 1.1), the Ordovician sediments in the northernmost part and the Silurian and then the Carboniferous sediments to the SE. Many sequences of Ordovician and Silurian in the Southern uplands show a succession from basalts through cherts and/or graptolitic shales to thick greywackes. The greywackes are a form of sandstone with a variety of mineral and rock fragments and a paste–like matrix of the same material. The shales are more persistently developed along a north eastward axis passing through Moffat. The Carboniferous system is well developed in the south of Scotland, especially near Langholm, where there are about 3500m. of beds representing the whole sequence of strata. The various rock types of these strata include thick beds of sandstone, mudstone, limestone and thin beds of coal, seatclay, ironstone and cementstone together with basalts and tuffs of volcanic origin. This system extends over an area of about 470 sq. km. and for a distance of some 75 km. along the border between Scotland and England, stretching through Langholm, Canonbie and Newcastleton from Ecclefechan to the Cheviot hills.

The dominant structural feature in the Southern Uplands is the Southern Upland Fault (SUF) which separates the two major units, the Southern Uplands and the Midland Valley. The crustal structure associated with the fault is, however, not yet fully known, especially the total throw. In a classic memoir, Peach and Horne (1899) divided the Southern Uplands into northern, central and southern belts. Although their model has undergone radical revision (Craig and Walton 1959, Mitchell and Mckerrow 1975, Mckerrow et al 1977, etc.), this division is still in use. The broad structural pattern in the Southern Uplands is clearly due to horizontal compression in a NNW to a SSE direction, resulting in folding along ENE axes and the development of strike faults of minor scale. In a recent paper Anderson and Oliver (1986), have however, demonstrated that the boundary between the northern and central belts is a major fault – the Orlock Bridge Fault – whose trace extends for about 400 km. across Scotland and Ireland. Reversed strike faults and subsequent wrench faults are well developed. These in turn are closely related to the main folding and there is ample evidence of the later reactivation of many faults under different stress conditions. The Carboniferous strata are faulted against the

FIGURE 1.1

General geology around the study region. SUF= Southern Uplands Fault; SBF= Stublick Fault.

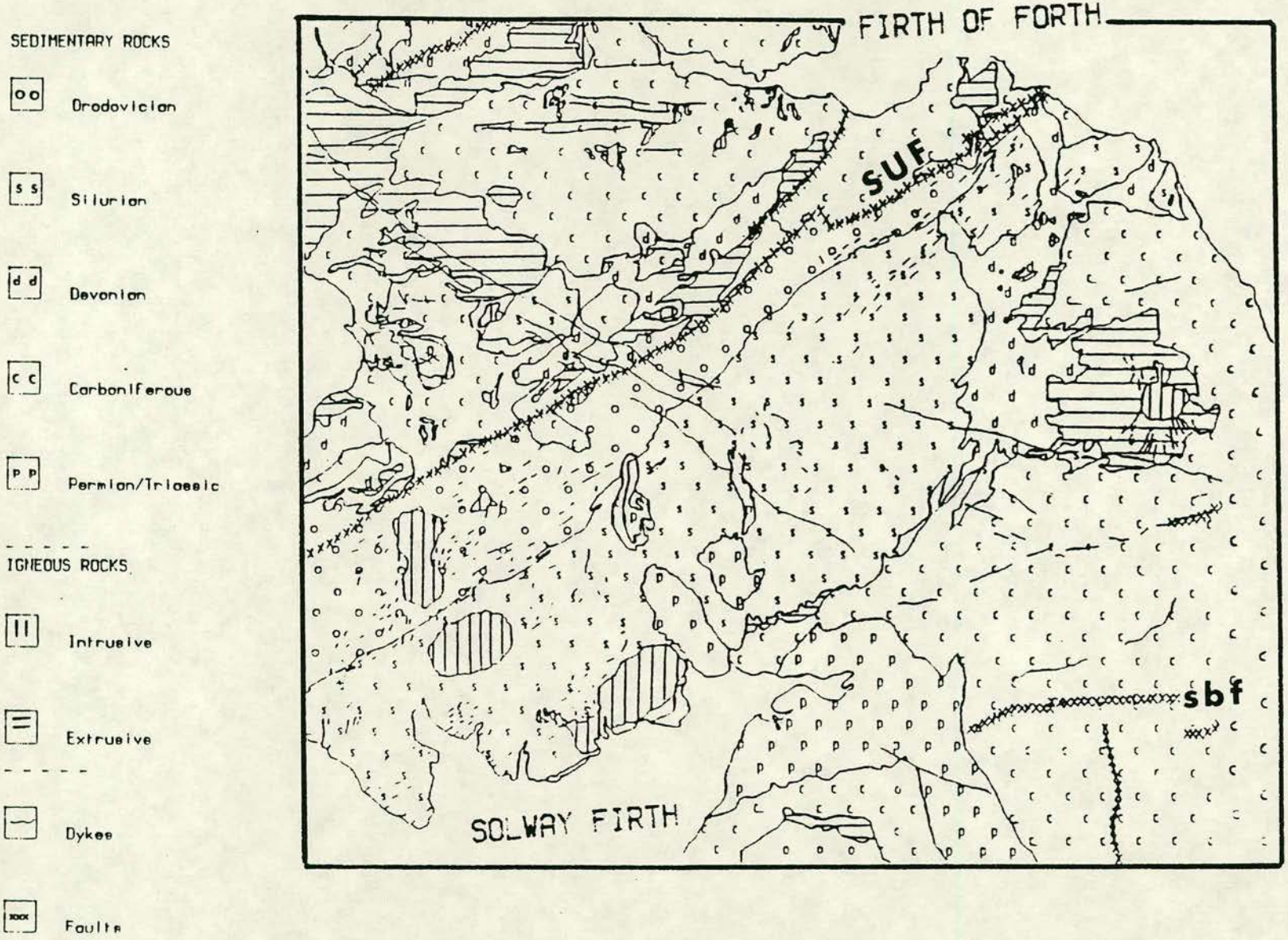
SEDIMENTARY ROCKS
Ordovician
Silurian
Devonian
Carboniferous
Permian/Triassic
IGNEOUS ROCKS
Intrusive
Extrusive
Dykes
Faults
FIRTH OF FORTH
SUF
sbf
SOLWAY FIRTH

Silurian rocks towards the north but there are also several good sections showing the unconformable relationship of the Carboniferous to the underlying Silurian strata. Intrusion activity can be seen as emplacement of numerous small volcanic necks which now protrude above the Carboniferous strata to form prominent topographical features.

Northern England is mostly covered with Carboniferous sediments formed in a trough -the Northumberland Trough- known as a major east west structural unit bounded by the northern Pennine block in the south and the Southern Uplands block in the north. This trough stretches across Britain from the North sea to the Solway Firth and contains two sedimentary basins, the Northumberland Basin and the Solway Basin. While the Northumberland basin is well exposed, the Solway Basin is mostly covered by younger strata and only margins are exposed along the Scottish coast and Cumbria.

The major surface lineaments in Northern England are the Stublick and Ninety Fathom Fault structures, which provide an unambiguous southern margin of the Northumberland trough. The northern margin of the trough is more varied across Northern England. In the west, however, the margin is clear at the junction between the Carboniferous outcrop and the Silurian Greywacke basement of the Southern Uplands. Here, the Northumberland trough is deeply concealed below younger deposits, the Permo-Triassic of the Carlisle basin. The origin of the Northumberland basin has been studied in detail by Leeder (1976 and 1982). He showed that down-warping started early in the Dinantian owing to deep seated instability and an independent graben developed between the Antonstown and Harrettlinn faults, where the sediments of the upper border group thicken to more than 2 km. near Bewcastle. From geological mapping of the region, the block and basin structure of the Lower Carboniferous system was recognized (Johnson 1982). It comprises, from north to south, the Cheviot block, the Northumberland trough, the Alston block and south of the MT traverse followed by the Stainmore trough, the Askrigg block and the Craven basin.

Intrusion of a vast amount of igneous material during compression and uplift is evidenced by the granites of Shap, Skiddaw, Eskdale and the Isle of Man. The Weardale granite is concealed below the sediments of the Alston block. Igneous rocks associated with Carboniferous strata include both

volcanic and intrusive rocks. The volcanic rocks which are confined to the Lower Carboniferous consist mainly of Olivine-basalts, lavas and tuffs near the western end of the Borders region - a thick series of Olivine-basalts near Cumberland and the Scarlet volcanic group of the Isle of Man. The intrusive rocks consist of sills and dykes. By far the most important intrusion is the Great Whin sill and its associated dykes. The sill is shallow (about 200m. deep) and its thickness varies from 12m. to as much as 73m..

1.3.2. Tectonic setting

From faunal, tectonic and stratigraphical evidence from rocks of the Southern Uplands, it has been postulated that there was an ocean between Scotland and England (Wilson 1966). This hypothesis was derived from the concept of sea floor spreading and it envisaged an early or 'proto' Atlantic ocean separating the Laurentian continent to the north and west from the European continent to the south-east. From this seminal paper and the emerging concepts of plate tectonics, Dewey (1971) was the first to propose a plate tectonic model for the Caledonides. This model involved parallel closure of the ocean referred to as the 'Iapetus' by Hartland and Gayer (1972), with one subduction zone in the north and two in the south (see fig. 8.5). In later years, different workers have proposed a sequence of increasingly complex models (Fitton and Hughes 1970, Jeans 1973, Gunn 1973, Church and Gayer 1973, Lambert and Mckerrow 1976, Wright 1976 and Phillips et al 1976). Some differences exist between the models due to: a) workers considering different geological time periods and areas; b) conflicting interpretations and c) application of new concepts arising from modern oceanographical investigations. The majority of authors, however, prefer a northerly dipping subduction zone. These models have been discussed in review papers by Moseley (1977) and Holland et al (1979).

Using a different approach, Mckerrow et al (1977) and Leggett et al. (1983) have constructed plate tectonic models based on an accretion hypothesis. According to this hypothesis, during the closure of the Iapetus ocean in Ordovician and Silurian times, the sedimentary strata of the subducting oceanic plate were sequentially stripped from the down going oceanic basement and accreted to the inner wall of the Laurentian continental margin. Evidence for the accretionary prism thus formed is provided by exposures in

the Southern Uplands and a number of Lower Palaeozoic in-liers to the north of the Iapetus suture in Ireland. In a recent paper Leggett et al (1983) have proposed a tectonic model and assessed it using analogies in terms of present day tectonics. In this way they have compared the Ordovician and Silurian history of the Southern Uplands with the Tertiary and Recent development of the Sumatra accretionary prism and the English margin of the Iapetus with the Queen Charlotte islands transform margin. (Fig. 7 in Leggett et al 1983).

In more recent years, a fuller understanding of the tectonics of the region has emerged from geophysical investigations. Evidence from various geophysical and geochemical studies, however, suggests a basement quite distinct from oceanic crust (Leggett et al 1983). From seismic, magnetic and conductivity results, Powell (1971) postulated the existence of Lewisian type basement rocks beneath the central part of the Southern Uplands. A more detailed account of previous geophysical work in the study region is given in the following section.

From the above discussion it is clear that the tectonic setting of the Southern Uplands and Northern England is quite complex. This topic has recently been debated in a recent Geological Society of London meeting entitled 'Southern Uplands controversy' (Mc Kerrow 1987). However, it is generally accepted that the Southern Uplands massif has an imbricate thrust on both major and minor scales and that the most probable location for the Iapetus suture is the Solway Firth line. This preference arises from the existence of an elongated basin in this location during the Lower Carboniferous. The chief differences within this interpretation are related to the acceptance of a simple subduction-accretion model.

1.4. Earlier geophysical studies

Various geophysical techniques have previously been applied in the study region both on a local as well as on a regional scale. These electric, electromagnetic, gravity, seismic and heat flow studies are now reviewed.

Firstly, the main results of electrical and electromagnetic methods, which include direct current (DC) resistivity, magnetotelluric, magnetovariational, are presented. Early magnetotelluric measurements in the study region, made by

Jain (1964) and Jain and Wilson (1967), suggested the presence of a lower crustal conductor. From application of the geomagnetic deep sounding (GDS) technique, Osmeikhian and Everett (1968) observed an attenuation of the vertical magnetic field component at Eskdalemuir approximately 40km. south of the Southern Uplands Fault (SUF). From subsequent magnetometer array studies, Edwards et al (1971) also showed an anomalous region passing through Eskdalemuir. Their interpretation of this anomaly was that electric currents induced in the North Sea leak through the lower crustal conductor - indicated by Jain and Wilson (1967) - into the Irish sea. This may be considered as an example of a phenomenon now known as 'current channelling'. Reinterpreting these data Bailey et al. (1974) and Bailey and Edwards (1976) suggested a relationship between the lower crustal conductor and the Iapetus oceanic crust. From short (10-600 s) period micropulsation studies Green (1975) observed a resistivity contrast across the SUF between the sediments of the Southern Uplands and the Midland valley, the former (Palaeozoic) being more resistive than the latter (Carboniferous). Hutton et al (1977) from their magnetometer array studies for the whole of Scotland have located the elongated Eskdalemuir anomaly with greater precision, especially to the NE of the Southern Uplands where it is approximately parallel to and south of the SUF. Intense magnetovariational studies in the southern part of the study region have been discussed by Banks et al. (1983), Beamish and Banks (1983), Banks and Beamish (1984) and Banks (1986). Fig.1.2 shows the locations of previous magnetotelluric measurements in the study region. Jones (1977) made magnetovariational and magnetotelluric measurements in the Midland valley, Southern Uplands and Northern England regions and indicated a crustal conductor at a depth of 24 km. beneath the Southern Uplands and less than 5km. beneath the Northumberland basin. Ingham (1981) made MT measurements along a traverse AA' (Fig. 1.2) and presented a two dimensional geoelectrical model across the Southern Uplands to the Highlands. This model also indicated the presence of a crustal conductor at varying depths below the Southern Uplands. Novak (1981) made a broad band magnetotelluric study along traverse BB' (fig. 1.2) covering two different frequency bands (ranging about 1000-2 Hz. and 0.1-0.001 Hz.) and discussed both the shallow and deeper crustal structure. Sule (1985) made detailed broad band MT investigations with close station spacing along a traverse CC' and in the Duns area (fig. 1.2) and presented a two dimensional geoelectrical

Fig. 1.2 Locations of earlier magnetotelluric stations in the Southern Uplands and the Northern England. Stations in parts of the Midland valley and the Highlands are also shown. Stippled lines shows the Duns area where an areal MT study has been carried out (Sule, 1985). Numbers represent the National grid references. SUF= Southern Uplands. Fault. The dashed line indicates the location of the present study traverse.

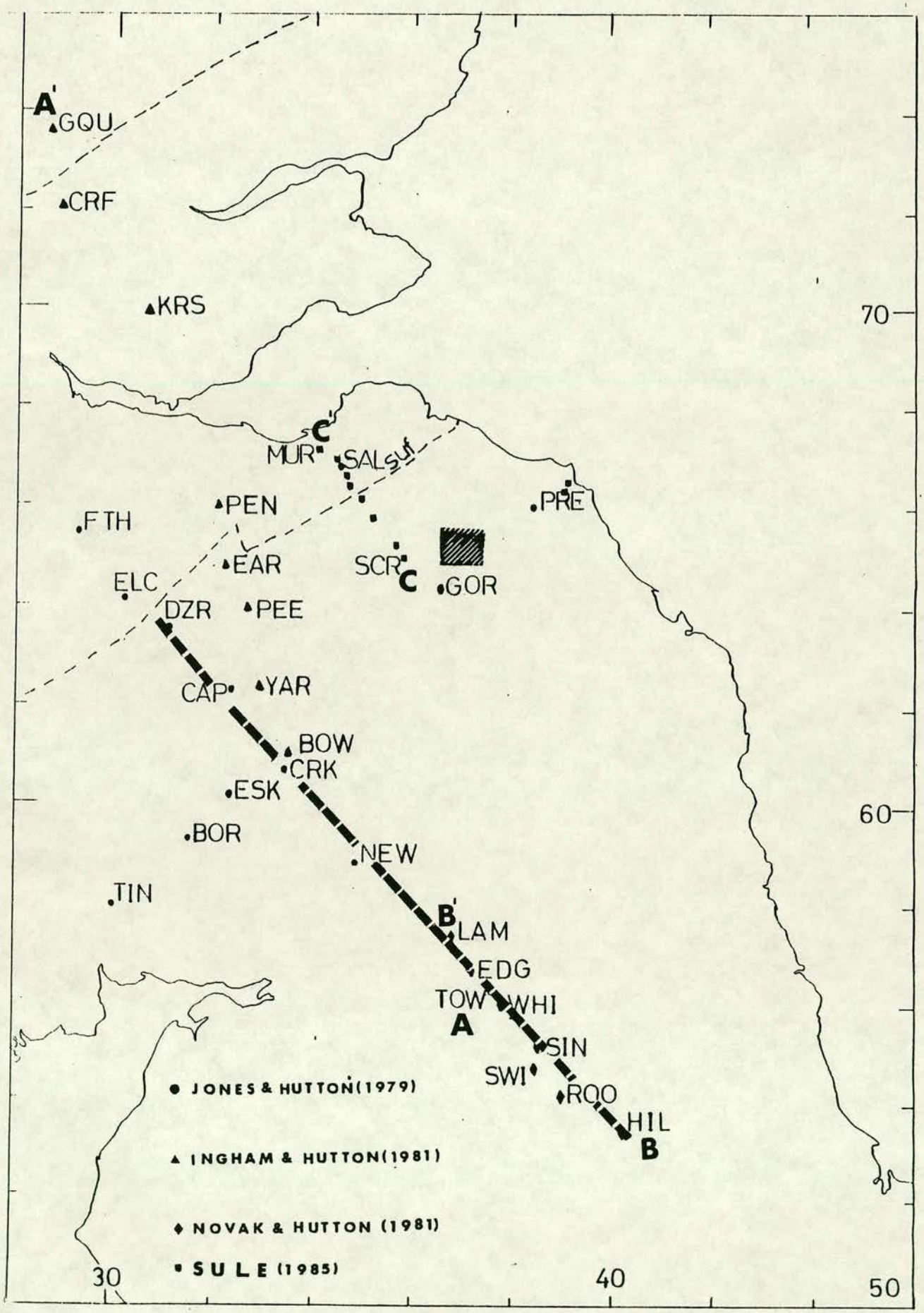
A'
GQU
CRF
KRS
C'
MUR
SAL
PEN
PRE
FTH
EAR
SCR
C
GOR
ELC
DZR
PEE
CAP
YAR
BOW
CRK
ESK
BOR
NEW
TIN
B'
LAM
EDG
TOW
WHI
A
SIN
SWI
ROO
HIL
B
70
60
50
40
30
JONES & HUTTON (1979)
INGHAM & HUTTON (1981)
NOVAK & HUTTON (1981)
SULE (1985)

model for his 36km. traverse. His study has not only provided an estimate of the thickness of the shallow sedimentary layers but also resolved the upper boundary of the crustal conductor (Sule and Hutton 1986). Some of the results of the above studies had been compiled and discussed recently by Hutton et al (1985).

The Earth Sciences department of Leeds University has carried out several deep D.C. resistivity soundings across Northern England and Southern Scotland- as M.Sc. projects- using the square array and dipole-dipole array configurations proposed by Habberjam and Thanassoulas (1979). These were later compiled and reinterpreted by Roxis (1984), who has provided the resistivity structure upto a depth of about 1 to 2km. reproduced in figure 1.3.

An extensive gravity survey has been carried out by members of the Geophysics department, University of Edinburgh and a long wavelength negative gravity anomaly over the Southern Uplands running SW-NE parallel to Caledonian trend has been reported (Lagios and Hipkin 1979). This gravity anomaly has been interpreted as due to the presence of a granitic batholith near Tweeddale (Lagios and Hipkin 1982, Lagios 1984). From gravity and magnetic surveys of the northern Pennines region, Bott and Masson-Smith (1957a) have proposed the existence of a granite batholith beneath the Alston block. This has later been confirmed by drilling (Dunham et al 1965). Block and basin structures have also been proposed from gravity studies and a variable thickness for the Carboniferous succession has been suggested (Bott 1961, 1967, Bott et al 1984).

From a regional aeromagnetic map, Hall and Dagley (1970) have observed a low amplitude magnetic anomaly (50-100 nT) trending parallel to the SUF. This magnetic 'low' is located across the Southern Uplands, while there is no prominent change at the SUF itself. From sheet 11 of the aeromagnetic map (Bullerwell 1968) it can be seen that the eastern part of the Southern Uplands is generally characterized by smooth, weak magnetic anomalies. In Northern England, a vertical field magnetic survey (Bott and Masson-Smith 1957b) has been made over the Alston block. Irregular variations in the magnetic field caused by the Whin sill and associated dykes have been observed in this survey. These variations are superimposed on a negative magnetic anomaly (nearly 70 nT in amplitude) which can be seen on both the vertical field and

Fig. 1.3 The circles indicate the locations of deep DC resistivity soundings in Southern Uplands and Northern England. The station numbers are also indicated. The resistivity structure along the profile is shown at the bottom of the figure (from Roxis 1984). The dashed line indicates the location of the present study traverse.

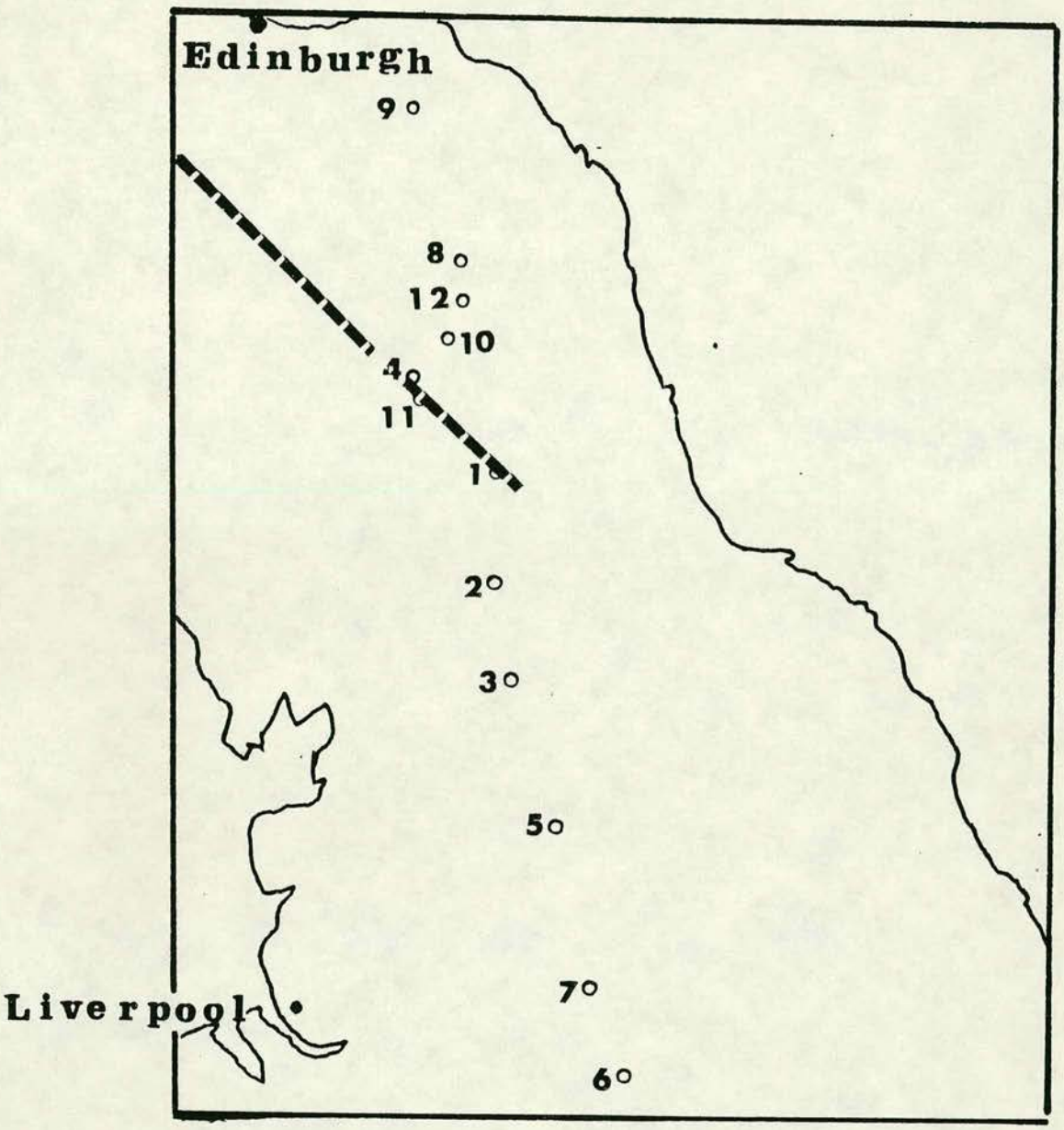
Edinburgh
9
8
12
10
4
11
2
3
5
7
6
Liverpool

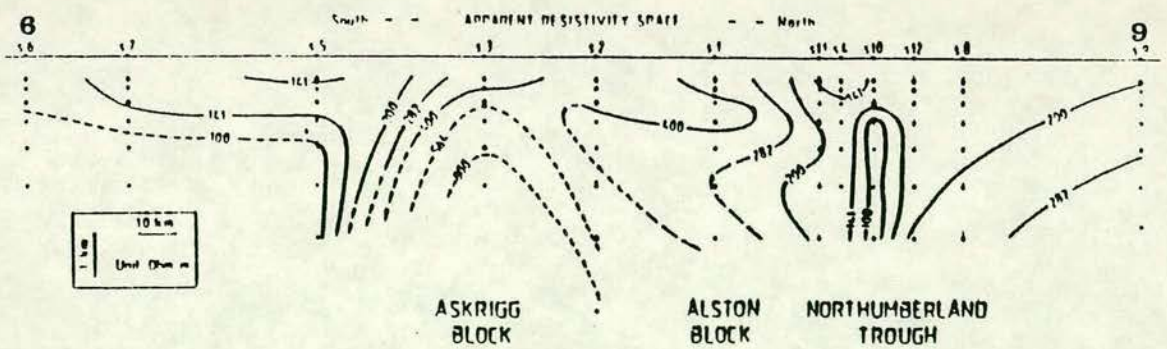
6
9
ASKRIGG BLOCK
ALSTON BLOCK
NORTHUMBERLAND TROUGH

aeromagnetic total field maps.

Jacob (1969) has reported a distinct refraction horizon at 12 km. under the Southern Uplands from Eskdalemuir seismological array studies. From seismic data obtained in the Firth of Forth and from seismological studies of Jacob (1969), continental crust has been indicated upto a depth 30 km. (Christie 1978). From the deep seismic refraction traverse trending NS across Great Britain (Bamford et al 1977, 1978) a contrast in the velocities of the pre-Caledonian crustal layers on either side of the Southern Uplands has been observed. This study indicated a major horizontal discontinuity in the pre-Caledonian basement near the SUF and a shallow lower crustal layer beneath the Southern Uplands. Reinterpreting these investigations, Hall et al (1983) have presented evidence for the existence of crystalline rocks of continental nature below the Southern Uplands at the shallow depth of about 1-5 km., trending approximately parallel to the Caledonian strike. The Southern Uplands Seismic Profile (SUSP) which was parallel to and south of the SUF showed a lateral variation in the seismic velocity layering at a depth of 1 km. and 3-4 km. (Warner et al 1982). Quarry blast observations with the Broughton array (El Isa, 1977) showed high apparent velocities from sources along strike (i.e., parallel to the SUF) but low apparent velocities across it. From quarry blast observations in Northern England, the depth of the Northumberland basin has been estimated at a number of locations (Bott et al 1984). The sedimentary thickness has been observed to be greater towards the east thinning towards the west. From wide angle explosion seismology results (CSSP) Bott et al (1985) showed the presence of pre-Caledonian metamorphic basement below Northern England and observed a well defined mid-crustal refractor at approximately 16 km. depth. Apart from these on-shore seismic investigations, various off-shore seismic investigations around the study region have also been reported.

Since 1977, the British Geological Survey has carried out several programmes to assess the geothermal potential of the U.K.. The results have been reviewed by Downing and Gray (1986 a,b). A high heat flow value (95 mW/m^2) has been observed near the Weardale granite of Northern England with an estimated temperature of about 200° C at a depth of 6 km. (Lee et al 1984). Blaxland et al (1979), from their Pb-isotope analysis of feldspar separates from different granite bodies of Scotland have observed that the

granites in the Southern Uplands are more radiogenic than those of other areas and concluded that the rocks north of the SUF belong to Lewisian crust, while those in the south are younger formations.

Palaeomagnetic studies have also contributed to the discussion of the tectonic history of the study region. For example, Briden et al (1984) have proposed a width of about 1000 km. for the Iapetus ocean. They could not, however, estimate precisely the rate of its subsequent closure.

1.5. Contents of this thesis

Following this introductory chapter, a brief description is given in Chapter 2 of the basic theory of electromagnetic induction for one and two dimensional situations. Chapter 3 contains descriptions of the various instruments, recorders and sensors used in the present investigation, together with the survey logistics. Conventional frequency domain processing procedures and consideration of time domain processing are presented in Chapter 4. In Chapter 5, the various noise sources observed during the acquisition of the field data are discussed and several methods for removing or reducing them using digital filtering techniques are presented. Errors in observations arising from topography are derived in this chapter by use of the Schwarz–Christoffel conformal transformation technique. The results of one dimensional modelling of the response functions are presented in Chapter 6. These include the results of joint inversion of AMT and DC resisitivity data for Northern England sites and the resolution study of derived model parameters. Chapter 7 is concerned with the effect of near surface inhomogeneities and two dimensional modelling results. Finally in Chapter 8, the resulting electrical resistivity model is compared with those of previous studies and its geophysical interpretation i.e., the significance of the resistivity values and the relation between the model and the present geology and regional tectonics, is also discussed.

CHAPTER 2

THEORY

This chapter begins in section 2.1 with a brief introductory account of the development of the theory of the magnetotelluric (MT) method which has been used for the field studies of the present investigation. In section 2.2 the relationships between the electric and magnetic fields are discussed and in section 2.3 the theory of electromagnetic induction in different media is presented.

2.1. Introduction

Though the relations between electric and magnetic fields were reported by Airy as early as 1868, it was not until the 1950's, from the classic work of Tikhonov (1950) and Cagniard (1953), that the properties of these fields were exploited for geophysical prospecting. In particular Cagniard demonstrated that the electrical resistivity distribution with depth could be derived from surface observations of natural magnetic and telluric fields. In 1954, however, Wait raised doubts about Cagniard's assumption of plane wave sources as ionospheric sources are finite and do not give rise to normally incident plane waves. In defence of Cagniard's theory, Price (1962, 1963) developed a general theory of the magnetotelluric method with finite source field dimension and introduced in the basic equations a term which depends on this dimension, the frequency of the inducing field and the earth resistivity. It has been shown that this term is negligible for normal earth structures and for periods less than 1000 sec.. Srivatsava (1965) investigated the effect of the earth's curvature on magnetotelluric soundings and this is found to be negligible for periods less than a day (Porstendorfer 1975). Cantwell (1960), Berdichevsky (1960, 1963) and Tichonov and Berdichevsky (1966) recognized that the scalar nature of the MT response function is inadequate in the presence of lateral inhomogeneities in electrical structure. They suggested that the magnetic fields tangential to the earth can be related to each electric field component, in general by a two dimensional tensor quantity.

As will be discussed in section 2.3.1.1 short period signals give information

about shallow structure and long period signals on deeper structure due to a phenomenon called the 'skin effect'. Till the 1970's the principles of the MT method had been primarily applied to signals of period between 1 and 1000 seconds to study deep crustal structures, Since then (eg. Strangway et al 1973), however, they have been extended increasingly to shorter periods as far as the audio range. This has enabled the use of this method for exploration of both the shallow as well as the deep earth electrical structure.

2.2. Field relationships

In the following the basic MT theory is briefly discussed. Consider Maxwell's equations,

$$\nabla \Lambda \bar{H} = \bar{J} + \frac{\partial \bar{D}}{\partial t} \qquad \text{.....2.1}$$

$$\nabla \Lambda \bar{E} = - \frac{\partial \bar{B}}{\partial t} \qquad \text{.....2.2}$$

$$\nabla \quad \bar{B} = o \qquad \text{.....2.3}$$

$$\nabla \quad \bar{D} = \rho^* \qquad \text{.....2.4}$$

The constitutive relations are,

$$\bar{D} = \varepsilon \bar{E} \qquad \text{.....2.5}$$

$$\bar{B} = \mu \bar{H} \qquad \text{.....2.6}$$

$$\bar{J} = \sigma \bar{E} \qquad \text{.....2.7}$$

$$\rho = \frac{1}{\sigma} \qquad \text{.....2.8}$$

where,

$\bar{H}$ = the magnetic field vector

$\bar{E}$ = the electric field vector

$\bar{B}$ = the magnetic induction vector

$\bar{D}$ = the electric displacement vector

$\bar{J}$ = the electric current density vector (A/m^2)

ρ^* = Volume charge distribution (C/m^3)

ρ = Resistivity (Ohm.m.)

σ = Conductivity (S/m)

ε = Permitivity in free space (F/m)

μ = magnetic permeability (H/m)

Let us consider an isotropic medium, where, ε μ and σ are uniform.

Substituting equations 2.5 and 2.7 in equation 2.1 and taking the curl on both the sides we get,

$$\nabla \Lambda \nabla \Lambda \bar{H} = \sigma \nabla \Lambda \bar{E} + \varepsilon \frac{\partial}{\partial t} \nabla \Lambda \bar{E}$$

.....2.9

Substituting equation 2.2 in equation 2.9 we have,

$$\nabla \Lambda \nabla \Lambda \bar{H} = -\sigma \frac{\partial}{\partial t} \bar{B} - \sigma \varepsilon \frac{\partial}{\partial t} \bar{B}$$

.....2.10

which can be rewritten as,

$$\nabla (\nabla . \bar{H}) - \nabla^2 \bar{H} = - \sigma \frac{\partial}{\partial t} \bar{B} - \sigma \varepsilon \frac{\partial^2}{\partial t^2} \bar{B}$$

.....2.11

Using equations 2.6 and 2.3, equation 2.11 can be written as,

$$\nabla^2 \bar{H} - \sigma \mu \frac{\partial \bar{H}}{\partial t} - \varepsilon \mu \frac{\partial^2}{\partial t^2} \bar{H} = 0$$

.....2.12

The electric field E satisfies an equation of similar form provided ρ^* is equal to 0. Within a conductor, ρ^* can be considered to be zero. Taking the divergence of equation 2.1 we have,

$$\sigma \operatorname{div} \bar{E} + \frac{\partial \rho^*}{\partial t} = 0$$

.....2.13

This can be written as

$$\frac{\sigma}{\varepsilon} \rho^* + \frac{\partial \rho^*}{\partial t} = 0$$

.....2.14

The solution for this differential equation is

$$\rho^* = A\, e^{\frac{-\sigma t}{\varepsilon}}$$

.....2.15

For saturated porous rocks with a dielectric capacitivity of 80, $\sigma_{min} = 10^{-5}$ Sm^{-1} and $\epsilon_{max} = 7 \times 10^{-10}$ F. m^{-1} (Grant and West 1965), hence,

$$\frac{\sigma}{\varepsilon} \approx 10^5$$

.....2.16

From equation 2.15 it is clear that any initial volume charge distribution decays rapidly. Hence equation 2.4 reduces to

$$\nabla . \bar{D} = o$$

.....2.17

In a uniform isotropic region the field $\bar{F}$ satisies the equation

$$\nabla^2 \bar{F} = \mu \sigma \frac{\partial}{\partial t} \bar{F} + \mu \varepsilon \frac{\partial^2}{\partial t^2} \bar{F}$$

.....2.18

where, $\bar{F}$ is either the electric or magnetic field.

The field $\bar{F}$ therefore satisfies the diffusion equation or the wave equation according to whether the second or the third term in the above equation is dominant respectively.

Assuming a time dependence of the form $e^{i\omega t}$, where ω is the angular frequency of the source field and $i = \sqrt{-1}$, equation 2.18 can be written as

$$\nabla^2 \bar{F} = \omega^2 \mu \varepsilon \left(\frac{i\sigma}{\omega\varepsilon} - 1\right) \bar{F}$$

.....2.19

Considering the maximum frequency of interest as 100 Hz. (as used in the present study) $\sigma = 10^{-5}$ S m^{-1} and $\varepsilon = 7 \times 10^{-10}$ F m^{-1} we get,

$\sigma/\omega = 160$ which is $>> 1$

This implies that the displacement currents are negligible compared to the conduction currents. Hence equation 2.19 reduces to

$$\nabla^2 \bar{F} = i \omega \mu \sigma \bar{F}$$

.....2.20

The induction problem can thus be considered as one of diffusion of the field into the Earth (Price 1962).

2.3. Induction in different media

In the following sections, this diffusion type of induction problem described for one and two dimensional Earth models and the three dimensional situation is also briefly discussed.

2.3.1. The one dimensional case

2.3.1.1. Uniform half space

Let us assume the conductivity varies only with depth, i.e., along the z direction.

The field equation inside the conducting Earth (i.e., for $z < 0$) is

$$\nabla^2 \bar{E} = \mu \sigma \frac{\partial}{\partial t} \bar{E}$$

.....2.21

and above it (i.e., for $z > 0$)

$$\nabla^2 \bar{E} = 0$$

.....2.22

and

$$\nabla . \bar{E} = 0$$

.....2.23

Separation of variables for $\bar{E}$ in the Cartesian co-ordinate system leads to

$$\bar{E}(x, y, z, t) = Z(z, t)\, \bar{F}(x, y)$$

.....2.24

Substituting 2.24 in 2.23 we have,

$$\nabla \bar{E} = Z \left(\frac{\partial}{\partial x} F_x + \frac{\partial}{\partial y} F_y\right) + F_z \frac{\partial Z}{\partial z} = 0$$

..... 2.25

Equation 2.25 may be solved if either

(i) $F_z = 0$ and $\frac{\partial F_x}{\partial x} + \frac{\partial F_y}{\partial y} = 0$

or

(ii) $\frac{1}{F_z}\left(\frac{\partial F_x}{\partial x} + \frac{\partial F_y}{\partial y}\right) = -\frac{1}{Z}\frac{\partial Z}{\partial z} = \alpha$

.....2.26

where α is any (real or complex) constant. Substituting equation 2.24 into 2.22 and proceeding as before we get,

$$\frac{1}{F_z}\left(\frac{\partial^2 F_x}{\partial x^2} + \frac{\partial^2 F_y}{\partial y^2}\right) = -\frac{1}{Z}\frac{\partial^2 Z}{\partial z^2}$$

.....2.27

Now let us consider the region within the conductor by substituting equation 2.24 into 2.21

$$\frac{\partial^2}{\partial x^2}(Z\bar{F}) + \frac{\partial^2}{\partial y^2}(Z\bar{F}) + \frac{\partial^2}{\partial z^2}(Z\bar{F}) = \mu\sigma\frac{\partial}{\partial t}(Z\bar{F})$$

$$\Rightarrow \frac{1}{\bar{F}}\left(\frac{\partial^2}{\partial x^2}\bar{F} + \frac{\partial^2}{\partial y^2}\bar{F}\right) = \frac{1}{Z}\left(\mu\sigma\frac{\partial}{\partial t}Z - \frac{\partial^2}{\partial z^2}Z\right) \quad \text{.....2.28}$$

Since $\bar{F}$ is a function of x and y only equations 2.27 and 2.28 can be written in the following form,

$$\frac{\partial^2 \bar{F}}{\partial x^2} + \frac{\partial^2 \bar{F}}{\partial y^2} + \lambda^2 = 0$$

.....2.29

where λ is some constant.

Then from equation 2.27

$$\frac{\partial^2 Z}{\partial z^2} = \lambda^2 Z \text{ for } Z > 0$$

.....2.30

and from equation 2.28

$$\frac{\partial^2 Z}{\partial z^2} = (\lambda^2 + \mu\sigma \frac{\partial}{\partial t}) Z \text{ for } Z < 0$$

.....2.31

Equation 2.30 shows that λ is real and positive. Price (1950) showed that condition (ii) in equation 2.26 is associated with varying electric currents which produce no external magnetic field and hence are of no interest in the induction problem. From condition (i), however, it is possible to solve the general problem of induction for any inducing field. The solution of the one dimensional induction problem can be easily obtained from the above results.

Consider the problem of an electrically uniform half space Earth and let the magnetic field outside it be uniform and varying harmonically with time i.e.,

$$\bar{H} = - H_o e^{i\omega t} \bar{j}$$

.....2.32

where, $\bar{j}$ is a unit vector. Then inside,

$$\bar{E} = E(z)\ e^{i\omega t}\ \bar{j}$$

.....2.33

Substituting 2.33 in 2.21 we have,

$$\nabla^2 E(z) = \mu\ \sigma\ i\ \omega\ E(z)$$

.....2.34

i.e.,

$$\frac{\partial^2}{\partial z^2} E(z) = \mu\ \sigma\ i\ \omega\ E(z)$$

.....2.35

The solution of this differential equation can be written as

$$E(z) = C \exp\left(\pm \sqrt{\mu\ \sigma\ i\ \omega}\ .\ Z\right)$$

.....2.36

From equation 2.2 and 2.36 we have,

$$\mu\ \frac{\partial \bar{H}}{\partial t} = -C\sqrt{\mu\sigma i\omega}\ \exp\left(\sqrt{\mu\sigma i\omega}\ .\ Z\right)\bar{j}$$

.....2.37

considering the boundary condition as H_t is continuous at z = 0 gives,

$$C = \frac{\sqrt{i\omega\mu}}{\sigma} \cdot H_o e^{i\omega t}$$

.....2.38

Now equation 2.36 can be written as

$$\bar{E} = \frac{\sqrt{i\omega\mu}}{\sigma} \quad H_o e^{i\omega t} \cdot \exp\left(\sqrt{\mu\sigma i\omega} \cdot Z\right) \cdot dz$$

.....2.39

and at z = 0

$$\frac{E_x}{H_y} = \sqrt{\frac{i\omega\mu}{\sigma}}$$

.....2.40

Since $\rho = \frac{1}{\sigma}$ we have,

$$\rho = \frac{-i}{\omega\mu}\left(\frac{E_x}{H_y}\right)^2$$

.....2.41

This is the basis of Cagniard's magnetotelluric theory. Equation 2.41 shows that resistivity is an imaginary quanitity. This indicates that there is a 45° phase difference between the oscillations of magnetic and electric fields.

The electric field decays exponentially with depth as shown by equation 2.36. The depth at which the amplitude is reduced to 1/e of its surface value

is termed 'the skin depth'. For a uniform earth this is given by

$$\delta = \left(\frac{2}{\mu \omega \sigma}\right)^{1/2}$$

.....2.42

The depth of penetration in magnetotellurics is thus related to the period of observation such that the longer the signal period the greater the depth of penetration. In an inhomogeneous medium, Sims and Bostick (1969) have defined a generalized skin depth dw, from

$$\text{Re} \quad [\int_o^{dw} \sqrt{i \omega \mu \sigma (z)}\, dz] = 1$$

.....2.43

2.3.1.2. Layered medium

In an n-layered earth, both the electric field E_x and the magnetic field H_y must be continuous across the boundaries and between the layers, since, there exists neither charge accumulations nor free poles at the boundaries. The wave impedance at the bottom of each layer must equal the wave impedance at the top of the adjacent lower layer. The general equation for an n-layered earth (Weaver 1973) is given by,

$$Z(o)=\frac{-i\mu\omega}{\theta_1} \coth[\theta_1 h_1+\coth^{-1}$$

$$\{ \quad \frac{\theta_1}{\theta_2}\coth(\theta_2 h_2+\coth^{-1}$$

$$\{ \quad \frac{\theta_2}{\theta_3}.....\{ \quad \frac{\theta_{n-2}}{\theta_{n-1}} \coth (\theta_{m-1} h_{m-1} +$$

$$\coth^{-1} \quad \frac{\theta_{n-1}}{\theta_m} \quad) \quad \}.....]$$

.....2.44

where, Z(o) is the impedance at the earth's surface above an n-layered structure of conductivities $\sigma_1, \sigma_2, \sigma_3, \ldots\ldots\sigma_n$ with layer depths $h_1, h_2, \ldots\ldots h_n$ and θ_n is given by

$$\theta_n^2 = \lambda^2 + i\ \mu\ \omega\sigma_n$$

.....2.45

2.3.2. The two dimensional case

It is not always possible to interpret the observed earth response functions in terms of horizontal layered structures. The presence of lateral variations in conductivity related to, for example, fault structures are not uncommon. In such a situation, the model parameters derived for the one dimensional case may be unsatisfactory and lead to mis-interpretation. In the 2D case, the conductivity is assumed to be a function of two coordinates eg. y and z, with no variation of conductivity along the x-direction. With the assumptions that the conductivity, $\sigma = \sigma(y,z)$ and that the displacement currents can be neglected, Maxwell's equations 2.1 and 2.2 can be rewritten as,

$$\nabla \Lambda \bar{H} = \sigma\ (y,z\ )\bar{E}$$

.....2.46

and

$$\nabla \Lambda\ \bar{E} = -i\ \omega\ \mu \bar{H}$$

.....2.47

These equations in Cartesian coordinates de-couple into two distinct modes and the relationships for the field components can be written as

$$\frac{\partial E_x}{\partial z} = -i\ \omega\ \mu\ H_y$$

$$\frac{\partial E_x}{\partial y} = i\ \omega\ \mu H_z$$

$$\frac{\partial H_z}{\partial y} - \frac{\partial H_y}{\partial z} = \sigma E_x$$

.....2.48

$$\frac{\partial E_z}{\partial y} - \frac{\partial E_y}{\partial z} = -i\omega\ \mu\ H_x$$

$$\frac{\partial H_x}{\partial z} = \sigma E_y$$

$$-\frac{\partial H_x}{\partial y} = \sigma E_z$$

.....2.49

In equations 2.48 only E_x, H_y and H_z components and in equation 2.49 only E_y, E_z and H_x are involved. Thus in this situation two polarizations arise. These are termed the E and B (or sometimes H) polarization cases.

In the E- polarization (E-pol) case, the electric currents are constrained to flow along the direction of invariant conductivity distribution i.e., the x-direction. By eliminating H_y and H_z equation 2.48 can be reduced to the

scalar Helmholtz equation with respect to E_x

$$\frac{\partial^2 E_x}{\partial y^2} + \frac{\partial^2 E_x}{\partial z^2} - i\omega \mu_0 \sigma E_x = 0$$

.....2.50

For the B-polarization (B-pol) case, as for the E-polarization case, the field component B_x can, from equation 2.49, be shown to satisfy

$$\frac{\partial^2 H_x}{\partial y^2} + \frac{\partial^2 H_x}{\partial z^2} + \frac{1}{\sigma}\left(\frac{\partial \sigma}{\partial y}\cdot\frac{\partial H_x}{\partial y} + \frac{\partial \sigma}{\partial z}\cdot\frac{\partial H_x}{\partial z}\right) - i\omega\sigma H_x = 0$$

.....2.51

From equation 2.49, it can be seen that when $\sigma = 0$,(for example, in air) there is no variation of the magnetic field along the y and z directions. Hence, the magnetic field remains constant at the boundary of the conductor irrespective of the conductivity distribution inside it. Electric currents, however, may cross the interfaces and as result a) volume charges may appear in zones of rapid lateral conductivity variation and b) surface charges may appear at intersections of a discontinuous variation of conductivity.

The effect of these charges is commonly known as 'galvanic' being frequency independent (Rokityansky 1982, p 52). Since the differential equations derived for the E and B polarization cases are non - linear, they can in general only be solved numerically. Analytical solutions are only available for simple geometrical earth structures such as faults, dykes etc., (eg. Rankin 1962, D'erceville and Kunetz 1962 etc.) as reviewed by Hobbs (1975). There are various numerical techniques available for solution of general E- and B-pol differential equations. These include the finite element, the finite difference,

the integral equation methods etc., and are discussed later in Chapter 7.

2.3.3. The three dimensional case

Although three dimensional modelling has not been attempted in the present study, a few comments about the problem follow.

In this case $\sigma = \sigma(x,y,z)$, and hence it is difficult to reduce Maxwell's equations to a simple form. Numerical solutions obtained by Jones and Pascoe (1972), Lines and Jones (1973) require large computer storage and time. Several attempts have since been made to reduce the computer storage and CPU time required (e.g. Raiche 1974, Weidelt 1975, Hohmann 1983). In these attempts the use of integral equations seems to be the most successful for solving complicated structures (Ting and Hohmann 1981, Das and Verma 1982 and Wannamaker et al 1984). For some 3D problems, a 'thin sheet' model approach as described in Vasseur and Weidelt (1977), Hermance (1982), McKirdy et al. (1985) is useful. An application of this approach to the region of this study has been made by Jowiak and Beamish (1986) and this will be discussed in chapter 8.

CHAPTER 3
Instrumentation and data acquisition

This chapter deals with a description of the instruments used and data acquisition procedures applied in this project. In section 3.1, a brief introduction to the basic requirements of an MT system is given. Details of the instruments and the survey logistics are described in sections 3.2 and 3.3 respectively.

3.1. Introduction

As discussed in chapter 1, the source fields used in the magnetotelluric method cannot be controlled since they are natural electromagnetic variation fields and as such their occurrence frequency is dependent on local time, season and latitude and their amplitudes vary from about 0.001 nT to 100 nT. A satisfactory magnetotelluric data acquisition system must be designed to take all these factors into account. A system with a high gain, low noise amplifier-filter unit and a digital recording facility is normally regarded as the basic requirement. In recent years, however, with the advent of microcomputers, analysis of the data in the field is becoming more common, especially for the higher frequencies. This assists in the acquisition of relatively noise free data and thus good quality response functions.

In the present study, all the data were recorded digitally during two field seasons- Aug 1985 and July 1986. The following four MT systems were used.

1. The short period audiomagnetotelluric (S.P.A.M.)Mk-I system with an operational range of 100 Hz. to 0.125 Hz, with CM-11 induction coils.

2.The S.P.A.M. MK-II system (128 Hz. to 0.031 Hz.) with CM-11 induction coils.

3. A long period magnetotelluric system with digital recording on magnetic tape and a range of 5 sec. to 190 sec. This also utilised CM-11 induction coils as magnetic sensors.

4. Long period magnetotelluric systems (40 sec. to D.C.), with digital recording as above and EDA fluxgate magnetometers as magnetic sensors.

The electric field sensors comprise pairs of electrodes between which the

potential differences are measured. In this study, non-polarizing electrodes Pb - Pb Cl_2 were used for the longer period (>10 sec.) observations and copper metal electrodes for the short period signals (< 10sec.). Induction coils (Societe Eca CM11E) were used as magnetic sensors for the 128 Hz. to .01 Hz. range and EDA fluxgate magnetometers for signals in the 0.025 Hz. to DC. range.

3.2. Instrumentation

Details of the S.P.A.M. system are given in an internal report of the Geophysics Department (Dawes, 1984) and of the NERC geologger in a technical hand book (Valiant, 1976). The long period MT systems (Bands 4, 5) were developed by Hill (1986, personal communication) and Dawes(1987, personal communication) respectively. In the following sections, a summary of these reports is presented.

3.2.1. The S.P.A.M. system

In the S.P.A.M. (Mk.II) system used in this study, signals in the frequency range 128 to 0.031 Hz. were studied in four overlapping bands called sequentially Band 0 (-3DB points at 128-16Hz.), band 1 (16-2Hz.), band 2 (2-0.25Hz.) and band 3 (0.25-0.0312 Hz.). The system consists mainly of three units, a pre-amplifier (sensor distribution) unit, an analogue unit and a computer unit. This portable system can be operated with one 12V battery for the analogue and preamplifier units and a 24V battery for the computer unit. A block diagram of the complete system can be seen in fig 3.1 (from Dawes 1984).

The preamplifier unit is located about 50-100m. from the analogue and computer units and normally within 5m. of the magnetic sensors. A schematic diagram of this unit illustrating its main functions is given in fig 3.2a. This unit contains telluric amplifiers and filters with a wide frequency range (1000Hz. and 0.001 Hz.). This box also contains a voltage regulator and supplies power to the magnetic induction coils. All the five sensors, two electric and three magnetic components (Ex, Ey, Hx, Hy and Hz) are connected to this unit and the output signals are fed to the analogue unit via a multi-core single cable. The response function of this unit can be seen in

Fig.3.2b. The signals entering this system first pass through amplifier-filter units in which the radio frequencies greater than 10.6 K Hz. are suppressed before being amplified. Later the signals pass through a differential amplifier and band pass filtering unit (-3DB points at 0.033 Hz. and 2040 Hz). Finally the signals are amplified in the post-amplification unit with a fixed gain of 8.

3.2.1.1. The analogue unit

This can be divided into six sections- the input amplifier unit, the notch filtering unit, the band pass - post amplifier units, the clock unit, the A/D converter unit and the DC-DC converter unit.

The input amplifier unit has a fixed gain of 2 with a high impedance buffer followed by high and low pass filters. The notch filter unit consists of two twin T notch filters for each channel with notch frequencies of 50 and 150 Hz. and a notch width (Q value) of 10. The post amplification unit consists of a low gain buffer followed by a switchable band pass filter. A sharp low pass filter prevents anti-aliasing problems in digitizing. The band pass filters are followed by a single pole high pass filter to eliminate any D.C. present. Now the signals are amplified with a digitally controlled amplifier with a dynamic range from 2^0 to 2^7 in steps of 2. This unit is followed by a clock and A/D converter unit. The crystal clock generator provides the timing pulses to control the automatic gain ranging and digitizing frequency which is 4 times the corner frequency. The A/D converter consists of 5 identical sections. There are no time delays in digitizing each channel since the system is provided with separate A/D converters for each channel. The A/D converter is 12 bit with a range of +/- 10V and a conversion time of 25 micro sec. The final unit in the analogue box is the DC-DC converter which provides a supply voltage of +5V and +/- 15V from the 12V input. The current consumption of the analogue unit, preamplifier unit and magnetic induction coils is about 1.5 amps. Hence a 20 Ahr. battery should provide 12 hours of continuous supply. The response functions of the different frequency bands of the analogue unit is shown in Fig. 3.3. Since the response functions of each channel of this unit are identical no correction is applied for the band pass filter of this unit.

FIGURE 3.1

Block diagram showing the AMT/MT data acquisition system (S.P.A.M.) (from Dawes 1984).

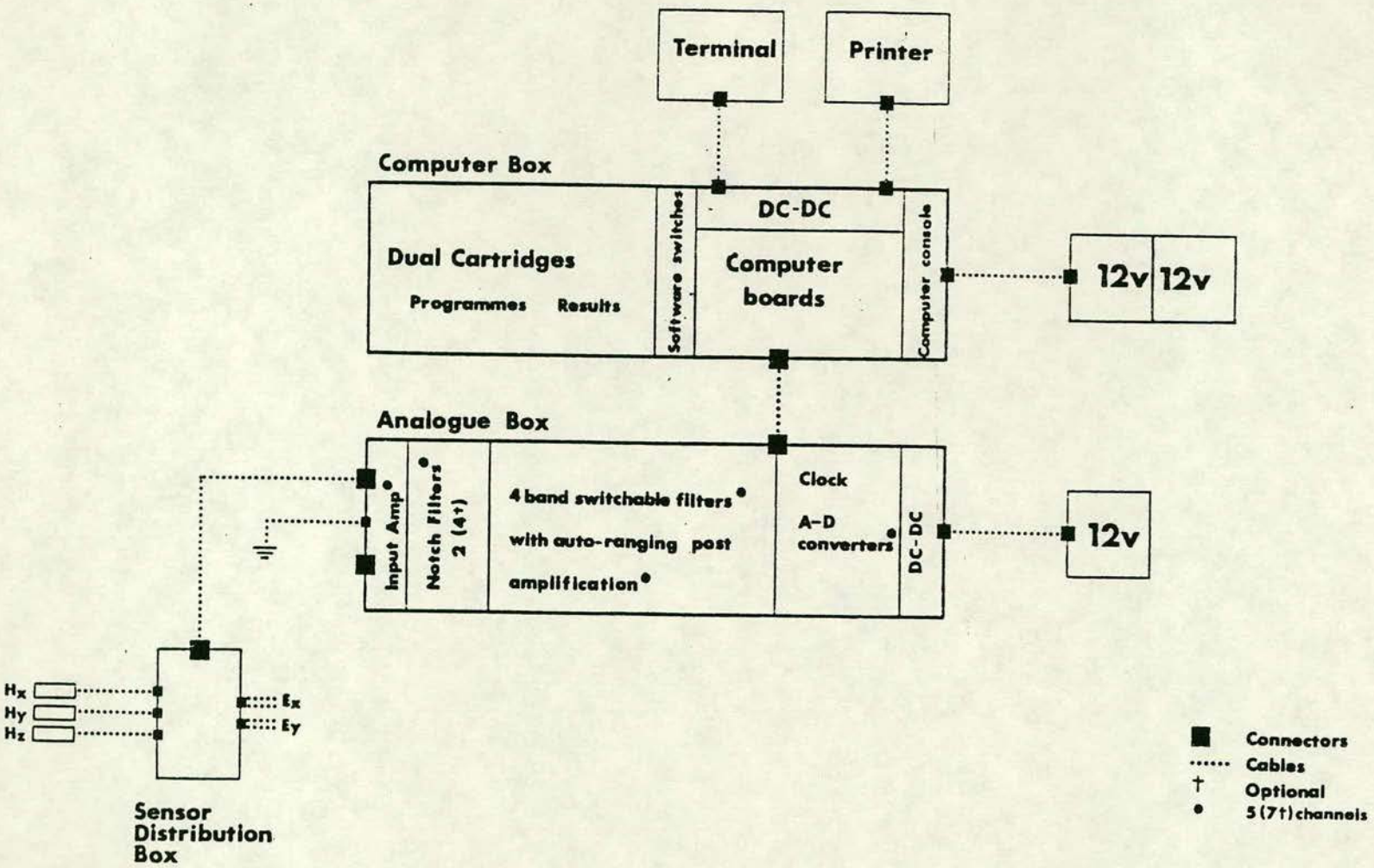

Complete System

FIGURE 3.2

a. A schematic block diagram for the pre-amplifier unit of SPAM.

b. Calibarated response curves for the pre-amplifier unit.

a) PRE-AMPLIFICATION UNIT (S.P.A.M.)

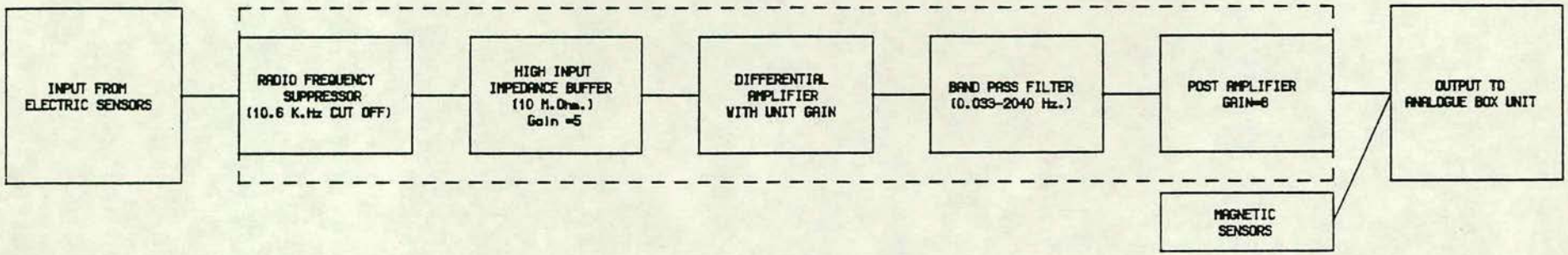

b) PREAMPLIFIER UNIT (AMT)

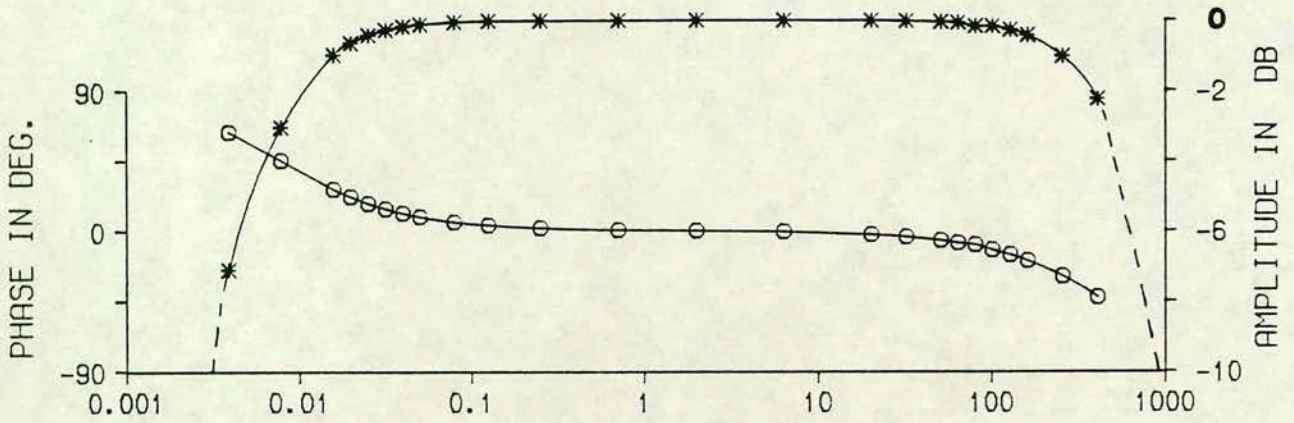

FIGURE 3.3

The response curves for the analogue unit of the SPAM system for the five identical channels. (from Dawes 1984)

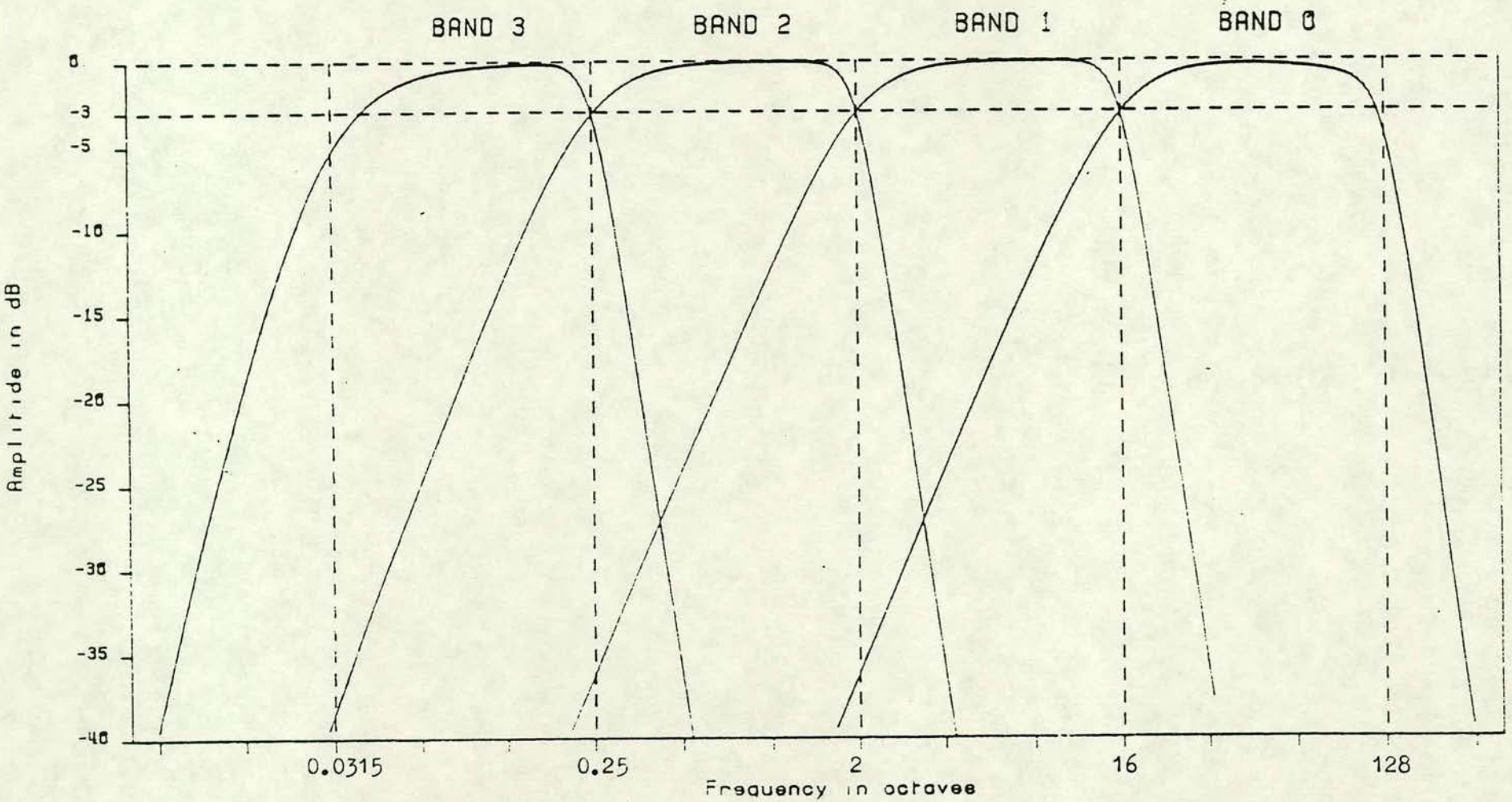
BAND 3
BAND 2
BAND 1
BAND 0
0
-3
-5
-10
-15
-20
-25
-30
-35
-40
Amplitude in dB
0.0315
0.25
2
16
128
Frequency in octaves

3.2.1.2. The computer unit

The computer unit is based on the DEC LSI 11 bus architecture. This consists mainly of a) a central processor (CPU), b) the LSI 11/2 with a KEV 11 floating point chip c) the main memory (RAM) of 64 K bytes d) a boot strap board (ROM) to load the system from cartridge on power up e)a quard serial line (SLU), f) an input-output board to interface with the terminal, printer and cartridge controller and a 64 parallel line TTL compatible to interface with the analogue box- and software switches. The recording system has a DEC TU58 system of dual cartrides one of which holds the user programmes and the system software while the other stores the raw digitized time series and the analysed results. There are two peripherals- a Brother HR-5 thermal transfer printer using A4 rolled paper and a miniature double line liquid display terminal. The terminal is powered with internal batteries which can be operative for 60 hours on full charge and the printer is powered by a 6V battery. The current consumption of the computer system is 2.5 amps. The operations performed by the computer such as analysis, plotting and recording of the data can be controlled from the terminal. Details of the in-field processing will be discussed in section 3.3.2.

3.2.2. The Long period (Band-4) magnetotelluric system

This system consists of three units- a preamplifier unit, a post-amplification unit and a recording unit. The block diagram of this system can be seen in fig. 3.4a. The preamplifier unit is similar to that of the S.P.A.M. system but differs in the band pass frequency range. The response curves of this unit can be seen in Fig 3.4b. The response curves for the CM11 magnetic sensors used with this system and also SPAM are shown in Fig. 3.4 c. The post-amplification unit consists of a) an input amplifier (gain=2), b) a band pass filter (-3DB point at 0.005 Hz. and 0.185 Hz.), c) pre_amplification (gain=7.2), d) an active low pass filter (-3 DB points at 0.079Hz.) and e) a high pass (0.00265Hz.) noise suppressor (4.52Hz.). The geologger unit has a digital magnetic cassette recording system with a range for each channel of +/- 10V. The sampling rate for recording the Band-4 data was selected in this study to be 1Hz. with a digitizing step of 5 mV. Each digital cassette could then record the data for about 6 1/2 hours.

FIGURE 3.4

a. A schematic block diagram for the Band-4 MT system.

b. Calibrated response curves for Band-4 system.

c. Response curves for a CM-11 induction coil.

a) BAND-4 MAGNETOTELLURIC SYSTEM

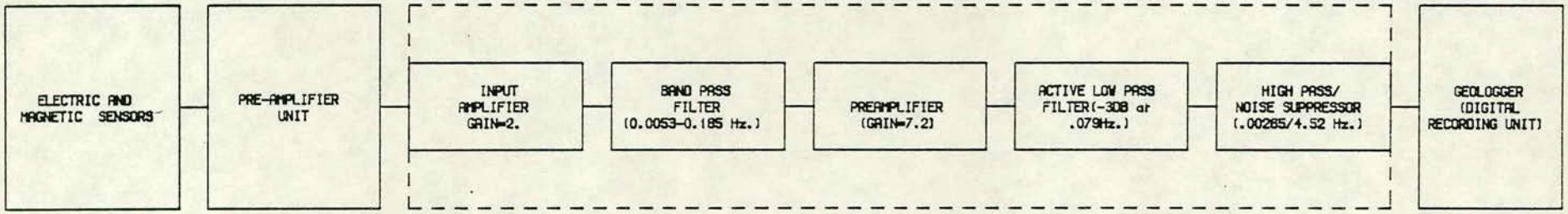

b) PREAMPLIFIER UNIT (BAND-4)

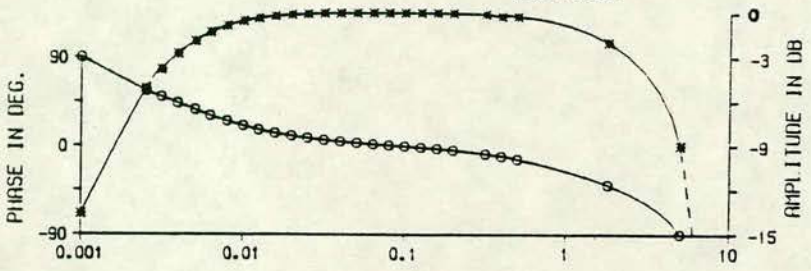

C) CM11 INDUCTION COIL

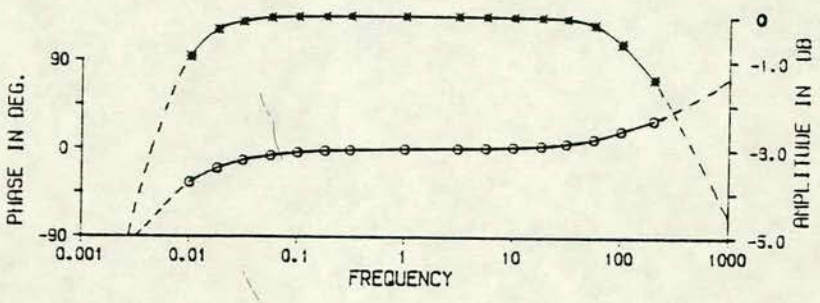

3.2.3. The long period (Band-5) magnetotelluric system

The block diagram of this system can be seen in Fig 3.5. The magnetic signal assembly consists of a 3 component E.D.A. fluxgate magnetometer with a low pass filter (0.025 Hz.) The total sensitivity for the magnetic assembly including the sensors is 50 mV/nT. Electric field assembly consists of an input amplifier with a fixed gain of 100 with back-off, a 2 two pole Butterworth low pass filter (0.025 Hz.) and a variable post-amplifier (Gain 2 to 100); all the 5 signals are finally input to the geologger for recording. The author assisted during the construction of the system (preparation of the PCB circuitary boards for the amplifier-filter units etc.,) and in its field testing.

3.3. Survey logistics

The instruments were calibrated before the field measurements using a frequency generator and analyser as shown in Figs. 3.2b and 3.4b. Subsequently, the following procedure was adopted.

3.3.1. The field procedure

Ideally, to record natural signals with minimum noise and error the magnetotelluric station should be distant from power lines and other cultural noise and it should have reasonably flat topography. Care should also be taken to locate the station in an area with uniform geology, distant from highly conducting regions such as rivers, lakes etc. which might introduce surface distortion (Rokityansky 1982).

In this study the sites were selected along the chosen traverse to satisfy the above requirements as far as possible. Then the following field procedure was adopted.

First, electric cables of about 50m. long were laid out along the NS and EW directions using a cross spread configuration and the electrodes were buried at the end points of the cables. Next the magnetic induction coils were laid along the NS and EW directions and another coil buried vertically to a depth of about 0.5m deep. The coils were supported with clamps and covered with wind shields. The cables from the electric and magnetic sensors were connected to the preamplifier unit. The distances between the electrodes were measured. A 50/100m. long multi-core cable connected the preamplifier

FIGURE 3.5

A schematic block diagram for the Band-5 MT system.

BAND-5 MAGNETOTELLURIC SYSTEM

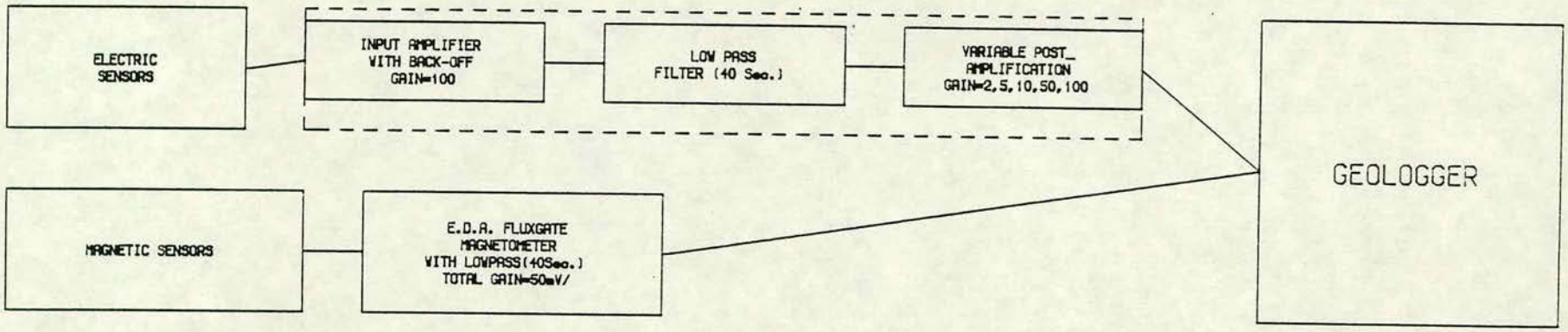

unit to the analogue unit. A common reference (earth) electrode was buried away from the sensors and was connected to the analogue unit. The analogue and computer units were kept in the vehicle at a distance of about 50 to 100m. from the sensors. The period of recording at each site was about 1 to 1 1/2 days using the SPAM system. The field installation procedure for the long period (Band 4) magnetotelluric system was similar except that the amplifier-recording assembly was kept in an aluminium box for continuous recording of the data for about 3 to 4 days at each site. In the long period (Band 5) magnetotelluric system the 3 component fluxgate sensing head was buried to a depth of about 0.3m and covered from the wind. The duration of recording for this system was about 7 days per site. Upto 68 hours of data could be recorded on one cassette with the 10s sampling rate used for this Band-5 system. The adjustment for back-off of the electrode self potentials was required at least twice per day.

3.3.2. The in-field processing of the short period (AMT/MT) data

As described earlier the signals were recorded in four overlapping frequency bands, one band at a time. In each band about 60 to 90 windows of data (1 window = 256 samples per channel) which satisfied certain preset conditions were accepted for analysis. The acceptance criteria were established in the following manner:

After a window was read the data could be checked visually by plotting i) the time series of all channels ii) their power spectra and iii) their response functions. By visual inspection of these plots at each site acceptance criteria could be changed by the observer.

In this study the data were normally selected if they satisfied the following criteria: a) the power level is greater than 0.3 for 5 frequencies in a window and b) the predicted coherence is greater than 0.8. Infield processing was undertaken as shown in the flow chart presented by Dawes (1984) and reproduced in fig. 3.6. The field data were recorded on a digital cartridge using four tracks, with each track storing 24 windows of five channel data. An example of the in-field processing results for Whitfield (station code=508) in N. England is shown in fig.3.7. The time series with automatically selected gain for each channel are shown for the window 28 of band 3 in fig. 3.7a. Only 4 channels of data can be seen in this example as the recording of the vertical

FIGURE 3.6

The flow chart showing the various steps and options during in-field data acquisition and processing (from Dawes 1984).

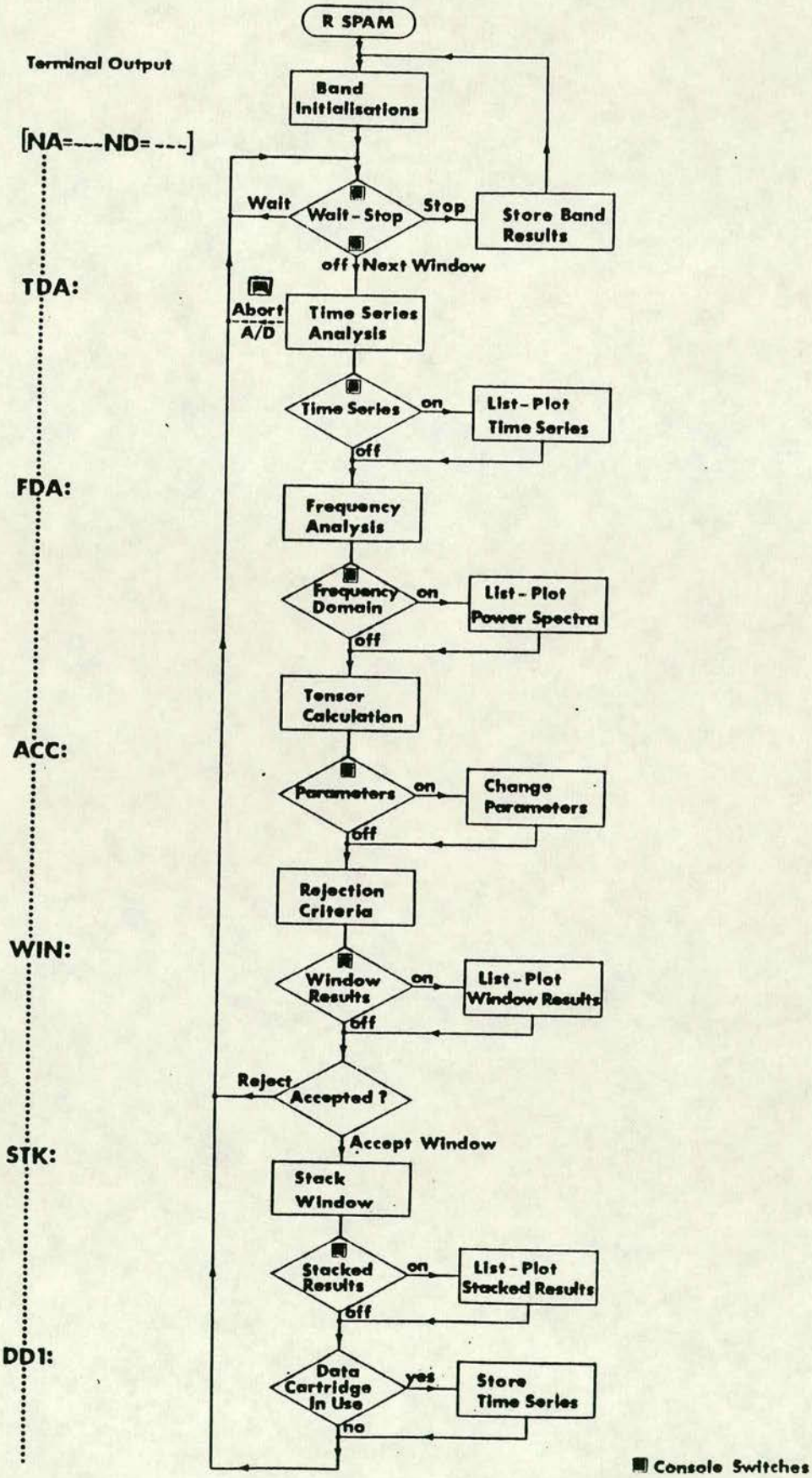

FIGURE 3.7

An example of in-field data results from WHI station showing a) the time series of 4 channels, b) the power spectra and c) frequency variations of Cagniard apparent resistivity (RHOXY, RHOYX), phase (PHXY, PHYX), coherency (COHER), skew etc. Nxy, Nyx and NEST are the number of estimates accepted; ERHXY, ERHYX are the errors in the estimation of apparent resistivity values.

TIME SERIES SITE: 508 BAND: 3 WINDOW: 28

(a)

CHAN		MING	MAXG	GAIN	MEAN	NSAT
1	HX1	5	5	5	29	0
2	HY1	5	7	5	0	0
3	EX1	7	7	7	7	0
4	EY1	7	7	7	9	0

BAND : 03 I/P GAIN: 03 NOTCHES : 00 00 00 00

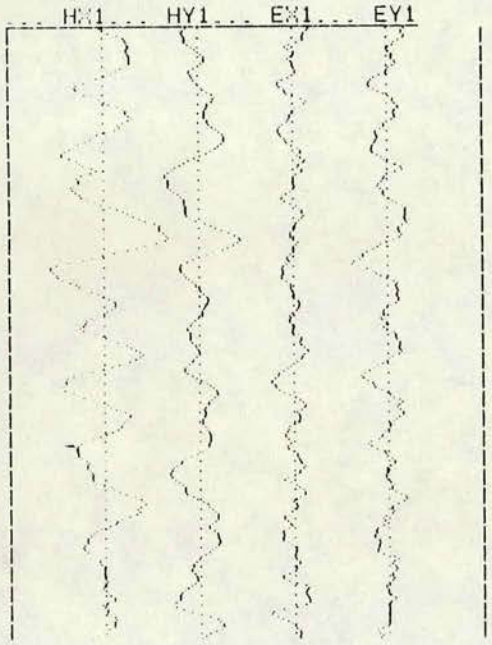

(b)

FFT AMPLITUDE SITE: 508 BAND: 3 WINDOW: 2

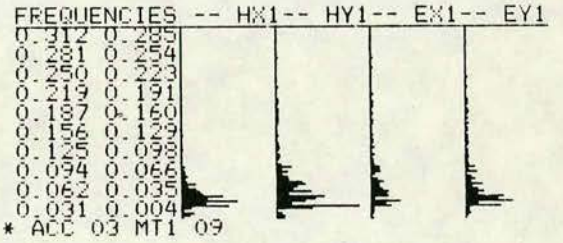

(c)

STACKED RESULTS SITE: 508 BAND: 3 WINDOW: 49

MT1	FREQ	SKEW	RHOXY	PHXY	COHXY	RHOYX	PHYX	COHYX	NXY	ERHXY	NYX	ERHYX
1	0.250	0.37	40.21	-136.	0.53	17.35	36.	0.72	11	24.82	11	3.82
2	0.195	0.32	98.44	-131.	0.46	20.76	23.	0.72	7	28.39	7	9.89
3	0.156	0.29	82.80	-136.	0.43	30.76	24.	0.61	5	33.07	5	15.86
4	0.125	0.19	148.70	-129.	0.52	41.71	36.	0.64	17	48.00	17	9.94
5	0.098	0.22	79.42	-124.	0.55	42.57	30.	0.68	18	26.78	18	8.62
6	0.078	0.21	59.75	-107.	0.69	38.08	41.	0.76	27	8.86	27	4.98
7	0.062	0.25	56.63	-102.	0.73	41.64	46.	0.84	34	8.42	34	7.50
8	0.051	0.29	44.79	-96.	0.72	43.61	57.	0.88	32	4.93	32	3.42
9	0.039	0.24	56.23	-104.	0.68	46.71	63.	0.92	31	30.70	31	3.40
10	0.031	0.32	35.94	-87.	0.78	42.94	71.	0.91	37	17.58	37	3.66
11	0.025	0.30	22.76	-78.	0.82	46.19	80.	0.92	40	4.30	40	2.75
12	0.020	0.33	34.37	-91.	0.89	42.83	90.	0.98	35	17.72	35	3.17
13	0.016	0.25	33.29	-50.	1.45	51.68	105.	2.62	16	16.67	16	6.51

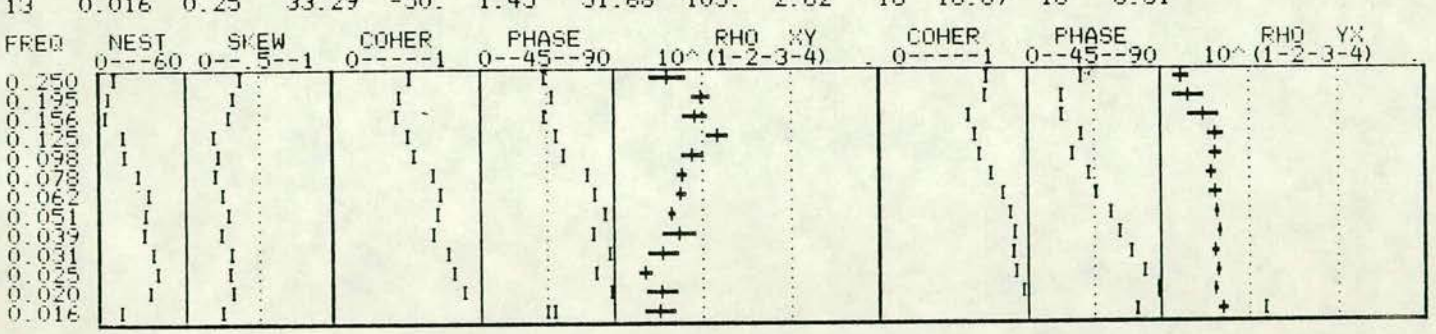

component Hz, had been abandoned due to high noise level. The power spectra for the same band but for window 2 can be seen in fig. 3.7 b and the stacked results are shown for 49 windows. The resistivities in the measured directions are plotted on a log scale (fig. 3.7c). Apart from this form of analysis the data were also inverted in the field after obtaining all the data bands. For this purpose the Bostick transformation (Bostick 1977), to obtain the resistivity–depth profiles in the measured and rotated directions, was used.

3.3.3. Data transcription

After the completion of the field work the S.P.A.M. data were transferred to 9" magnetic diskettes, then to 1/2" magnetic tapes using a DEC MINC-11 computer and finally transferred to the main frame computer of the Edinburgh multi-access system (EMAS). The longer period data were first read to 9" floppy discs then a series of windows were selected by visual examination of the time series, their spectra were then transferred to the main frame computer as for the AMT/MT data. All the results presented in this thesis were obtained by use of the EMAS system.

3.3.4. Station location

In total 22 S.P.A.M. soundings were made along a traverse starting from near the Southern Uplands Fault and ending in the Weardale granite region of Northern England. Soundings at three of the stations- Edges green (EDG), Sinderhope (SIN) and Rookhope (ROO) were repeated due to noise problems and to check the repeatability of the results of the data analysis. Band - 4 recordings were made at four locations- Drumezlier (DZR), Sinderhope (SIN), Rookhope (ROO) and Hillend (HIL) and Band-5 recordings at six locations- Rookhope(Roo), Sinderhope(Sin), Whitfield (WHI), Bewcastle (BEW), Eskdalemuir (ESK) and Cappercluech (CAP). Unfortunately, data at a few stations (eg. BIG, NEW, CRK, ESK etc.,) were corrupted with noise and could not be considered for modelling. Discussion of these noise problems is given in Chapter 5. Fig. 3.8 shows the station locations occupied in this study. Their grid references, codes and the names of adjacent villages or towns are given in table 3.1.

3.8 The station location map showing the AMT/MT stations occupied in the present study. The numbers represents the national grid eastings (105–505) and northings (500–700). The grid references for these stations are given table 3.1. The dashed line indicates the locations of the major faults. SUF= Southern Uplands Fault; OBF= Orlock Bridge Fault and SBF= Stublick Fault. The approximate boundary between Silurian (Si) and Carboniferous (Cr) sediments; Or = Ordovician sediments.

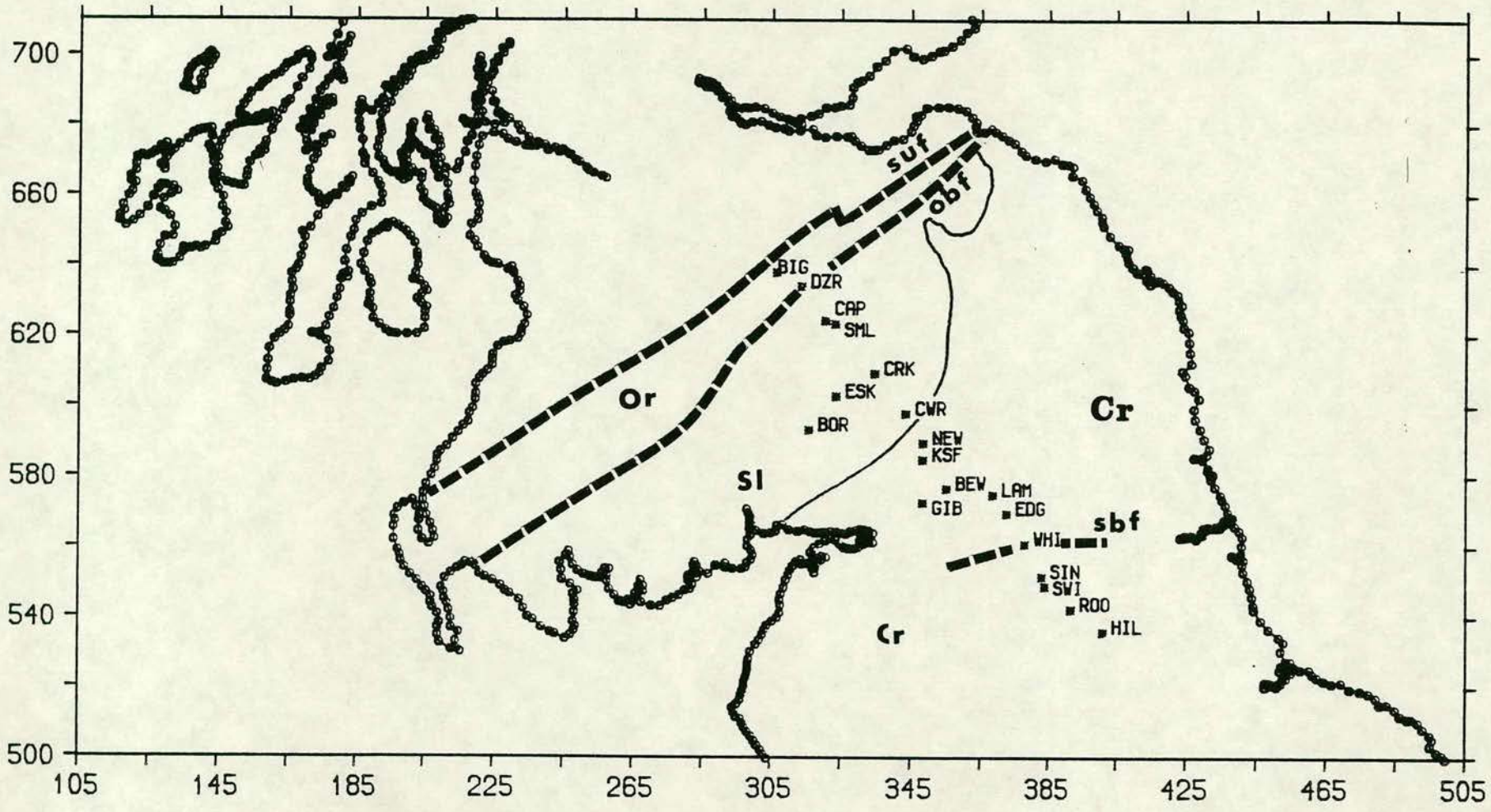
700
660
620
580
540
500
105
145
185
225
265
305
345
385
425
465
505
suf
obf
sbf
Or
Cr
Sl
Cr
BIG
DZR
CAP
SML
CRK
ESK
BOR
CWR
NEW
KSF
BEW
LAM
GIB
EDG
WHI
SIN
SWI
ROO
HIL

56

L

TABLE 3.1

List of MT stations occupied in the present study. Station codes, its numbers and nearest popular location name are given. The national grid reference (Eastings and Northings) for each station can also be seen.

TABLE 3.1

SITE NO.	SITE CODE	SITE NAME	EASTINGS	NORTHINGS
601	BIG	Biggar	30640	63790
515	DZR	Drumezlier	31365	63380
514	CAP	Cappercluch	32050	62410
607	SML	St.Mary'sLoch	32330	62310
503	CRK	Craik	33465	60900
608	ESK	Eskdalemuir	32360	60260
504	BOR	Boreland	31575	59300
502	CWR	Carewoodrig	34355	59760
501	NEW	Newcastleton	34840	58925
605	KSF	Newcastleton	34830	58450
505	BEW	Bewcastle	35510	57630
506	LAM	Lampert	36850	57455
509	GIB	Gibstown	34830	57240
507	EDG1	Edgesgreen	37245	56900
606	EDG	Edgesgreen	37255	56920
508	WHI	Whitfield	37785	56062
510	SIN1	Sinderhope	38330	55120
604	SIN	Sinderhope	38300	55130
513	SWI	Swinhope	38385	54860
511	ROO1	Rookhope	39175	54200
603	ROO	Rookhope	39175	54200
512	HIL	Hillend	40110	53560

CHAPTER 4
Data Processing

In this chapter the processing procedures used in this study are described and the results presented. In section 4.1 a brief introduction to the processing is given. Frequency domain processing procedures and the properties of impedance elements are discussed along with a few field examples in section 4.2, while in section 4.3 the results obtained from processing are presented. Some consideration is given in section 4.4 to the time domain processing technique for estimation of the impulse response functions of the earth, although this procedure was not developed sufficiently for application to the present field study.

4.1. Introduction

As discussed in the previous chapter, the data acquired consist of simultaneous records of time dependent magnetic field variations and the electric field variations induced in the ground by the magnetic fields. The aim of processing these observed time variational fields is to determine the earth response functions. The response functions of interest in this study are functions that can be determined from surface magnetotelluric (MT) measurements.

The observed horizontal components of electric and magnetic fields are related by the impedance 'Z' and the determination of this quantity is the fundamental problem in MT data processing. Due to the presence of inhomogeneous earth structures, 'Z' is treated as a tensor of rank 2. The problem of estimation of the impedance tensor may be regarded as a two input and single output linear system. The computations involving the solution of this linear system can be carried out either in the time domain or in the frequency domain. The linear equations to be solved in the time domain can be written as

$$E_x(t) = Z_{xx}(t) * H_x(t) + Z_{xy}(t) * H_y(t) + \delta E_x(t) \qquad \text{.....4.1a}$$

$$E_y(t) = Z_{xy}(t) * H_x(t) + Z_{yy}(t) * H_y(t) + \delta E_y(t) \qquad \text{.....4.1b}$$

where * represents the convolution operation.

In the frequency domain, the equations are

$$E_x(\omega) = Z_{xx}(\omega)\ H_x(\omega) + Z_{xy}(\omega)H_y(\omega)$$

.....4.2a

$$E_y(\omega) = Z_{xy}(\omega)\ H_x(\omega) + Z_{yy}(\omega)\ H_y(\omega)$$

.....4.2b

where $E_x(\omega)$, $H_x(\omega)$...etc., are Fourier coefficients of

$E_x(t)$, $H_x(t)$... etc., respectively.

Processing of all the data in the present study has been carried out in the frequency domain as described in detail in the next section.

4.2. Frequency domain analysis

Estimation of the impedance tensor suffers from random and bias errors. Bias errors arise from the noise associated with both the electric and the magnetic fields. To reduce these errors, the impedance tensor is estimated from a large number of data sets. Some understanding of the effects of bias due to incoherent noise has been provided by Sims et al (1971), and Pedersen (1982).

4.2.1. Estimation of the impedance tensor

There are various ways of estimating the impedance tensor from single site analysis as discussed by Hermance (1973) or by using remote reference technique (Gamble et al 1979, Goubau et al 1984). One method of estimation is by using least squares cross spectral analysis (Sims et al 1971). In this

approach, by using the complex conjugates of each measured component and minimizing the noise power on either the electric field components or the magnetic field components, four equations can be obtained. For example, by multiplying equations 4.2b by the complex conjugates of E_x, E_y, H_x and H_y one can get four equations. Since the four equations are independent any two of them can be solved simultaneously for Z_{yx} and Z_{yy}. Impedance tensors can be solved, however, from six different possible pairs of equations, thus producing six ways of estimating Z_{yx} and Z_{yy}. For example, the least squares solution for the element Z_{yx} can be written as,

$$Z_{yx} = \frac{(E_y A^*)(H_y B^*) - (E_y B^*)(H_y A^*)}{(H_x A^*)(H_y B^*) - (H_x B^*)(H_y A^*)} \qquad \text{.....4.3}$$

The terms in the brackets represent the average spectral values over a finite frequency band. The six estimates for the Z_{xy} element are obtained by substituting,

$$\begin{aligned}
&Hx^* = A^* \;;\; Hy^* = B^* && (a)\\
&Ey^* = A^* \;;\; Hy^* = B^* && (b)\\
&Ex^* = A^* \;;\; Hy^* = B^* && (c)\\
&Ex^* = A^* \;;\; Ey^* = B^* && (d)\\
&Hx^* = A^* \;;\; Ey^* = B^* && (e)\\
&Hx^* = A^* \;;\; Ey^* = B^* && (f) \qquad \text{.....4.4}
\end{aligned}$$

From studying the solutions of 4.4, it is clear that 4.4(a) assumes E_y as output, solution (d) assumes H_x as output and 4.4 (f) assumes H_y as output. Thus the three solutions are obtained by minimizing the noise in their respective outputs. All these three solutions are biased, however, by noise in their respective inputs. Solution 4.4(a) is downward biased by noise in H_x and solution 4.4(d) is biased upward by noise in E_y. Solution 4.4 (f) is either downward biased by noise in H_x or upward biased by noise in E_y.

Solutions of 4.4 b, c and e can be similarly explained. However, all the six solutions are unstable for highly polarized incident fields and two

solutions, 4.4(c) and (f), are unstable in a one dimensional earth situation. Sims et al. (1971) have suggested that the arithmetic mean of the remaining four stable solutions for each impedance element provides the most reliable estimate possible for the element. More recently, however, several attempts have been made to obtain bias free transfer functions for a single site data analysis. For example, Kao and Rankin (1977) have suggested a correction for auto-power noise and Pedersen and Svennekjaer (1984) have discussed the conditions for and extent of bias effects. These latter studies aid the understanding of the distortion of transfer functions. Park and Chave (1984) have presented a method involving use of using singular value decomposition and Chave et al (1987) have discussed the use of robust estimation methods. In the present study, the least square approach (Sims et al 1971) is used. Since the magnetic field has been observed to be generally less noisy compared to the electric field, a downward biased estimate of the impedance has been computed.

4.2.2 The Coherence function

After determining the impedance elements from equation 4.3 they can be substituted back into equations 4.2 a and b to compute E_x and E_y. Differences between computed values and observed values can be directly attributed to the noise in E or H. Hence the coherence between the output and two inputs is generally used as a good measure of the noise. This is termed as 'multiple' coherence or 'predicted' coherence and is given (Swift 1967) by

$$\mathrm{Coh}(E_x^{pred}E_x)=\frac{<E_x^{pred}E_x^{*}>}{[<E_x^{pred}E_x^{pred*}><E_xE_x^{*}>]^{1/2}} \qquad \text{.....4.5}$$

Terms within <> indicate the average values in a subfrequency band. Where,

$E_x^{pred}=Z_{xx}H_x+Z_{xy}H_y$

and

$<E_x^{pred}E_x^{*}>=Z_{xx}<H_xE_x^{*}>+Z_{xy}<H_yE_x^{*}>$.

Expanding equation 4.5 gives,

$$\mathrm{Coh}(E_x^{pred}E_x)=\frac{|H_x|Z_{xx}\,\mathrm{Coh}(H_xE_x)+|H_y|Z_{xy}\,\mathrm{Coh}(H_yE_x)}{\left[|Z_{xx}|^2|H_x|^2+|Z_{xy}|^2|H_y|^2+2|H_x||H_y|\,\mathrm{Re}(Z_{xx}Z_{xy}\,\mathrm{Coh}(H_xH_y))\right]^{\frac{1}{2}}}$$

4.2.3. Apparent resistivity and phase

Expressing equations 4.2 a and b in tensor matrix form we have,

$$\begin{pmatrix} E_x \\ E_y \end{pmatrix} = \begin{pmatrix} Z_{xx} & Z_{xy} \\ Z_{yx} & Z_{yy} \end{pmatrix} \begin{pmatrix} H_x \\ H_y \end{pmatrix}$$

.....4.6

where Z_{xy}, Z_{yx} are called the principle impedances or off diagonal elements and Z_{xx}, Z_{yy} are called the diagonal elements, which are additional impedances due to contributions from parallel components of the magnetic field. For a one dimensional earth structure, $Z_{xx} = Z_{yy} = 0$ and $Z_{xy} = -Z_{yx}$. For such a structure, Cagniard (1953) has defined the apparent resistivity 'ρ_a' and phase 'ϕ' in the measured direction as

$$\rho_a = \frac{1}{\mu_o \omega} \left| Z_{ij} \right|^2$$

.....4.7

where, i,j are x,y or y,x. Applying the practical units, mv/km and nT, to electric and magnetic fields respectively, the apparent resistivity in Ohm.m. can be obtained from equation 4.7 as,

$$\rho_a = 0.2T \left| Z_{ij} \right|^2$$

.....4.8

4.2.4. Directionality and dimensionality indicators

4.2.4.1. DIRECTIONALITY PARAMETER

After obtaining the impedance elements in the measured arbitrary axes, they can be rotated to any other Cartesian co-ordinate axes. In a strictly one dimensional situation, the impedance elements are invariant to rotation. In the presence of lateral inhomogeneous earth structures, however, the values of these elements are variable with rotation. In this case, the properties of the impedance elements are, in general,

$$Z_{xy} + Z_{yx} \neq 0$$

$$Z_{xx} + Z_{yy} = 0$$

and after rotation

$$Z'_{xx} = Z'_{yy} = 0$$

.....4.9

The angle of strike 'α_s' can be obtained by maximizing either Z_{xy} (Everett and Hyndmann 1967a) or $Z'^{2}_{xy} + Z'^{2}_{yx}$ (Swift 1967) under rotation. The rotated elements can be obtained by the matrix equation,

$$\overline{\overline{Z}} = \overline{\overline{R}}\ \overline{\overline{Z}}\ \overline{\overline{R}}^{T}$$

.....4.10

where 'R' is the Cartesian rotation matrix given by,

$$R = \begin{bmatrix} \cos\theta & \sin\theta \\ -\sin\theta & \cos\theta \end{bmatrix}$$

.....4.11

From the analytical approach, the azimuth or strike angle can be obtained (Swift 1967) as

$$\theta_s = \frac{1/4 \ \tan^{-1} (Z_{xx}-Z_{yy})(Z_{xy}+Z_{yx})^{*}+(Z_{xx}-Z_{yy})^{*}(Z_{xy}+Z_{yx})}{Z_{xx} - Z_{yy}^{2} - Z_{xy} + Z_{yx}^{2}}$$

.....4.12

where, * denotes the complex conjugate.

As shown in equation 4.9 in an ideal two dimensional situation, after rotation to the principal directions, $Z'_{xx} = Z'_{yy} = 0$. In practice, however, they seldom become zero but only attain a minimum value compared to Z'_{yx}, Z'_{yx}. For these directions the major and minor apparent resistivities corresponding to Z_{xy} and Z_{yx} can be obtained from,

$$\rho_{max} = 0.2\ T \left| Z'_{xy} \right|^2$$

$$\rho_{min} = 0.2\ T \left| Z'_{yx} \right|^2$$

.....4.13

The ρ_{max} and ρ_{min}, cannot, however, be consistently identified as ρ-parallel and ρ-perpendicular due to the 90° ambiguity in the determination of θ_s as it can be seen that $\theta_s + \pi/2$ can also satisfy the equation 4.12.

4.2.4.2. DIMENSIONALITY PARAMETER

The estimations of the impedance elements are affected, in general, by contributions from one dimensional, two dimensional or three dimensional structures either singly or in combination. Commonly used dimensionality indicators are the skew, eccentricity and ellipticity as reviewed recently by Beamish (1986).

The skew parameter is defined (Swift 1967) as

$$S = \left| \frac{Z_{xx} + Z_{yy}}{Z_{xy} - Z_{yx}} \right| \qquad \text{.....4.14}$$

As previously discussed, for a one dimensional situation, the diagonal elements(Z_{xx},Z_{yy}) are zero and Z_{xy} is equal to $-Z_{yx}$. From equation 4.14 then it is clear that skew is zero. Under rotation in this situation the Z_{xy} and Z_{yx} should show small or no variation with angle. In a two dimensional situation, the off-diagonal impedance elements (Z_{xy} and Z_{yx}) maximize and minimize in the principal directions and the diagonal elements become zero. For this situation also skew should be zero. When the lateral resistivity variation is low, it is possible however that $|Z_{xy} - Z_{yx}|$ attains a value near zero, in which case, it is clear from equation 4.14 that skew can have a large value (provided zxx+zyy $\neq$ 0). For a general three dimensional situation, the maxima and minima for Z_{xy} and Z_{yx} may not coincide under rotation and also, Z_{xx}, Z_{yy} are large. The rotational properties are illustrated for one field example in figure 4.1. The variations of the impedance elements with rotation are presented here for nine frequencies for the Rookhope (Code =603) data (Band-0). It is clear from the figure that between 45° and 90° the values of Z_{xy} and Z_{yx} attain maxima and minima while Z_{xx} and Z_{yy} attain a value of nearly zero.

Noting the inherent difficulties in using this parameter as an indicator of dimensionality in certain conditions, Kao and Orr (1982) introduced a set of three normalized weights D1, D2 and D3. These weights have been shown by these authors to be better indicators than skew in assessing the relative importance of the different dimensional structural contributions. These weights can be written (Beamish 1986) as

$$D_1 = |Z_1| / S \qquad \text{(a)}$$

$$D_2 = |M_1| / S \qquad \text{(b)}$$

Fig. 4.1 The rotational properties of the impedance elements are shown for a field example - Band 0 data from ROO station. 91.0 Hz. etc. represent the frequencies and 0,45... represent the rotation angles.

Zxy
Zyx
Zxx
Zyy
91.0 HZ
72.8 HZ
35.9 HZ
30.0 HZ
22.9 HZ
17.0 HZ
14.0 HZ
11.0 HZ
9.00 HZ
100
64
38
16
4
0
0
45
90
135
180

$$D_3 = |M_2| / S \qquad (c)$$

.....4.15

where,

$$Z_1 = (Z_{xy} - Z_{yx}) / 2$$

$$M_1 = [Z'_{xy}(\theta) + Z'_{yx}(\theta)]/2$$

$$M_2 = [Z'_{xx}(\theta) - Z'_{yy}(\theta)]/2$$

$$S = |Z_1| + |M_1| + [|Z_2| + |M_2|]/2$$

$$Z_2 = Z_{xx} + Z_{yy}$$

$Z'_{xy}(\theta)$ $Z'_{yx}(\theta)$...etc., are the impedance values in the principal directions.

Studying the analytical properties of the complex response function $C(\omega)$ of the earth, Weidelt (1972) presented 19 inequalities involving the real and imaginary parts of C, which every realizable one dimensional data set should obey. Summarizing these inequalities recently, Weidelt (1986) has given 4 conditions for checking existence of the one dimensionality. These are stated below:

Assuming the time factor as $e^{i\omega t}$ and SI units the transfer function $C(\omega)$ can be defined as

$$C(\omega) = \frac{E_x(\omega)}{i\,\omega\,\mu_0\,H_y(\omega)}$$

$$= g(\omega) - ih(\omega)$$

$$= C(\omega)e^{-i\phi\omega}$$

.....4.16

where E_x and H_y are electric and magnetic field components at the surface in the x and y directions. These transfer functions can be related to the impedance Z and apparent resistivity ρ_a and phase ϕ as

$$Z = i\,\omega\mu_0\,C$$

$$\rho_a = \omega\,\mu_0\,|C|^2$$

$$\phi = 90^0 - \psi$$

.....4.17

The four conditions can now be written as

i) $$\frac{h_2 / \omega_2 - h_1 / \omega_1}{\omega_2 - \omega_1} < 0$$

ii) $$\frac{g_2 - g_1}{\omega_2 - \omega_1} < 0$$

iii) $$\left[\frac{C_2 - C_1}{\omega_2 - \omega_1}\right]^2 < \frac{h_1 h_2}{\omega_1 \omega_2}$$

and iv) $$\frac{\omega_2 C_2 - \omega_1 C_1}{\omega_2 - \omega_1} < g_1 g_2$$

.....4.18

where h_1, h_2..... correspond to the two different frequencies under consideration.

Considering the response functions for a theoretical one dimensional earth structure, the dimensionality indicators (equation 4.14) and existence checks (equations 4.18) are presented in figures 4.2a and b. It can be seen from figure 4.2a that at all frequencies, the weights for a one dimensional structure are unity and for two and three dimensional structure the weights vanish. In figure 4.2 b, the '+' sign indicates that for the pair of frequencies considered the existence condition for one dimensional structure is satisfied.

In figures 4.3 a–m, the dimensional weights on a logarithmic scale over the frequency range for all the field stations of the present study are presented. It can be seen from these that at all stations the weights for one dimensionality are dominant compared to the two or three dimensional weights, especially, at the higher frequencies. As the frequency decreases the weights for two and three dimensionality also become prominent. This can be observed, for example, for LAM and WHI (Fig. 4.3h and 4.3j respectively).

FIGURE 4.2

a) Dimensionality weights (Kao and Orr 1982) are shown for a theoretical one dimensional structure.

b) Weidelt's (1986) existence checks for 1D case, for the same theoretical exmple considered in a)

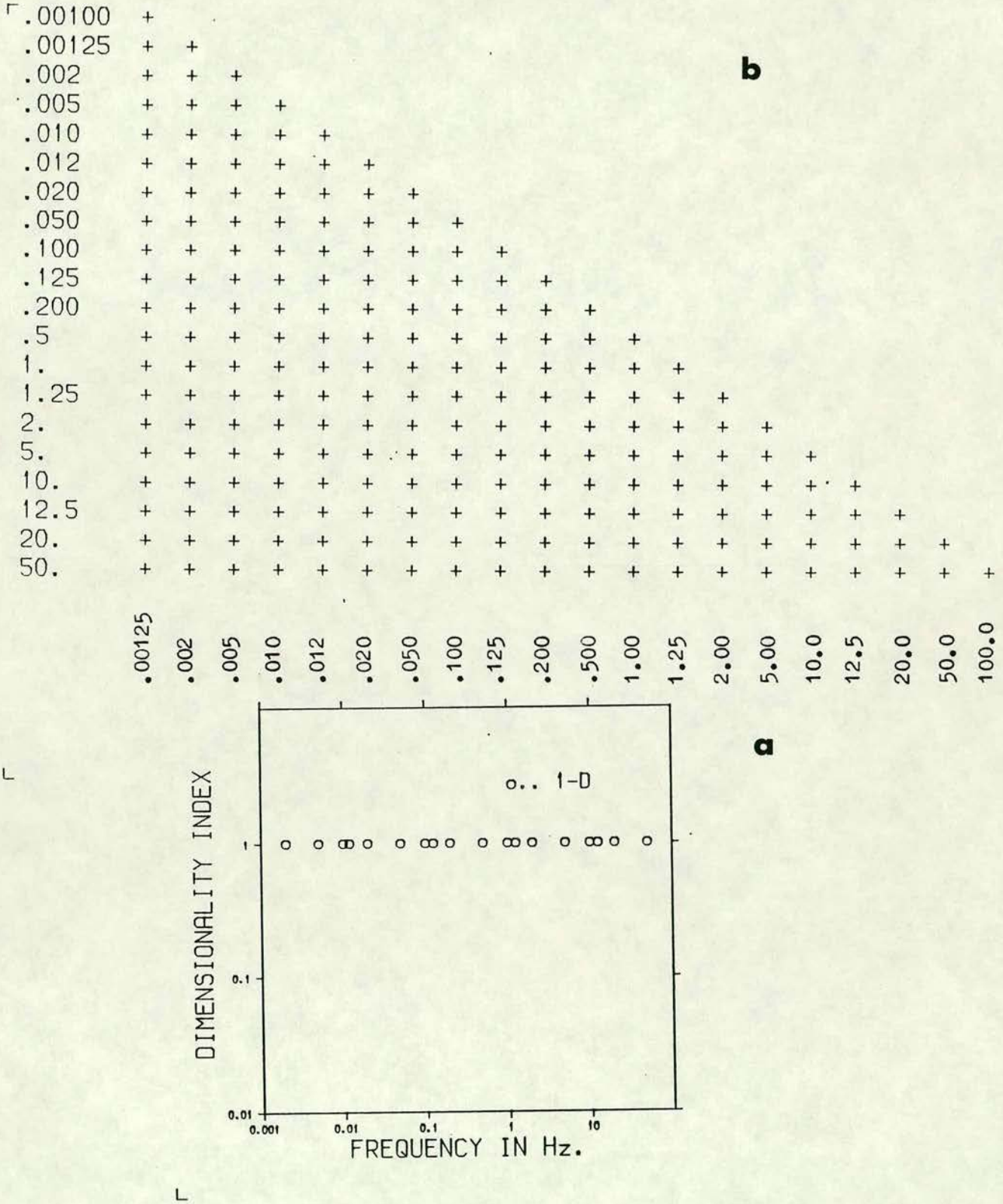
.00100
.00125
.002
.005
.010
.012
.020
.050
.100
.125
.200
.5
1.
1.25
2.
5.
10.
12.5
20.
50.
.00125
.002
.005
.010
.012
.020
.050
.100
.125
.200
.500
1.00
1.25
2.00
5.00
10.0
12.5
20.0
50.0
100.0
b
a
o.. 1-D
DIMENSIONALITY INDEX
1
0.1
0.01
0.001
0.01
0.1
1
10
FREQUENCY IN Hz.

FIGURE 4.3

a-m Dimensionality indicators for all the field stations of the present study, plotted as a function of frequency.

SITE NO.	SITE CODE	SITE NAME
515	DZR	Drumezlier
514	CAP	Cappercluch
607	SML	St.Mary'sLoch
503	CRK	Craik
502	CWR	Carewoodrig
505	BEW	Bewcastle
506	LAM	Lampert
509	GIB	Gibstown
606	EDG	Edgesgreen
508	WHI	Whitfield
604	SIN	Sinderhope
603	ROO	Rookhope
512	HIL	Hillend

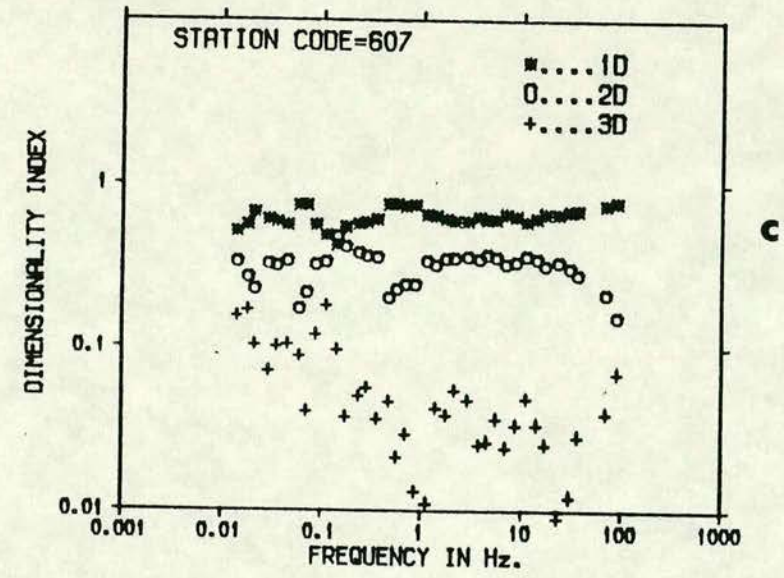
STATION CODE=607
*....1D
O....2D
+....3D
DIMENSIONALITY INDEX
1
0.1
0.01
0.001
0.01
0.1
1
10
100
1000
FREQUENCY IN Hz.

c

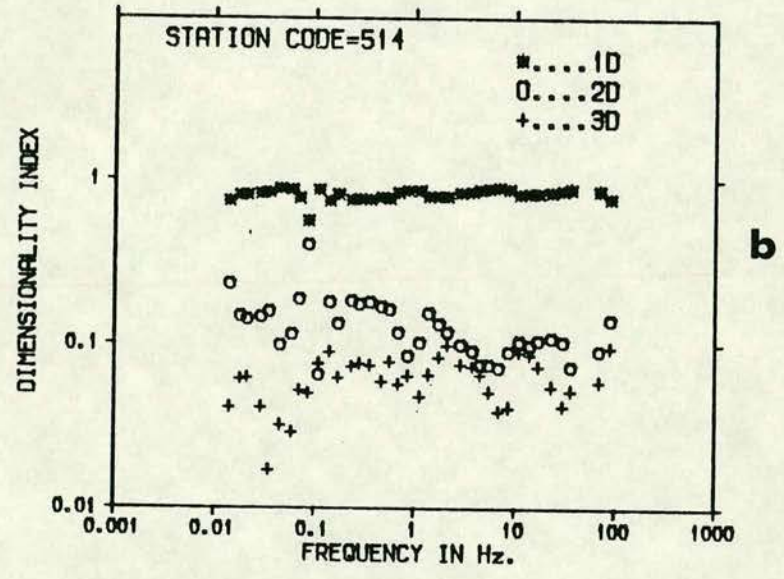
STATION CODE=514
*....1D
O....2D
+....3D
DIMENSIONALITY INDEX
1
0.1
0.01
0.001
0.01
0.1
1
10
100
1000
FREQUENCY IN Hz.

b

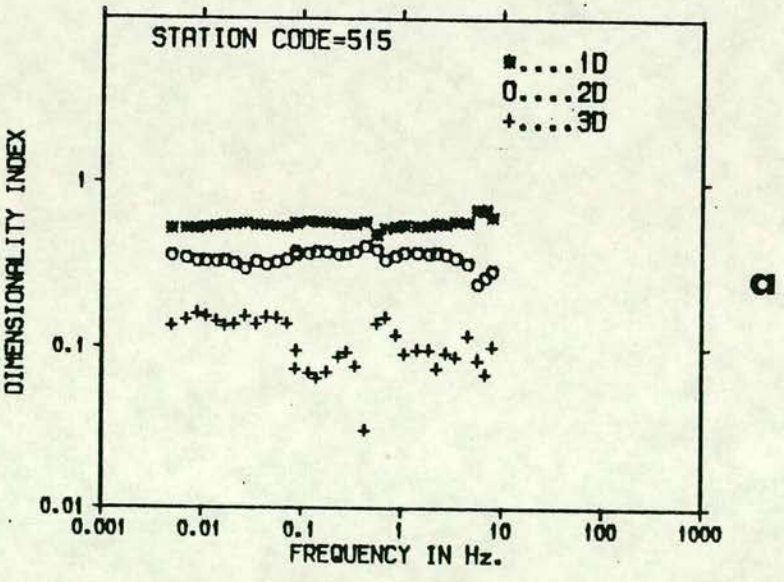
STATION CODE=515
*....1D
O....2D
+....3D
DIMENSIONALITY INDEX
1
0.1
0.01
0.001
0.01
0.1
1
10
100
1000
FREQUENCY IN Hz.

a

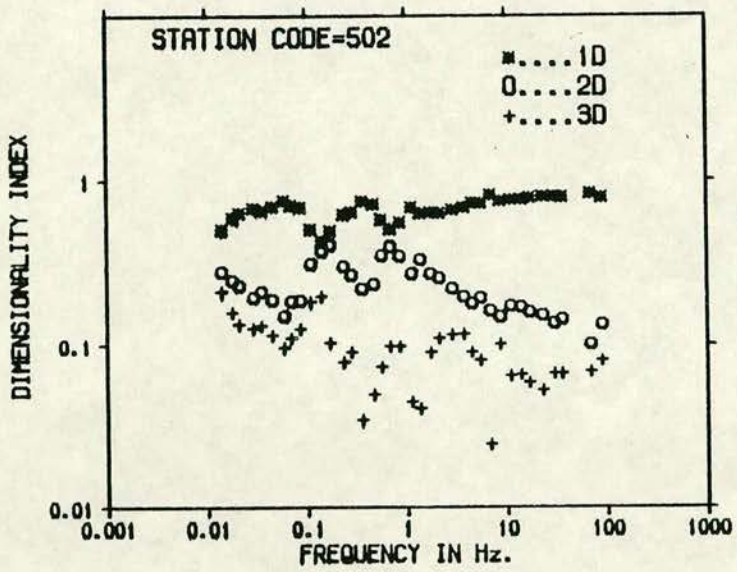
STATION CODE=502
*....1D
O....2D
+....3D
DIMENSIONALITY INDEX
1
0.1
0.01
0.001
0.01
0.1
1
10
100
1000
FREQUENCY IN Hz.

d

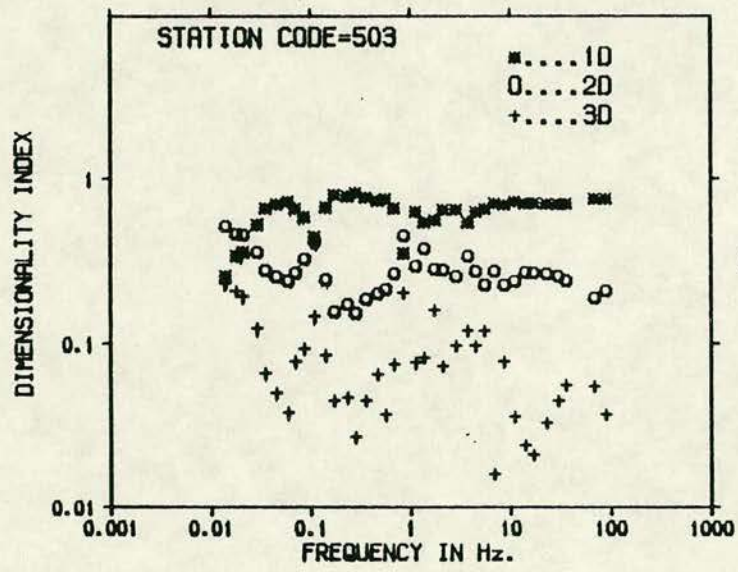
STATION CODE=503
*....1D
O....2D
+....3D
DIMENSIONALITY INDEX
1
0.1
0.01
0.001
0.01
0.1
1
10
100
1000
FREQUENCY IN Hz.

e

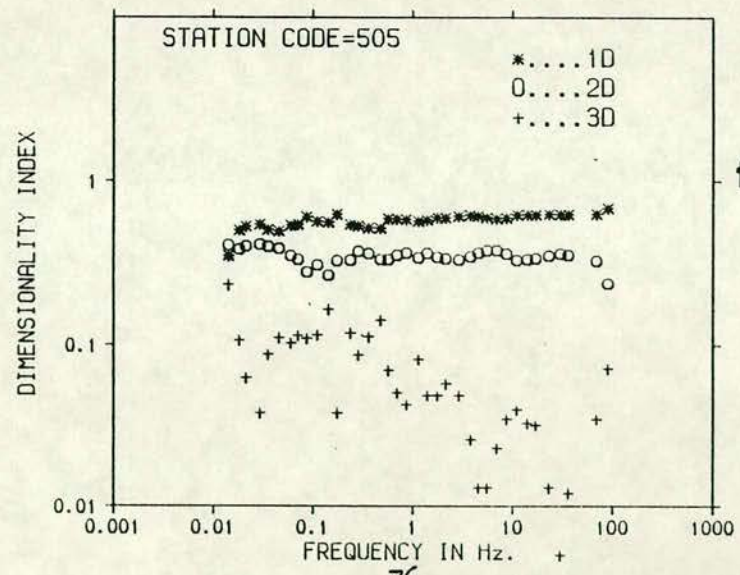
STATION CODE=505
*....1D
O....2D
+....3D
DIMENSIONALITY INDEX
1
0.1
0.01
0.001
0.01
0.1
1
10
100
1000
FREQUENCY IN Hz.

f

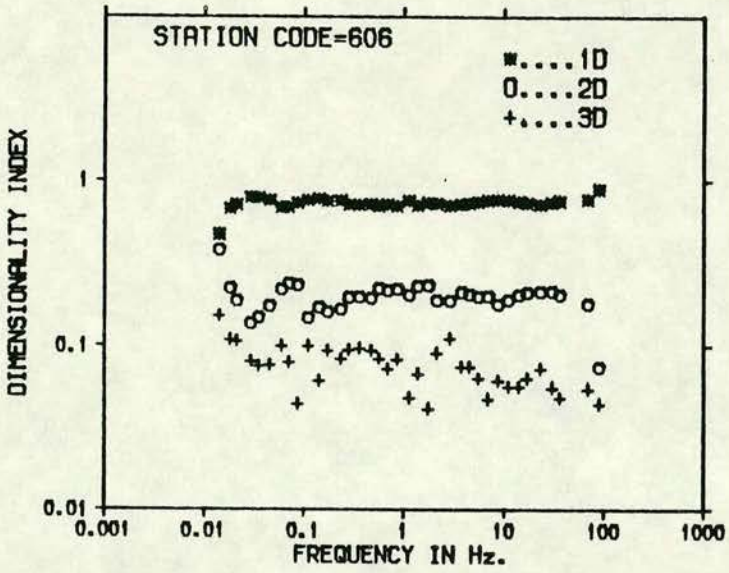
STATION CODE=606
*....1D
O....2D
+....3D
DIMENSIONALITY INDEX
1
0.1
0.01
0.001
0.01
0.1
1
10
100
1000
FREQUENCY IN Hz.

i

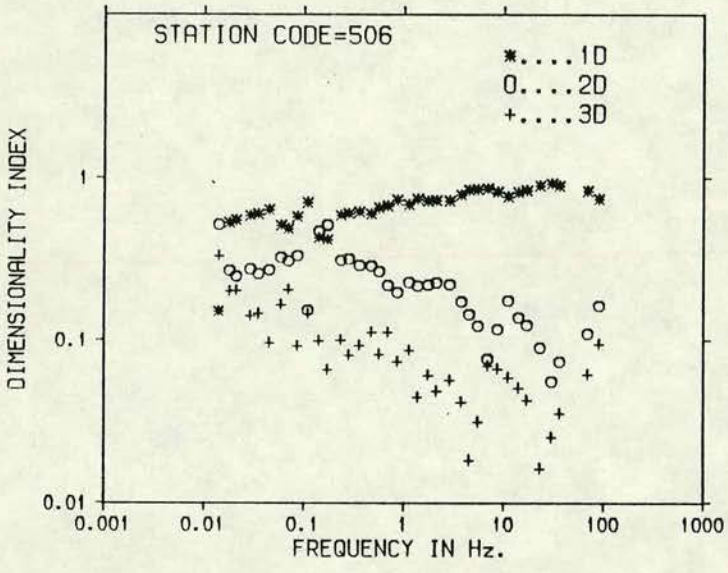
STATION CODE=506
*....1D
O....2D
+....3D
DIMENSIONALITY INDEX
1
0.1
0.01
0.001
0.01
0.1
1
10
100
1000
FREQUENCY IN Hz.

h

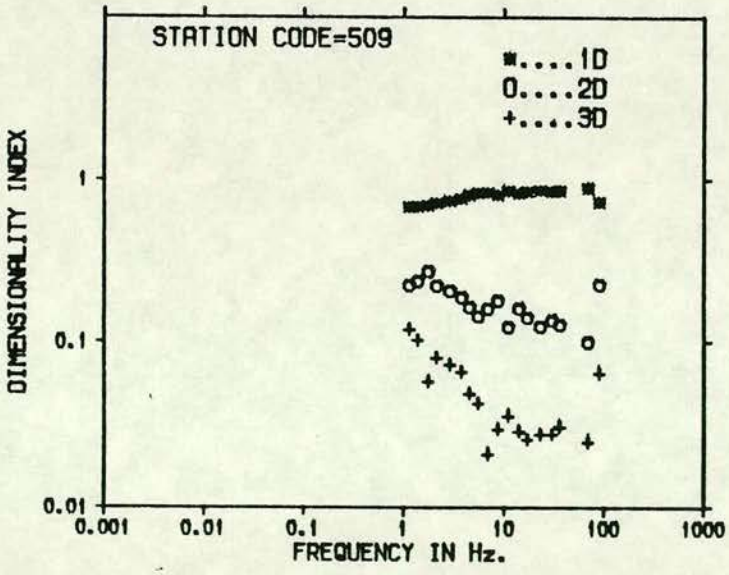
STATION CODE=509
*....1D
O....2D
+....3D
DIMENSIONALITY INDEX
1
0.1
0.01
0.001
0.01
0.1
1
10
100
1000
FREQUENCY IN Hz.

g

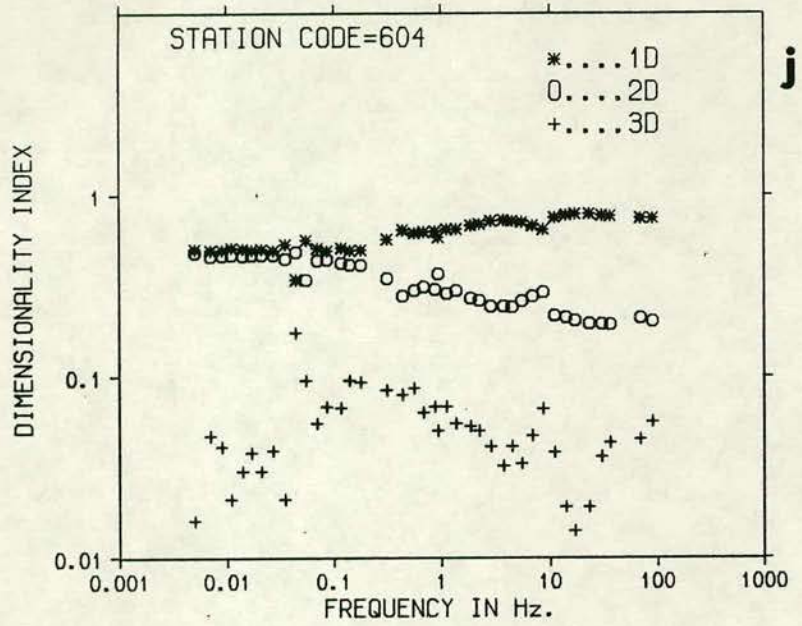
STATION CODE=604
*....1D
O....2D
+....3D
DIMENSIONALITY INDEX
FREQUENCY IN Hz.
0.001
0.01
0.1
1
10
100
1000
0.01
0.1
1

j

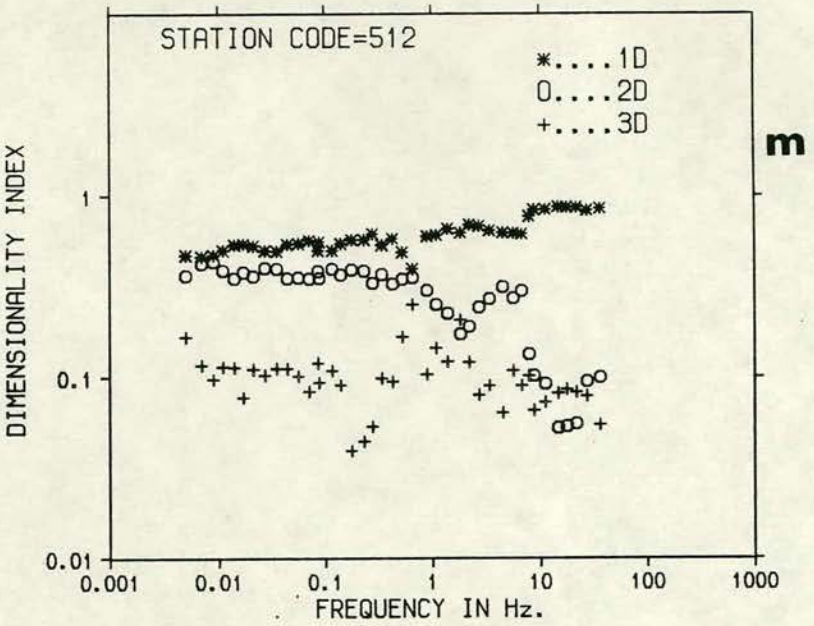
STATION CODE=512
*....1D
O....2D
+....3D
DIMENSIONALITY INDEX
FREQUENCY IN Hz.
0.001
0.01
0.1
1
10
100
1000
0.01
0.1
1

m

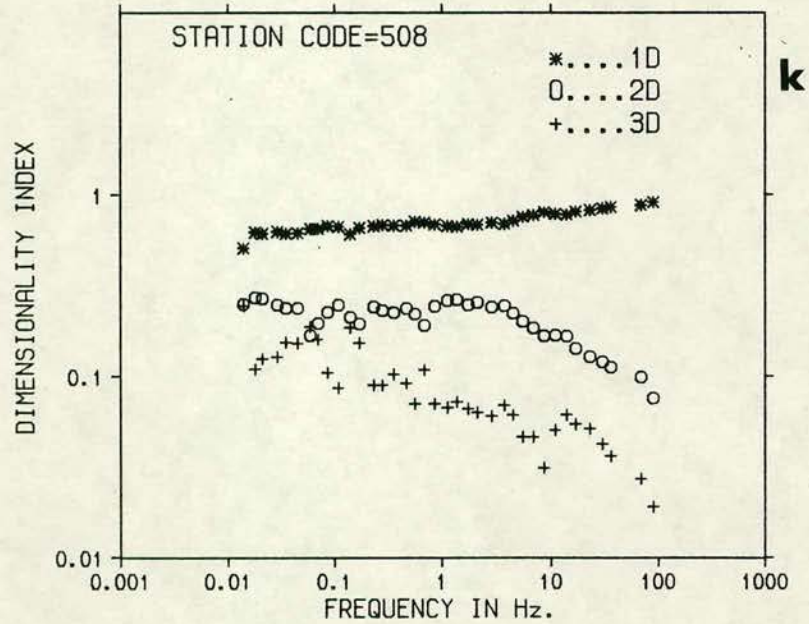
STATION CODE=508
*....1D
O....2D
+....3D
DIMENSIONALITY INDEX
FREQUENCY IN Hz.
0.001
0.01
0.1
1
10
100
1000
0.01
0.1
1

k

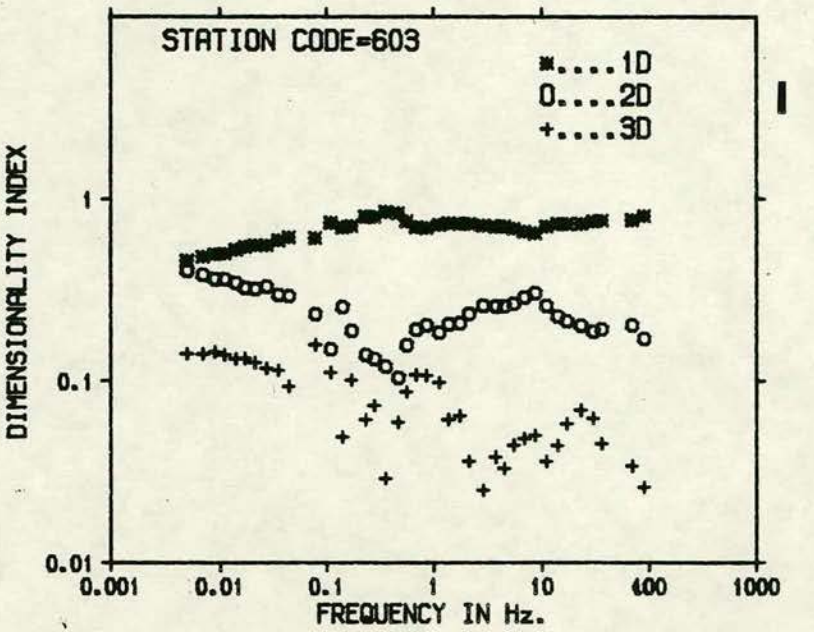
STATION CODE=603
*....1D
O....2D
+....3D
DIMENSIONALITY INDEX
FREQUENCY IN Hz.
0.001
0.01
0.1
1
10
100
1000
0.01
0.1
1

l

4.2.5. Single station geomagnetic transfer functions

So far the discussion has been concerned with the horizontal magnetic components H_x and H_y. When the vertical component H_z is also measured this component can be related to the horizontal components with the following general assumptions:

- a) the vertical component of the inducing field is relatively small compared to the observed vertical magnetic component.
- b) the anomalous horizontal field components are negligible compared to the inducing horizontal fields.
- c) the inducing horizontal field and the inducing vertical fields do not correlate with each other.

With these assumptions, the relation (Everett and Hyndmann 1967b, Schmucker 1970) can be written as,

$$H_z = A\,H_x + B\,H_y + \delta\,H_z \qquad \text{.....4.19}$$

where, H_z is the residual which does not correlate with the horizontal fields H_x and H_y. A and B are the geomagnetic single station transfer functions.

Equation 4.19 can be treated as the equation of a plane. This is the preferred plane in which the magnetic variations tend to occur (Parkinson 1962). The horizontal unit vector projected perpendicular to this plane is popularly known as the 'Parkinson vector'. The direction of this vector is used to locate the anomalous current concentration inside the earth. From the equation 4.19 the real and imaginary parts of this induction vector can be written as,

$$|\overline{R}| = (A_r^{\,2} + B_r^{\,2})^{1/2},$$

$$\theta_r = \tan^{-1}\left(\frac{B_r}{A_r}\right)$$

$$|\tilde{I}| = (A_i^2 + B_i^2)^{1/2},$$

$$\theta_i = \tan^{-1}\left(\frac{B_i}{A_i}\right)$$

.....4.20

where suffixes r,i represents the real and imaginary parts. θ_r and θ_i represent the directions (azimuth) of the induction vectors. R is called the 'Weise vector' and when this vector is reversed in direction, it is equivalent to the 'Parkinson vector'.

In the present study, the vertical magnetic component 'Hz' at the measured stations was corrupted by noise and hence no useful analysis was possible. As an example, the magnitude and azimuth of the real and imaginary components of the induction vector from Cap (Code= 514) are presented in figure 4.4. However studies involving magnetic responses have previously been undertaken in the study region and will be referenced in Chapter8.

4.2.6. Field polarization

Polarization is an important parameter which can affect the estimates of both the impedance elements and the geomagnetic transfer functions. Problems can arise due to the characteristics of magnetic source fields, especially when they are highly polarized as then the denominator in equation 4.3 will tend to zero. In such cases, the tensor impedances are not well behaved under rotational transformations (Hermance 1973). Hence it is preferable that the source field be totally unpolarized. The effects of polarization have been discussed by Lilley (1976) and Lineart (1980).

Polarization can be represented either in the time domain or in the frequency domain. Study of polarization characteristics in the frequency domain has been proven to be advantageous compared to the time domain hodogram (Reddy and Rankin, 1972).

The polarization angle θ for a field F (E or H) is the inclination of the

FIGURE 4.4

An example of the induction vectors obtained in the present study at CAP station. The directions of the azimuths are presented rotating in clockwise from magnetic north (represented by 0 in the figure). Number of estimates at each frequency can also be seen. The band details of this station can also be seen at the top right hand corner.

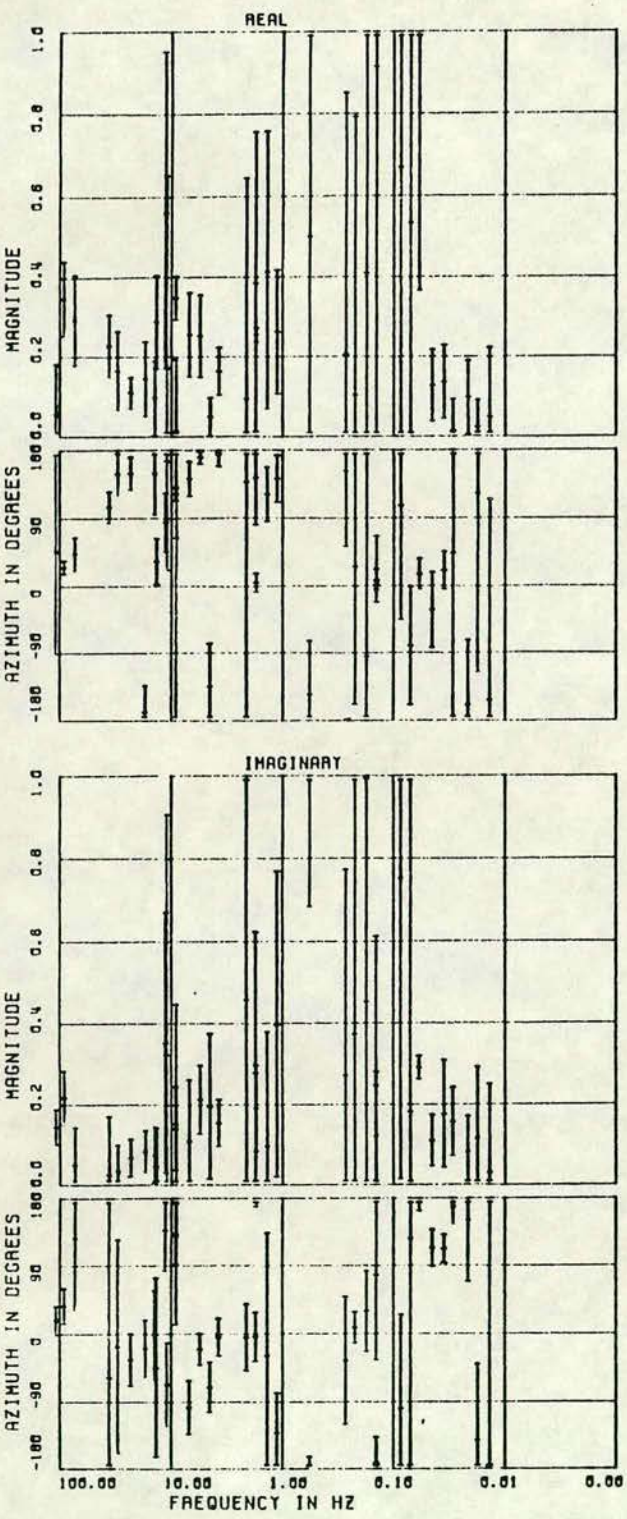

SITE : 514A MAGNETIC

CARTRIDGE	514GA	514IA	514ZA	514JA
BAND	1	2	3	4
COMPONENTS	5	5	5	5
SAMPLES/WINDOW	256	256	256	256
NUMBER WINDOWS	0	0	0	0
SAMPLE RATE HZ	512	64	8	1
PLOT HPF	64.00	8.00	0.50	0.05
PLOT LPF	700.00	64.00	8.00	1.00
FREQS/DECADE	10	10	10	10
FREQS/BAND	11	13	13	13
MIN COHERENCY	0.80	0.80	0.80	0.80
REJECTION LOOPS	2	2	2	2

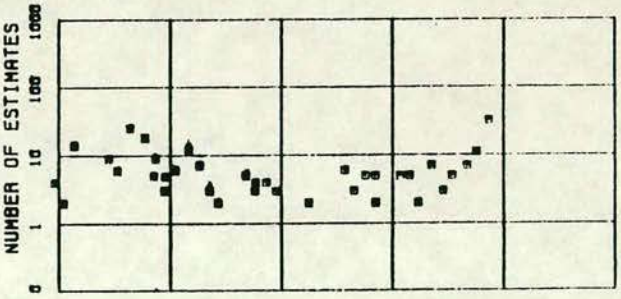

major axis of the ellipse, which is given by,

$$\tan 2\theta = \frac{2 F_x F_y \cos\phi}{F_y^2 - F_x^2}$$

.....4.21

where F is either E or H and ϕ is the phase difference between F_x and F_y.

Another parameter which can be obtained from the polarization ellipse is the 'ellipticity' which is given by (Smith and Word 1974)

$$e = \frac{F_x F_y \sin\phi}{F^2}$$

where

$$F = \left| F_x e^{i\phi} \text{Sin } \theta + F_y \text{Cos } \theta \right|$$

.....4.22

Examples of the variation of the polarization for different events for both telluric and magnetic fields are presented in figure 4.5 considering Band-0 data from Rookhope (Code=603). In general, the magnetic field is polarized between -90° and 10° and the dominant polarization direction of the telluric field is between -70° and 40°, indicating that there is a considerable variation of polarization angle for this station.

FIGURE 4.5

An example of the telluric and magnetic polarization (-90 to 90) plots for band-0 data for ROO station at different sub-frequency bands.91.0 Hz. etc. represents the frequencies.

TELLURIC
MAGNETIC
90
-90
6030A
91.0 HZ
72.8 HZ
35.9 HZ
30.0 HZ
22.9 HZ
17.0 HZ
14.0 HZ
11.0 HZ
9.00 HZ

4.3. Processing of field data

As described in chapter 3, the study data were acquired using three different types of instrument- the S.P.A.M., Band-4 and Band-5 systems. Firstly, the processing procedures carried out for the data acquired using the S.P.A.M. and Band-4 systems are discussed.

4.3.1. Event selection

As described in the previous chapter, the S.P.A.M. data were automatically selected in the field according to preselected criteria one of which was coherency. All the data thus selected, however, were not accepted for main frame analysis as some events had been found to be corrupted by coherent noise, which had been accepted along with good signal. To eliminate coherent noisy events, the following qualitative approach was adopted.

Firstly, the cross spectra, Cagniard apparent resistivity and phase plots were studied. By visually examining these plots, events showing spurious apparent resistivity and phase values compared to the rest of the events were discarded. This procedure had been successfully used by Dawes (1986) observing the form of the frequency variations of apparent resistivity.

Since the Band-4 data had been recorded continuously on digital cassettes, they were first transferred to floppy discs without pre-selection and then examined using a PDP-11 computer and Dawes (1986) interactive event selection program. Time series of successive events for all components and their FFT spectra were examined and time intervals with traces free from extraneous noise and showing high levels of magnetic and telluric field activity were then selected as events, for transfer to the main frame computer and further analysis. The duration of these events was 16 minutes. Typical examples of the time series for Bands 0,1,2 and 3 data are shown in figures 4.6a, b, c and d, recorded at WHI station in N.England during the day time on 15-8-85. Band-0 and band-1 show the signals in the audio to sub-audio frequency range and band-2 and band-3 are the examples for Pc1 - Pc3 pulsations (cf. Jacobs 1970).

FIGURE 4.6

A typical time series data recorded at WHI station (No. 508) showing for a) band-0, b) band-1, c) band-2, and d) band-3; 5080A 35 represents- station= 508, Band=0, dataset=A, window=35; NCHAN= Number of channels, in this case 4; NSAMP= number of samples per window; SRATE= Digitising frequency; XTICK= time interval between two '+' marks shown in the figure for each channel. The four traces shown for each band are Ex, Ey, Hx and Hy reading from top to bottom. The corresponding scale values shown on the left of each trace are mV/km. for electric field and nT. for the magnetic field. These data were recorded on 15-8-85 during day time.

FILE : AM5081A
STATION: 508
BAND : 1
NCHAN : 4
NSAMP : 256
SRATE : 64 HZ
XTICK : 0.20 SEC

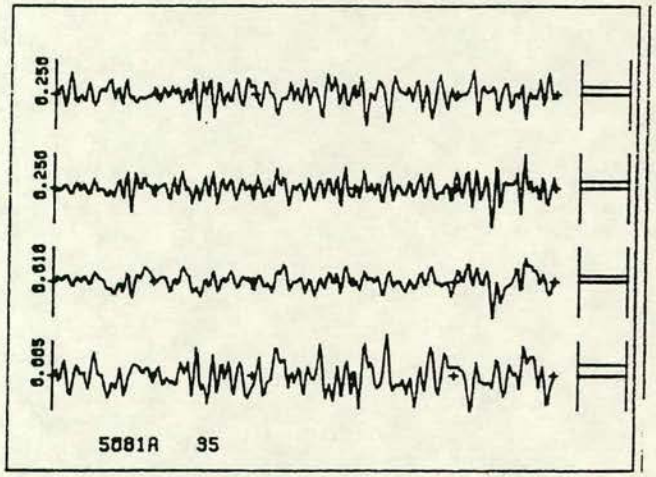

FILE : AM5083A
STATION: 508
BAND : 3
NCHAN : 4
NSAMP : 256
SRATE : 1 HZ
XTICK : 16.00 SEC

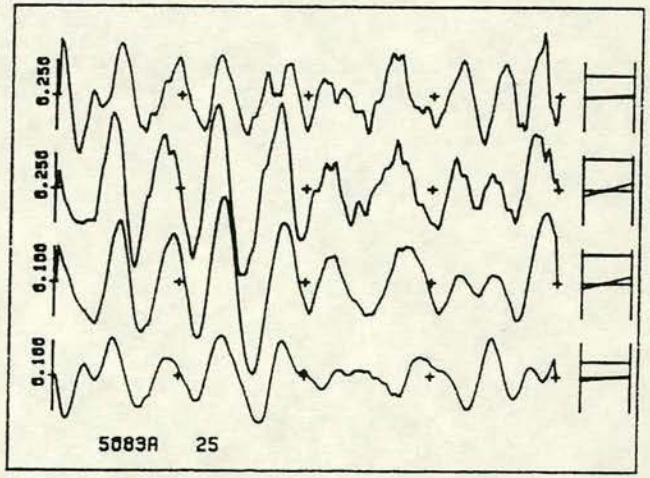

FILE : AM5080A
STATION: 508
BAND : 0
NCHAN : 4
NSAMP : 256
SRATE : 512 HZ
XTICK : 0.02 SEC

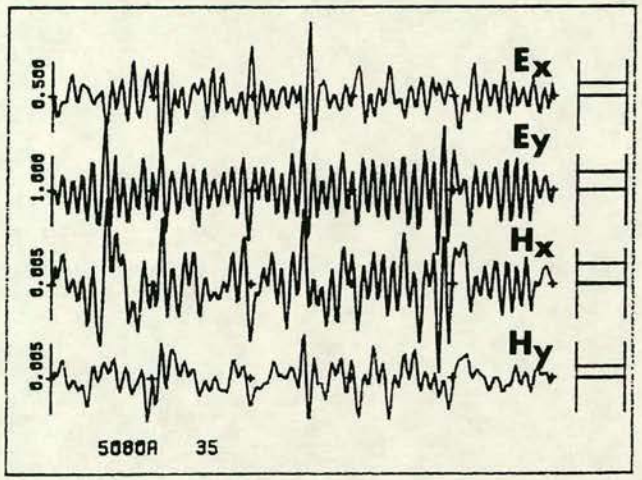

FILE : AM5082A
STATION: 508
BAND : 2
NCHAN : 4
NSAMP : 256
SRATE : 8 HZ
XTICK : 2.00 SEC

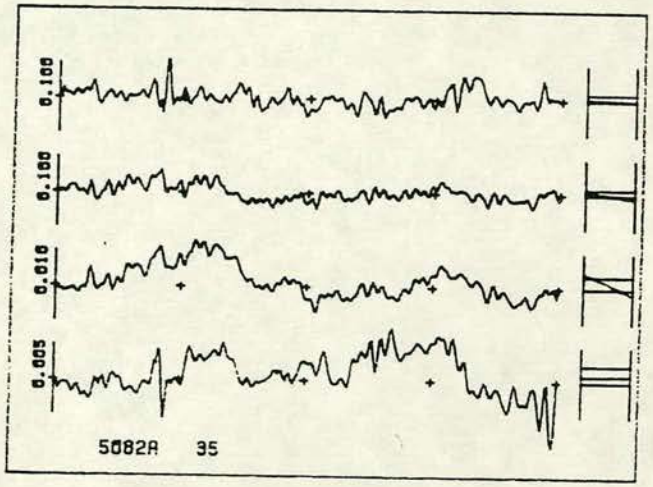

4.3.2. Event analysis and averaging

As previously stated, the analysis of all the events was carried out on the Edinburgh Multi Access system (EMAS)-twin ICL 2972 and 2980 computers. The necessary software was originally written by Rooney (1976) and modified for use with more efficent graphic packages by Dawes (1980). The author has made small modifications to these packages incorporating options such as rejection on magnetic coherency criteria weighting the response functions depending on its coherency. A summary of the important steps involved in the software packages are described below.

The basic data processing can be divided into three stages, which are illustrated in figures 4.7a, b and c. In the first stage, the linear trends in the data are removed and cosine tapering applied to 10% of data points at both ends of the event. The data are then transferred from the time to the frequency domain to obtain the FFT coefficients. In the second stage, the instrument response corrections (Telluric pre-amplifier and induction coils) are applied to the FFT coefficients and auto- and cross spectra are computed. This is followed by the computation of various parameters for each event as shown in the figure. All the events for a site are then subjected to the selection criteria.

In the third stage, all the analysed events are averaged at discrete frequencies. Before averaging the data are weighted, the weights being proportional to the coherency.

The main steps involved in the data averaging are presented in fig 4.7c as stage 3. This involves a) application of the coherency weight criterion, b) computation of statistics such as mean and standard deviation, c) rejection of data values lying outside +/- 2.2 standard deviations followed by recalculation of step b) and d) computation of transfer functions, azimuth and skew parameters. Computation of statistics (step-b) for the tensor elements is carried out assuming a log normal distribution (Bentley 1973) and 68% confidence intervals (one standard deviation) as error bars for estimates of the

FIGURE 4.7

A flow diagram showing the principal steps involved in the processing of the software package used in this study. Three stages in the processing are illustrated in a), b) and c).

a) STAGE-1

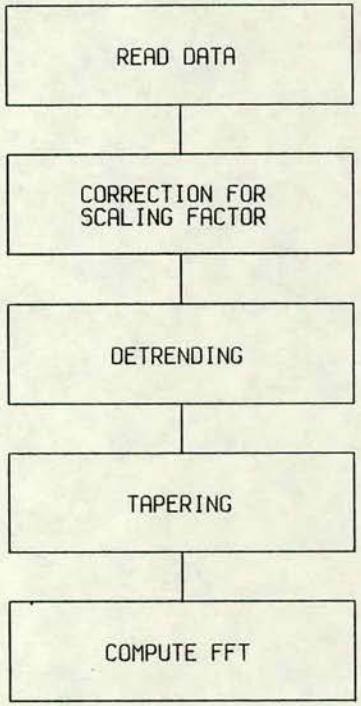

b) STAGE-2

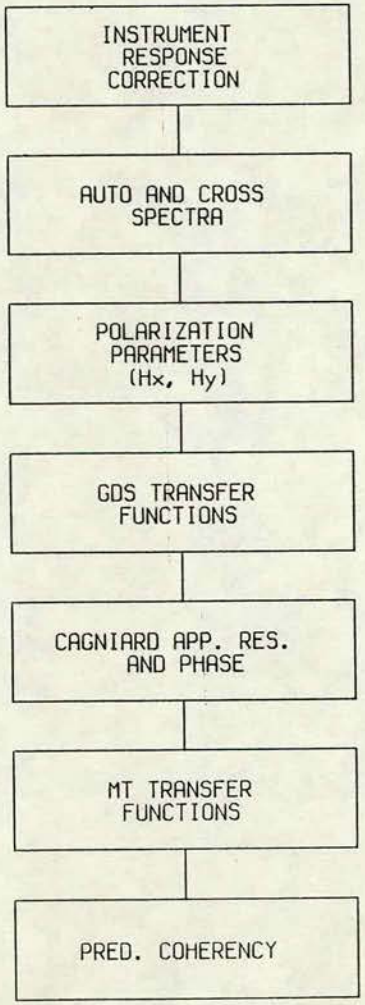

c) STAGE-3

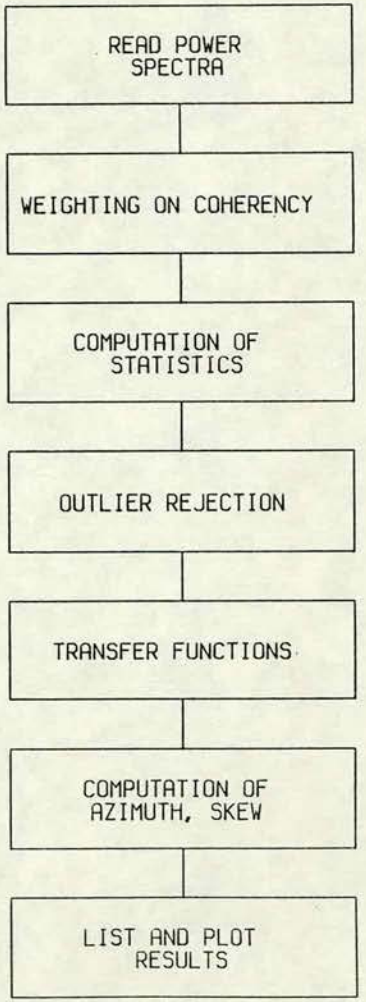

means. The results thus obtained for 13 stations are shown in figures 4.8 a-m; these include the frequency variations of the apparent resistivity and phase in the measured directions, the skew, the azimuth of major apparent resistivity and the number of estimates. The apparent resistivity and phase in the principal directions and the invariant (Berdichevskiy and Dmitriev 1976) apparent resistivity and phase can also be seen in the same figure. The station number and code are given at the top of the figure. No claim is made that the estimated response functions are high quality. However, at all the stations, in general, the phase response function is well estimated compared to the apparent resistivity. Some minor discrepancies can be seen at a few stations in the apparent resistivity of adjacent bands. At station, LAM, the apparent resistivity (ρ_{xy}) is inconsistent with the phase near 1Hz.. Definite reasons for these discrepancies are not clear. However, the probable reason may be associated with upward bias effects due to the presence of electrical noise as discussed in section 4.2.1.

4.3.3 Processing of long period (Band 5) data

Since attention during the fieldwork was primarily concentrated on the use of the SPAM system and since the field work duration was constrained for financial reasons no useful Band-5 data were obtained during its recording at 6 stations. A recording period of one week at each station seems to be insufficient to ensure the acquisiton of good magnetic and telluric signals with the system as used.

4.4 Time domain processing

4.4.1 Introduction

As previously stated, estimation of the impedance tensor is the main objective of MT data processing. The data processing involves the solution of a linear vector equation. The general vector equation which can be written from equation 4.1a and b in the time domain is,

$$O = X * A + Y * B \qquad \text{.....4.23}$$

where, X,Y are the input field .

O is the output field.

A,B are the impulse response functions

FIGURE 4.8

a-m Response functions obtained from processing at each of the sites shown as a function of frequency. The various plots show apparent resistivity and phase in measuring (RHOXY and RHOYX i.e., magnetic NS and EW) and in principal (major and minor) directions, the rotationally invariant apparent resistivity and phase, the no. of estimates, the skew parameter and the azimuth for the major. The station no. and the station code can be seen at the top of the figure in each case.

SITE NO.	SITE CODE	SITE NAME
515	DZR	Drumezlier
514	CAP	Cappercluch
607	SML	St.Mary'sLoch
503	CRK	Craik
502	CWR	Carewoodrig
505	BEW	Bewcastle
506	LAM	Lampert
509	GIB	Gibstown
606	EDG	Edgesgreen
508	WHI	Whitfield
604	SIN	Sinderhope
603	ROO	Rookhope
512	HIL	Hillend

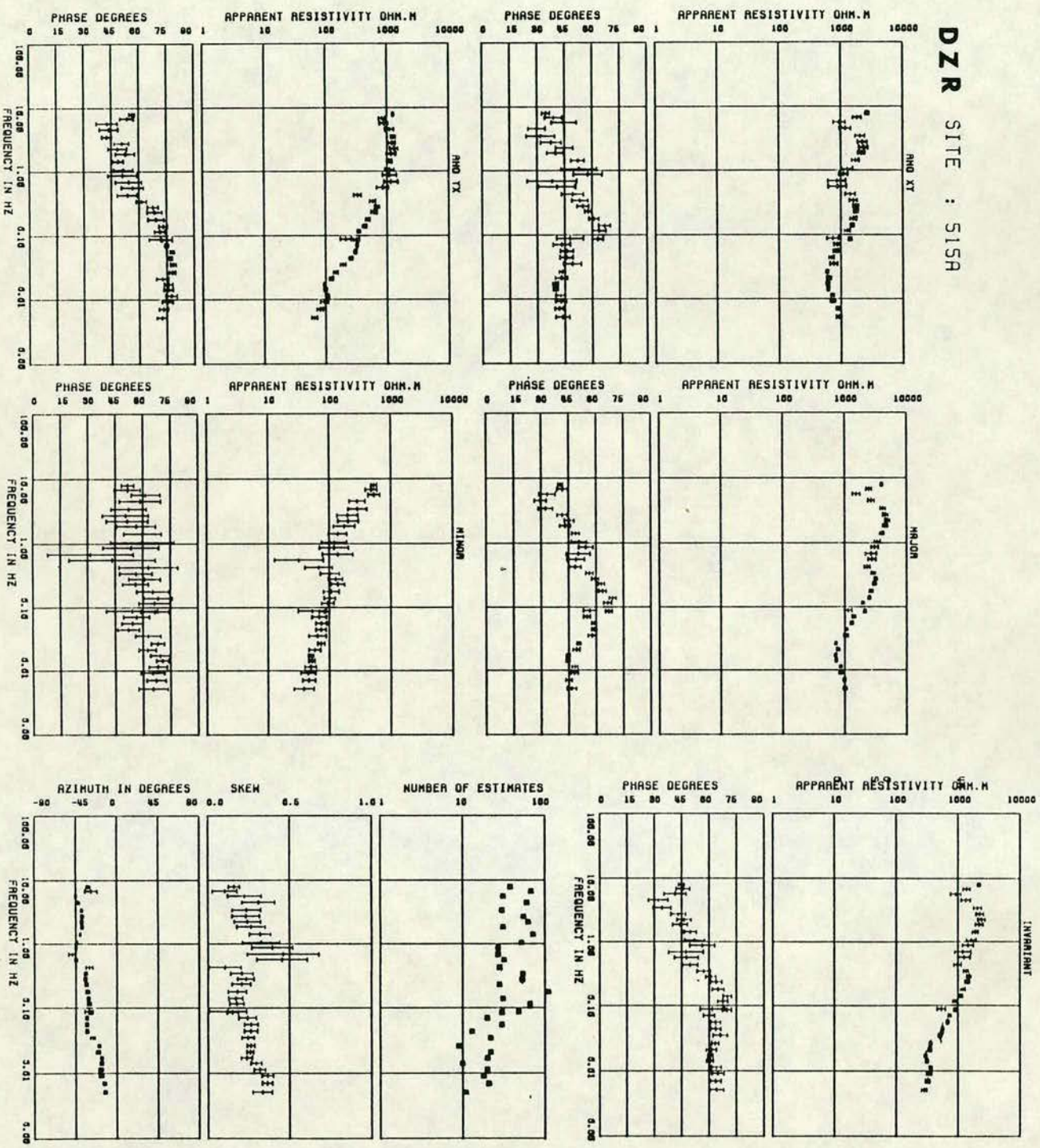
a DZR SITE : SISA
PHASE DEGREES
APPARENT RESISTIVITY OHM.M
FREQUENCY IN HZ
RHO TX
RHO XT
MINRH
MAXRH
AZIMUTH IN DEGREES
SKEW
NUMBER OF ESTIMATES
INVARIANT

b CAP SITE : S14C

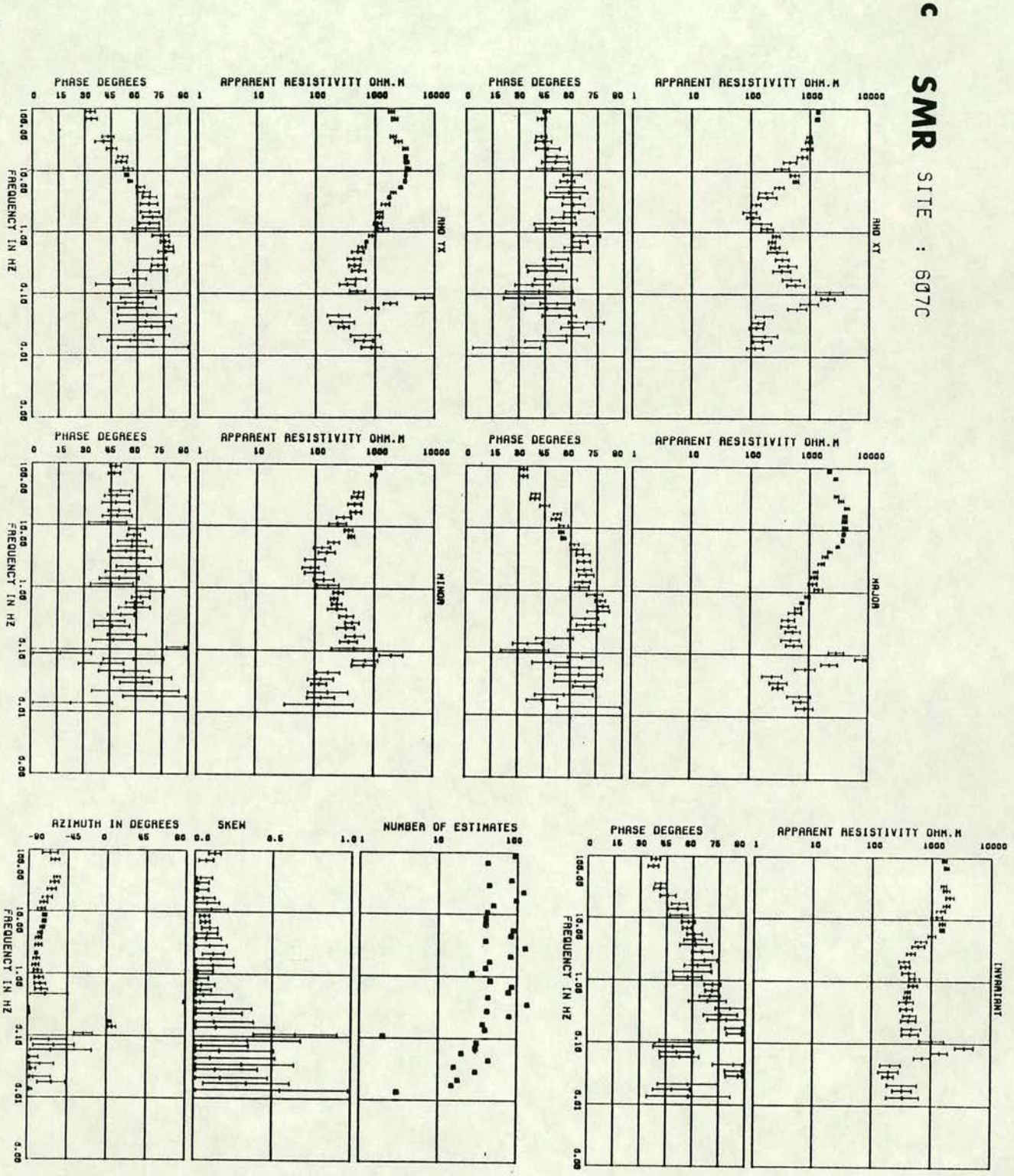
SMR SITE : 6076
PHASE DEGREES
APPARENT RESISTIVITY OHM.M
FREQUENCY IN HZ
RHO TX
RHO TY
RHO XY
RHO YX
AZIMUTH IN DEGREES
SKEW
NUMBER OF ESTIMATES
INVARIANT

d **CRK** SITE : 503A

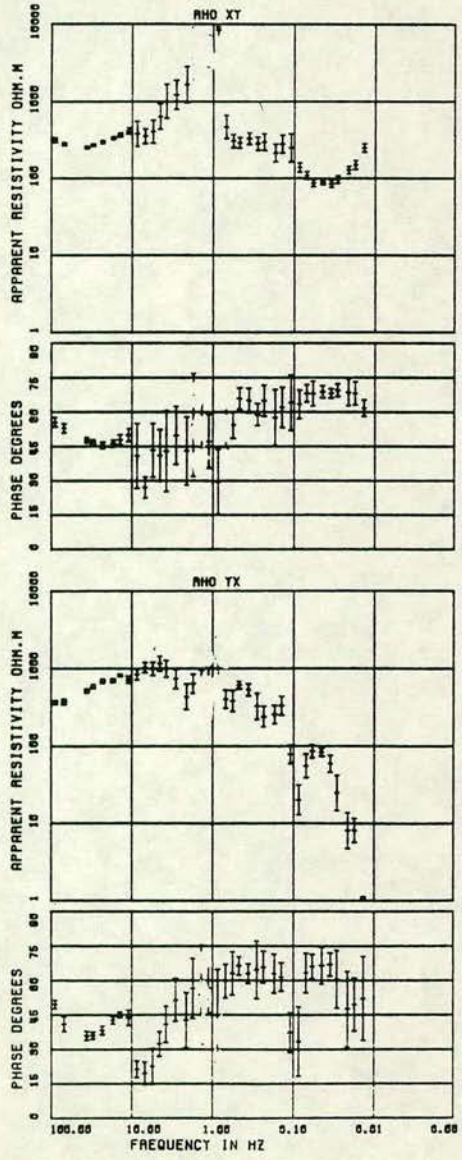

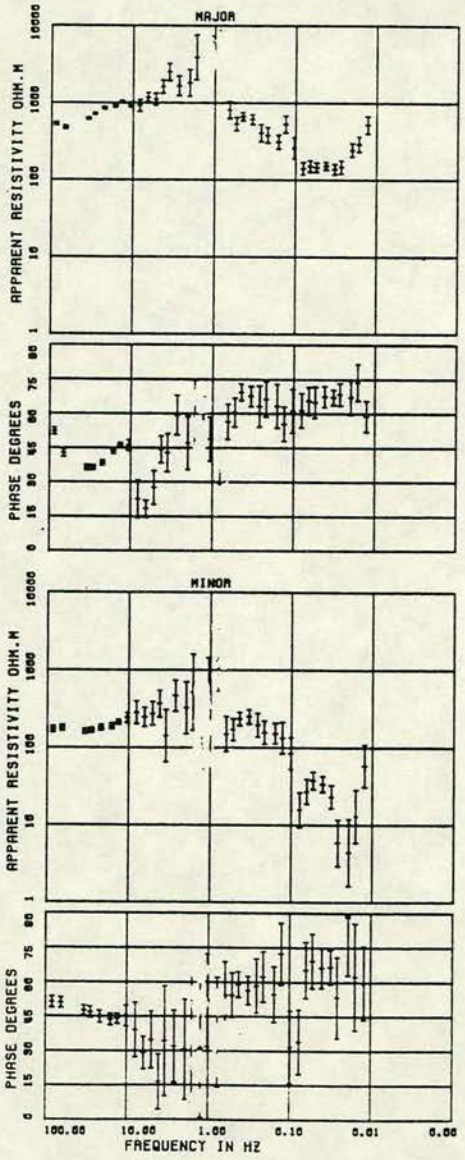

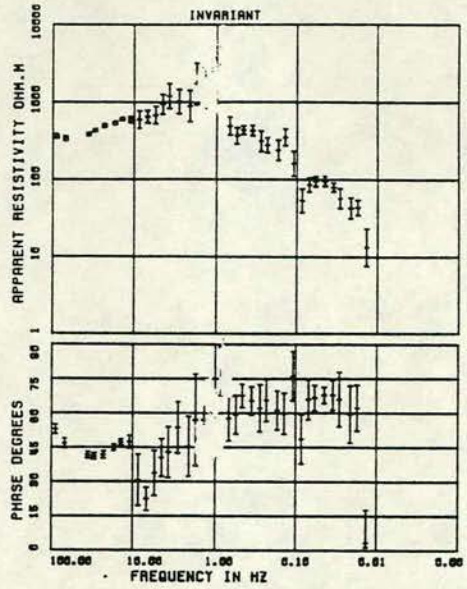

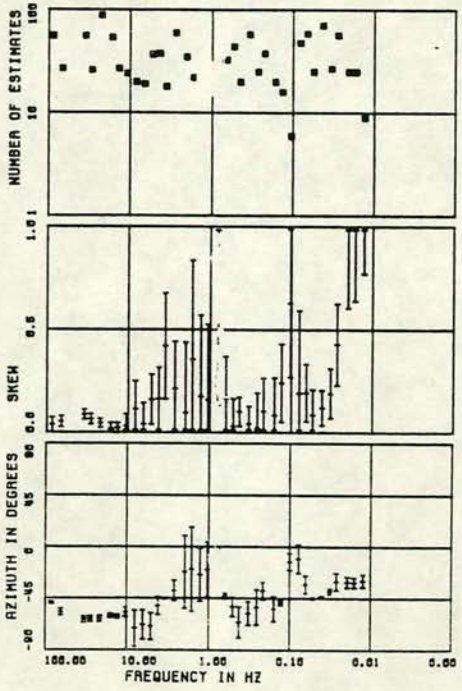

CWR SITE : 502C
ANO XY
ANO YX
MAJOR
MINOR
INVARIANT
APPARENT RESISTIVITY OHM.M
PHASE DEGREES
FREQUENCY IN HZ
AZIMUTH IN DEGREES
SKEW
NUMBER OF ESTIMATES

f **BEW** SITE : 505C

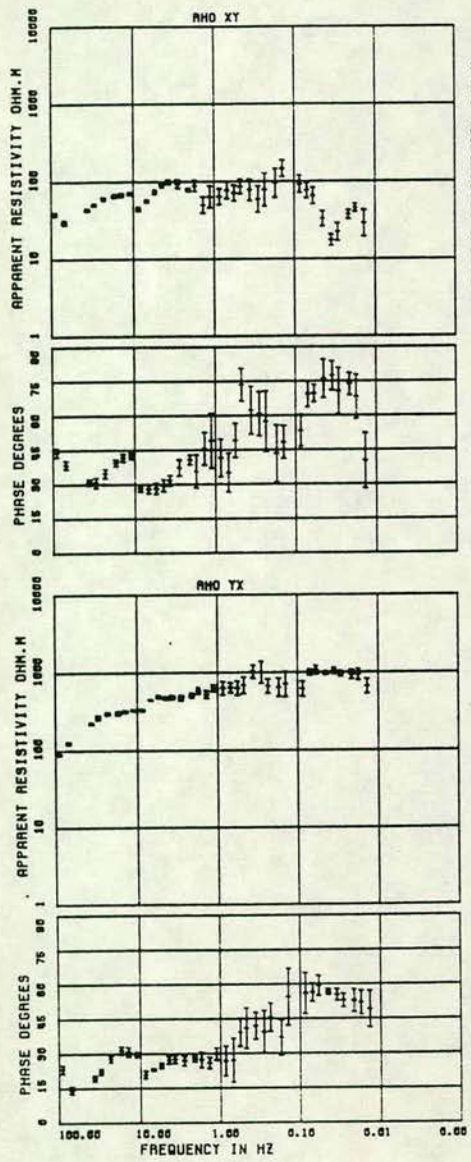

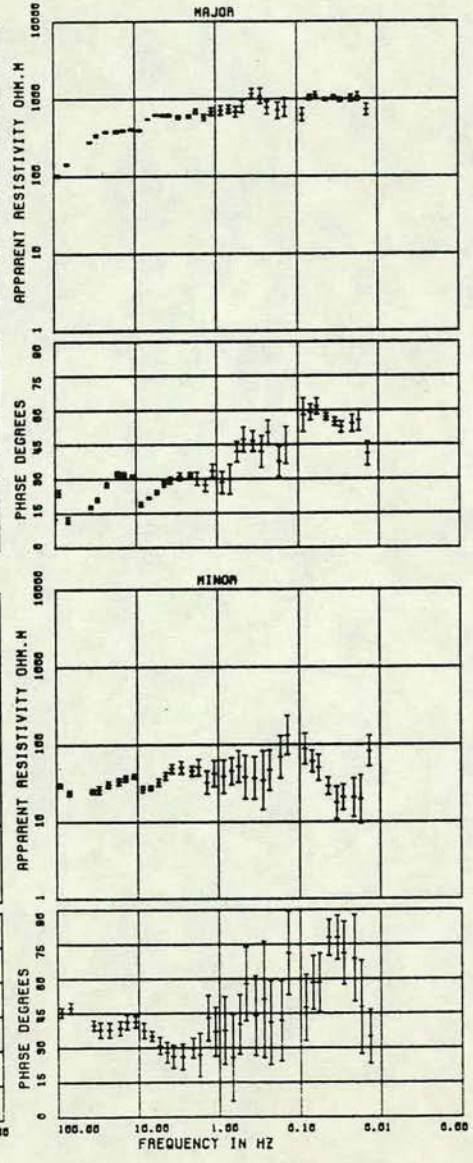

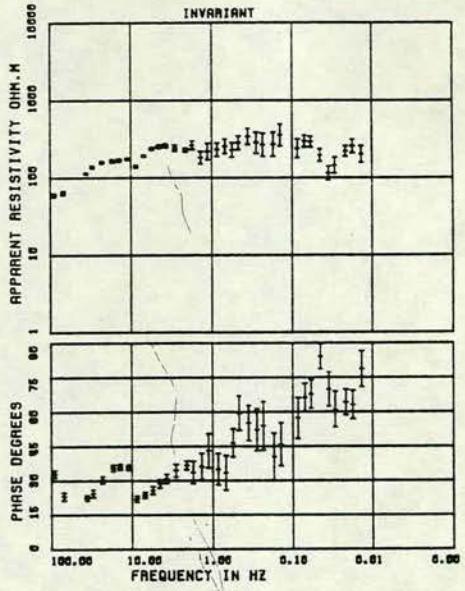

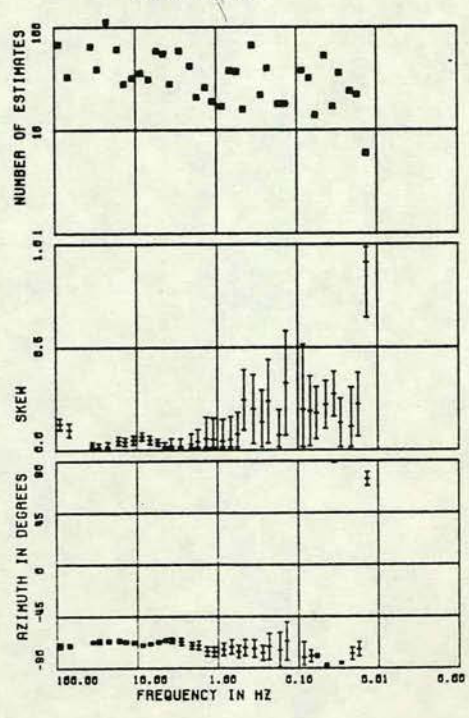

9

GIB SITE : 509C

h

LAM SITE : 506C

EDG SITE : 606C

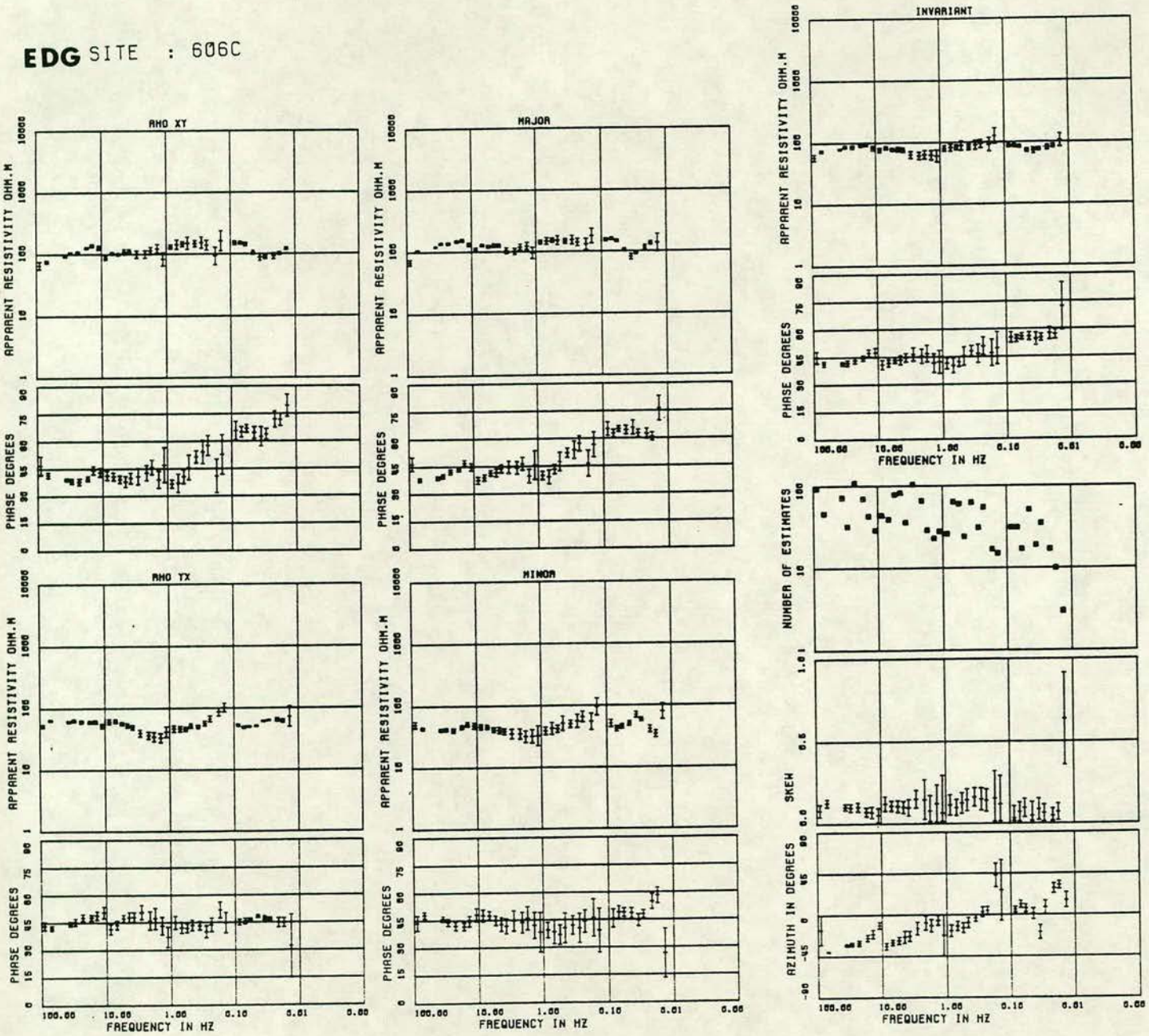

j **WHI** SITE : 508C

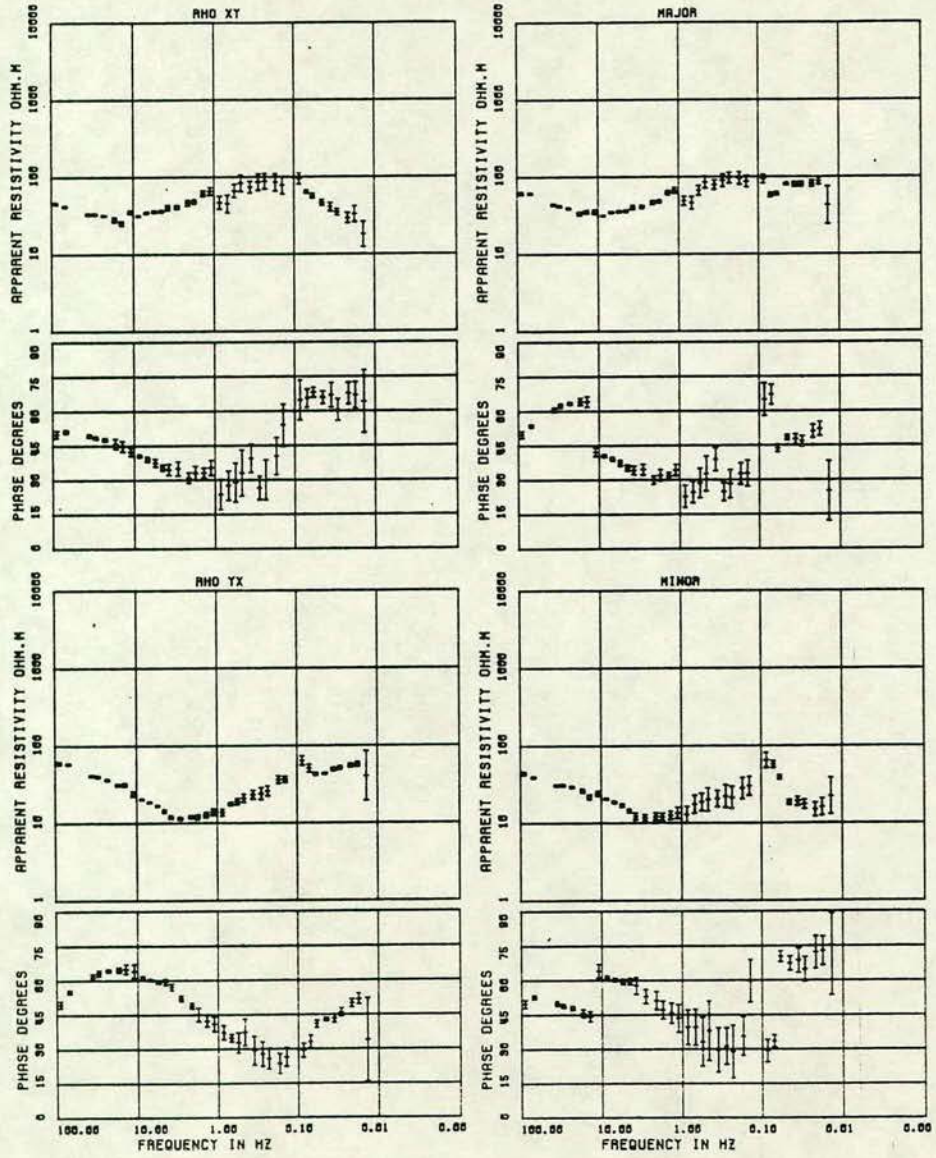

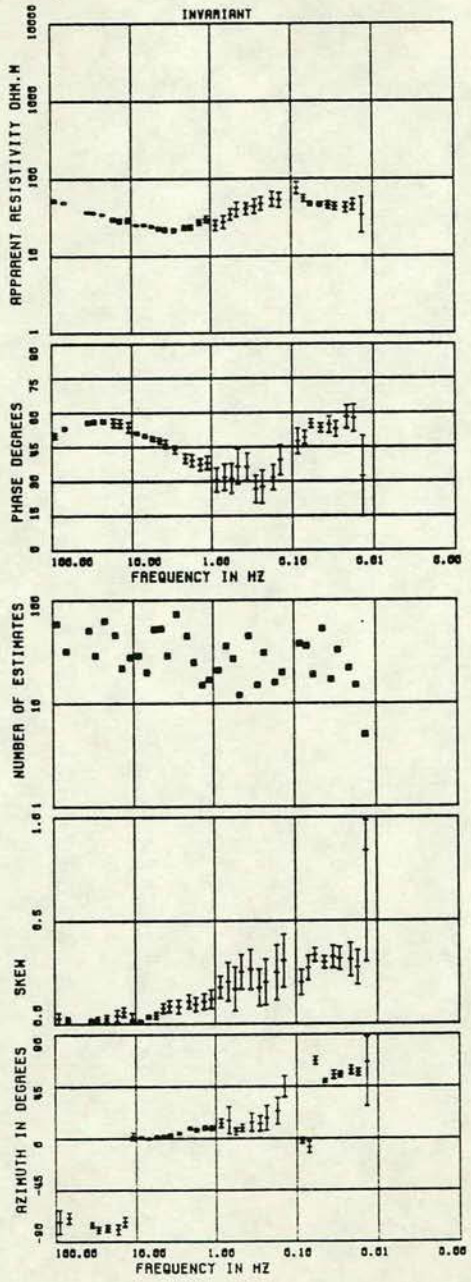

SIN SITE : 604C
k
INVARIANT
APPARENT RESISTIVITY OHM.M
PHASE DEGREES
FREQUENCY IN HZ
NUMBER OF ESTIMATES
SKEW
AZIMUTH IN DEGREES
MAJOR
MINOR
RHO XY
RHO YX

ROOSITE : 603C
RHO XY
RHO YX
MAJOR
MINOR
INVARIANT
APPARENT RESISTIVITY OHM.M
PHASE DEGREES
AZIMUTH IN DEGREES
SKEW
NUMBER OF ESTIMATES
FREQUENCY IN HZ

HIL SITE : S12A
RHO XY
RHO YX
MAJOR
MINOR
INVARIANT
APPARENT RESISTIVITY OHM.M
PHASE DEGREES
NUMBER OF ESTIMATES
SKEW
AZIMUTH IN DEGREES
FREQUENCY IN HZ

and * denotes the convolution operation.

X and Y can be considered as the horizontal components of the magnetic field and O is one of the electrical components. Data processing in the time domain is less used than frequency domain processing mainly because of the required increase in computational time. However Wieladek and Ernst (1977), Ernst (1981) and McMechan and Barrowdale (1985) have stressed its advantages over conventional frequency domain analysis, especially when the data are corrupted by spiky noise.

For example, Weiladek and Ernst (1977) applied a linear least squares method to determine the impulse response of the system and showed that this involves fewer assumptions compared to the corresponding frequency domain analysis. They showed that frequency domain processing is an approximation to time domain processing. It is likely that errors can creep into frequency domain processing due to removal of the mean, detrending, tapering (eg. using cosine window) etc., before computation of spectra and due to smoothing of the spectra. Ernst (1981) compared the results of processing geomagnetic sounding data in the frequency and time domains and showed the superiority of the least squares method in the time domain. Comparing the use of the least squares (l2) solution and the least absolute (l1) solution, McMechan and Barrowdale (1985) have shown that the 'l1' solution is more satisfactory when certain types of noise are present. In the present study, in view of the noise contamination of some of the data, it thus seemed worthwhile to undertake a preliminary study of further techniques for time domain processing. This involved use of a least mean square adaptive algorithm applied to synthetic data. The details of this technique are presented in Appendix–A of this thesis.

CHAPTER 5
Noise and Error during field measurements

Although the magnetotelluric (MT) method can be effective and fast in probing the electrical conductivity structure of the earth at crustal depths, the results are often degraded by industrial and cultural noise. To obtain reliable processed results for modelling, it is first necessary to extract or select the natural signals from frequently contaminated time series. Topography is another parameter which could distort the measurements (eg. see Thayer 1975, Harinarayana and Sarma 1982) and knowledge of the effect of undulating earth surfaces can help the planning of a field survey in a manner which minimises its effects.

In this chapter since the data from the present study show some evidence of degradation the effects of noise and error during field measurements are described and some procedures are suggested for their reduction. In section 5.1 various cultural noise reduction techniques based on digital filters are described with special reference to persistant noise signals and in section 5.2 the effect of topography is discussed by consideration of a conducting hill. This chapter is based mainly on two papers, Harinarayana (1987 in preparation) and Fontes et al (1987). The author contributed about 30% to the latter paper.

5.1. Processing of noisy data using digital filtering techniques and additional data selection criteria

The publication by Fontes et al (1987) which includes a field example from this study is attached to this thesis as an Appendix-B. Additional field examples from the author's field work and a laboratory study of spike noise are described here.

5.1.1. Field examples of noisy data in S.Scotland

The data recorded at different noisy stations have different characteristics and the sources of noise cannot be explained in all cases. However, it is apparent that the noise recorded in S.Scotland is mainly from 50 Hz. power lines and electrical fences. Figures 5.1a to 5.1e show field examples from NEW, BOW BOR, ESK AND KSF. One way of recognising noise in the data is by observing the characteristics-amplitude, frequency etc.- of the signals. For example, by comparision of the data recorded at BIG, BOR (Fig. 5.1a and b) with the relatively noise free WHI data (Fig. 4.6) reproduced here for ease of comparision (Fig. 5.1f) it is clear that the data at BIG and BOR show

5.1 Signals recorded at various noisy stations for consecutive frequency bands showing the time series data for four components; Magnetic (nT) signals are Hx, Hy and electric (mV/km.) signals are Ex, Ey. Each trace consists of 256 samples; 6010A 10 represents- 601= station number; 0= band number; A= data set; 10= window number. The examples shown are for

a) Station BOW recorded on 12-1-86. (code number= 601)

b) Station BOR, recorde on 9-8-85. (Code number= 504)

c) Station NEW, recorded on 5/6-8-85. (Code number= 501)

d) Station ESK, recorded on 24-7-86. (Code number= 608)

e) Station KSF, recorded on 16-7-86. (Code number= 605)

f) Figure 4.7 reproduced here- Station WHI (Code number= 508, recorded on 15-8-85.)

a

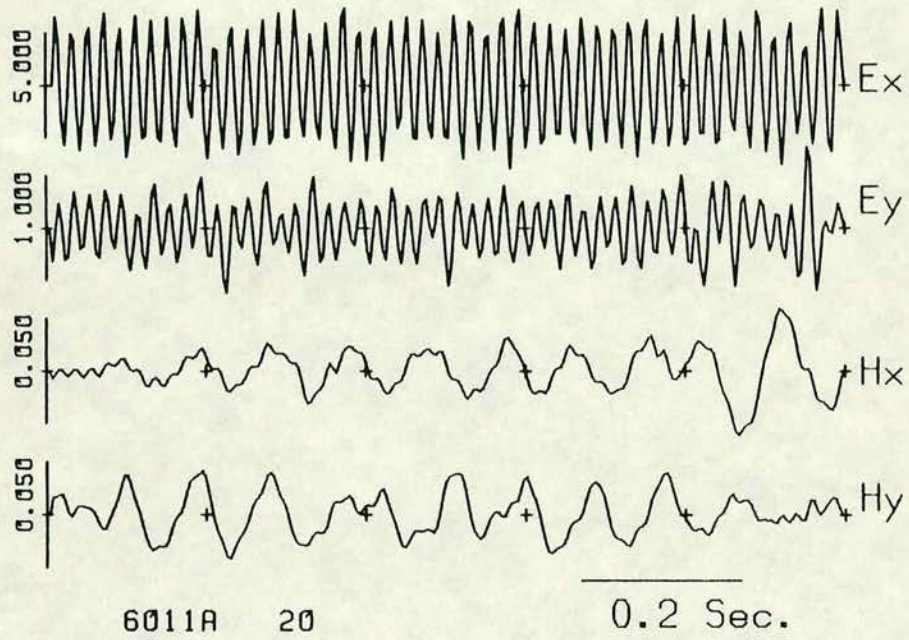
5.000
Ex
1.000
Ey
0.050
Hx
0.050
Hy
6011A 20
0.2 Sec.

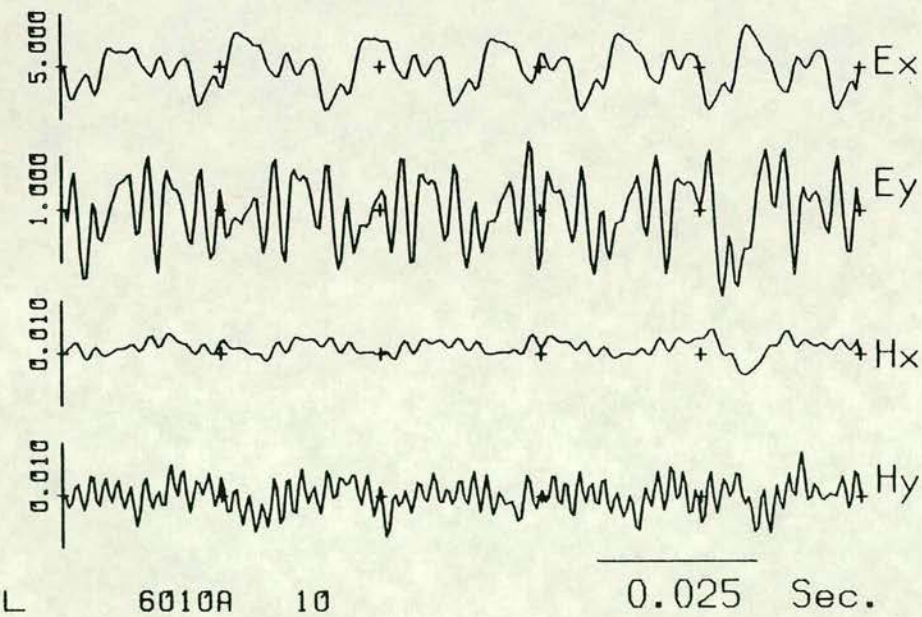
5.000
Ex
1.000
Ey
0.010
Hx
0.010
Hy
6010A 10
0.025 Sec.

b

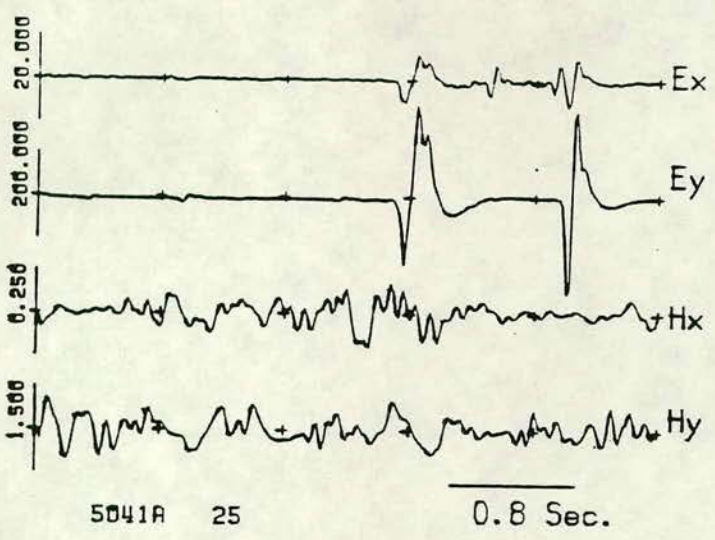
20.000
200.000
0.250
1.500
Ex
Ey
Hx
Hy
5041A 25
0.8 Sec.

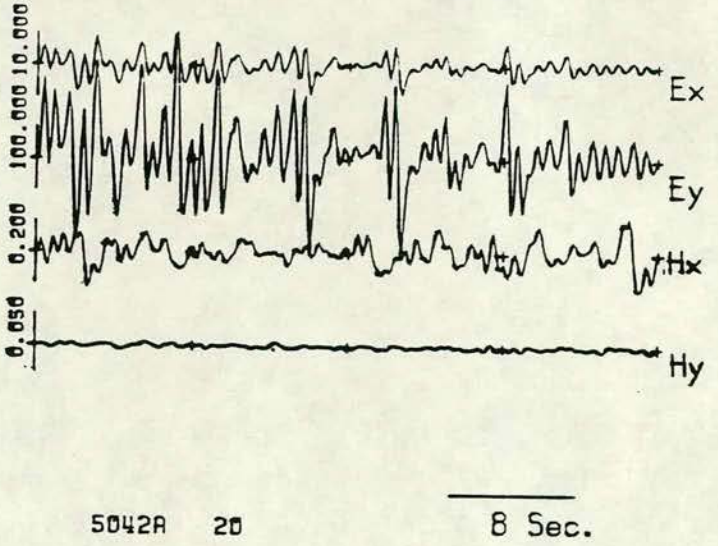
100.000 10.000
0.200
0.050
Ex
Ey
Hx
Hy
5042A 20
8 Sec.

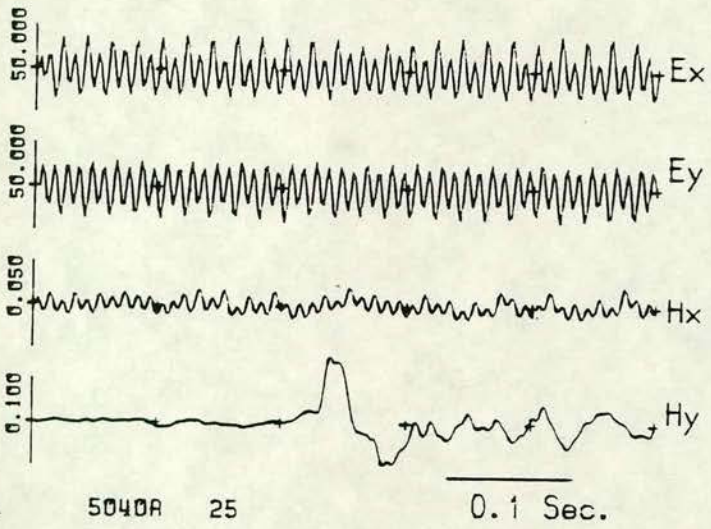
50.000
50.000
0.050
0.100
Ex
Ey
Hx
Hy
5040A 25
0.1 Sec.

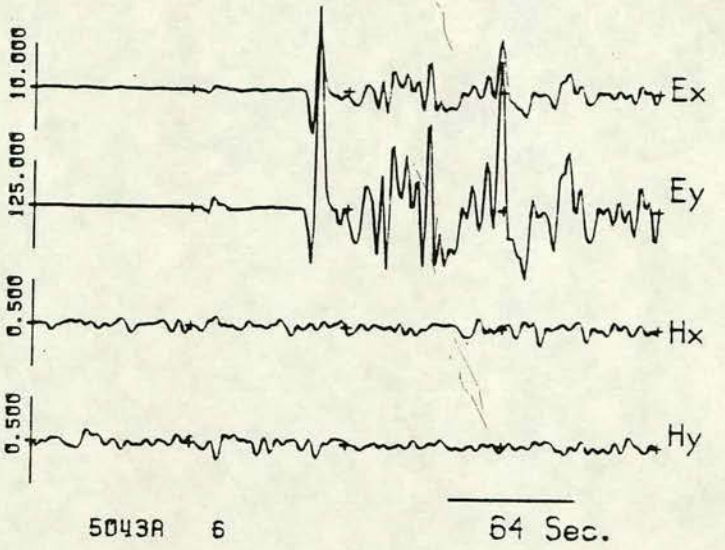
10.000
125.000
0.500
0.500
Ex
Ey
Hx
Hy
5043A 6
64 Sec.

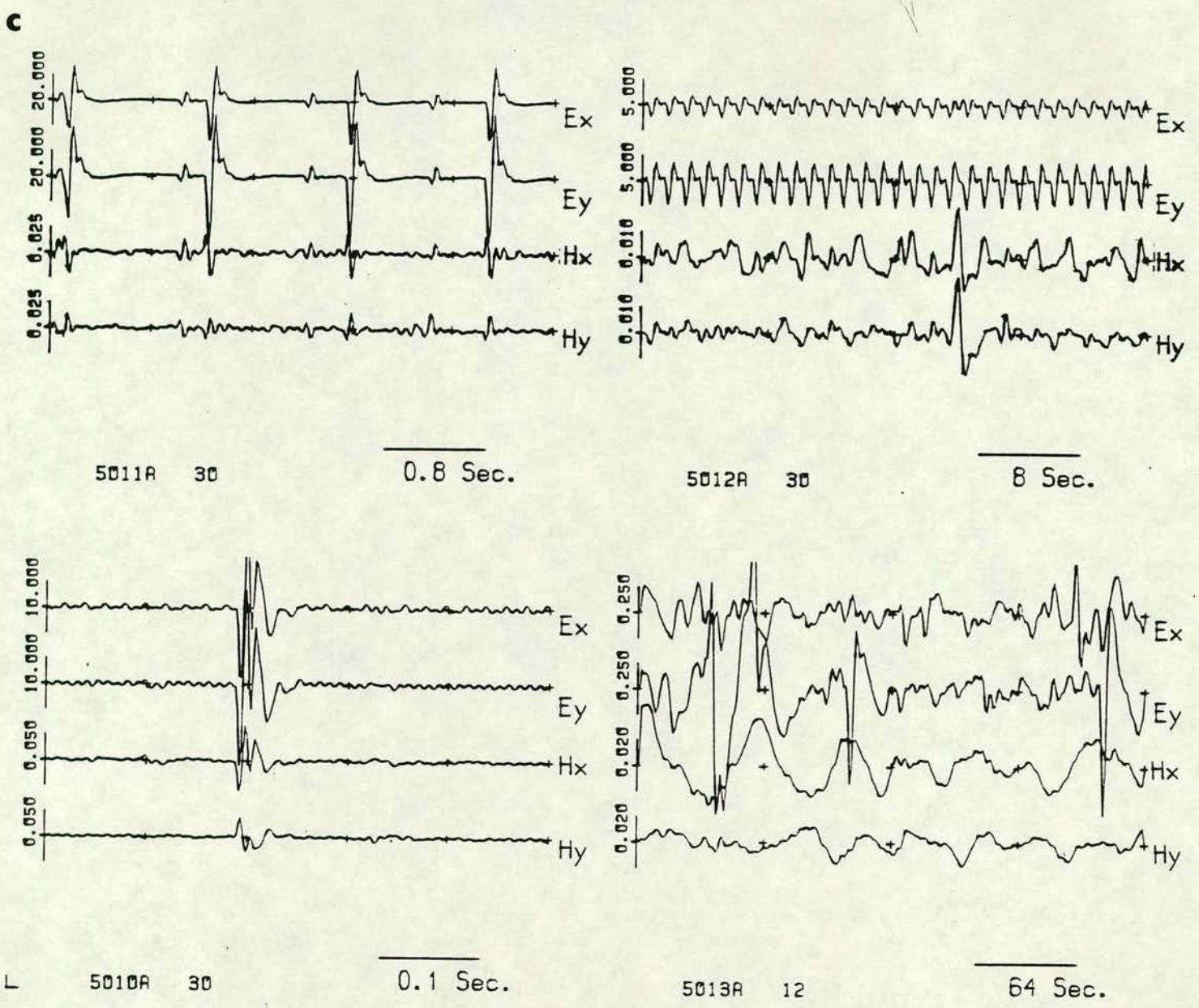
c
20.000
20.000
0.025
0.025
Ex
Ey
Hx
Hy
5011A 30
0.8 Sec.
5.000
5.000
0.010
0.010
Ex
Ey
Hx
Hy
5012A 30
8 Sec.
10.000
10.000
0.050
0.050
Ex
Ey
Hx
Hy
5010A 30
0.1 Sec.
0.250
0.250
0.020
0.020
Ex
Ey
Hx
Hy
5013A 12
64 Sec.

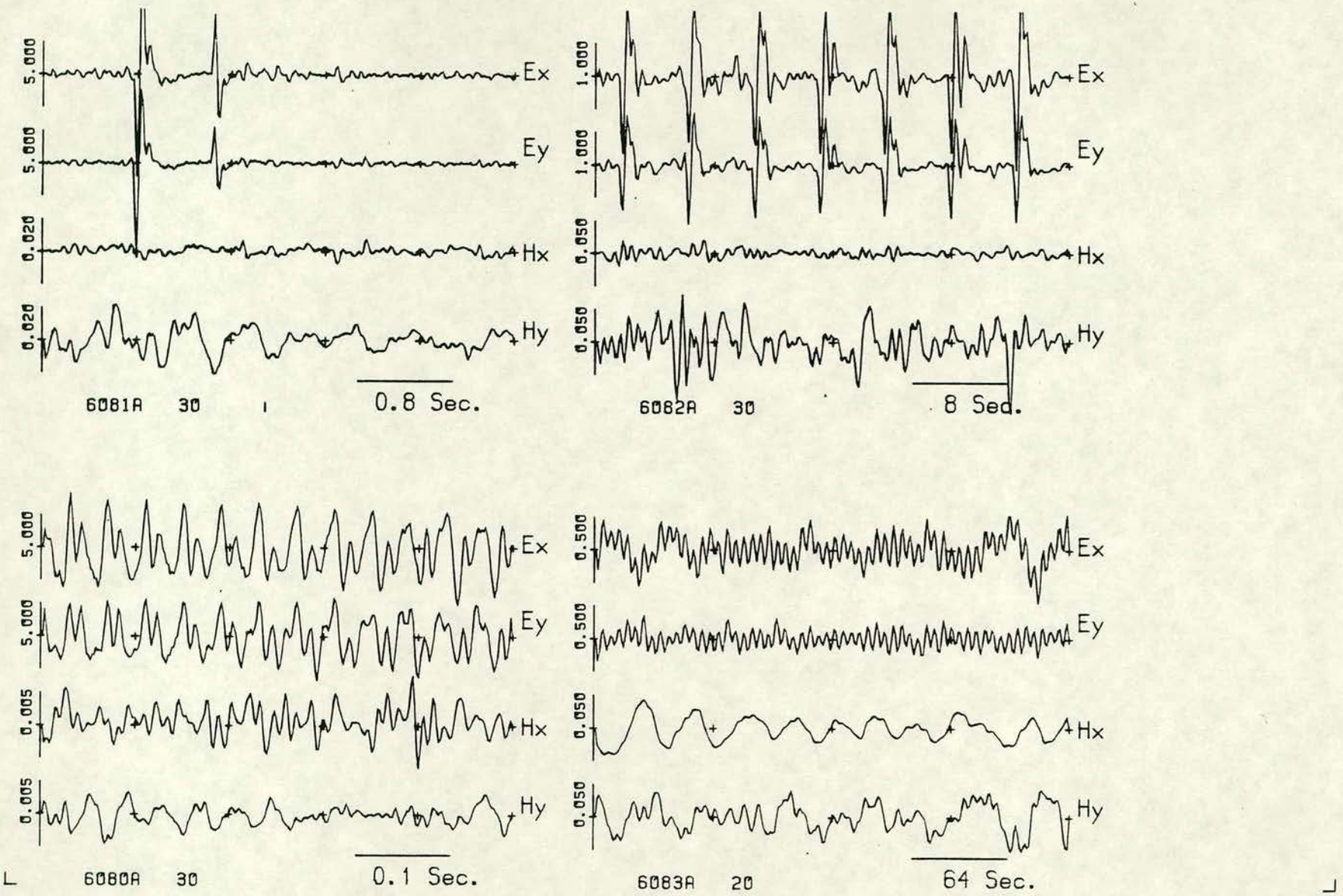
d
5.000
Ex
5.000
Ey
0.020
Hx
0.020
Hy
6081A 30
0.8 Sec.
1.000
Ex
1.000
Ey
0.050
Hx
0.050
Hy
6082A 30
8 Sec.
5.000
Ex
5.000
Ey
0.005
Hx
0.005
Hy
6080A 30
0.1 Sec.
0.500
Ex
0.500
Ey
0.050
Hx
0.050
Hy
6083A 20
64 Sec.

e

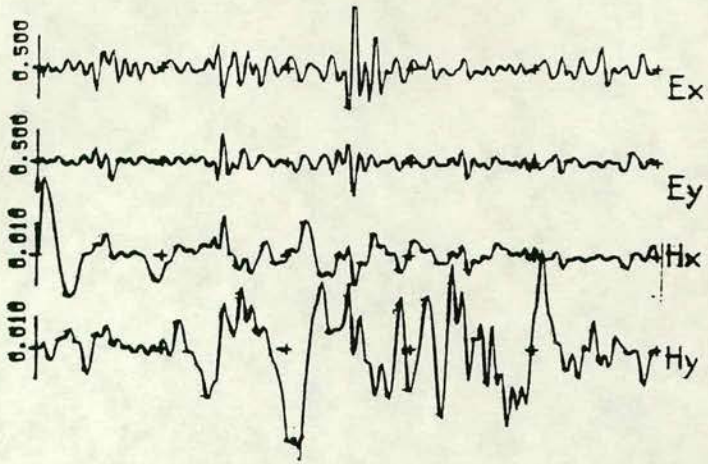

6051A 35 0.8 Sec.

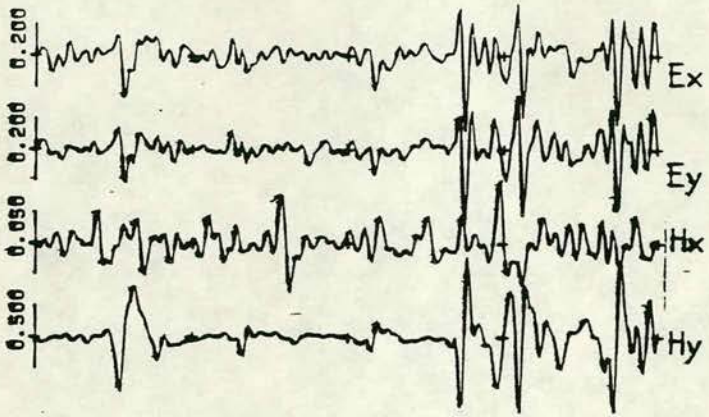

6052A 35 8 Sec.

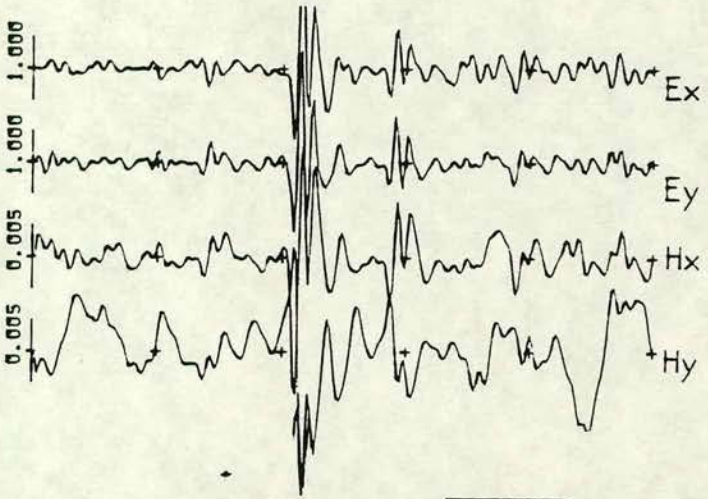

6050A 20 0.1 Sec.

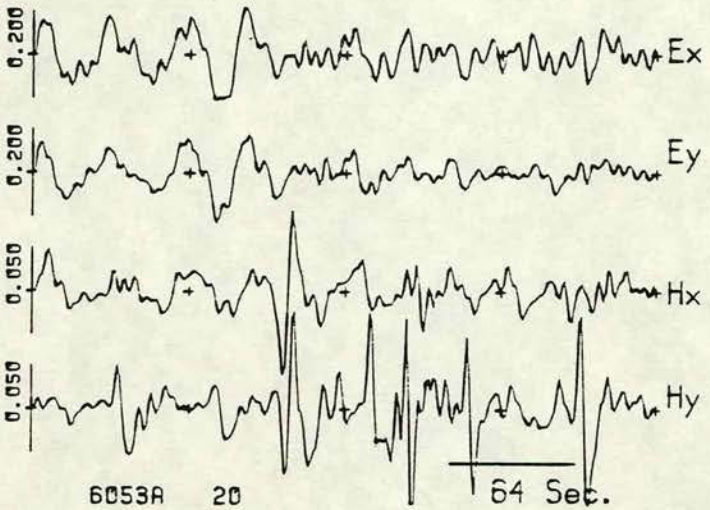

6053A 20 64 Sec.

f

FILE : AM5081A
STATION: 508
BAND : 1
NCHAN : 4
NSAMP : 256
SRATE : 64 HZ
XTICK : 0.20 SEC

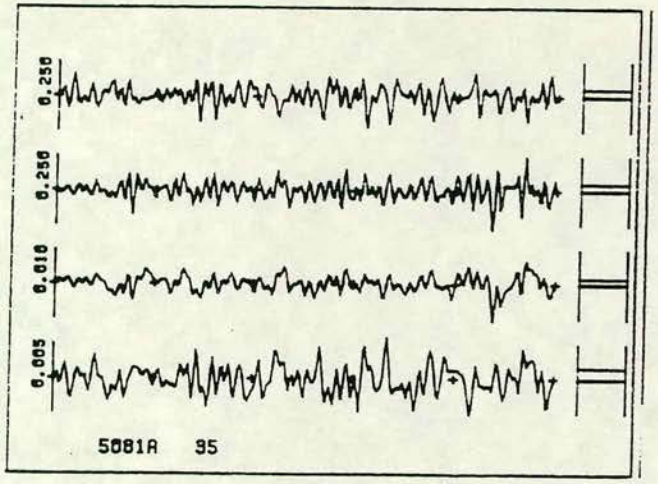

FILE : AM5083A
STATION: 508
BAND : 3
NCHAN : 4
NSAMP : 256
SRATE : 1 HZ
XTICK : 16.00 SEC

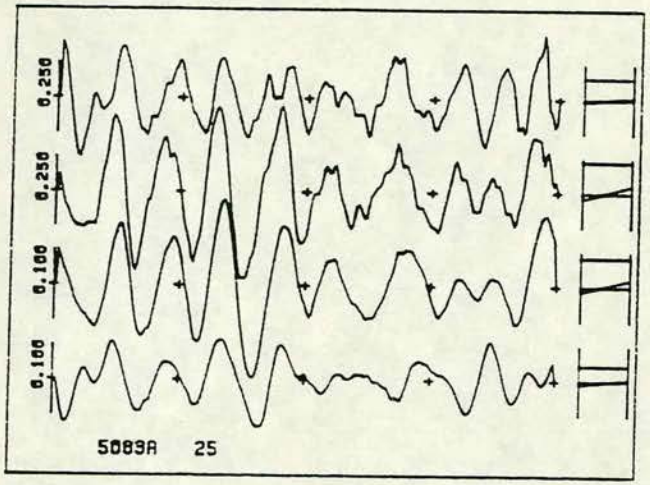

FILE : AM5080A
STATION: 508
BAND : 0
NCHAN : 4
NSAMP : 256
SRATE : 512 HZ
XTICK : 0.02 SEC

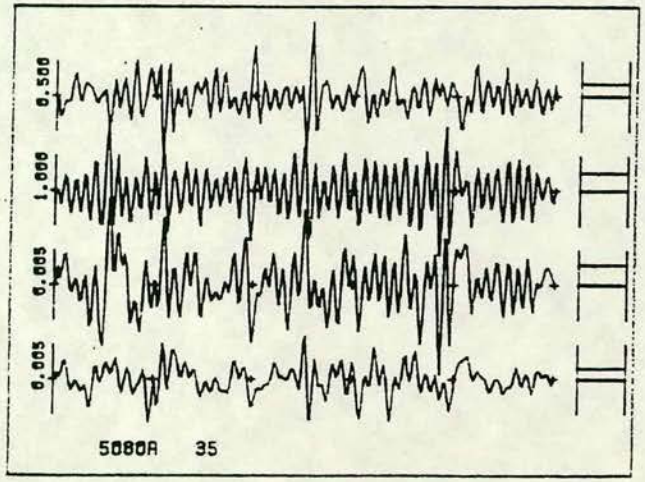

FILE : AM5082A
STATION: 508
BAND : 2
NCHAN : 4
NSAMP : 256
SRATE : 8 HZ
XTICK : 2.00 SEC

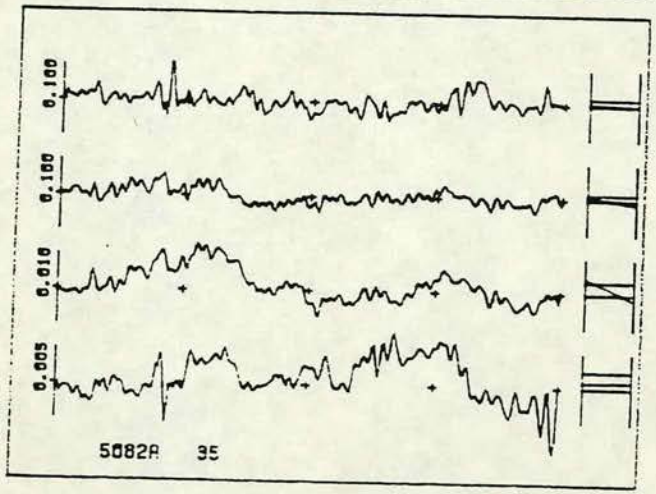

abnormally 'high' telluric field values of 5 mv/km. and 200 mv/km. respectively. It must be remembered, however, that these data were recorded at different local times, since it is known that amplitude charateristics of the signals are variable with location, local time and also depend on other factors such as the geology etc. Nevertheless, the abnormally 'high' values can probably be attributable to the effect of artificial sources of local nature. Similarly, by comparision of WHI data with NEW and ESK stations (Fig. 5.1 c,d), it can be seen that the signals at NEW and ESK stations have 'high' amplitudes and appear to show a periodic nature for bands 1 and 2.

As discussed in Appendix-B, if the 50 Hz. noise is neither a pure sinusoid nor has a fixed frequency, a notch filter in a data acquisition system is not completely effective in its elimination. Thus the noise recorded at stations BIG and BOR is possibly due to 50Hz. noise. Noise recorded at stations NEW, ESK (Fig.5.1c and d) and CRK (Fig.1 in Appendix-B) seems to originate from electrical fences and appears to show an irregular character in Band 0 and a periodic one in Bands 1 (16Hz.-2Hz.) and 2 (2Hz. -0.125 Hz.). The recordings from station KSF (Fig. 5.1e) are examples of irregular noise of a more intermittent nature and, as such, a spike can be seen in Band-0 and coherent noise of intermittent character in other bands. Since spike noise seems to corrupt at a few stations in the present field investigation, a laboratory study was made to analyse its effects, the details being given in the following section.

5.1.1.1. A laboratory study of the hypothetical spike source

To understand the nature of spike noise due to electrical fences, different types of signals such as a square pulse, ramp etc., with varying frequency and amplitude were input to the S.P.A.M. data acquisition system and the output signals were analysed both on analog as well as on digital recordings. When the noise source is a double spike of 6.5V amplitude and 0.8Hz. frequency and pulse width of about 0.5 to 1 ..sec. (Fig. 1 in Appendix-B), the signals appear to resemble the data at CRK. Figure 5.2 shows the results of this laboratory study. Comparing figures 1 in Appendix-B, and 5.2 it is clear that noise from electrical fences is probably of similar shape to that of a spike.

FIGURE 5.2

Electric field (mV/km.) data recorded by SPAM in the laboratory with a double spike of 6.5V amplitude and 0.8 Hz. frequency as input to the system. The different traces recorded in different frequency bands- a) Band-0 (128-16 Hz.); b) Band-1 (16-2 Hz.); c) Band-2 (2-0.125 Hz.); and d) Band-3 (0.125- 0.025 Hz.); The hypothetical spike source (e) can also be seen

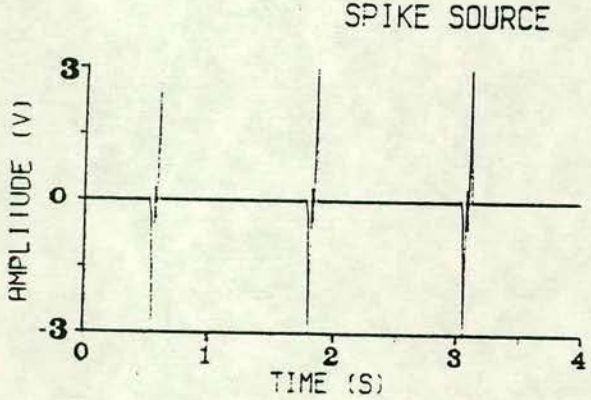
SPIKE SOURCE
AMPLITUDE (V)
3
0
-3
0
1
2
3
4
TIME (S)

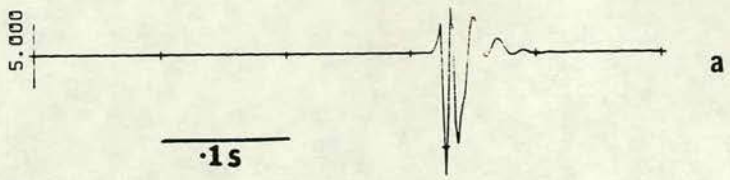
5.000
.1s

a

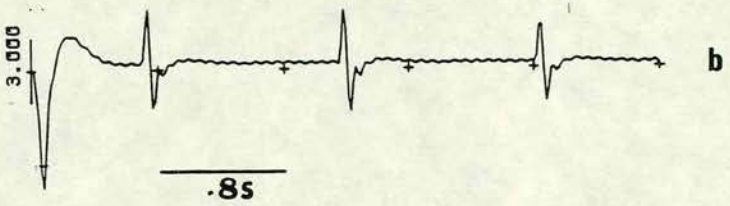
3.000
.8s

b

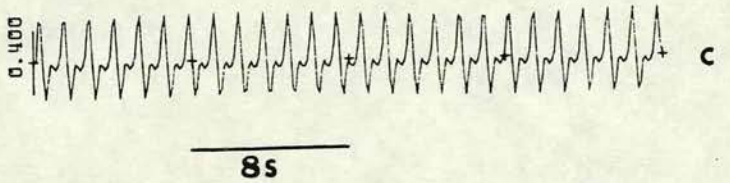
0.400
8s

c

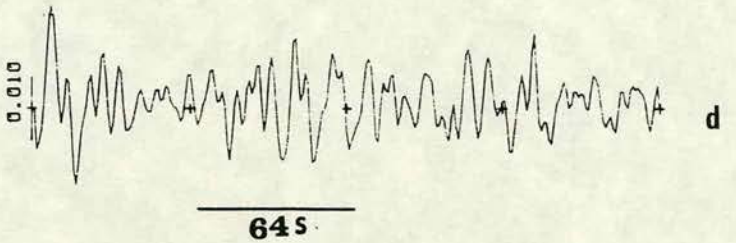
0.010
64s

d

5.2. Distortion of telluric field measurement near hills using conformal mapping methods

Hills are commonly seen topographic surfaces and their effect on MT field measurements is not fully known. The author thus undertook a study of a simple model to get some insight into the understanding of its effect. It was not anticipitated, however, that the topography in the present study region would cause a major obstacle as the undulations were not of comparable heights, for example, to the Himalayas or to the Alpine mountains. A preprint of the results of this study is attached to this thesis as Appendix-C.

The relevance of the model results presented in that paper are now considered with respect to this field study. In fig. 5.3 a smoothed surface topographic profile along the study traverse is presented. It may be noted that the model results could not, in general be applied to the estimation of accurate values of the distortion effects of complicated surface undulations since a simple symmetric hill surface (Fig. 1 of Appendix-C) was used as the model and DC fields only were considered. However, it is worthwhile to consider the implications of the computations to the present study. For this purpose, station WHI is chosen as this site is located on the conducting sediments of the Northumberland basin -a situation closely related to the assumed model. From fig. 5.3, a hill can be seen to the south of WHI. With the assumptions that- a) the hill surface is highly conducting compared to the basement, b) the hill is symmetric, c) the basement depth (H_1) is about 1km., as estimated from the present study (chapter- 6), d) the station is located at a distance (x) of about 10km. from the hill, e) the inclination 'α' is 30°, and f) the height of the hill (H_2) is 0.4 km., the following parameters can be obtained.

$H_2/H_1=0.4$; $\alpha = 30°$; $x/H_1=10$;

With these values and reference to fig.1 of Appendix-C, it can be concluded that the topographic effect is negligible at WHI for DC currents. If it can be assumed that the topographic distortion at a site is less for higher frequencies compared to DC fields the for the frequencies of signals considered at WHI (0.01 to 100 Hz.) the distortions are probably negligible.

FIGURE 5.3

A smoothed surface topography along the study traverse. The approximate symmetric hill is shown with a dotted line and its inclination is 30°. The distortion effect is studied at 'WHI' station.

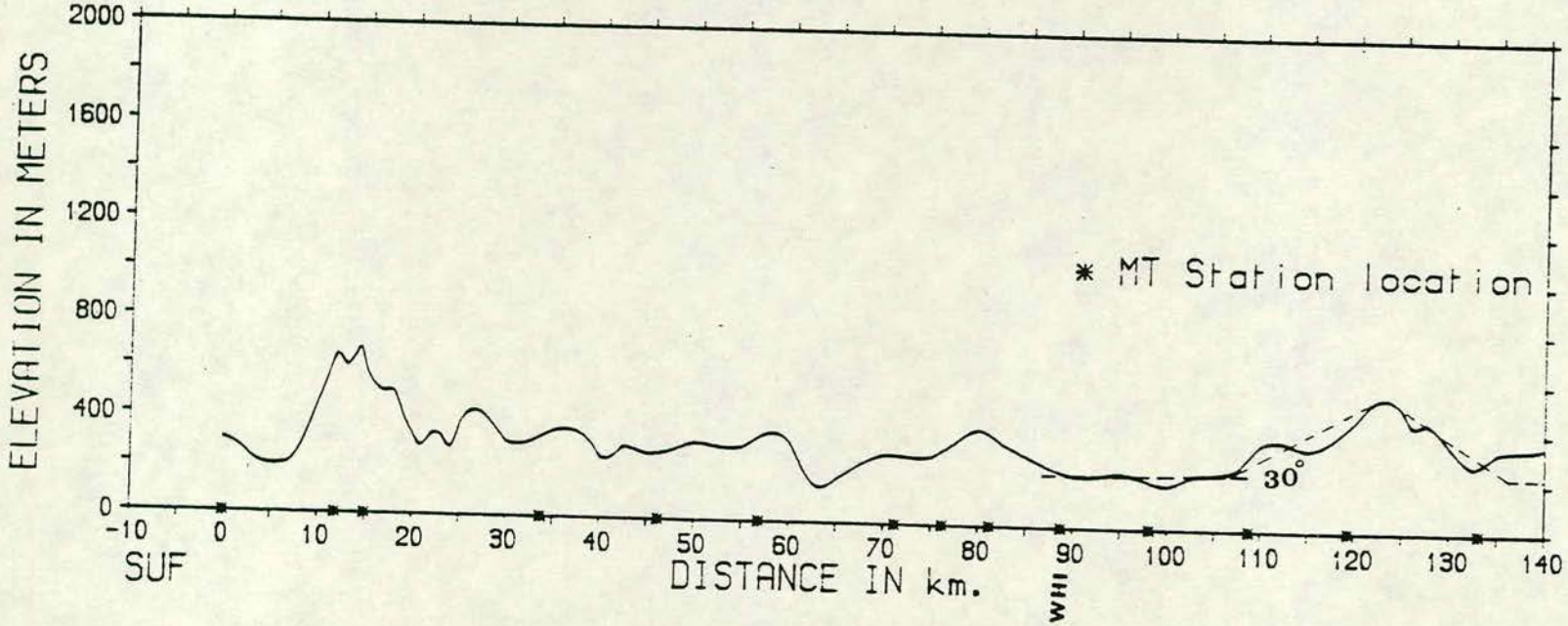
ELEVATION IN METERS
2000
1600
1200
800
400
0
* MT Station location
30°
-10
0
10
20
30
40
50
60
70
80
90
100
110
120
130
140
SUF
DISTANCE IN km.
WHI

Chapter 6

ONE DIMENSIONAL MODELLING RESULTS

This chapter deals with one dimensional modelling of both short period data obtained in this study (0.01 to nearly 100 sec.) and long period data (40–1000 sec. range) from earlier studies. In section 6.1 a brief description is given of the limitations and difficulties arising from use of one dimensional inversion schemes. In section 6.2, details of a qualitative study of the short period data obtained at all stations of this field investigation are presented. The results obtained from the application of two different inversion schemes are presented in section 6.3 and the resolution of the derived model parameters is discussed in section 6.4. Joint inversion, combining D.C resistivity sounding data with magnetotelluric (MT) data, is discussed in section 6.5 with respect to resolution of the shallow electrical structure in the Northumberland basin and the results of modelling of the long period data can be seen in section 6.6. Finally, in section 6.7 all the results of this chapter are summarized.

6.1. Introduction

The purpose of any geophysical modelling is to derive a physical parameter for the Earth that satisfies the observed data. Inferences can then be made about the nature and extent of the structure with respect to the geology and tectonics of the area. The approach is to construct the response function of a known Earth model and compare it with the observed response. Determination of the response function of simple Earth models is easily achieved using mathematical modelling procedures, especially with the advent in recent years of fast computers. However, analogue model studies in the laboratory are useful for three dimensional earth structures. This latter procedure has been applied to the British Isles (Nienaber et al 1981, Dosso and Nienaber, 1986) and it has also been used to study the topographic effect (eg. Faradzhev et al 1972). Mathematical modelling can be carried out through either a forward or an inverse approach. In the forward approach, a close fit is obtained by trial and error method between the observed experimental data and the theoretically computed response of a particular Earth model. If they

are in good agreement then the assumed model is considered to be an approximation to the real Earth. In the case of the inverse approach, in general, the above technique is carried out iteratively with successive model adjustments until the model with the minimum misfit between the observed and computed data is obtained.

As discussed earlier in chapter 4, the dimensionality parameters for the observed response data of this study have indicated that the structure is predominantly one dimensional. Although the contribution from the two dimensional earth structures is not negligible, the use of one dimensional inversion schemes is a good first approximation to two dimensional modelling. Generally, inversion schemes for induction problems can be carried out considering either a continuous variation of conductivity with depth, or a parametric layered Earth. In the first approach, the conductivity varies smoothly with a small gradient. The solutions are mainly variants of the process of Backus and Gilbert (1967) using Frechet derivatives (Parker 1970 and 1977, Oldenburg 1979, Hobbs 1982). Other examples in this category are direct inversion methods. In this approach, the derived models are not dependent on the minimization of misfit but on recovering the structure almost directly, considering the fact that high frequency responses give information about shallow Earth structures and low frequency about deeper structures (Nabetani and Rankin 1969, Patella 1976, Schmucker 1970 etc.,). In the second approach, the earth is divided into small number of uniform layers of variable thickness, conductivity discontinuities at the interfaces (eg. Wu 1968, Jupp and Vozoff 1975, Larsen 1981, Fisher and Le Quang 1981). Nonlinear methods such as the Montecarlo inversion scheme (Jones and Hutton, 1979) where the solution is sought randomly may fail to produce large sets of solution (Parker 1983), if the random search is incomplete. Complete nonlinear solutions can be used to study the range of model variability for the data sets by measuring the acceptability through the chi-square (χ^2) measure of misfit and providing three classes of models D^+, H^+ and C^{++} (Parker 1983). Though it is ideal to solve the inverse problem in a

nonlinear sense, surely a unique solution is impossible due to the 'equivalence property'. However, one generally requires a model to interpret the data according to a meaningful earth structure of the area. A procedure has recently been described (Constable et al 1987) for finding the smoothest model by linearising the nonlinear problem about the starting model and then solving explicitly for the desired model. Since most inversion schemes are based on the linearization of the nonlinear problem, use of any single such inversion scheme cannot provide a unique solution, and so application of different inversion schemes to assess the uniqueness is suggested by Oldenburg et al (1984). In the present study, two inversion schemes: a hedgehog modification of the modified Montecarlo inversion of Jones and Hutton (1979) and a linearised inversion (Jupp and Vozoff 1975) were used in addition to the Bostick transform (Bostick 1977).

As described earlier in chapter 4, the Earth response functions obtained in two perpendicular directions can be rotated to the strike direction to obtain major and minor apparent resistivities and phases. If the dominant geological strike is well known the axes can be rotated such that the electric field is parallel (E-pol) and perpendicular (H-POL) to the strike at all frequencies. One dimensional modelling can be carried out using any one of these response functions. However, some argue that when the Earth can approximate to a one dimensional structure, rotationally invariant impedance elements provide a better approximation to the real situation (Ingham and Hutton 1982, Jodicke et al 1983, Mbipom and Hutton, 1983, Beamish 1986, Jones and Garland 1986). The invariant used in these later studies was introduced by Berdichevisky and Dmitriev (1976) and termed 'the effective impedance', now frequently called the 'Berdichevisky average'

$$Z = (Z_{xy} - Z_{yx}) / 2 \qquad \text{.....6.1}$$

In another form, also introduced by Berdichevisky and Dmitriev (1976), the invariant representing all the four elements of the impedance, Z, is given by

$$Z = \sqrt{Z_{xx} Z_{yy} - Z_{xy} Z_{yx}}$$

.....6.2

This may be termed the 'determinant average', but in this thesis is simply called the invariant. Ranganayaki (1984) argues that compared to the effective impedance, it is a better average response of the real 3 dimensional Earth.

6.2. The qualitative study

Before attempting any inversion scheme, it is quite useful to study qualitatively the response functions which play a vital role in assessing the quantitative parameters of the model. Depending on the shapes of the invariant apparent resistivity and phase curves obtained in this study, they have been divided into three distinct groups as shown in figures 6.1 a, b and c. Fortunately, these groups belong to three different structural geological regions. The first group, for Southern Uplands stations (Fig. 6.1a) exhibits type 'K' apparent resistivity curves which tend to decrease from a resistivity of about 500 to 1000 Ohm.m. at short periods (0.01–0.1 sec.). The phase curves at the shorter periods have a value of about 45°, rise gradually in the 0.1–1 sec. range and finally reach a value of about 60 to 80° at about 0.01–0.1 sec. In the second group (Fig. 6.1b), for the Northumberland Basin sites, the short period apparent resistivity curves have only values of about 50 to 80 Ohm.m. but tend to increase at longer periods. The phase curves of this group have values of about 40°– 45° at short periods, decrease gradually to 30 to 35° at 1 sec. period and then rise to about 60°–70°. Finally the third group (Fig. 6.1c) belonging to the Alston block exhibits approximately 'Q'– type apparent resistivity curves. The curves at short periods have a value of about 20 to 50 Ohm.m. and then rise with a more or less steep gradient indicating the presence of a shallow high resistivity structure. The phase curves are about 60° at short periods then they decrease rapidly to a value of about 30 to 35°

FIGURE 6.1

Magnetotelluric invariant apparent resistivities and phases plotted as a function of period for (a) the Southern Uplands, (b) the Northumberland Basin and (c) the Alston block.

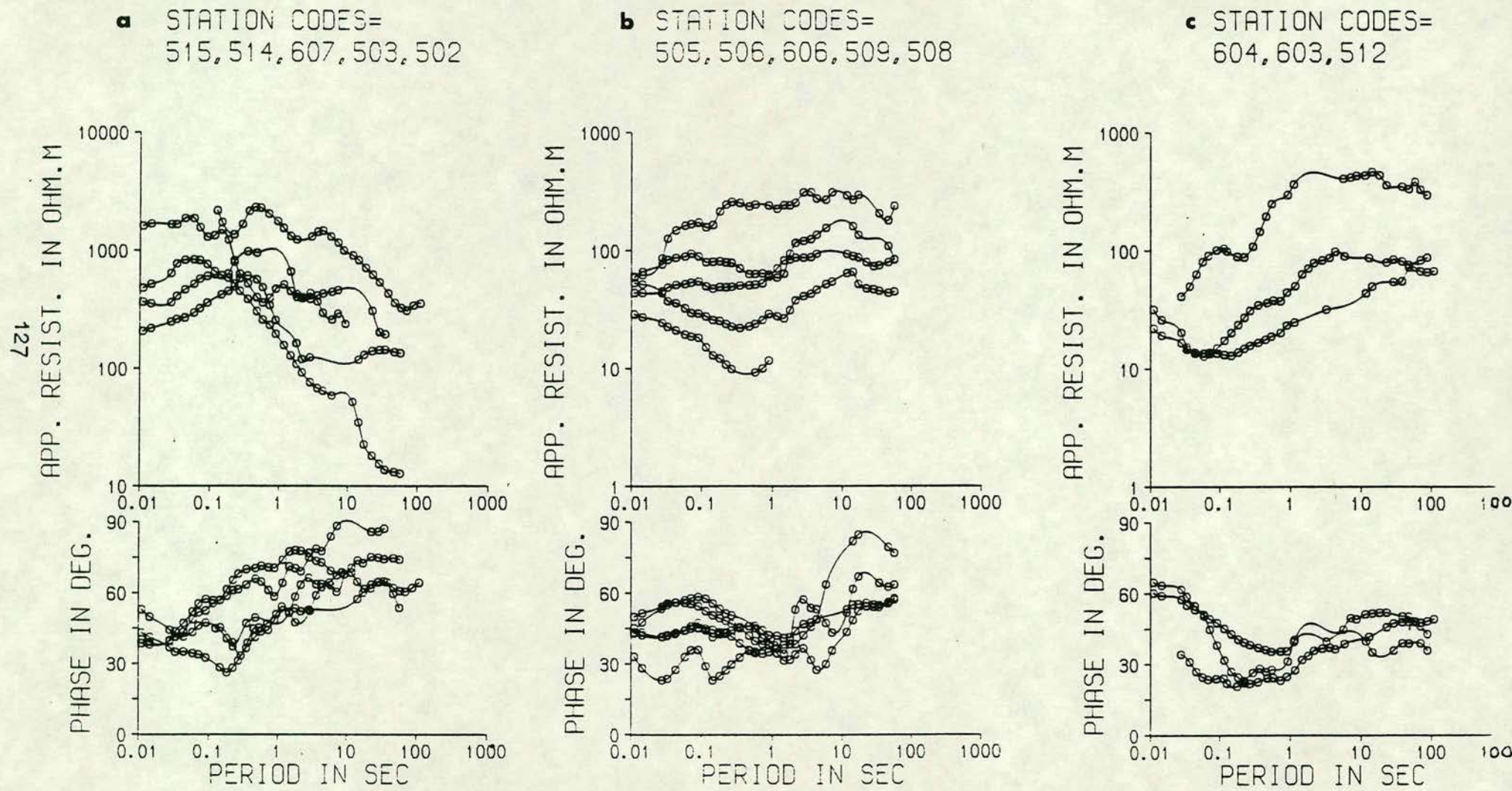
a STATION CODES=
515,514,607,503,502
b STATION CODES=
505,506,606,509,508
c STATION CODES=
604,603,512
APP. RESIST. IN OHM.M
PHASE IN DEG.
PERIOD IN SEC
10000
1000
100
10
1
90
60
30
0
0.01
0.1
1
10
100
1000

between 0.1 - 1 sec. finally rising gradually to about 40 to 45°.

For a qualitative determination of the resistivity structure the response functions were first subjected to an approximate inversion, using the Niblett-Bostick transformation (or simply Bostick transformation) to resistivity - depth parameters.

6.2.1. The approximate inversion

There are three main approximations presently in use for transforming measured magnetotelluric data into resistivity-depth distributions. These are the Niblett approximation (Niblett and Sayn_Wittgenstein 1960), the Schmucker ρ^*-z^* scheme (Schmucker 1970) and the Bostick approximation (Bostick, 1977). These approximations are all inter-related; Weidelt et al (1980) have demonstrated the relationship between the Schmucker and Bostick schemes, while Jones (1983b) showed the equivalence of the Niblett and Bostick transformations. These approximate resistivity - depth profiles are simple to compute and easy to incorporate in a real-time data acquisition system. Presentation of a resistivity-depth profile along with the conventional apparent resistivity and phase MT curves has been suggested by Goldberg and Rostein (1982). The field data obtained in the present study using the SPAM system have been transformed using the Bostick transformation. It has also been used to construct the starting model for the inversion schemes.

The Bostick transformation of apparent resistivity ρ_a and phase ϕ to the approximate resistivity and depth (Bostick 1977) is given by

$$\rho(D) = \rho_a(\omega) \; [(\pi/2\phi) - 1] \qquad \text{.....6.3}$$

and

$$D = [\rho_a(\omega) / \mu\omega]^{1/2}$$

The Bostick transformation of the response functions of Figs. 6.1 a-c are presented respectively in Figs. 6.2-6.4. In the first group -Fig. 6.2- for the Southern Uplands, the upper crustal resistivity is about 300-500 Ohm.m. except near station 607 (St. Mary's loch) and station 515 (Drumezlier), where it is about 1000 Ohm.m.. At a depth of about 5 to 10 km. the resistivity begins to decrease at all sites to about 10-100 Ohm.m.. In fig 6.3, for the Northumberland basin sites, the resistivity is very low (30 - 80 Ohm.m.) at shallow depths. It then rises to about 100 to 150 Ohm.m. and finally falls to about 10-50 Ohm.m. except near station 505 (Bewcastle) where it is about 100 Ohm.m.. In the Alston block group (Fig. 6.4) the resistivity at depths up to about 0.5 km. is 10-50 Ohm.m. as for the Northumberland Basin sites but in this case, the resistivity of the deeper structure rises gradually to about 100 Ohm.m. for stations 604 (Sinderhope) and 603 (Rookhope) and about 500 to 800 Ohm.m. for station 512 (Hill end). Initial parametric layered models have been established from the above information and used in the more rigorous iterative inversion schemes.

6.3. The inversion procedures

6.3.1. Modified Montecarlo-Hedgehog inversion

The basic strategy in this inversion scheme is to minimize the error between the model response and the observed response function, choosing the model at random. This scheme was originally proposed as a Montecarlo inversion by Jones and Hutton (1979), where a full description can be found. In the present study, it is used in Dawes's (1980) modified version which also incorporates a 'hedgehog procedure' as now described briefly.

Let us assume that M observations are represented by the vector

$$d^T = d_1, d_2, \ldots\ldots, d_M$$

FIGURE 6.2

Bostick transformation of apparent resistivity and phase to resistivity-depth profiles- Southern Scotland.

SITE 515C INVARIANT

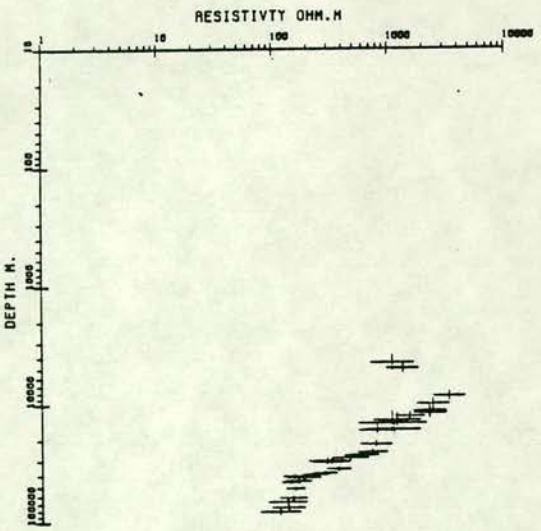

SITE 514C INVARIANT

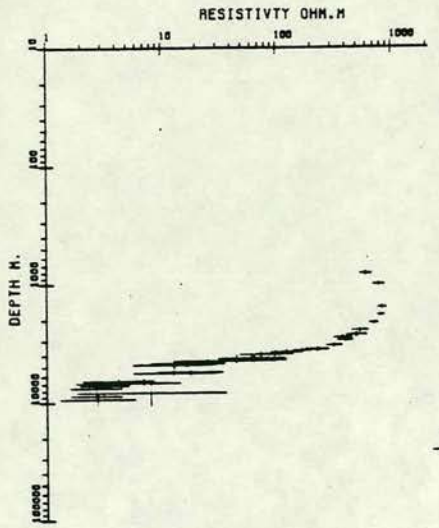

SITE 607C INVARIANT

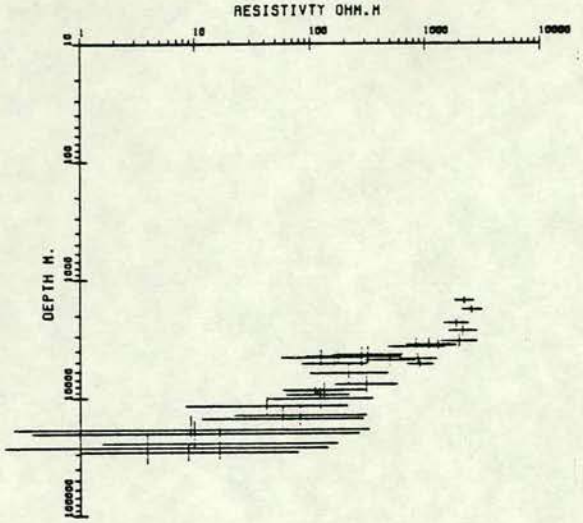

SITE 503C INVARIANT

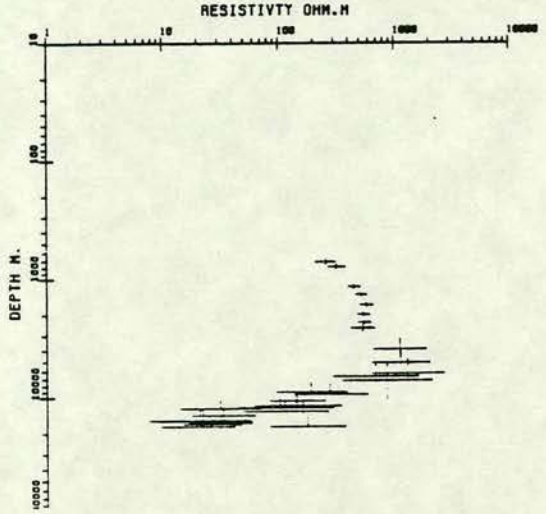

SITE 502C INVARIANT

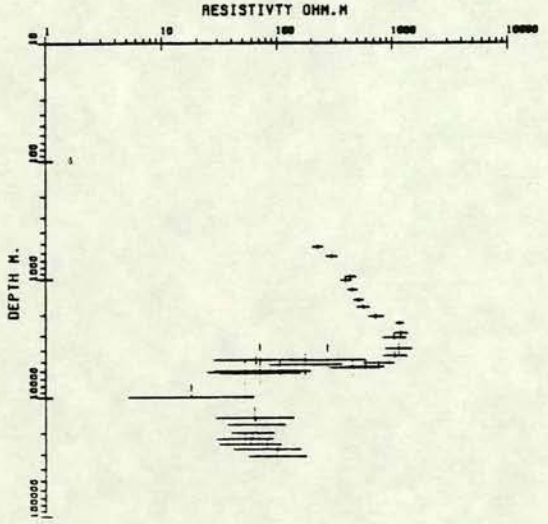

FIGURE 6.3

Bostick transformation of apparent resistivity and phase to resistivity-depth profiles- Northumberland basin.

SITE 505C INVARIANT

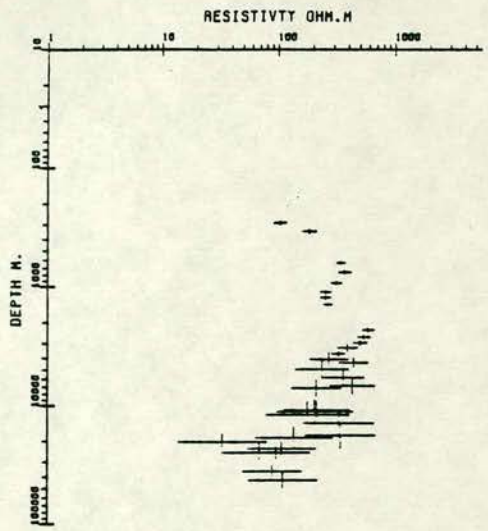

SITE 509C INVARIANT

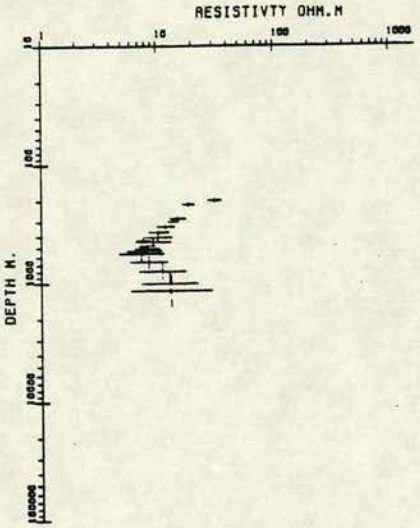

SITE 506C INVARIANT

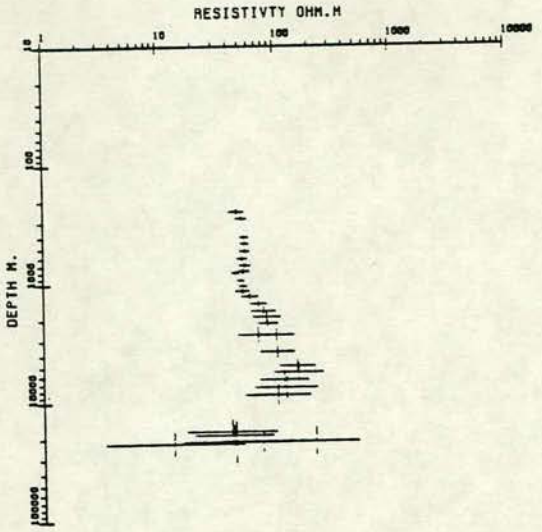

SITE 606C INVARIANT

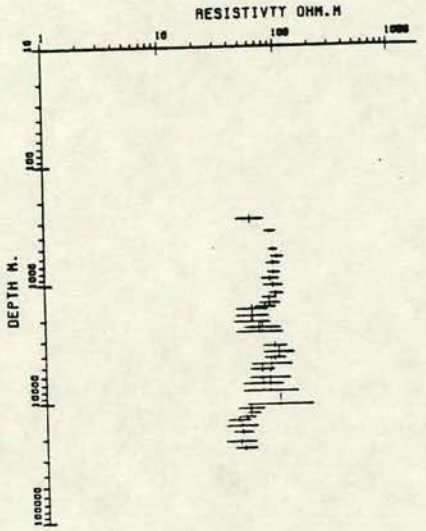

SITE 508C INVARIANT

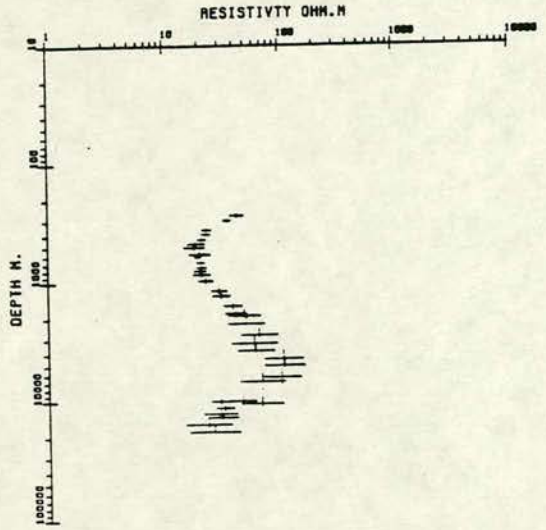

FIGURE 6.4

Bostick transformation of apparent resistivity and phase to resistivity–depth profiles– Alston block.

SITE 604C INVARIANT

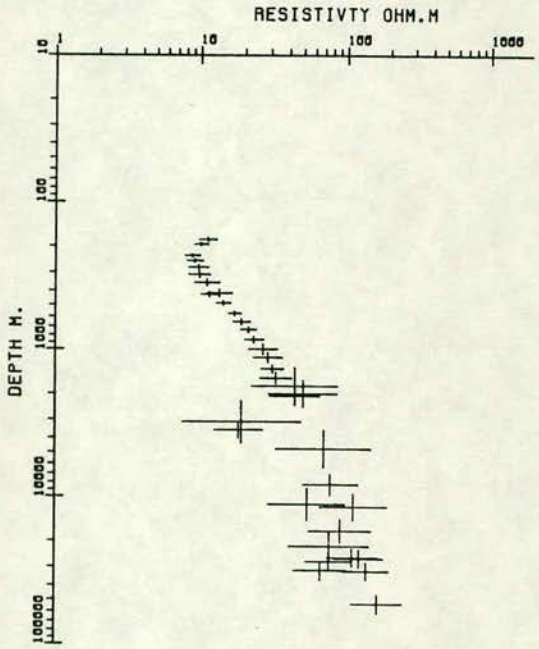

SITE 603C INVARIANT

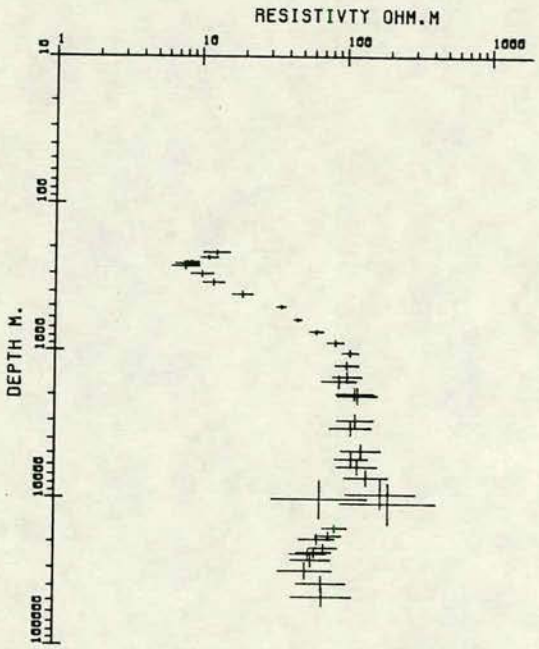

SITE 512C INVARIANT

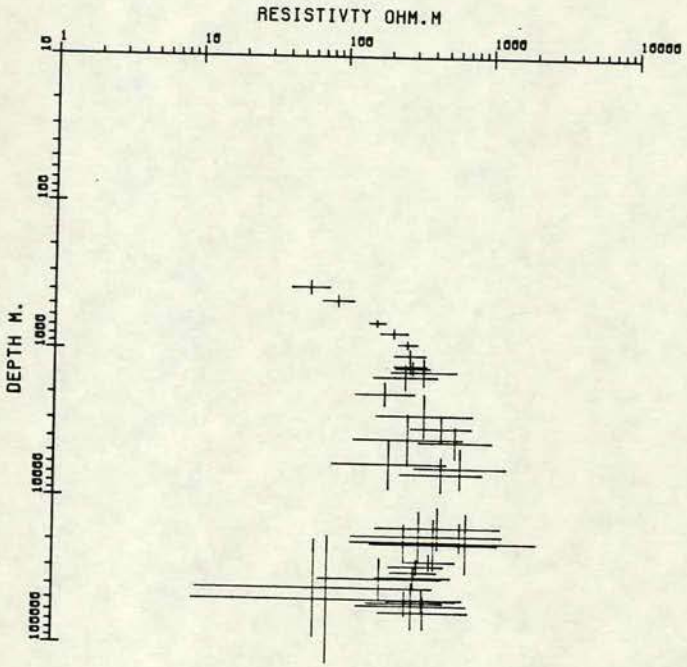

.....6.5

and the response function of the model X by

$$g^T = g_1, x, g_2 x, \ldots\ldots, g_M x$$

.....6.6

and the model X with N degrees of freedom be

$$x = x_1, x_2, \ldots\ldots x_N$$

.....6.7

Initially, a parametric layered model X consisting of resistivity and depth parameters for a fixed number of layers is required. Its response function g is then calculated and compared with the data vector $\bar{d}$. The response functions used in many earlier studies (eg. Sule 1985, Travassos 1987) were apparent resistivity and phase. In the present study the impedance values were considered.

The misfit between the model response and the observed data is given by

$$\psi = 1/N. \sum_{i=1}^{N} [|\hat{Z}-Z|]^2 / |\hat{Z}| \, |Z|]$$

.....6.8

where

$\hat{Z}$, Z represents the computed and observed impedance values for the initial model.

New models are generated by perturbing the initial model with a series of random numbers r1, r2,..... which are normally distributed with zero mean and unit variance. The parameters of the new model are also conditioned by the bounds imposed on the initial model. Each model parameter X is assigned three values, minimum value- X_{min}, optimum value- X_{opt} and maximum value- X_{max}. These chosen bounds depend in turn on the quality of the observed data and its associated errors. The perturbations imposed on each parameter of the model are given by

$$x_p = x_p * 10^{r \log(x_{max}/x_{opt})} \text{ for } r > 0 \qquad \text{.....6.9}$$

and

$$x_p = x_p * 10^{r \log(x_{opt}/x_{min})} \text{ for } r < 0 \qquad \text{.....6.10}$$

In each iteration, 50 random models are considered and at the end of each iteration the information from the previous best five models are used to readjust the bounds and provide an average model which is used as the starting model of the next iteration. Though this mechanism speeds up the computations, it also restricts the random search to the neighbourhood of the initial starting model. After each iteration, however, the range of the initial bounds narrows and tends to converge to a particular optimum model provided the misfit criterion decreases. In this study 10 iterations were used for each inversion. If the final misfit was very large, the initial starting model

was altered and the inversion scheme repeated.

6.3.2. The Linearised inversion

This scheme, published in Jupp and Vozoff (1977) where full details can be found, is based on local linearization, achieving the solution through iteration. An overview of the procedure is given here.

In solving the inverse problem, the model parameter x is determined such that the error between the response function g(x) and the data vector $\bar{d}$ is a minimum. The error parameter used in this scheme is the root mean square relative error between the response function and data vector.

$$F(x) = [\ 1/M. \sum_{i=1}^{M} (d_i - g_i)^2 / d_i^2\ ]^{1/2}$$

.....6.11

To start the iteration process, the partial derivatives of the model data with respect to its parameters are obtained. To derive this, a Taylor expansion of the vector g(x) around the starting model x is used.

$$\bar{g}(x+dx) = \bar{g}(x) + \bar{\bar{J}}\,\delta x + \bar{R}$$

.....6.12

where, J is an M x N Jacobian matrix of partial derivatives whose elements are

$$\partial g_i/\partial x_j \qquad i= 1,2.....M \text{ and } j= 1,2.....N$$

The Jacobian matrix is also called the 'sensitivity matrix' of the model with respect to its parameters. In any column of the matrix, if the value is zero or

very small compared to other column vector values, then the corresponding component vector $\bar{x}_j$ has no influence on the observed data and is considered as 'irrelevant' .

The remainder $\bar{R}$ in equation 6.12 depends on the nonlinearity of the response function $\bar{g}$. In this scheme $\bar{g}(x)$ is assumed to be a linear function and hence the remainder $\bar{R}$ is zero.

Hence the search for the model is confined to the neighbourhood of the starting model. From the starting model X, the technique iteratively changes by an amount which minimizes

(i) $\|\bar{\varepsilon} - \bar{J}\bar{\delta}_x\|$

and

(ii) $\|\bar{\delta x}\|$ and solutions of (i)

.....6.13

The above conditions provide a unique solution to the problem

$$\bar{\bar{J}}\,\bar{\delta x} = \bar{\varepsilon}$$

.....6.14

Usually the Jacobian M X N matrix is not square. In fact in most of the cases M > N: that is the number of data points is greater than the number of parameters to be determined and J may or may not be full rank.

The rank of $\bar{\bar{J}}$ is difficult to determine especially when it is < min (M,N) A

deficient rank results in the problem being undetermined with respect to some parameters. Hence it is useful to decompose the matrix J (Golub and Van loan 1983) as

$$\bar{\bar{J}} = U\ S\ V^T = \sum s_i\ u_i\ v_i^T$$

.....6.15

where S and V are N X N matrices, u_i and v_i are column vectors of U and V respectively and s_i is an element of the diagonal of S such that $S_1 > S_2 > \ldots\ldots > S_p$. These diagonal elements are called the singular values. If p is the rank of J this implies that (N–P) parameters are irrelevant, and cannot be determined from the data. The solution for the vector g(x) can be obtained from equations 6.14 and 6.15 and is given by

$$\bar{\nabla x} = V\ S^{-1}\ U^T \varepsilon$$

.....6.16

The stability of the solution is achieved through truncation of the S^{-1} matrix.

6.3.3 1–D models for the individual stations

One dimensional inversion has been carried out using the above two inversion schemes, generally with the same initial model for each algorithm. The models obtained for the rotationally invariant apparent resistivity and phase responses of individual stations are presented in Fig. 6.5a to 6.5m superposed on the Bostick transformation plots.

FIGURE 6.5

a-m One dimensional inversion of invariant apparent resistivity and phase responses using Linearised (upper half of the figure) and Montecarlo-Hedgehog (lower half of the figure) inversion schemes. The resistivity and depth scales are logarithmic. Bostick transformation plots are superposed in each case.

SITE NO.	SITE CODE	SITE NAME
515	DZR	Drumezlier
514	CAP	Cappercluch
607	SML	St.Mary'sLoch
503	CRK	Craik
502	CWR	Carewoodrig
505	BEW	Bewcastle
506	LAM	Lampert
509	GIB	Gibstown
606	EDG	Edgesgreen
508	WHI	Whitfield
604	SIN	Sinderhope
603	ROO	Rookhope
512	HIL	Hillend

DZR

a

1D MODEL FOR SITE 515C INVARIANT

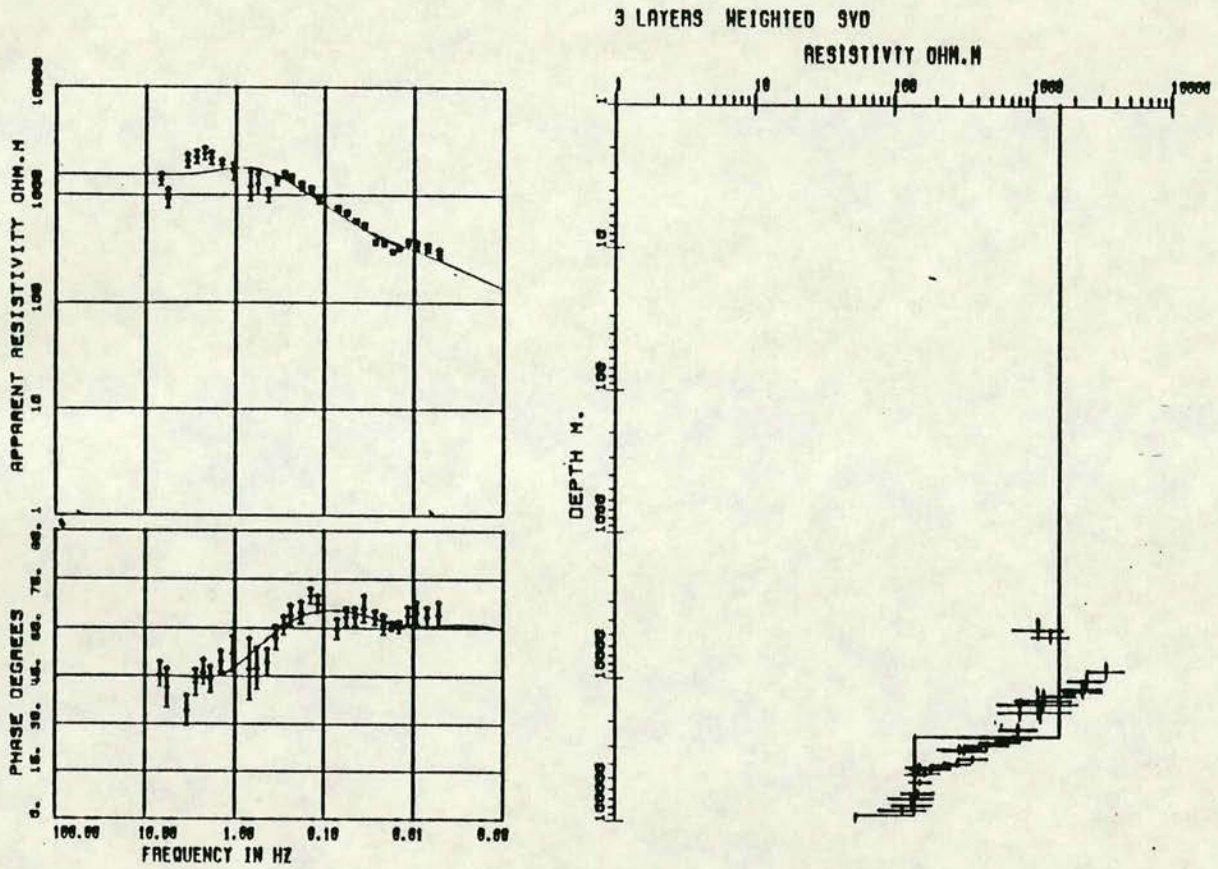

1D MODEL FOR SITE 515C INVARIANT

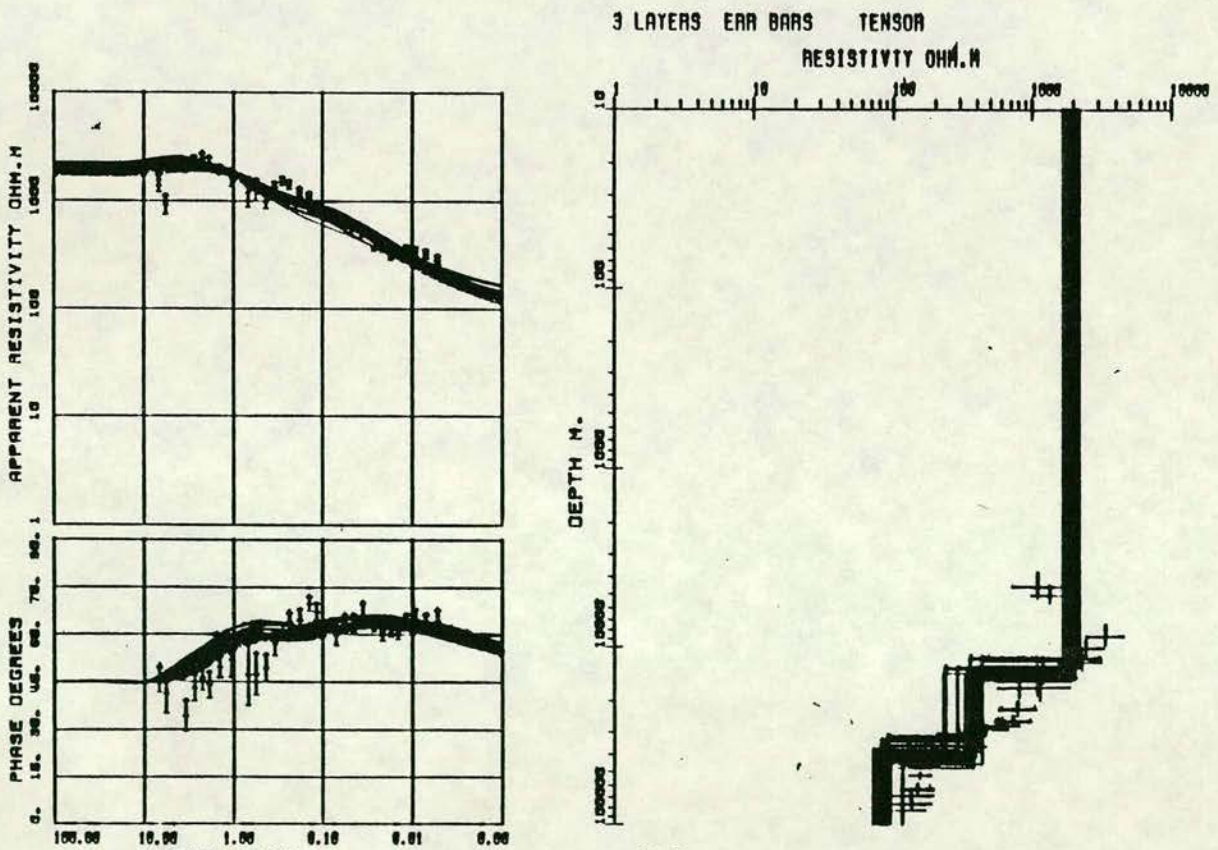

b

CAP

1D MODEL FOR SITE 514C INVARIANT

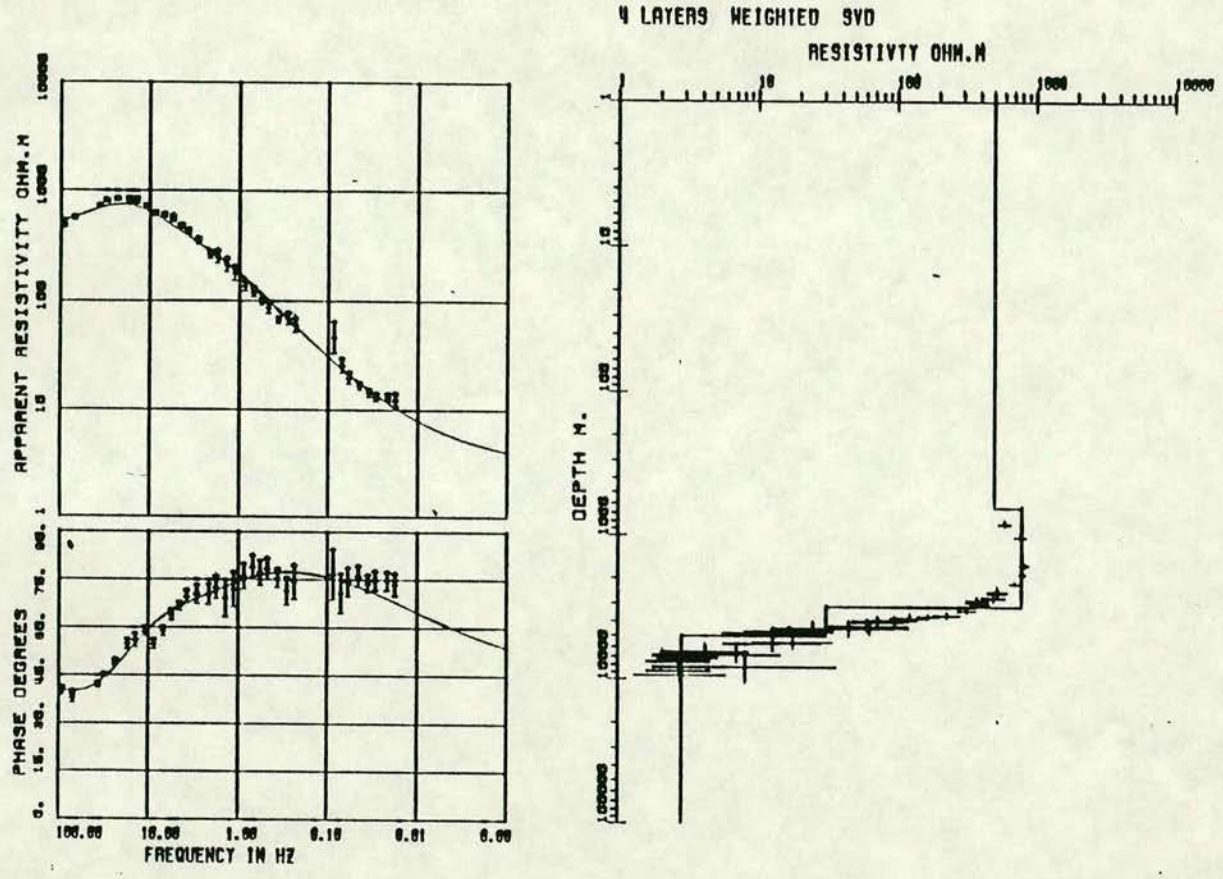

1D MODEL FOR SITE 514C INVARIANT

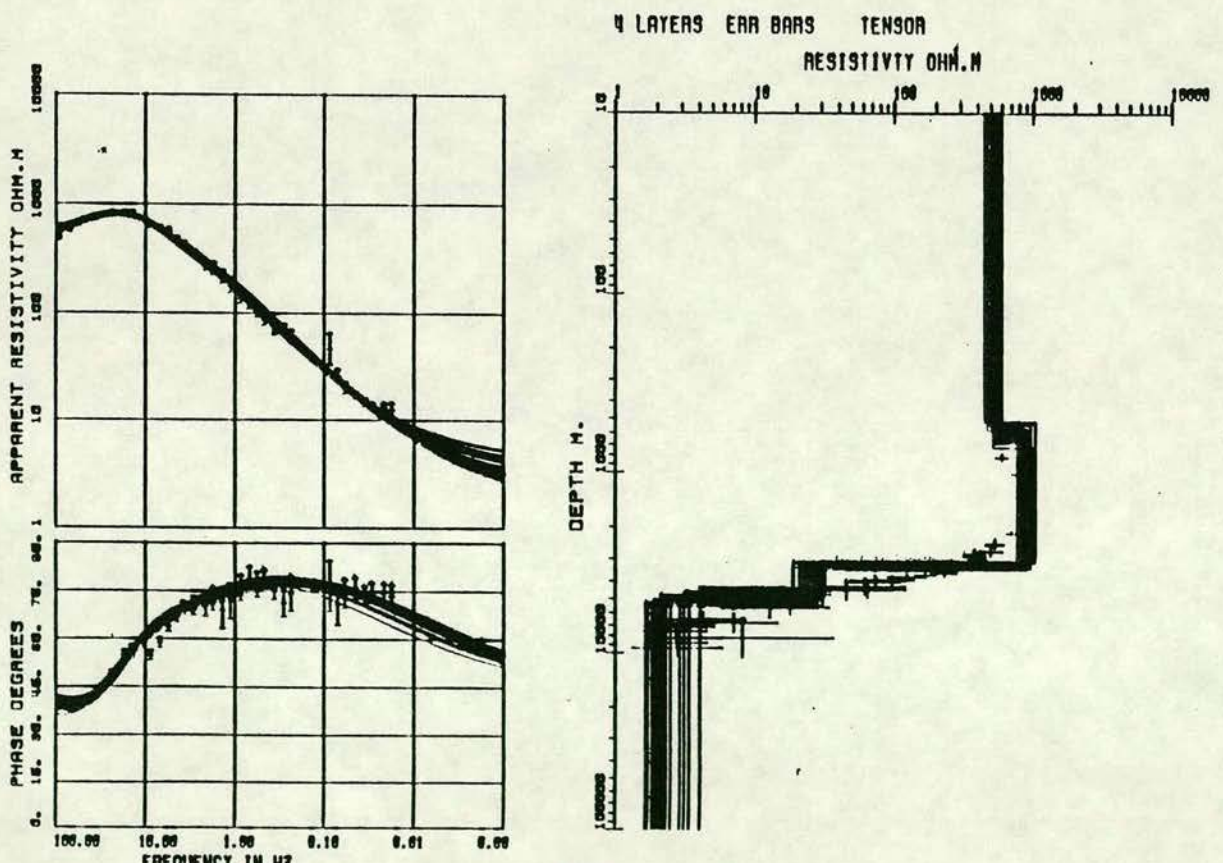

SML

c

1D MODEL FOR SITE 607C INVARIANT

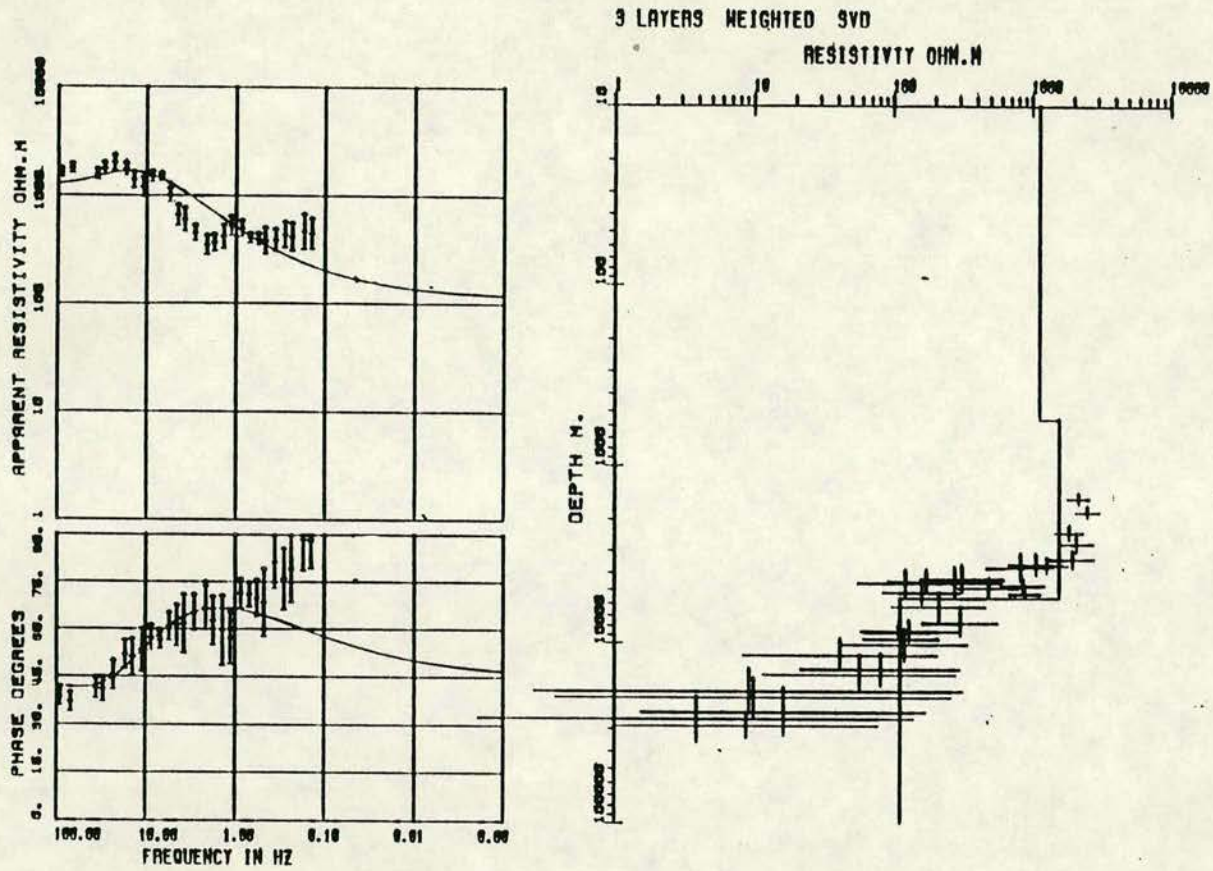

1D MODEL FOR SITE 607C INVARIANT

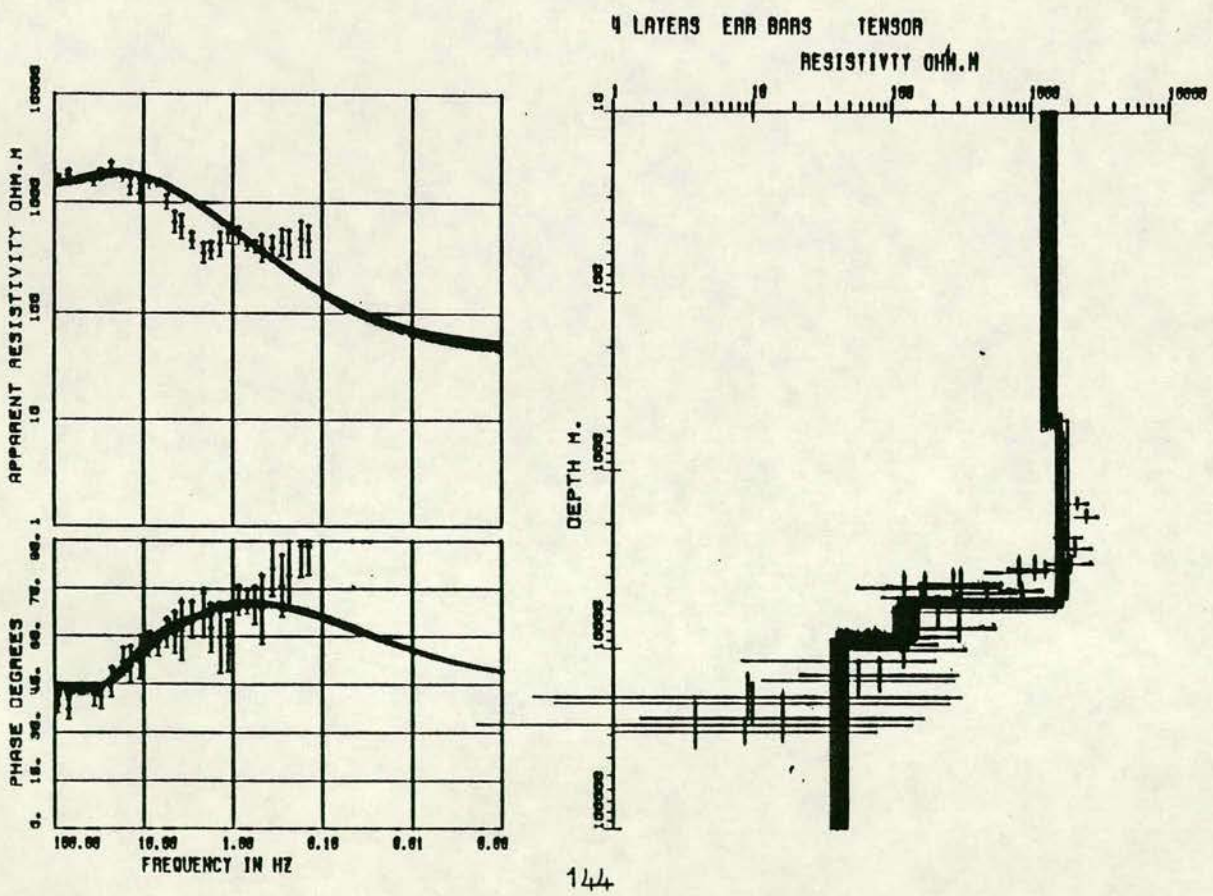

d

CRK

1D MODEL FOR SITE 503C INVARIANT

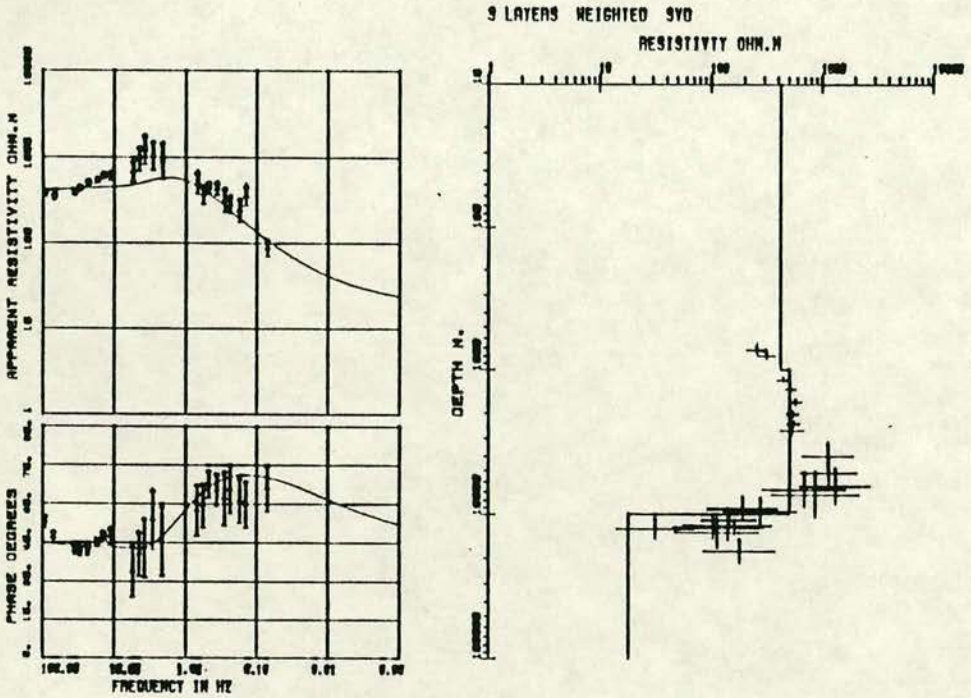

1D MODEL FOR SITE 503C INVARIANT

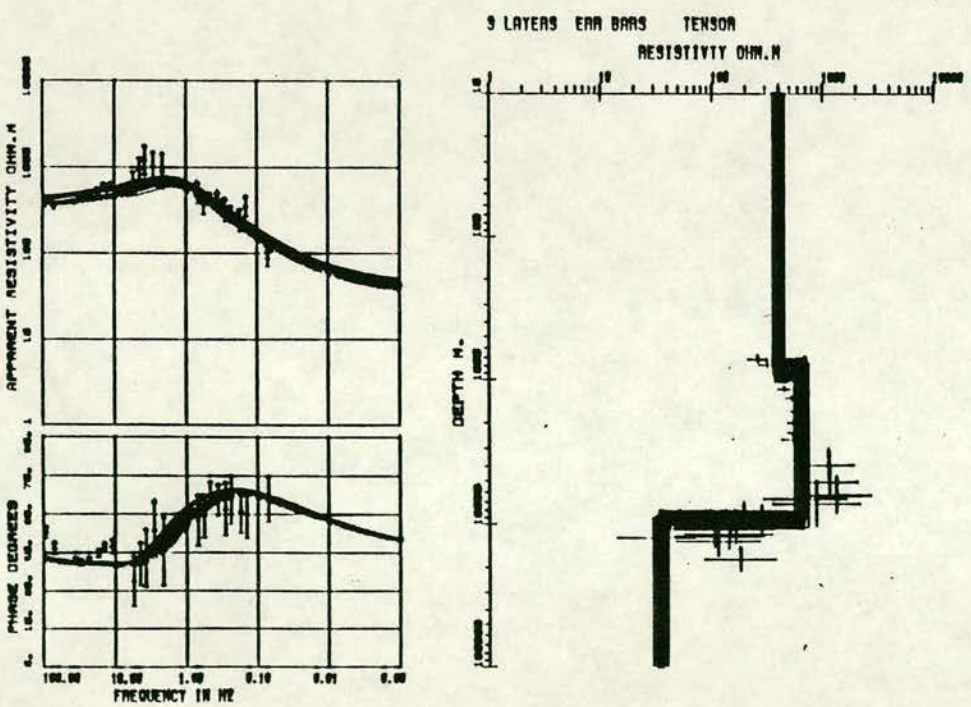

e

CWR

1D MODEL FOR SITE 502C INVARIANT

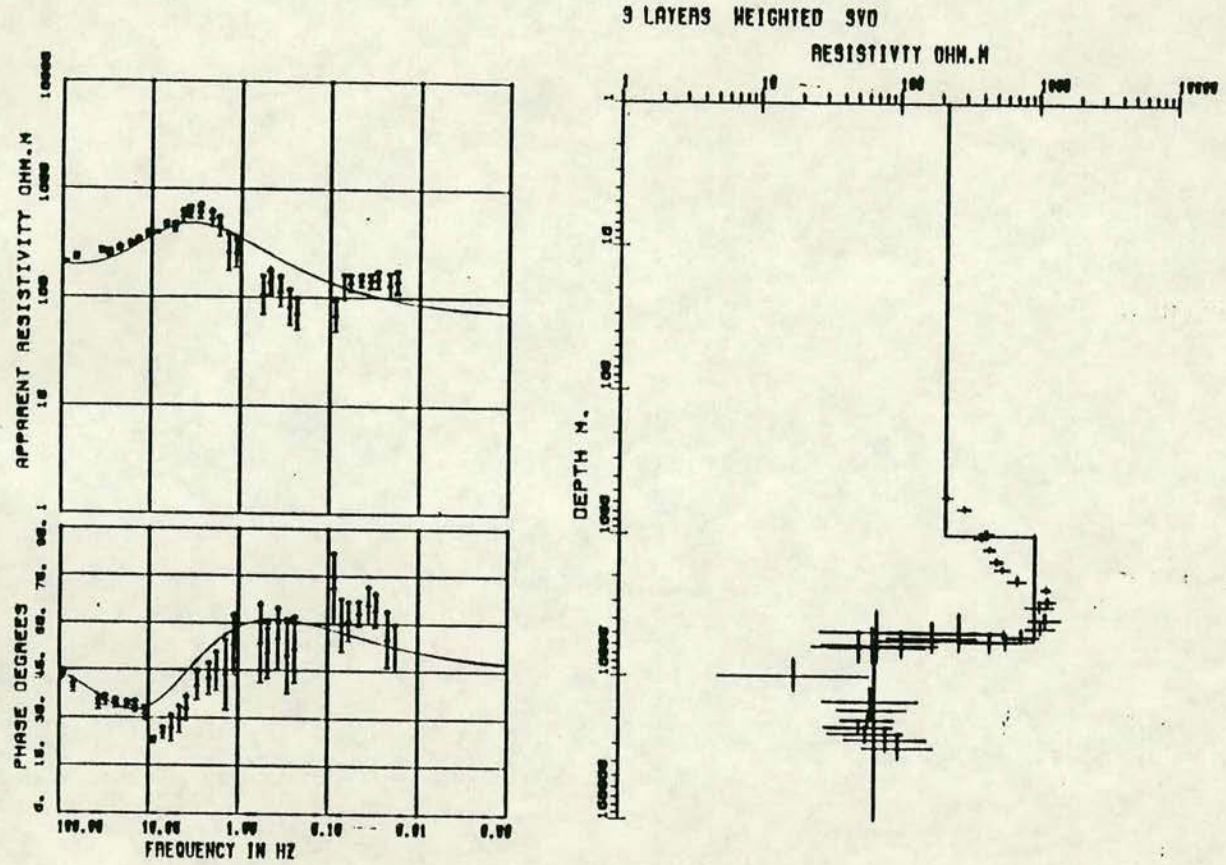

1D MODEL FOR SITE 502C INVARIANT

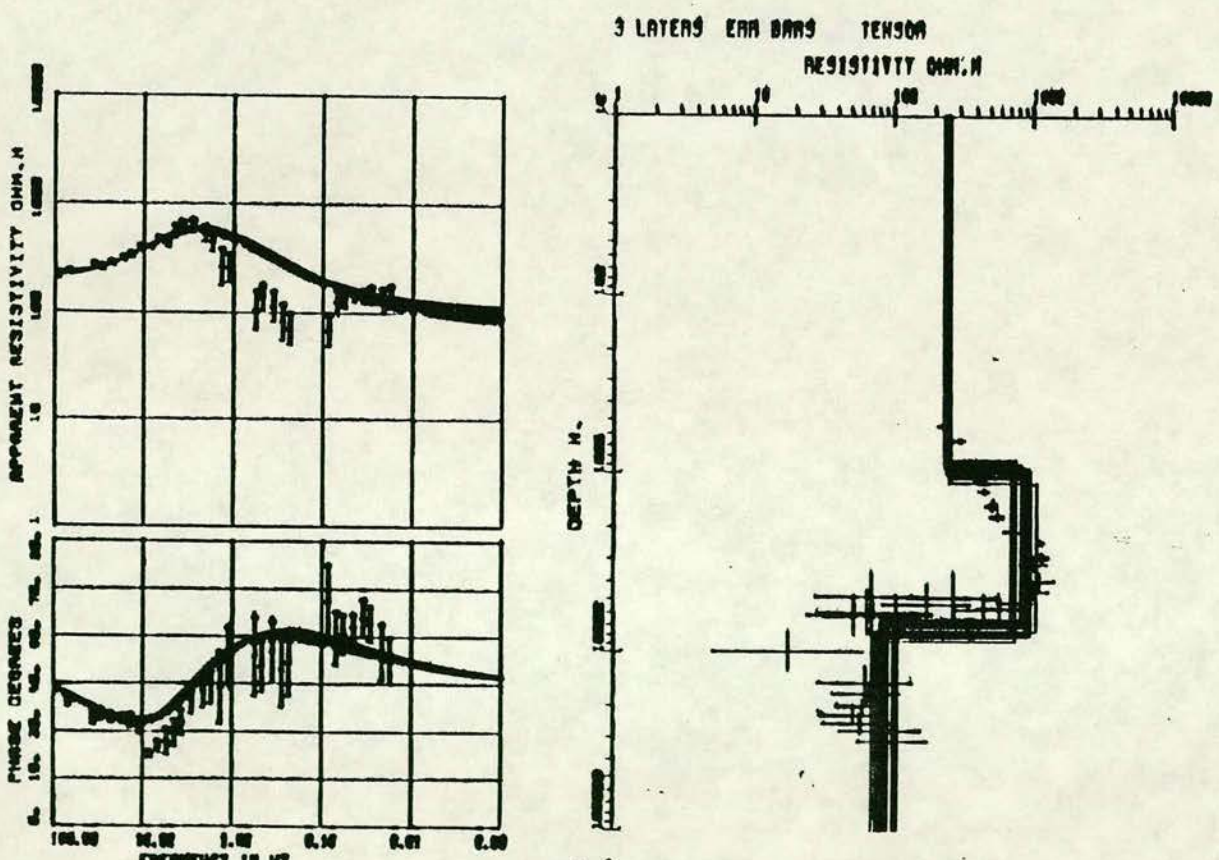

BEW

f

1D MODEL FOR SITE 505C INVARIANT

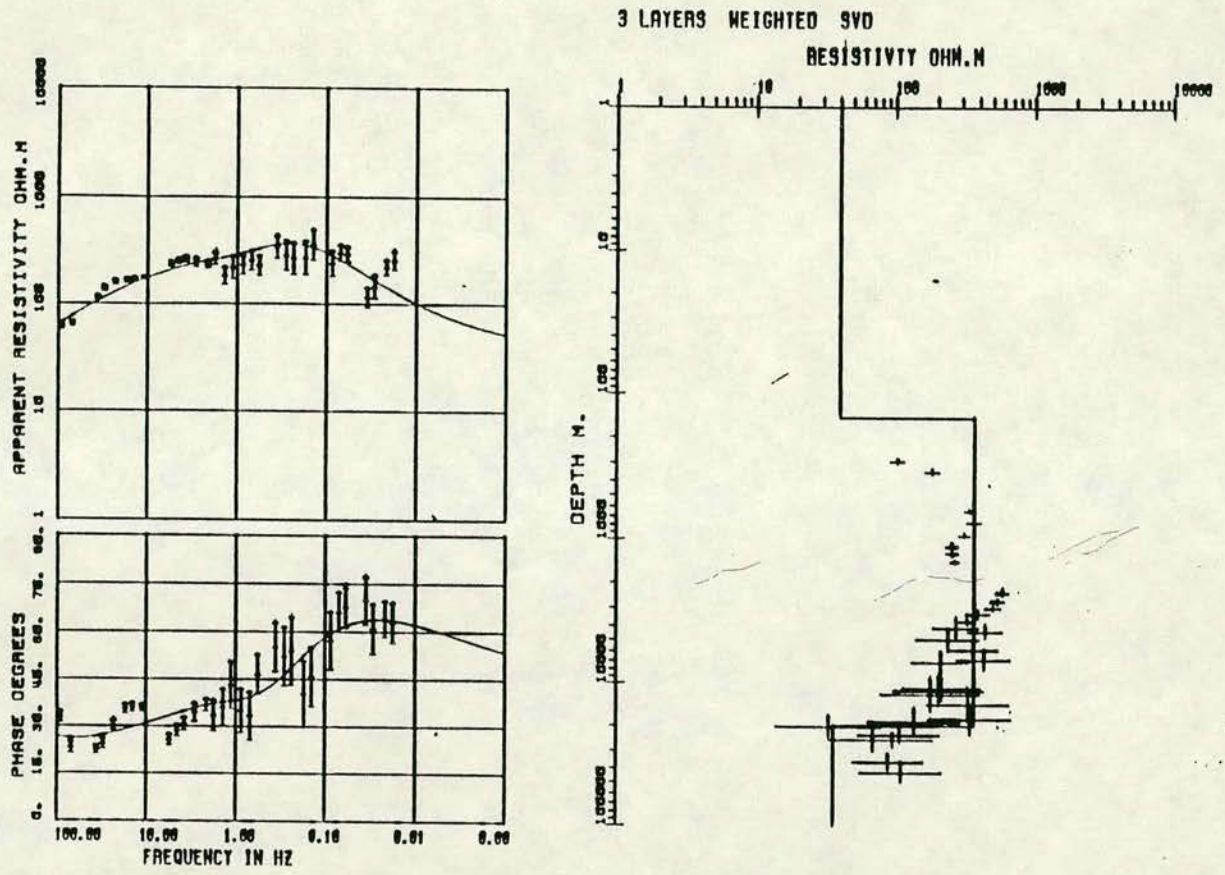

1D MODEL FOR SITE 505C INVARIANT

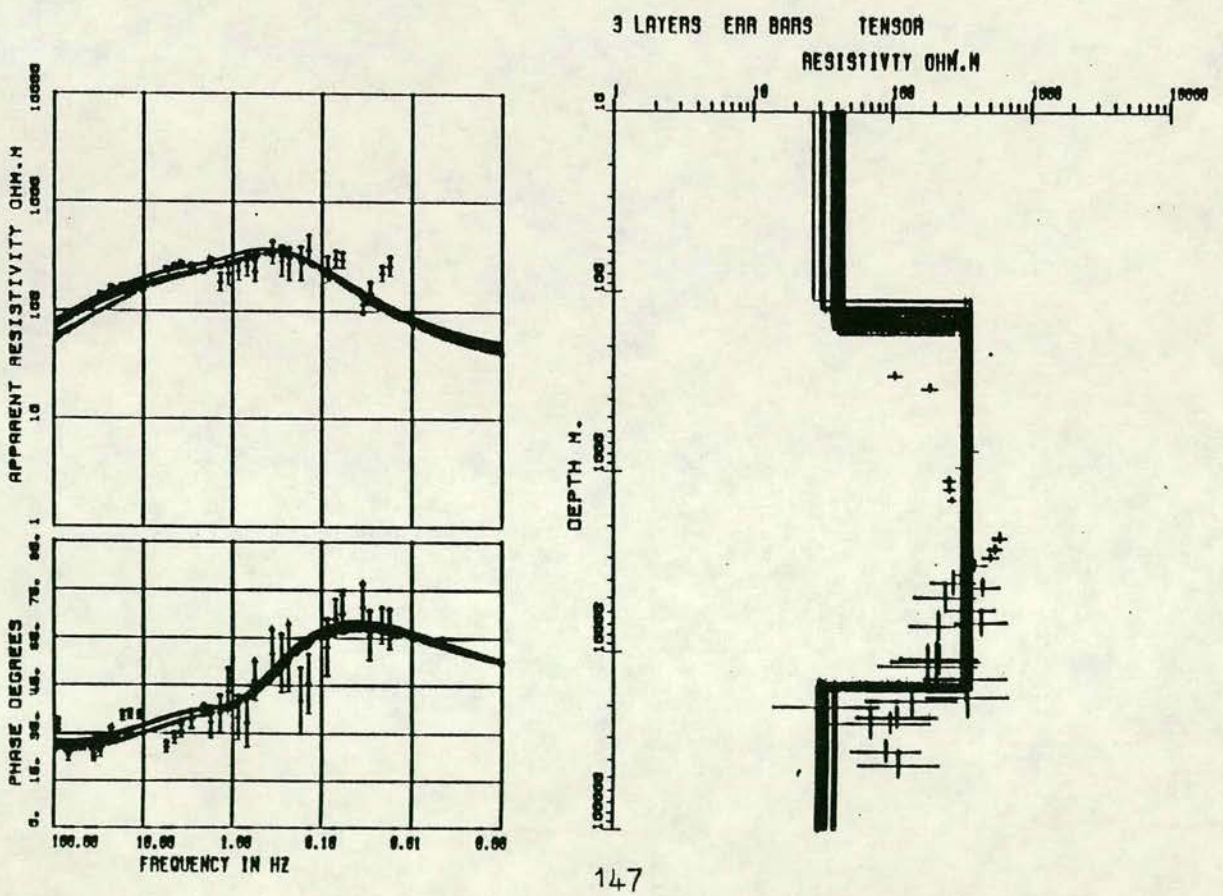

GIB

1D MODEL FOR SITE 509C INVARIANT

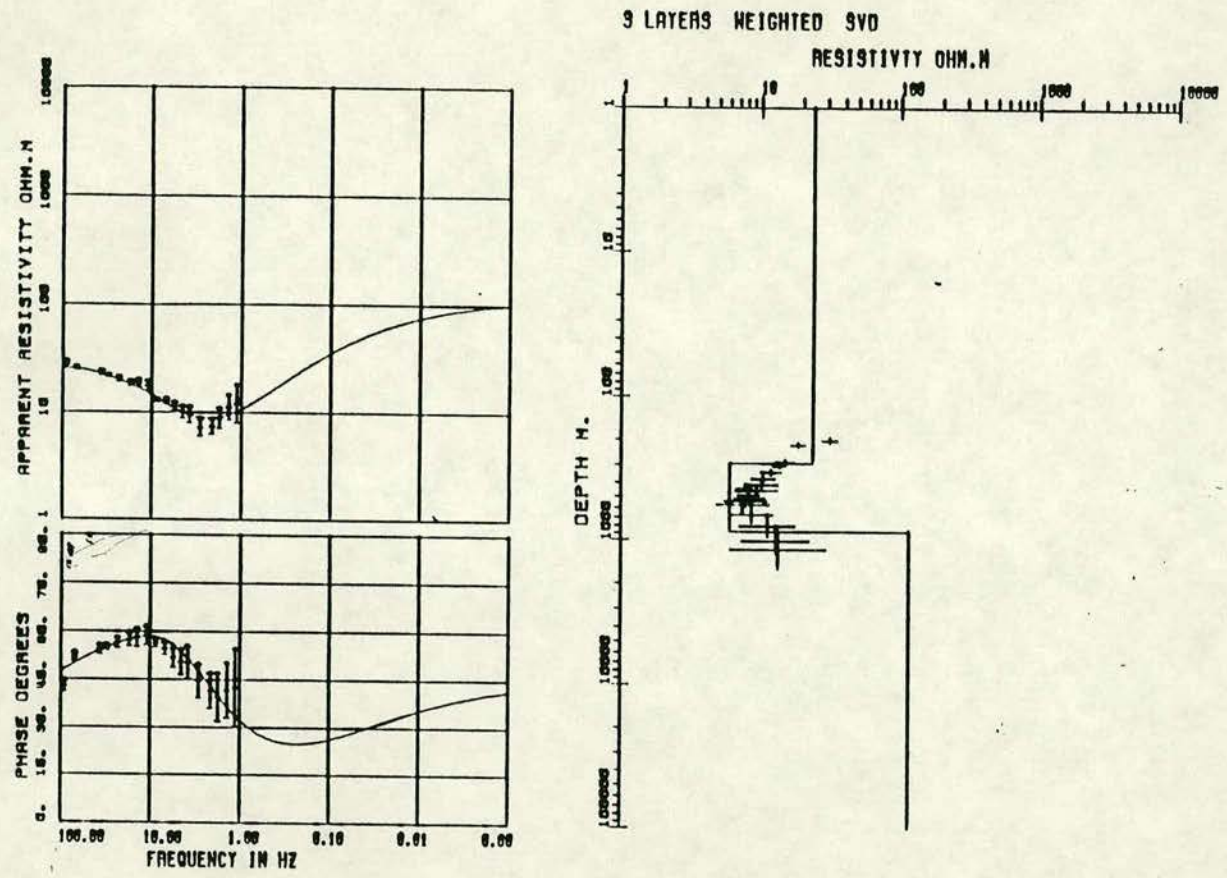

1D MODEL FOR SITE 509C INVARIANT

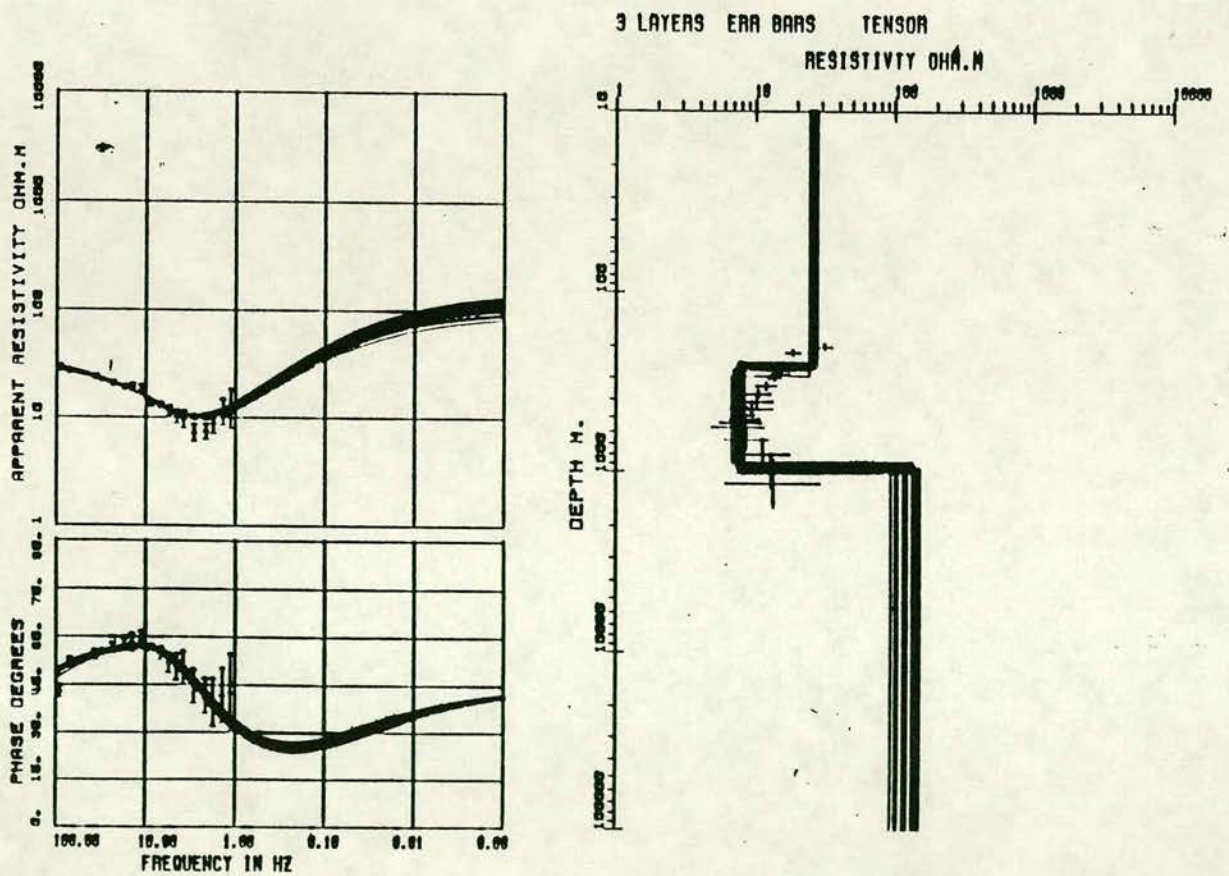

h

LAM

1D MODEL FOR SITE 506C INVARIANT

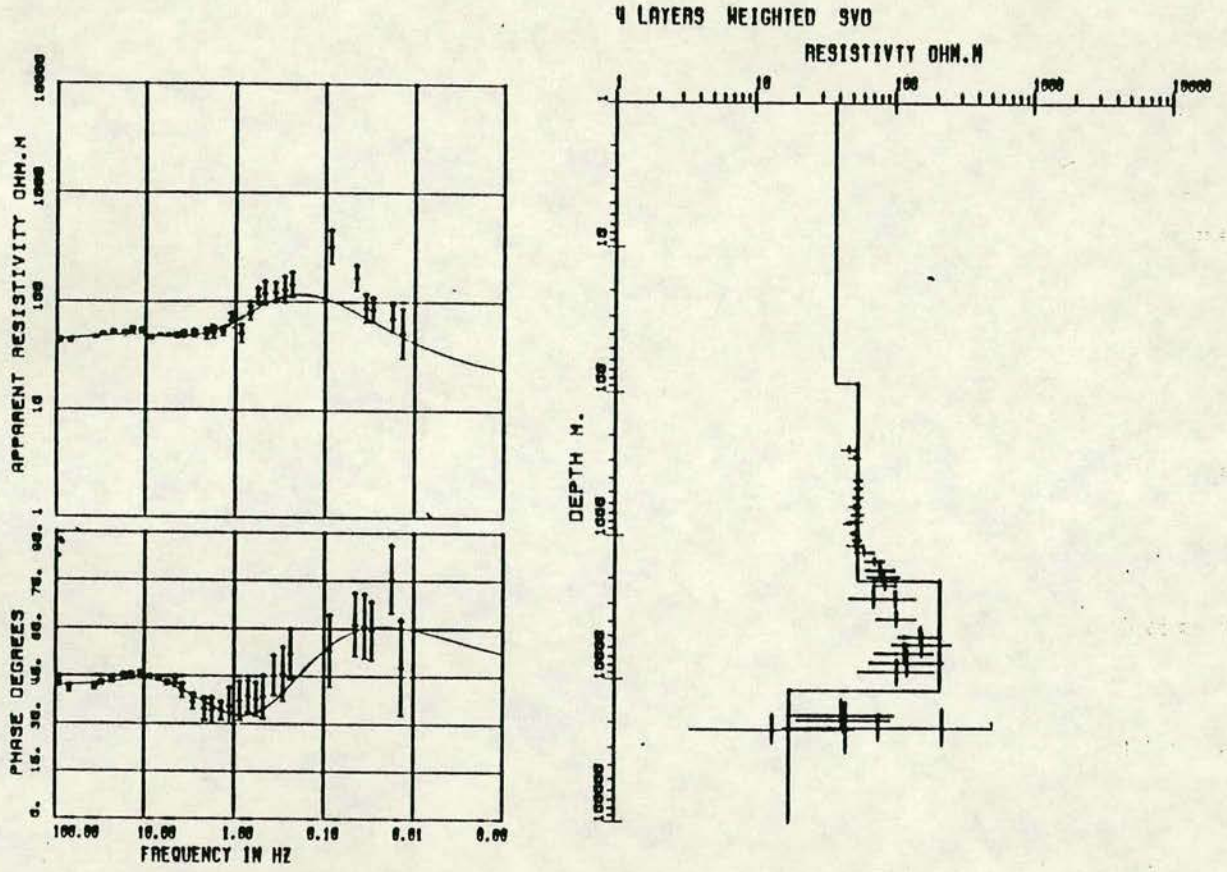

1D MODEL FOR SITE 506C INVARIANT

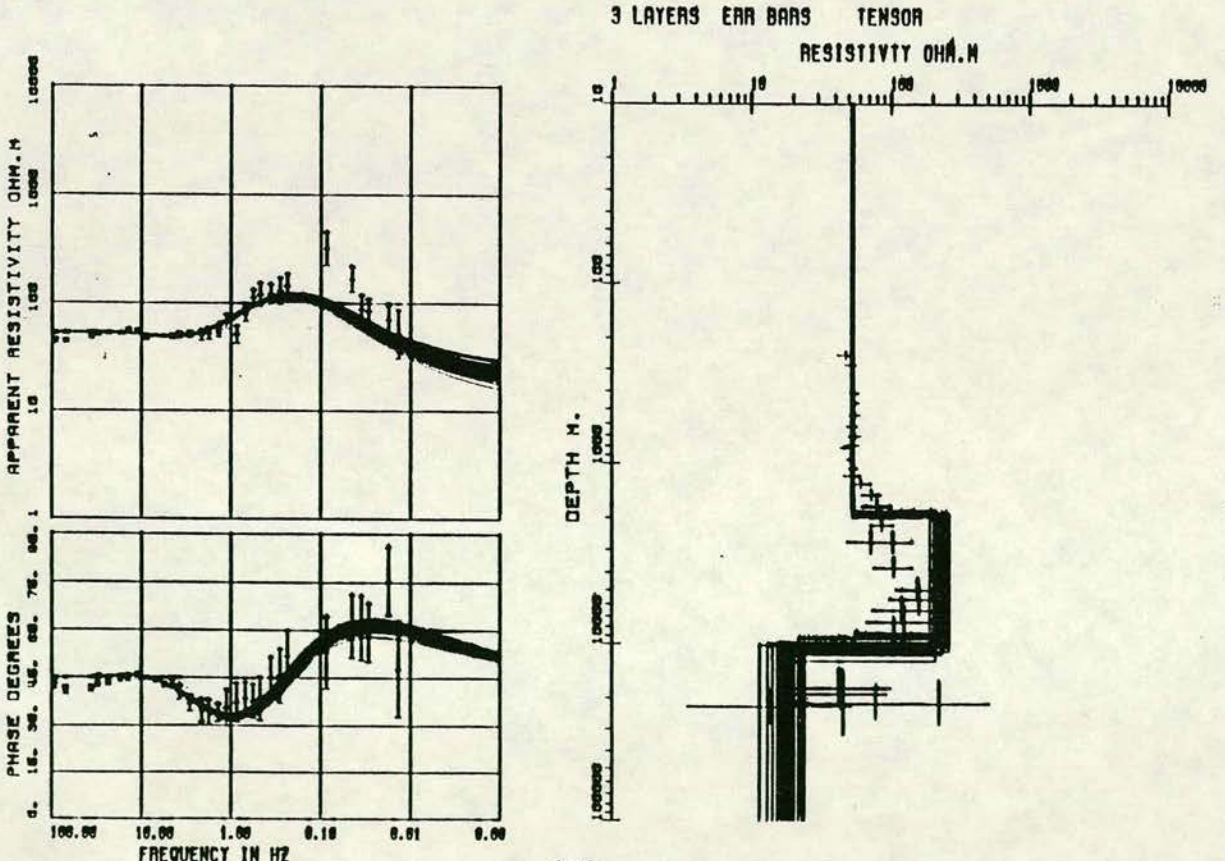

EDG

1D MODEL FOR SITE 606C INVARIANT

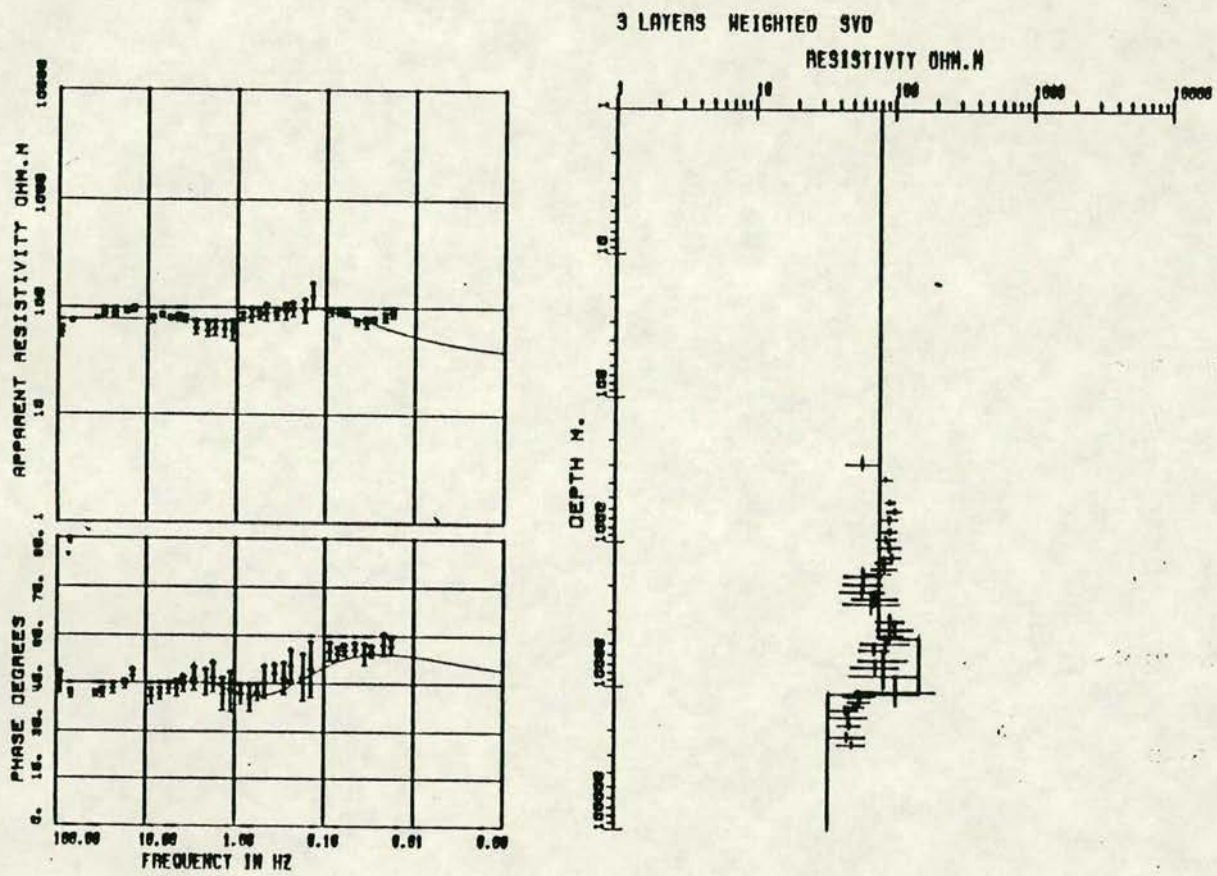

1D MODEL FOR SITE 606C INVARIANT

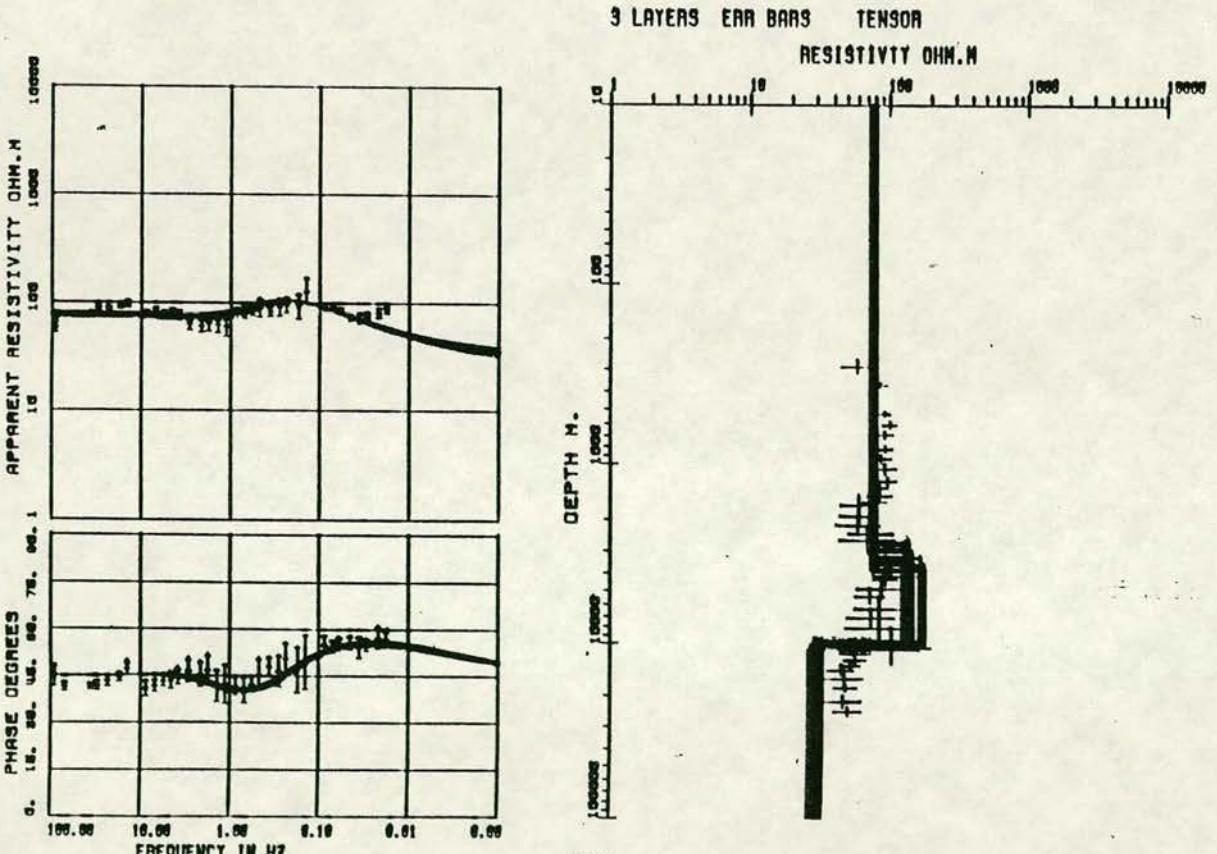

WHI

1D MODEL FOR SITE 508C INVARIANT

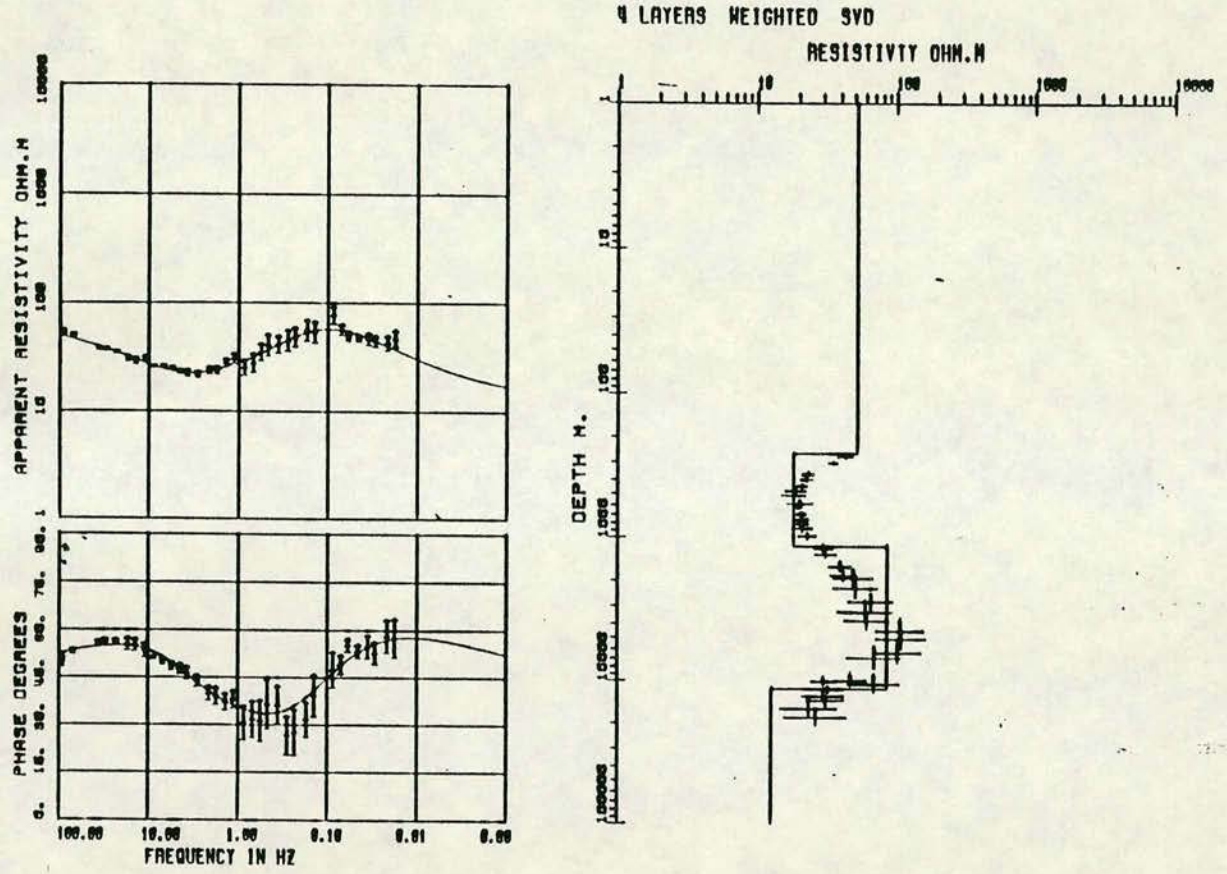

1D MODEL FOR SITE 508C INVARIANT

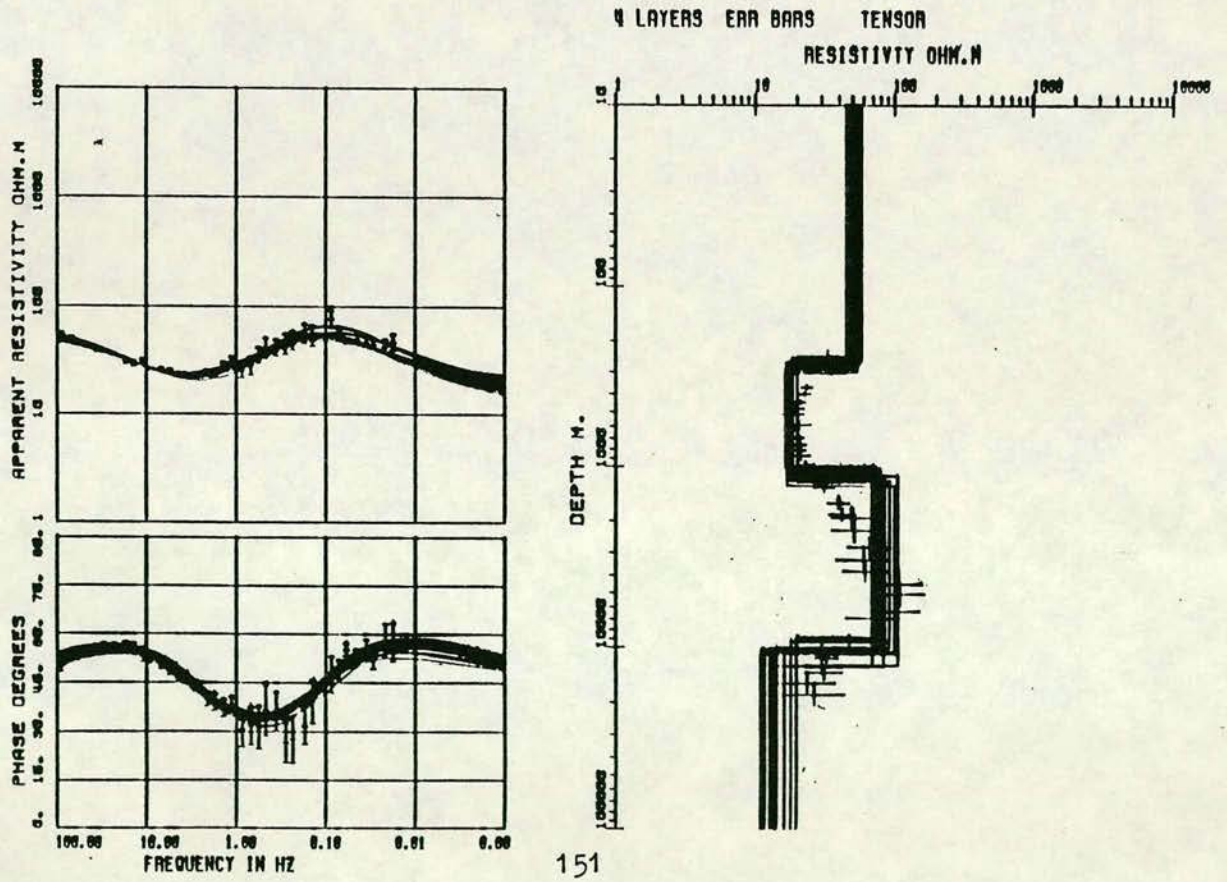

SIN

k 1D MODEL FOR SITE 604C INVARIANT

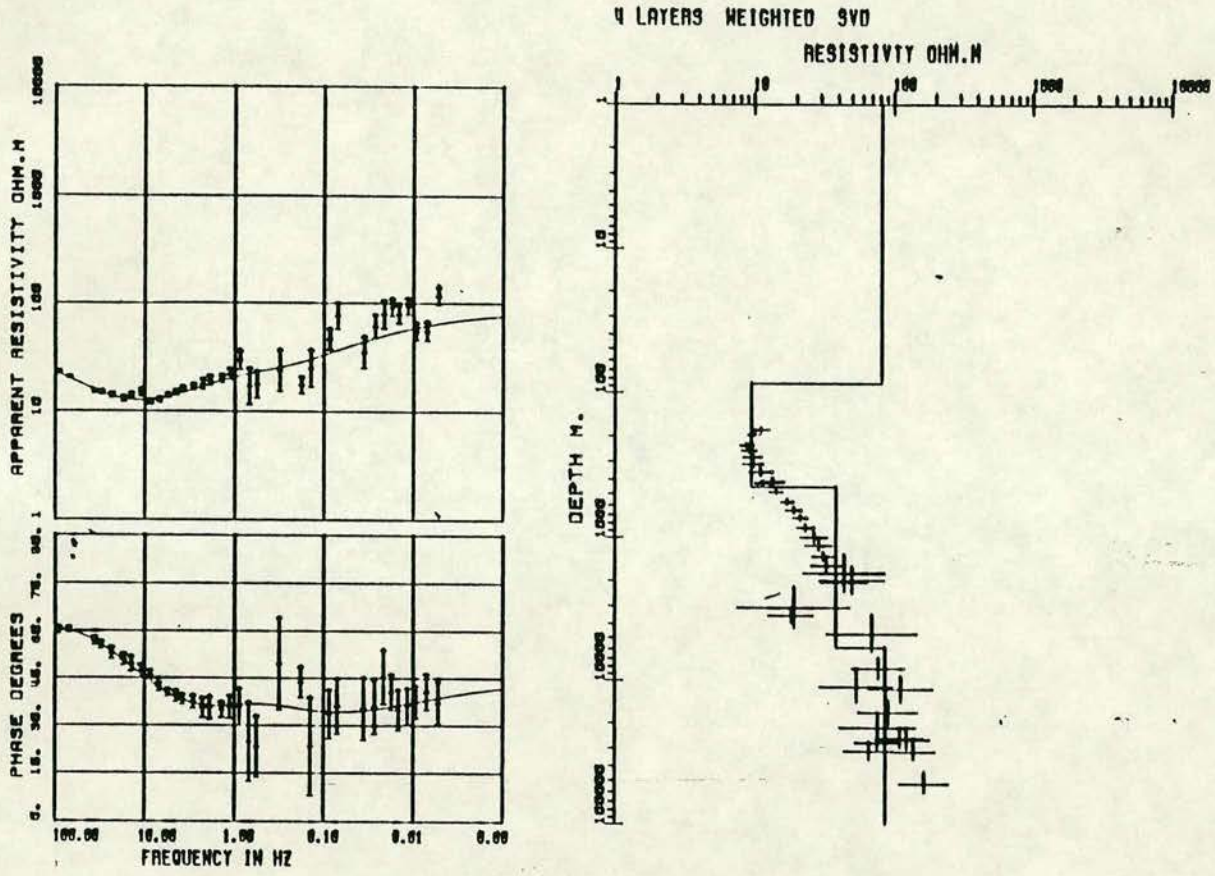

1D MODEL FOR SITE 604C INVARIANT

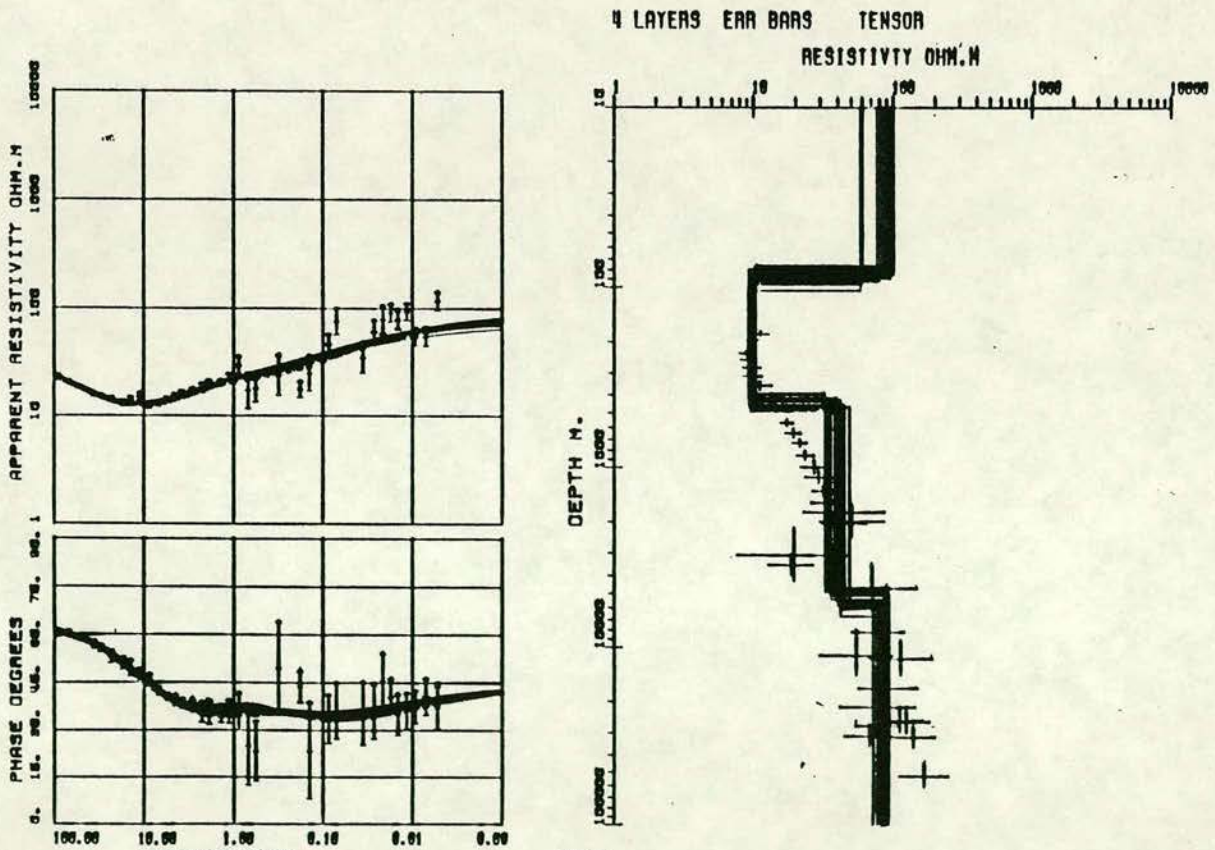

1D MODEL FOR SITE 603C INVARIANT

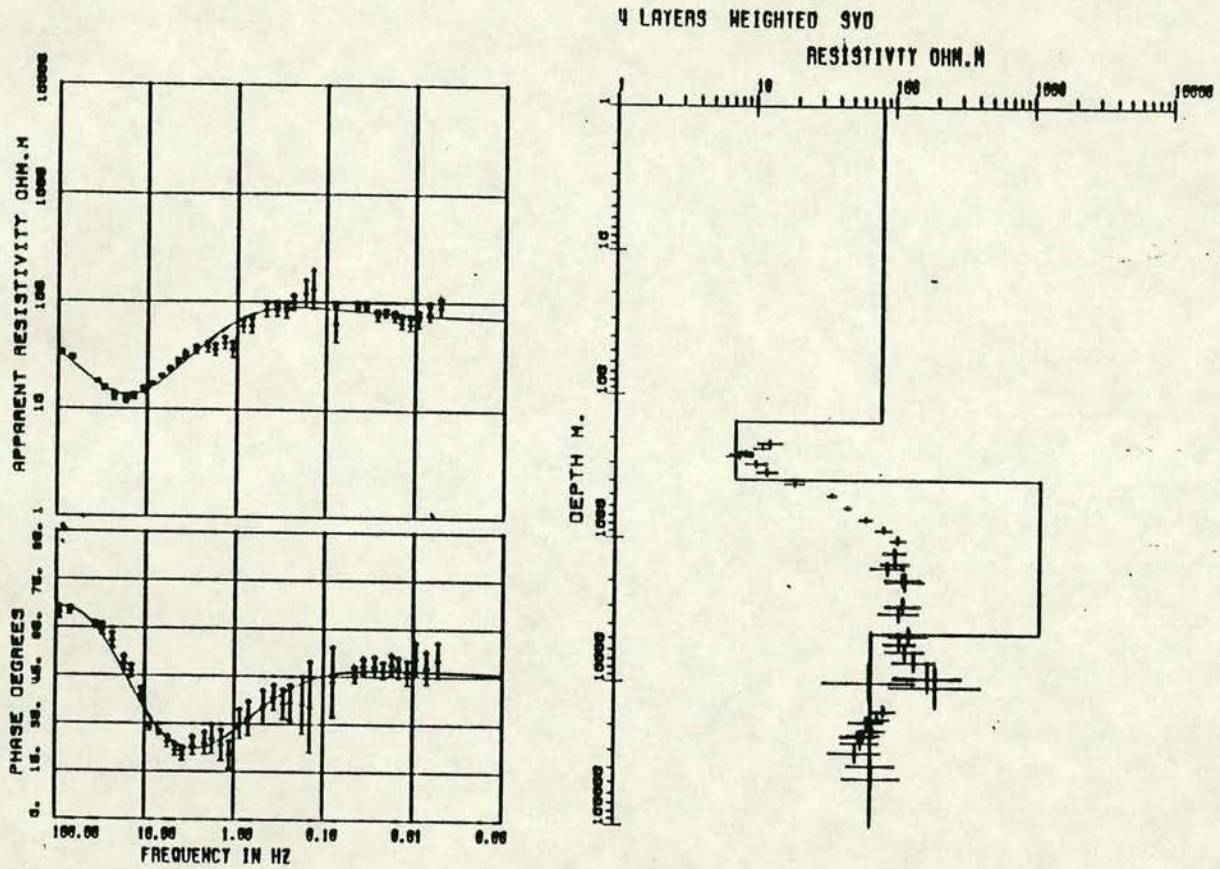

1D MODEL FOR SITE 603C INVARIANT

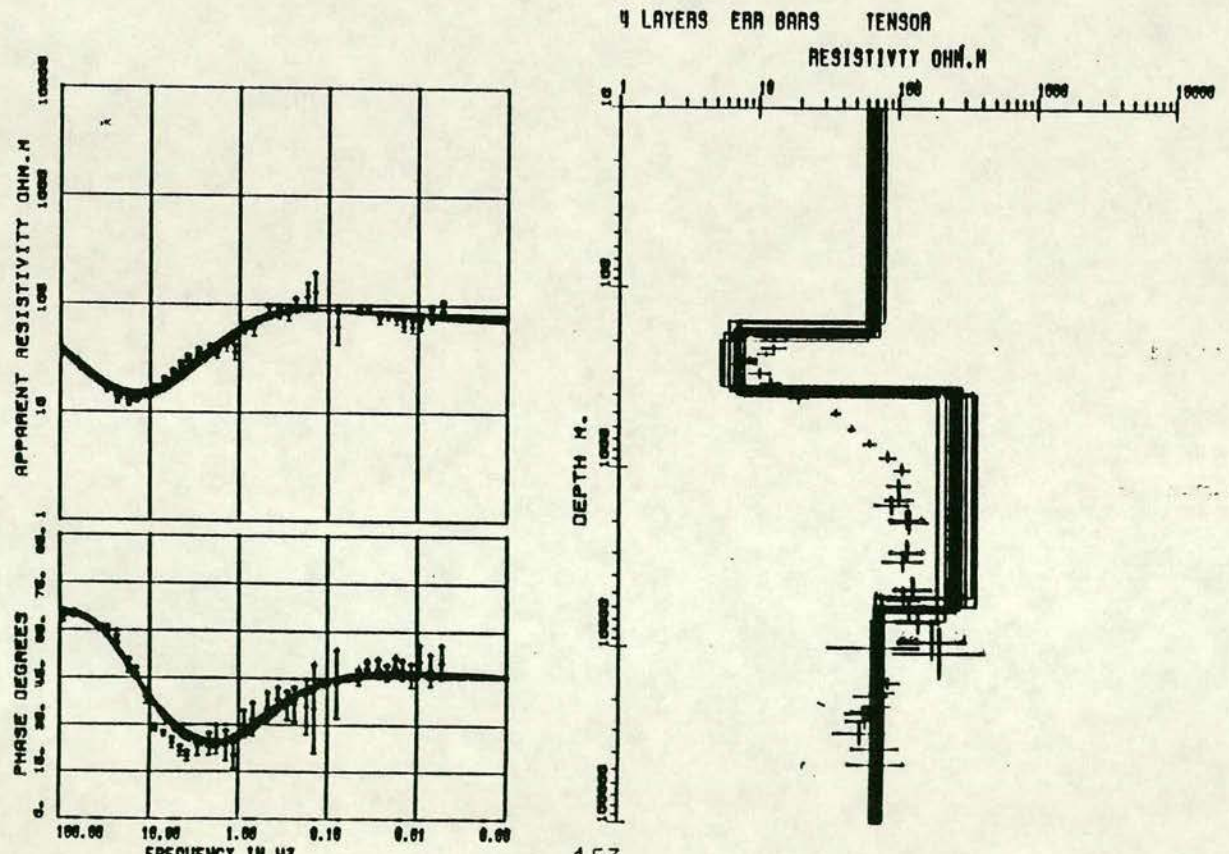

HIL

1D MODEL FOR SITE 512C INVARIANT

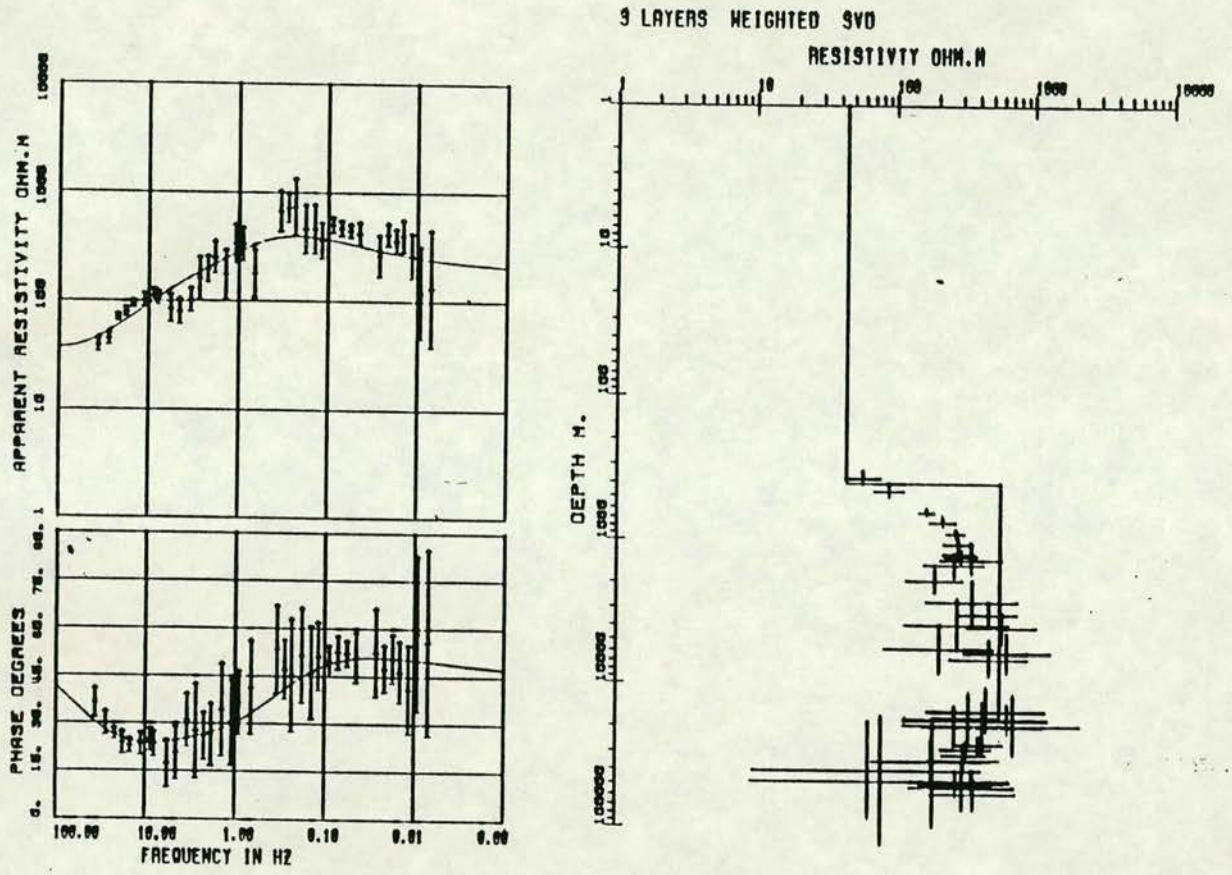

1D MODEL FOR SITE 512C INVARIANT

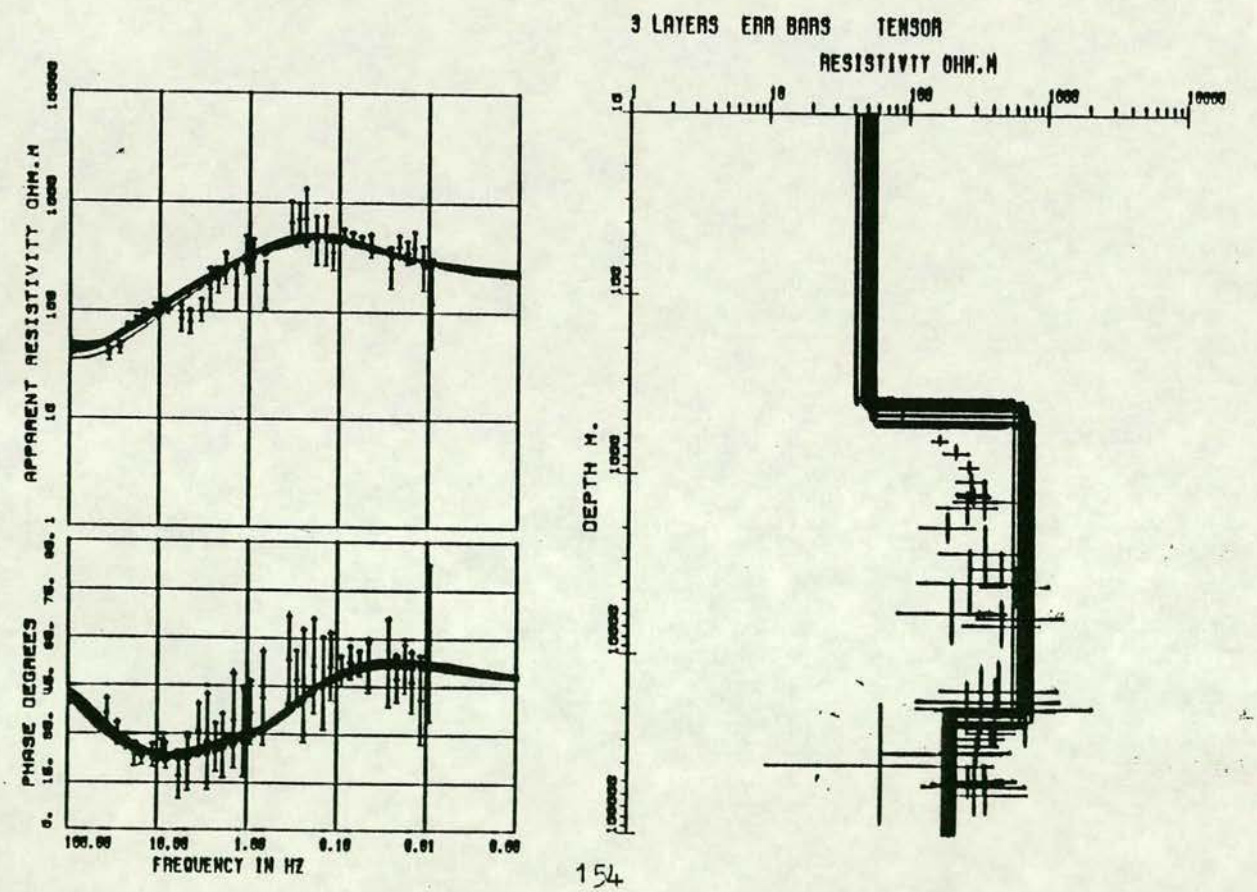

The general procedure adopted in carrying out these inversion schemes was as follows. In the modified Montecarlo-hedgehog (here afterwards simply called Montecarlo-hedgehog) scheme, for every resistivity and depth layer parameter assumed for the initial model, upper and lower bounds were given. The options used in the present study were i) to consider both the apparent resistivity and the phase values, ii) to allow all the initial model parameters to vary during iteration and iii) to use the mean square criterion as the basis of the misfit evaluation. For the linearised inversion, the apparent resistivity and phase data were additionally weighted such that they were inversely related to their associated errors.

The response functions were subjected to the inversion schemes several times by varying the number of layer parameters until a satisfactory misfit was achieved. The effect of each parameter on the response functions was also considered in altering the initial model which will be discussed later in this chapter. A greater number of layers was assumed for the initial model only when a satisfactory misfit could not be achieved with a smaller number. Adding extra layers to an initial model which already satisfactorily fitted the data was considered unjustified since it was equivalent to extracting more information than the responses actually contained. The problem of choosing the correct number of layers to achieve a minimum misfit has been discussed by Fischer and Le Quang (1982), who pointed out the dangers of modelling with an incorrect number. The effect of fictitious layers in a model has also been described by Jupp and Vozoff (1975) and is discussed again in later sections of this chapter.

For all the stations a satisfactory misfit (see table 6.1) was achieved with 3 or 4 layer models. At some sites, it was found that a three layer model could satisfy the apparent resistivity data alone but the phase misfit demanded another layer. This was observed for Cappercleuch station (station code = 514). It was also difficult on some occasions to choose the number of layers for the initial model because of the small apparent resistivity gradient. In such a situation, (eg. Edgesgreen, station code = 606) the phase response function played an important role in deciding the number of layers. At a station, such as the one near Bewcastle (Station code = 505), the model depth to the mid-crustal conductor differs by about 5-10 km. from that for the adjacent station, Lampert (Station code = 506). Since the dimensionality index

Table 6.1

List of station names and codes with mean power error between computed and observed values in 1-D model fit.

STA.	CODE	MEAN PERCENT ERROR		
		MONTECARLO -HEDGEHOG IMPED.	LINEAR INVERSION	
			RESIS.	PHASE
DZR	515	15	22	14
CAP	514	9	13	17
SMR	607	29	35	45
CRK	503	16	31	21
CWR	502	28	38	30
BEW	505	22	24	21
LAM	506	11	26	20
EDG	606	8	13	10
WHI	508	10	8	11
SIN	604	14	26	19
GIB	509	7	9	12
ROO	603	11	17	11
HIL	512	21	34	18

for Bewcastle had not indicated strong two dimensionality this difference requires further examination. It can be explained, however, by comparing ρ_{xy}, ρ_{yx} curves in Fig. 4.9f. The apparent resistivity ρ_{yx} is shifted upwards and is parallel to the ρ_{xy} apparent resistivity curve, while the phase curves for the two orthogonal directions are approximately identical. This type of distortion is now popularly known as the 'Static shift'; it arises from the presence of shallow surface heterogeneities near the observational location. Various procedures have been suggested for its correction (Berdichevisky et al , 1980, Moroz, 1985, 1985 and Jones 1987b). From the above discussion, it is clear that the phase responses play a significant role in modelling data at sites where this type of distortion is observed.

The computational time for the linearised inversion is 80% less than that for the Montecarlo–Hedgehog scheme. Moreover, the resolution of the model parameters derived from the linearised inversion scheme can be studied using the parameter sensitivity matrix 'J'. The details of this analysis are discussed later in this chapter.

In figures 6.6 and 6.7, the models resulting from the two inversion schemes have been collated and plotted for the traverse using a log depth scale. From these figures, the significant features for Southern Scotland are: a) a surface layer of about 200–1000 Ohm.m. to a depth of about 1 km., followed by a more resistive layer of the order of 500–1000 Ohm.m. to a depth of about 5–10 km. and then a conducting layer of about 20–100 Ohm.m. below the stations 503 (CRK) and 502 (CWR) and b) a highly conducting layer of about 25–30 Ohm.m and 2–3 Ohm.m. from a depth of about 3 to 3.5 km. near Cappercleuch station (Station code = 514). The Northern England stations showed a) a highly conducting surface layer with a resistivity of about 10–80 Ohm.m. and thickness increasing from about 0.5 km. near Hill End (station code = 512) to about 3 km. near Edgesgreen (station code = 606) and thinning to about 0.5 km. near Gibstown (station code = 509); b) a moderately resistive layer, of the order 150–300 Ohm.m., below the Northumberland Basin to about 10 km. overlying a second conducting layer of about 10–30 Ohm.m, and c) near the Alston Block, (station codes = 603 and 512) a comparatively resistive layer of 300–1000 Ohm.m to a depth of about 5 – 10 km. . The importance of these model parameters in relation to the geology and tectonics of the region will be discussed in chapter 8.

FIGURE 6.6

Compilation of one dimensional modelling results of invariant apparent resistivity and phase, obtained from the linearised inversion scheme for all stations for the traverse. Depth values are plotted on log scale; SUF= Southern Uplands Fault.

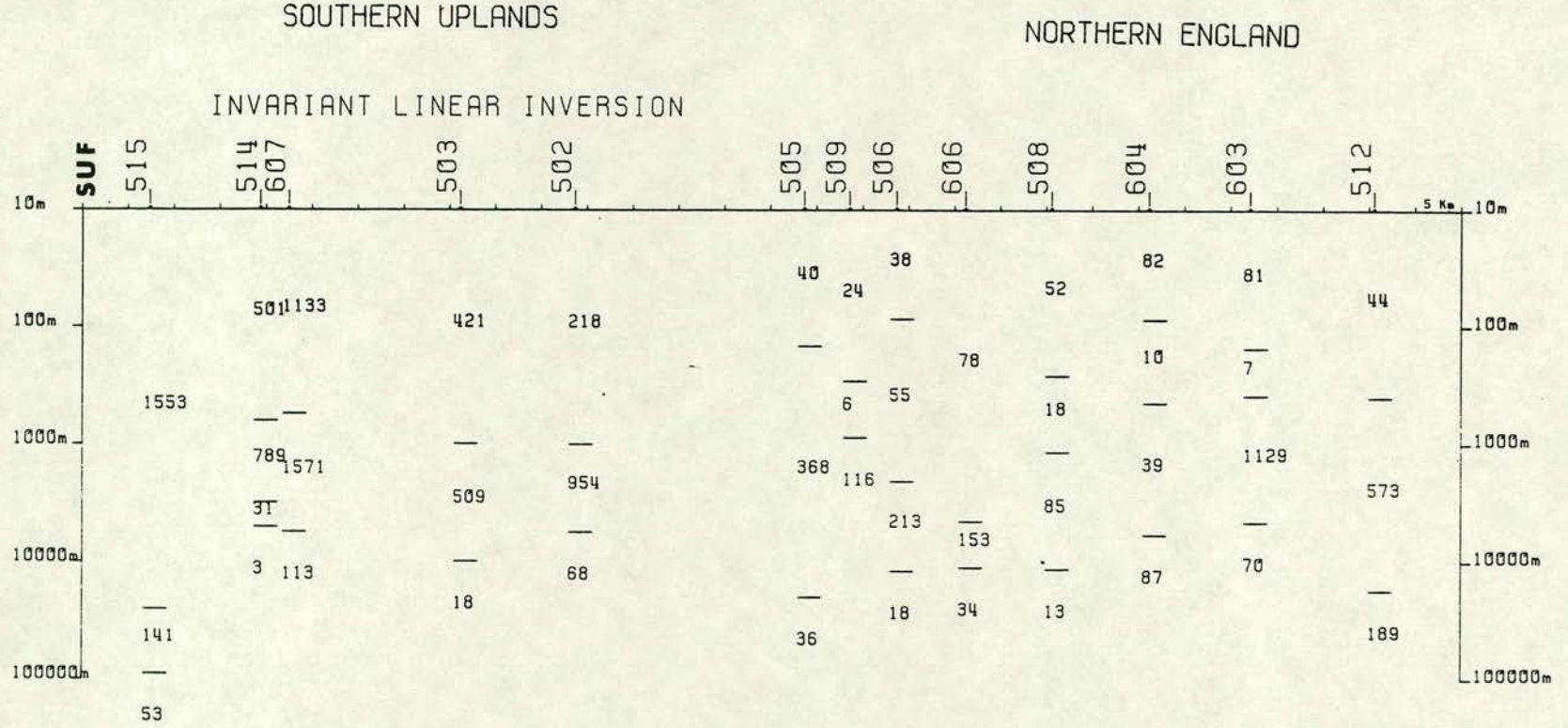
SOUTHERN UPLANDS
NORTHERN ENGLAND
INVARIANT LINEAR INVERSION
SUF
515
514
607
503
502
505
509
506
606
508
604
603
512
5 Km
10m
100m
1000m
10000m
100000m
1553
501
1133
421
218
789
1571
509
954
31
3
113
68
18
141
53
40
24
38
52
82
81
44
78
10
7
6
55
18
368
116
39
1129
213
85
573
153
87
70
34
13
36
189

FIGURE 6.7

Compilation of one dimensional modelling results of invariant apparent resistivity and phase, obtained from modified Montecarlo inversion scheme along the traverse. Depth scale is plotted on log scale; SUF= Southern Uplands Fault.

SOUTHERN UPLANDS

NORTHERN ENGLAND

INVARIANT MONTECARLO INVERSION

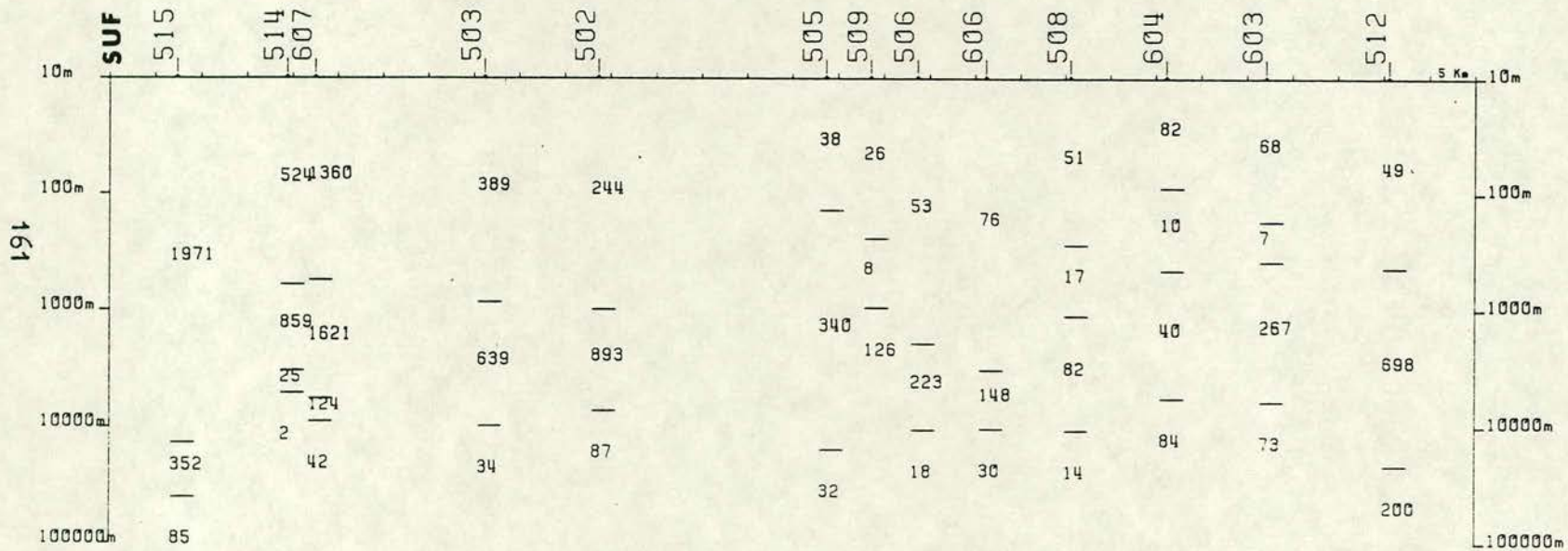

Although dimensionality index parameters supported the presence of dominantly one dimensional structures below the stations along the traverse, there was at a few adjacent stations a significant difference in the depths of the mid-lower crustal conductor. To study these lateral variations all the data sets were rotated 85° east of north i.e., along the average regional geological strike of Northern England and Southern Scotland and the resulting data sets (in E-pol and H-pol directions) were modelled using a linearised inversion (Jupp and Vozoff 1977) scheme. The results obtained are presented for the whole traverse in figures 6.8 (E-pol results) and 6.9 (H-pol results). E-pol data sets are known to be less distorted than H-pol data sets when the electric field is parallel to the strike (Schwarz et al 1984). From the E-pol section it can be seen that there is a significant improvement in the continuity of the depth parameters especially near Bewcastle (Code = 505), where a depth of about 10 km. to the mid crustal conductor is obtained - this is now compatible with its values at the adjacent station (LAM). It may be noted that for the same station in the H-pol section a depth of about 20 km. is observed - nearly the same as the result obtained from the invariant data. Thus it can be said that though invariant apparent resistivity-phase data can provide a good approximation to the two dimensional earth structure, in this study modelling of the E-pol data sets is likely to be more useful when the data sets are more anisotropic.

6.4. The joint inversion of the D.C and MT measurements

As mentioned in section 6.4, it is known that the magnetotelluric method can more easily in detect a thin conducting layer than a resistive one. D.C. resistivity methods are, however, equally responsive in both these situations, but longitudinal conductance is usually more resolvable for thin conducting layers and transverse resistance more resolvable for thin resistive layers. As a result of the difficulties inherent in modelling the results of a single sounding technique a joint inversion of D.C resistivity and magnetotelluric methods has been proposed by Vozoff and Jupp (1975).This has been applied in the present study for three stations in Northern England. In this scheme, the weighting of the influence of a particular earth model on these two (MT and DC) different type of earth response functions and the combination of the data sets are important. The MT and DC data measure

FIGURE 6.8

Compilation of one dimensional modelling results of E-pol apparent resistivity and phase for all stations along the traverse using the linearised inversion scheme. Depth scale is plotted on log scale; SUF= Southern Uplands Fault.

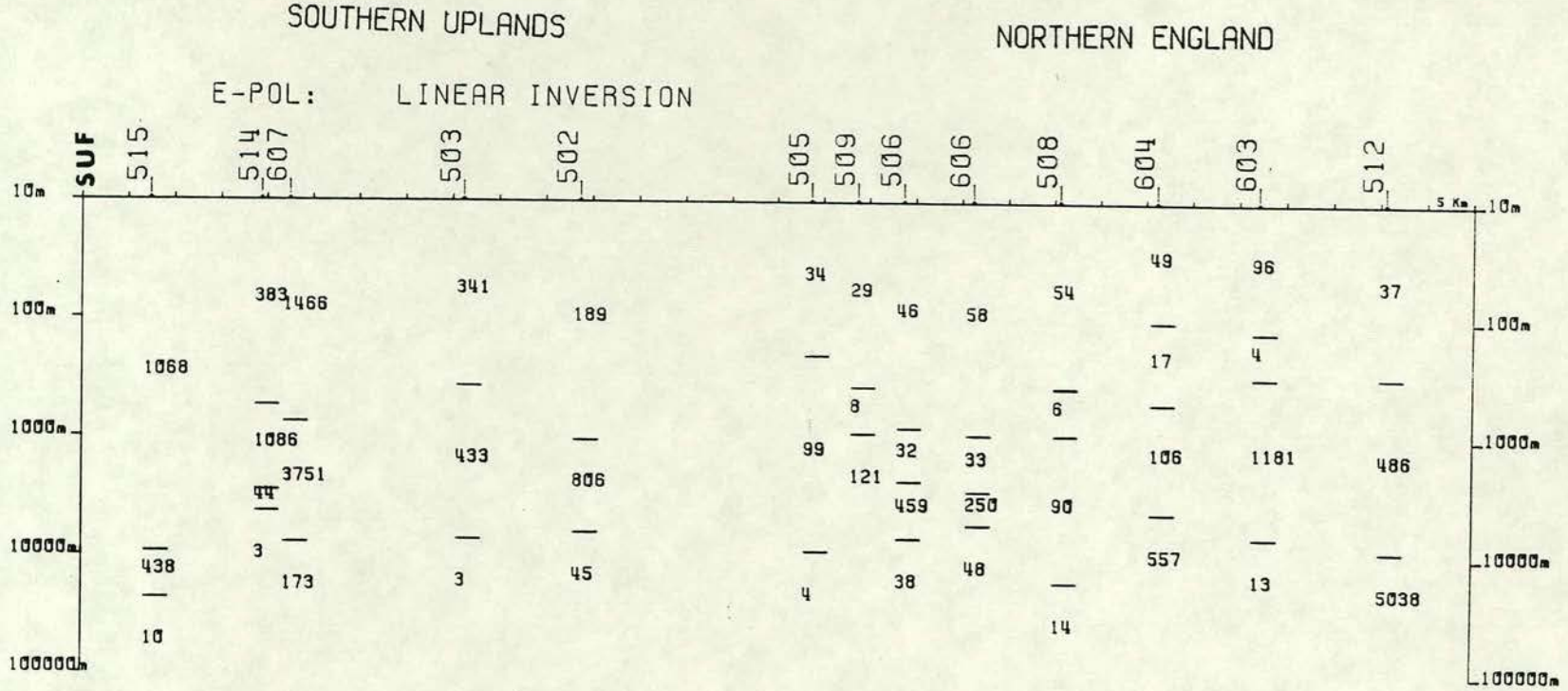
SOUTHERN UPLANDS
NORTHERN ENGLAND
E-POL: LINEAR INVERSION
SUF
515
514
607
503
502
505
509
506
606
508
604
603
512
5 Km
10m
100m
1000m
10000m
100000m
1068
383
1466
1086
3751
44
3
438
173
10
341
433
3
189
806
45
34
29
46
58
54
49
96
37
17
4
8
6
99
32
33
106
1181
486
121
459
250
90
557
13
5038
4
38
48
14

FIGURE 6.9

Compilation of one dimensional modelling results of H-pol apparent resistivity and phase for all stations along the traverse using the linearised inversion scheme. Depth scale is plotted on log scale; SUF= Southern Uplands Fault.

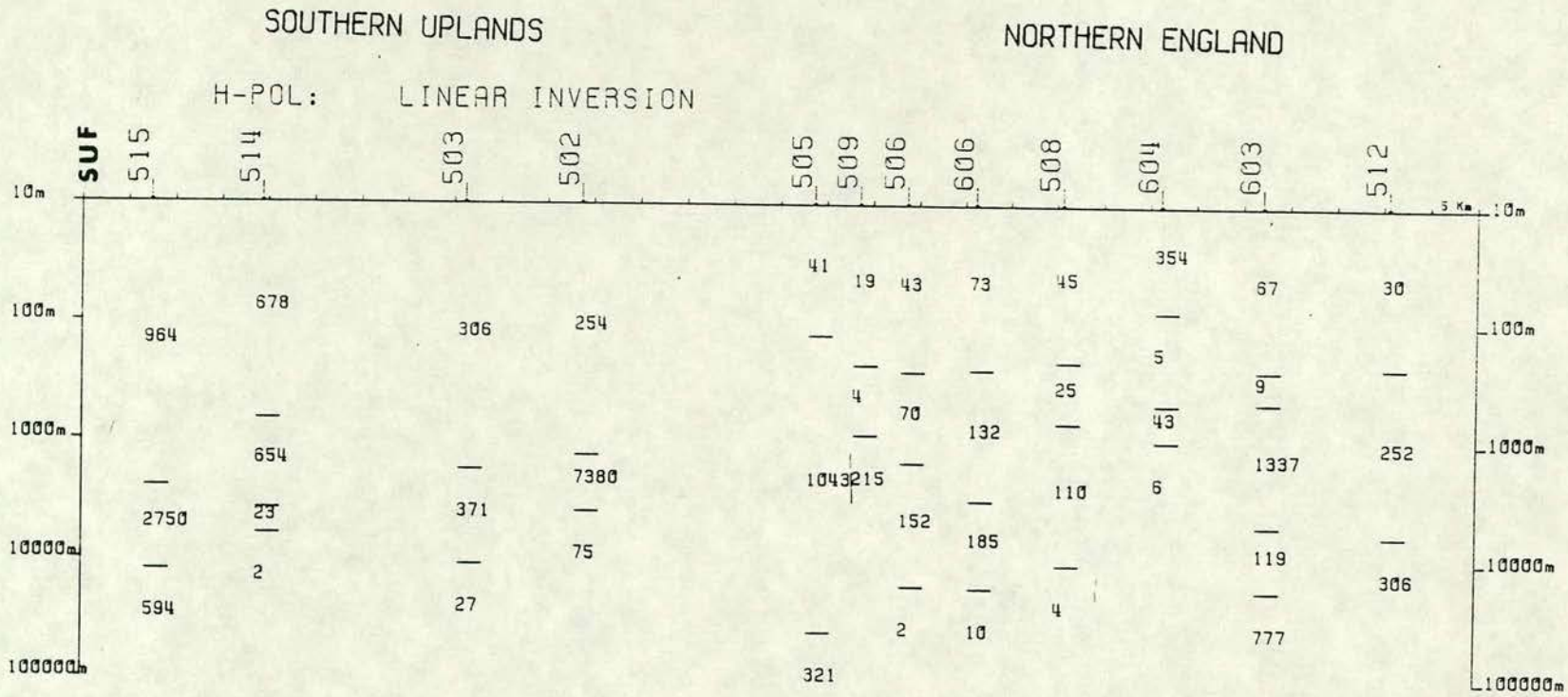
SOUTHERN UPLANDS
NORTHERN ENGLAND
H-POL: LINEAR INVERSION
SUF
515
514
503
502
505
509
506
606
508
604
603
512
5 Km
10m
100m
1000m
10000m
100000m
964
678
654
2750
23
2
594
306
371
27
254
7380
75
41
19
43
73
45
354
67
30
4
70
132
25
5
9
43
1043
215
1337
252
152
110
6
185
119
306
2
10
4
777
321

earth responses to two different inputs through quite different physical processes but their outputs, however, have some similar features. For example, the apparent resistivity curves are asymptotic to surface resistivity values, at shorter spacings (DC) and shorter periods (MT) and also asymptotic to the basement resistivity, at larger spacings (DC) and longer periods (MT). To combine the two data sets correctly, the separate 'parameter influence' (or Jacobian) matrices need to be balanced.

With regard to the present study a series of twelve deep D.C resistivity sounding data had previously been acquired by the Earth Sciences Department of Leeds University as part of several M.Sc. projects, and later compiled in a Ph.D., thesis (Roxis, 1984). These soundings were carried out along an approximately NS traverse covering Northern England and Southern Scotland with a square array configuration and electrode spacing at most stations upto 1024m. The spacing was extended further using bipole-bipole measurements. At most of these stations the bipole-bipole measurements were affected by lateral effects and surface topography. In the present study, the equivalent Schlumberger electrode spacings have been considered as described by Habberjam and Thanassoulas (1979).

Three of the MT stations, Lampert (Station code = 506), Edgesgreen (Station code = 606) and Rookhope (Station code = 603) were located in close vicinity (1-2 km.) to D.C sounding stations. The elevation differences and the horizontal distances between the D.C and MT stations can be seen in Table 6.2. It has been assumed that the geology is uniform between MT and DC stations.

Unfortunately, at two of these stations the maximum depth to which information can be obtained from the D.C data (Roxis 1984) hardly overlaps with that which can be obtained from the MT data as deduced from the Bostick plots. However, there is good overlap of resistivity information between D.C station, S1 and MT station, 603 located near Rookhope. Moreover, very near to the station 603 a deep bore hole was drilled to a depth of about 795m. and resistivity, S.P. and χ-ray logging data obtained. This station, thus provides useful data for a comparison of results. In the present study is the object was to approach the joint inversion problem with a priori information and then compare the resulting model with the bore hole

Table 6.2

Details of location of MT, DC and B.H. near Rookhope, N.England. Distance, elevation shown are with respect to the MT station.

Station Name	Code	Distance in km.	Elevation in meters.
Lampert	S4	1.1 SWS	10
Edgesgreen	S11	2.5 WSW	20
Rookhope	S1	2.2 NEN	-10
Rookhope	Bore hole	2.1 ESE	80

resistivity log.

The data sets for both the D.C and MT stations have been acquired in two perpendicular directions but in the joint inversion the mean apparent resistivity has been considered for the D.C data and the rotationally invariant apparent resistivity and phase for the MT data. The initial models chosen for the joint inversion were obtained by combining the model results of the individual methods. Since the parameters of the deepest layer (at about 10–20 km.) obtained from the MT data cannot influence the D.C data, these parameters were held fixed during the inversion. In figures 6.10 a, b and c, results of the joint inversion are presented for the three stations. A considerable mismatch between computed and observed data can be seen at the larger electrode spacings for the D.C resistivity stations S4 (Lampert) and S11 (Edgesgreen). The total misfit for these stations was found to be about 30%. It was observed that the model parameters obtained from D.C or MT data alone were considerably different from the results obtained from the joint inversion at both of these locations (Table 6.3).

Though the results obtained from the joint inversion for LAM and EDG locations were not very encouraging, some interesting comparisons can be made for Rookhope station between the present modelling results and those of various earlier investigations and the bore hole data. Moreover, this station is particularly significant from the geophysical point of view. The presence of the Weardale granite was predicted from Bouguer gravity (low) anomaly (Bott and Masson Smith 1957) and later proved by drilling (Dunham et al, 1965). At this location a number of earlier geoelectrical measurements had also been made and the resistivity models correlated with the bore hole data (Habberjam and Thanassoulas 1979, Novak 1981 and Roxis 1984). For example, Habberjam and Thanassoulas (1979) obtained reasonable agreement between computed and observed data when they used a model with the resistivity values and the thicknesses of the Great Limestone and Whin sill fixed to correspond with those of the bore hole. Constraining the bottom layer resistivity at 1500 Ohm.m., 1053 m. depth has been obtained for the Weardale granite from the ridge estimates for the D.C sounding data (Roxis, 1984). Constraining the depths by bore hole data and allowing the resistivity values to vary a good fit to AMT observations has been shown by Novak (1981).

FIGURE 6.10

Joint inversion of results of magnetotelluric and DC sounding showing the model fit with the data for- a) Magnetotelluric Station (code= 506) and DC sounding (Code = S4) near Lampert, b) Magnetotelluric Station (code= 606) and DC sounding (Code = S11) near Edgesgreen. and c) Magnetotelluric Station (code= 603) and DC sounding (Code = S1) near Rookhope.

a

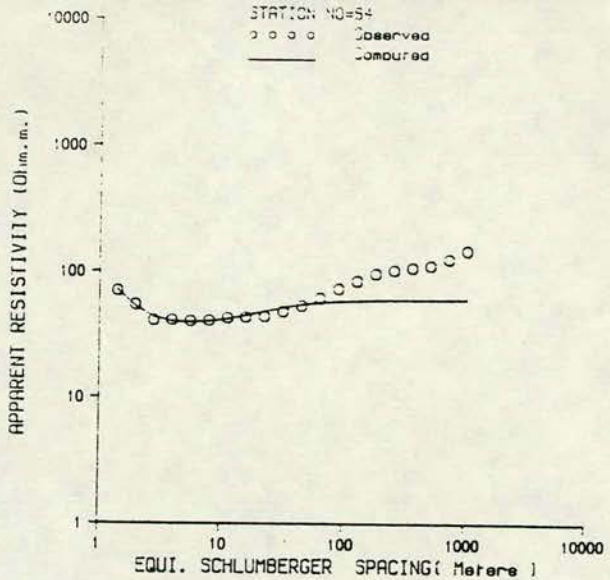

1D MODEL FOR SITE S06C INVARIANT

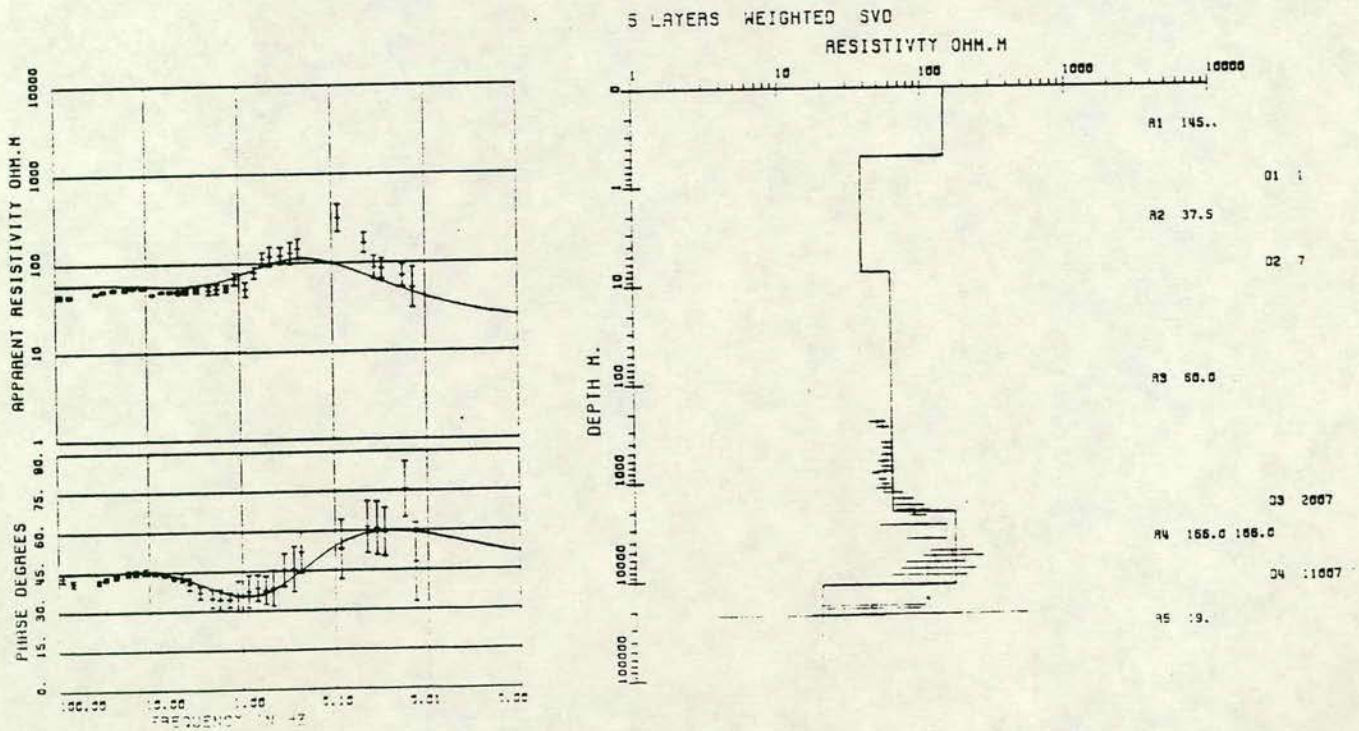

b

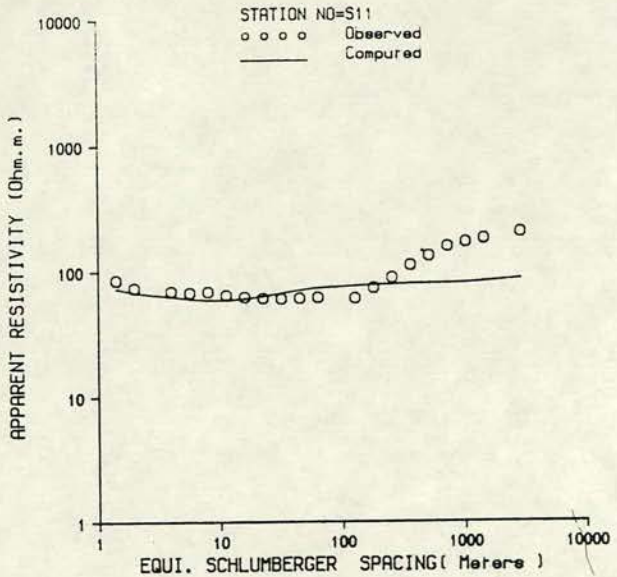

1D MODEL FOR SITE 606C INVARIANT

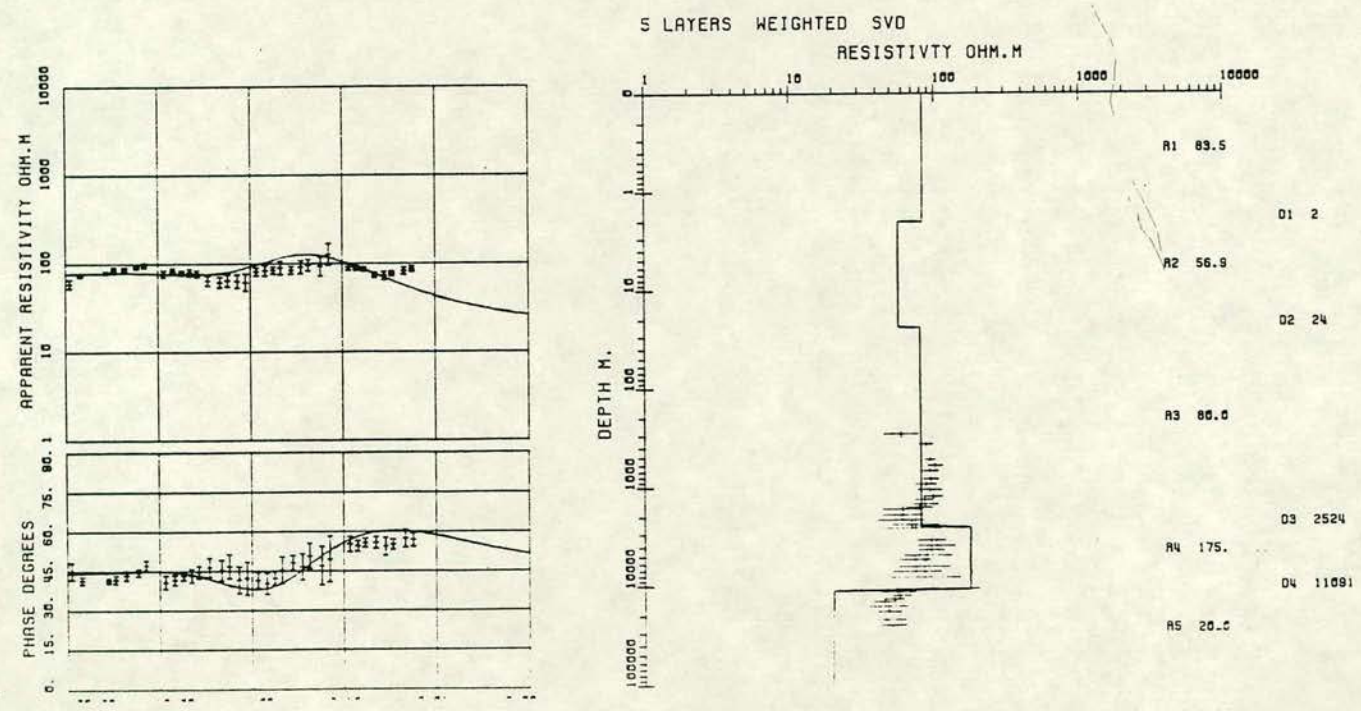

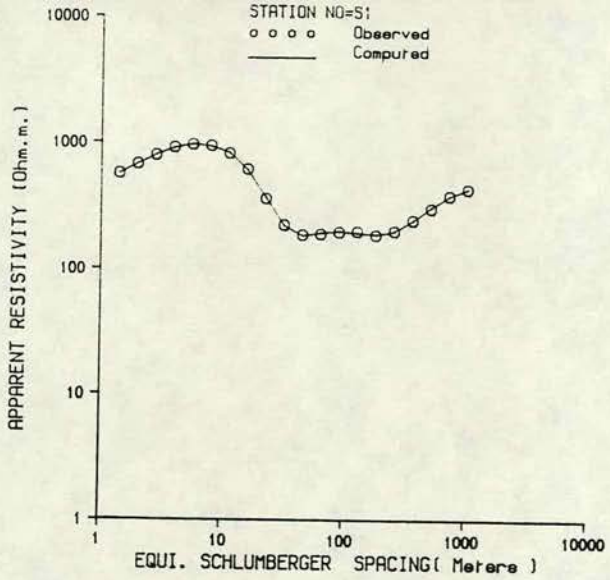

c

L

1D MODEL FOR SITE 603C INVARIANT

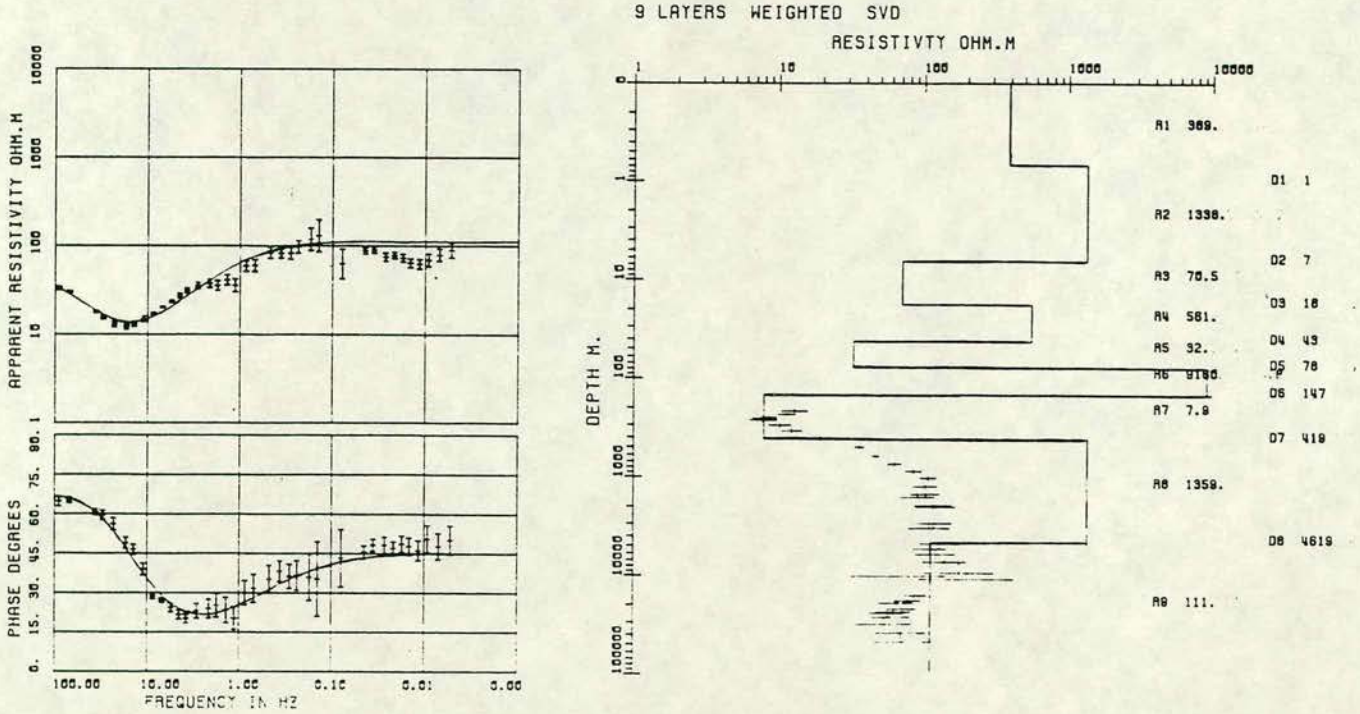

Table 6.3

Details of joint inversion results for 3 stations in N.England; Depths shown are to the top of each layer.

Station No. MT/DC	MT Resis Ohm.m.	MT Depth m.	DC Resis Ohm.m.	DC Depth m.	MT/DC Resis Ohm.m.	MT/DC Depth m.
506/ S4	38	86	132	.7	145.7	0.9
	55	2064	36	3.2	37.5	7.4
	213	11007	44	40.2	60	2007.
	18		184	101.2	165.9	11007.
			60	193.2	19	
			173			
606/ S11	76	3232	81	2.5	83	2.
	148	11090	61	149.5	56	24
	30		217		80	2524
					175	11090
					20	
603/ S1	81	154	385	.8	389	0.6
	7	390	1320	7.9	1338	6.5
	1129	4618	87	22	70	18
	70		308	75	561	42
			76	166	32	78
			3010	391	9161	147
			71	1053	8	418
			1500		1359	4618
					111	

The results obtained from the inversion of DC (ridge regression) by Roxis (1984), MT and combined DC-MT data of this study are summarized and in Fig. 6.11, together with the superposed borehole stratigraphy. It is clear from the figure that there are three prominent resistive layers at Rookhope - the Great Limestone, the Whin sill and the Weardale granite. The electrical boundaries derived from D.C, MT and combined DC-MT modelling results do not, in general, correspond to those of the resistivity-log. One important result from the joint inversion is that the shallow high resistivity layer (the Great Limestone) is well estimated. This would not have been possible with application of either one of individually. Another noticeable result from both MT and MT-DC inversion is that between the Great Limestone and the Whin sill is found to be highly conducting (about 8 Ohm.m.). Summing up these results- i) the thickness and depth of the Great Limestone are well estimated, ii) the Whin sill could not be identified, possibly due to its very small thickness compared to its depth of burial and iii) depth to the granite is less by 50m. compared to the bore hole, possibly due to separation of the stations and the Bore hole by about 1km..

6.5. Modelling of long period data

Though the first magnetotelluric measurements were made in the study region in the 1960's (Jain and Wilson 1967), during last decade, since this region is of special tectonic interest (see Chapter-1) several other investigations have been carried out using electromagnetic induction methods (Jones 1977, Ingham 1981 and Novak 1981).

As discussed in section 6.3, the present study has indicated a layer of about 50-100 Ohm.m. resistivity at a depth of about 10 km. under the Southern Uplands and about 10-50 Ohm.m. below Northern England. However, to understand the deep structure more fully by incorporating the structure as revealed by the earlier induction studies, four good data sets from earlier LMT-long period (> 10 sec.)- stations have been selected. These stations are located within 5 km. of the present traverse sites and it is necessarily assumed that the deep structure is uniform between these LMT and the author's AMT/MT locations. The selected LMT stations are Cappercleuch (CAP) (Jones, 1977), Borthwickbrae (BOW) (Ingham, 1981)- near Craik (station code=503)- and Lampert and Edgesgreen (LAM, EDG) (Novak,

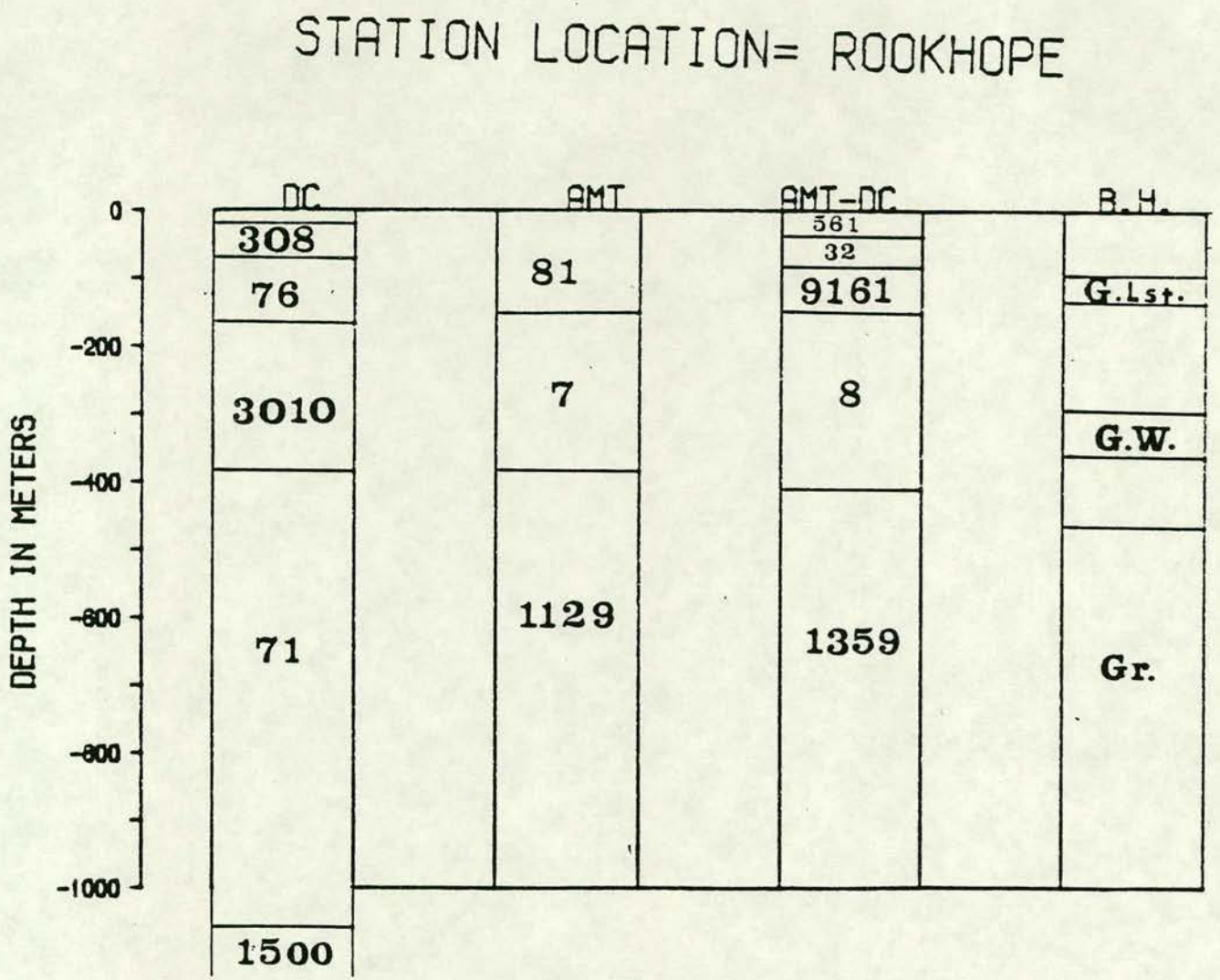

FIGURE 6.11

Comparison of the models obtained from DC, Magnetotelluric and Joint inversion of DC and MT data along with Bore hole data at Rookhope; Numbers represents the resistivity in Ohm.m; G.Lst= Great Limestone; GW= Great Whin sill; Gr= Granite.

1982). Since the longest observational period of the present investigation is about 40 sec., data longer than 40 sec. have been accepted for inclusion in the present analysis. E-pol data sets have been considered as they are quite consistent with those of the present study. As before, these data sets have been subjected to two inversion schemes, allowing all the assumed parameters of the initial model to vary. The modelling results from both of the inversion schemes are illustrated in figures 6.12 a-d. They show in Fig. 6.12a a low resistivity layer at a depth of about 30-35 km. below Borthwickbrae with a thickness of about 10-15 km. and a resistivity of about 40-50 Ohm.m. At CAP (Fig. 6.12b) the thickness of the low resistivity layer (5-10 Ohm.m.) obtained from modelling the MT data alone is still not well estimated even in this longer period modelling study. From the Bostick transformation plots, however, the thickness of the conductor seem to be approximately 15-20 km. A thickness of about 10 km. has been obtained for the deep low resisitivity layer at sites LAM and EDG below the Northumberland basin Figs. 6.12 c and d respectively.

6.6. Summary

Based on the results of both the short and long period 1-D modelling study discussed in earlier sections of this chapter, a schematic section has been prepared for the study traverse and is presented in fig. 6.13. The 1-D model result for NEW (see Fig. 6.13) has also been incorporated in the section. It may be noted that several workers have proposed various models using this data set (COPROD 1977). However, the result obtained by Jones (1977) is considered in Fig. 6.13.

The significant modelling results of this chapter can be summarized as follows.

1. In general, the structural features deduced from a qualitative study of apparent resistivity and phase curves and Bostick transformation plots have been confirmed by subsequent modelling.

2.The most prominent features of the electrical structure derived from the present modelling study are:

- a highly conducting (6-10 Ohm.m.) zone exists at the shallow

FIGURE 6.12

Model results obtained from application of Montecarlo and linearised inversion to

a) Cappercleuch (Station code = CAP {514}.

b) Borwickbrae (Station code = BOW {503}).

c) Lampert (Station code = LAM {506}).

d) Edgesgreen (Station code =EDG {606}.

In each figure upper half shows the linearised inversion results and the lower half shows the Montecarlo–Hedgehog results.

1D MODEL FOR SITE CAPD EPOL

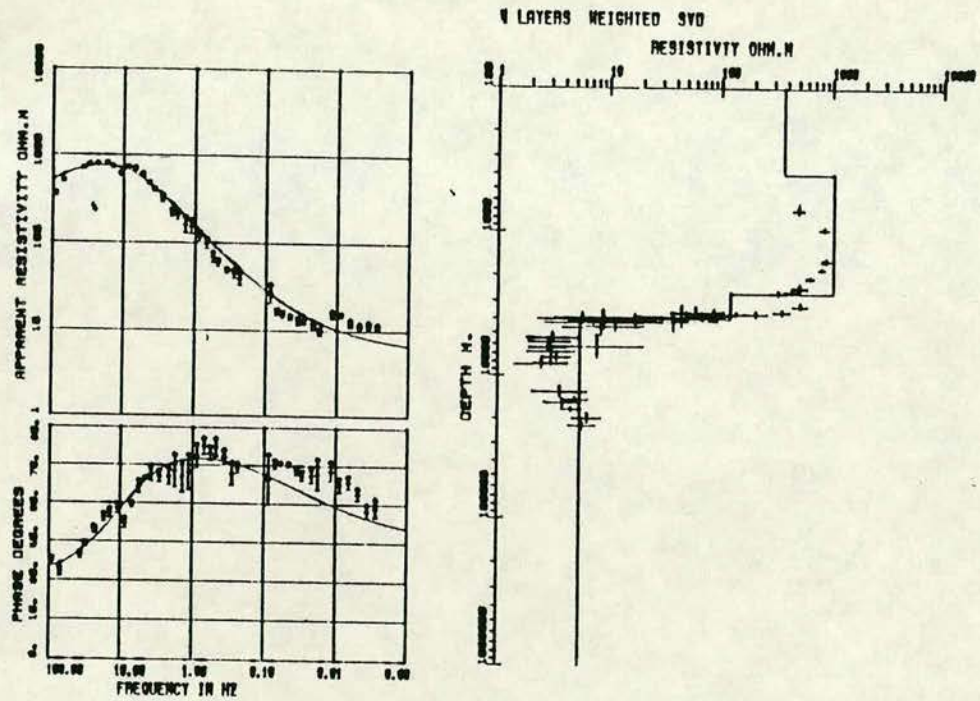

1D MODEL FOR SITE CAPD EPOL

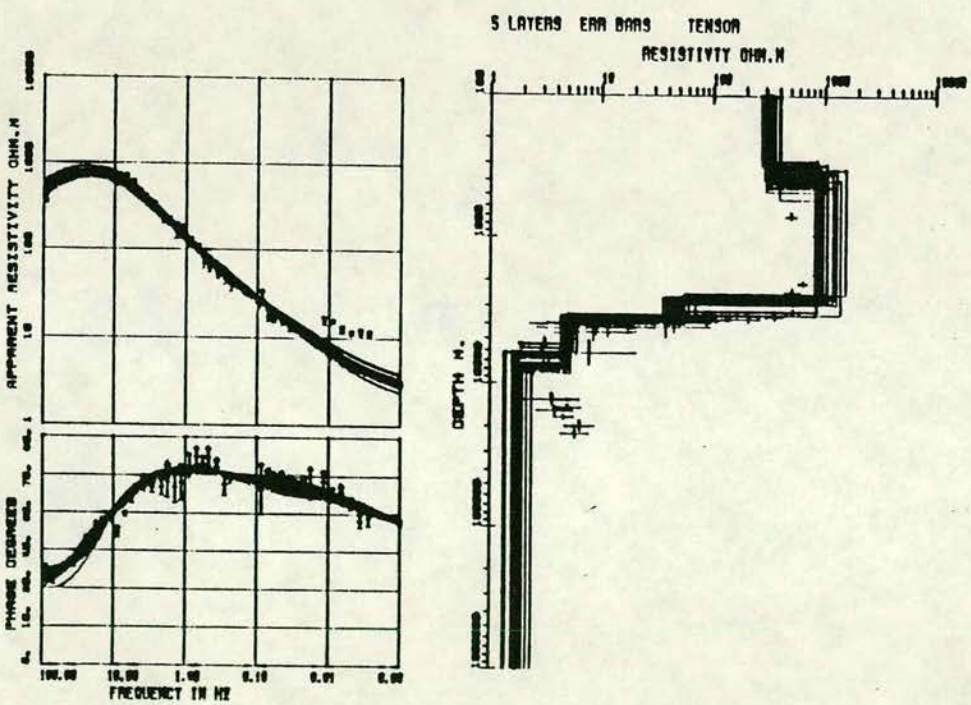

1D MODEL FOR SITE LAMD EPOL

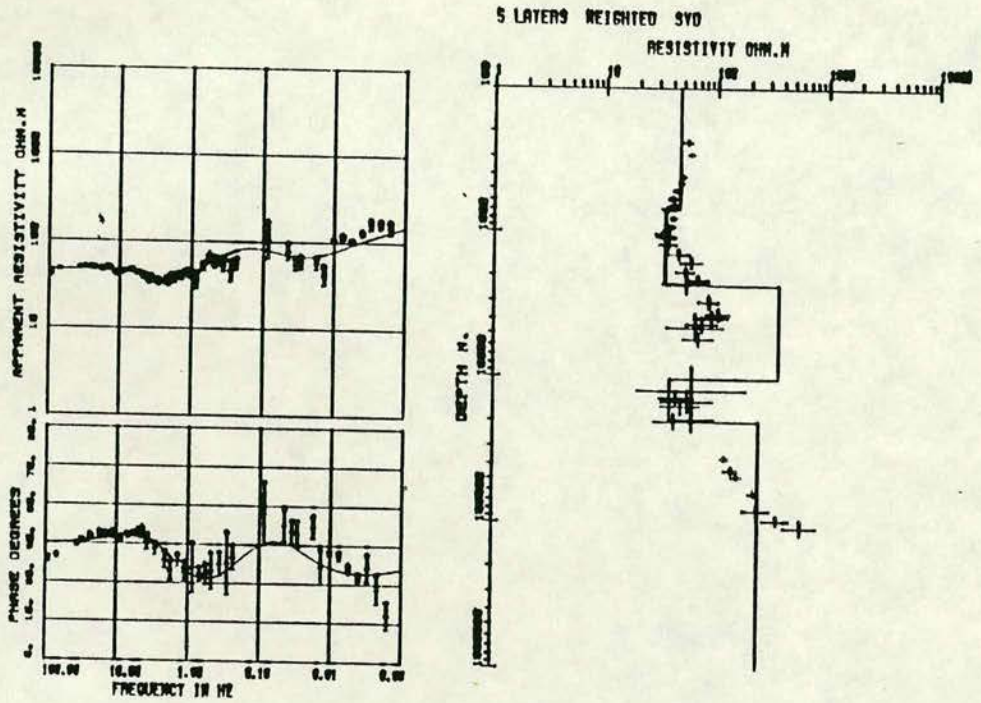

1D MODEL FOR SITE LAMD EPOL

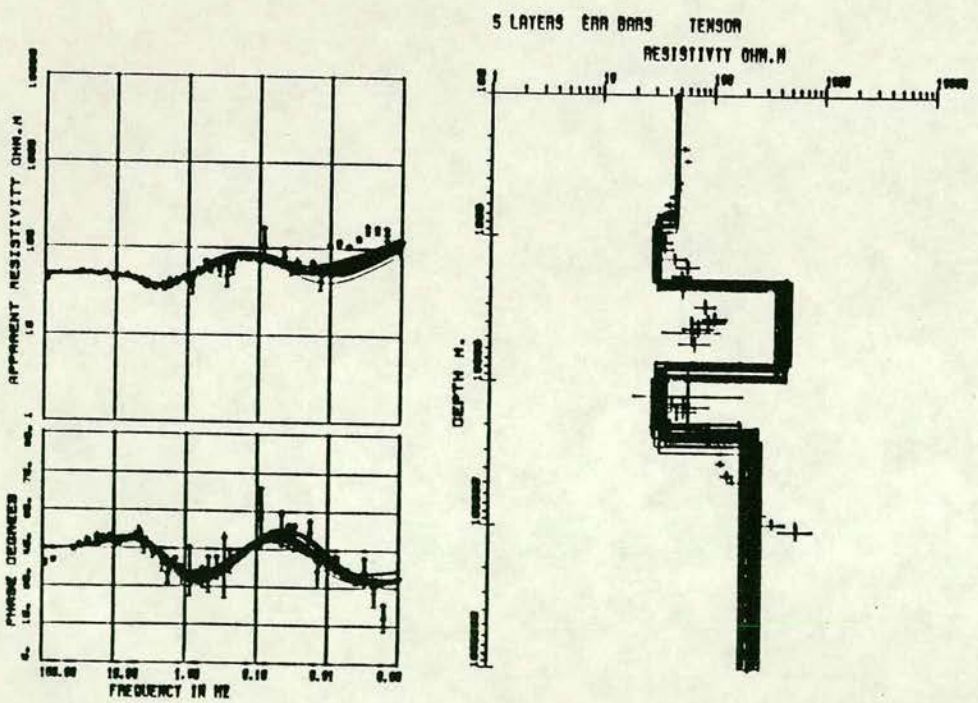

1D MODEL FOR SITE BOWD XY

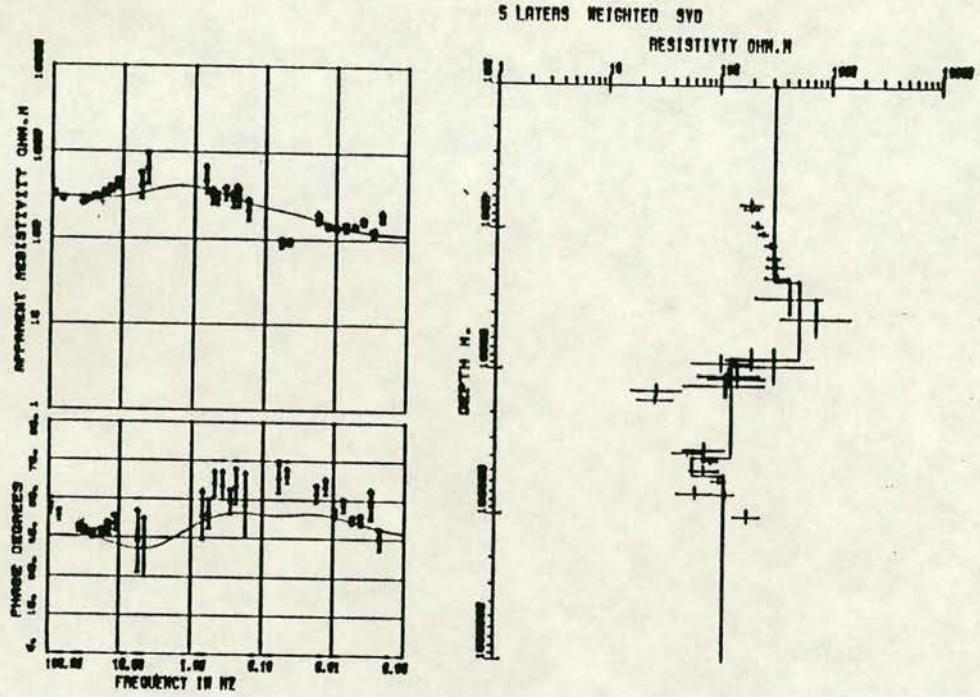

1D MODEL FOR SITE BOWD XY

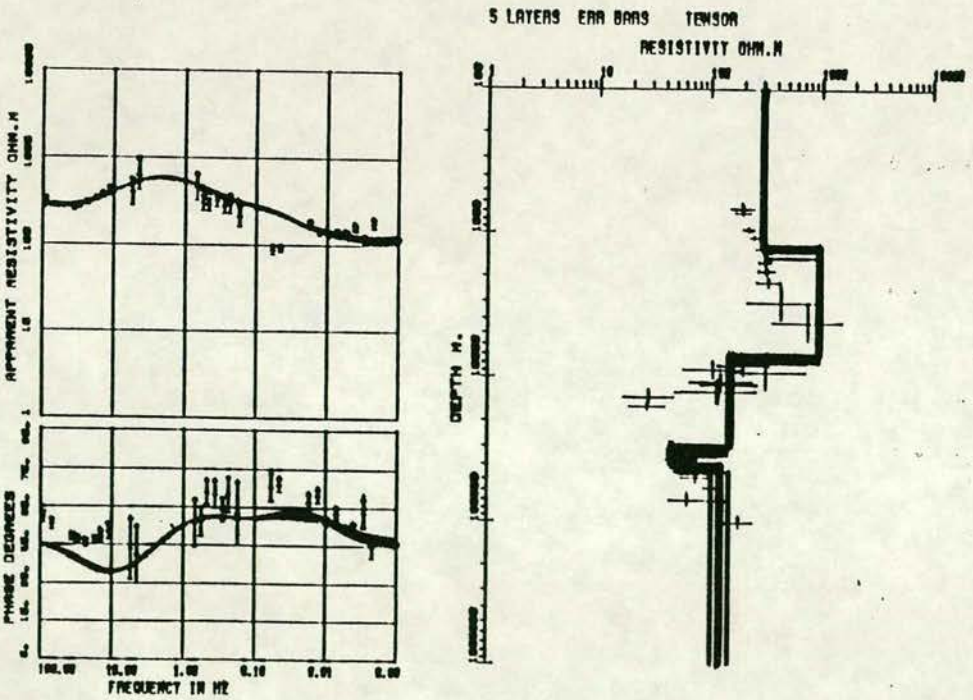

1D MODEL FOR SITE EDGD EPOL

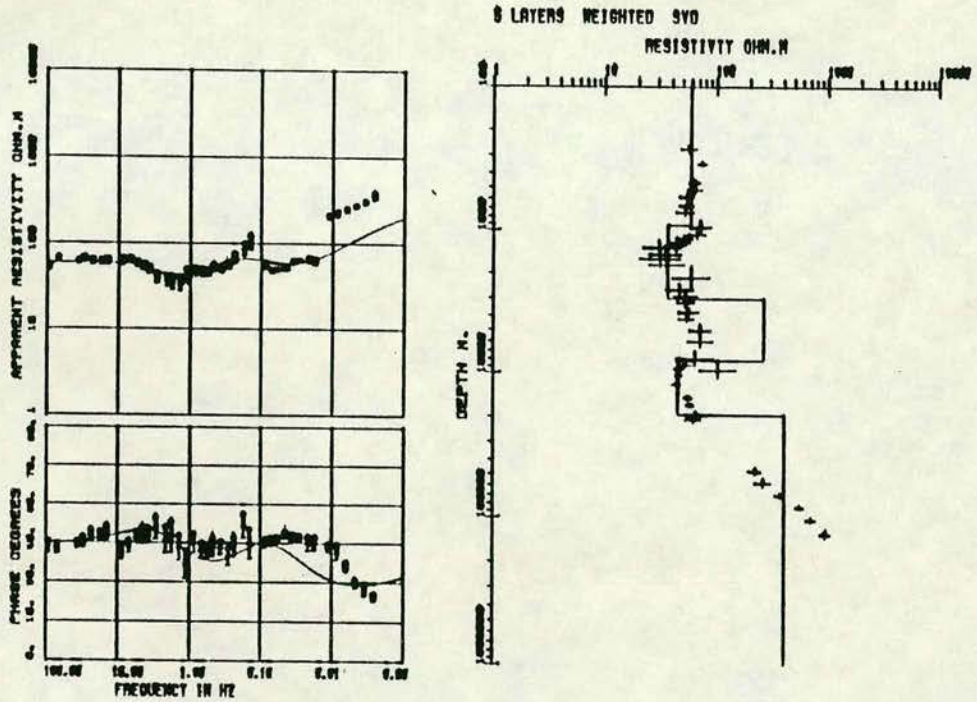

1D MODEL FOR SITE EDGD EPOL

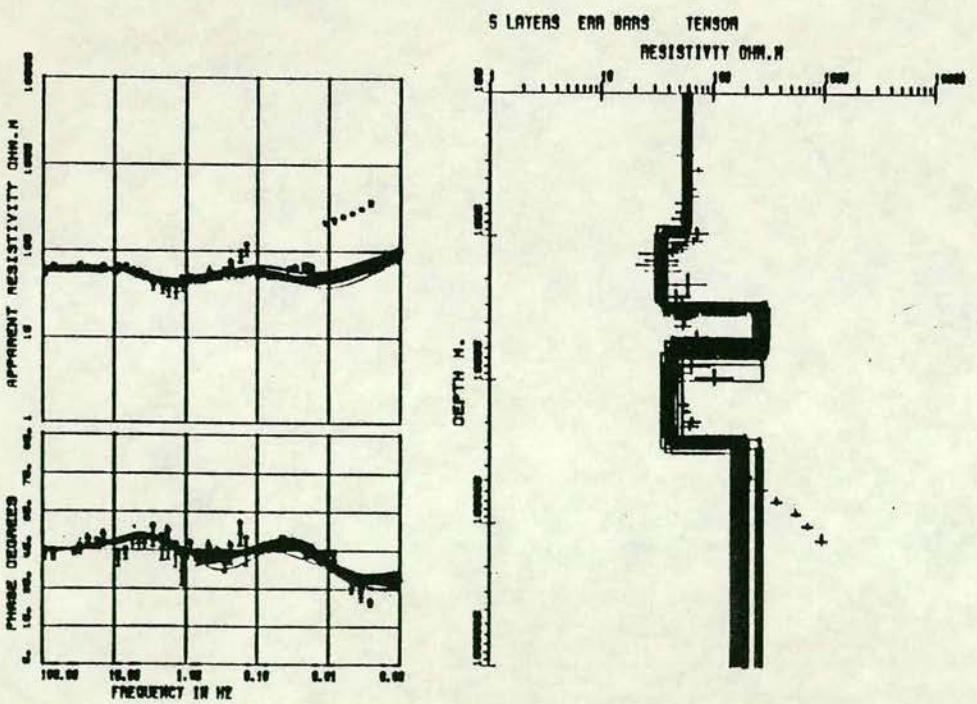

FIGURE 6.13

A schematic diagram based on the 1-D modelling results of both short and long period study and the NEW station result (Jones, 1977). Note that the depth scale is linear (actual)

SUF= SOUTHERN UPLANDS FAULT

OBF= ORLOCK BRIDGE FAULT

SBF= STUBLICK FAULT

DEPTH in Km.
0
-10
-20
-30
-40
-50
150 km.
SOUTHERN UPLANDS
NORTHUMBERLAND
ALSTON BLOCK
SUF
SBF
DZR
obf
CAP
SML
CRK (BOW)
CWR
NEW (LMT)
BEW
GIB
LAM+LMT
EDG+LMT
WHI
SIN
ROO
HIL
1000-2000
100-300
5-10
500-1000
100- 50
10-50
150 - 250
10-50
500-1000
100-200
100-200
SUF= Southern Uplands Fault
SBF = Stublick Fault
10-50= Resistivity in Ohm.m.
MAGNETOTELLURIC STATION

depth of 3-3.5 km. about 20km. south of the Southern Uplands Fault.

- a moderately conducting layer (50-100 Ohm.m.) exists at a depth of about 8-10 km. below the Southern Uplands.

- a shallow conductor (10-80 Ohm.m.) in the top 0.5-2.5km. corresponds to the sediments of the Northumberland Basin.

- a conductor (10-50 Ohm.m.) exists at a depth of 8-10 km. below the Northumberland Basin

- in the Northumberland basin the sedimentary thickness varies from about 0.5 km. near the Alston block to about 2.5-3.5 km. at the centre then thins to about .5 km. below Bewcastle.

- a resistive structure (500_1000 Ohm.m.) exists below the Alston block at a depth of about 0.5 km.

3.From joint inversion of D.C. and MT data at station ROO, the depth and thickness of the Great Limestone could be resolved.

4. The combined analysis of long and short period data indicates a conductor (30-40 Ohm.m.) with a thickness of about 10-15 km. at a depth of 8-10 km. below the Northumberland Basin and a conductor (50-80 Ohm.m) at a depth of about 30-35 km. below the Southern Uplands with approximately the same thickness. These results concerning a lower crustal conductor support those of the earlier induction studies (Jones 1977, Ingham 1981, Beamish 1986).

5. From comparision of Figs. 6.5-6.9 with 6.13, it can be seen that the schematic section is based on the smooth variation of depth to the different layers along the traverse. However, before accepting this section (Fig. 6.13), 2D modelling of the response functions is first necessary.

The interpretation of these modelling results in terms of the geology and tectonics of the region will be discussed in Chapter 8.

CHAPTER 7

TWO DIMENSIONAL MODELLING RESULTS

This chapter begins with an introduction describing various 2-D numerical modelling schemes with special reference to Brewitt- Taylor and Weaver (1976). In section 7.2, the effect of near surface inhomogeneties and edges are given while section 7.3 deals with the application of 2D forward and inversion schemes to the field data of the present study.

7.1. Introduction

The model parameters presented in chapter 6 are in general valid when the assumptions made in formulating the one dimensional modelling algorithm are closely met. MT response functions are, however, sensitive to various other factors such as surface inhomogeneities, anisotropy, topography, the current channelling effect, two and three dimensional structures etc.. When any of these factors is dominant, then the model parameters derived from one dimensional modelling are in general distorted. The effect of these factors on the observed data has been investigated by several workers and in such cases use of different modelling procedures or data corrections have been suggested. (eg.. Jones and Pascoe 1971, Silvester and Haslam 1972 Thayer 1975, Berdichevsky and Dmitriev 1976, Abramovici and Shoham 1977, Larsen 1977, Harinarayana and Sarma 1982, Jones 1983a, Park 1985, Wannamaker et al 1986, Jones 1987). When a number of these factors affects the data together, however, it becomes difficult to remove their effect. In this chapter, the effects of a) near surface inhomogeneities and b) two dimensional electrical structures on the response functions are discussed.

Two dimensional modelling can be carried out using either analytical or numerical schemes. Since it is difficult to construct an analytical scheme for complicated structures, such as in the present study, a numerical modelling procedure has been used. There are four main types of two dimensional numerical modelling procedures - finite element, transmission line analogy, integral equations and finite difference - presently in use. These are now summarized.

The finite element method is based on the principle that any electromagnetic system behaves in such a way so as to minimize its total energy. The total energy function in each element of a mesh is numerically minimized. This minimization gives a set of linear equations with field values at the nodal points. Since the pioneering work of Coggan (1971), there have been several studies based on this method (eg. Silvestor and Haslam 1972, Reddy and Rankin 1973, Kaikkonen 1977, Pridmore et al 1981 and Wannamaker et al 1986).

The method of solution in the transmission line method is the analogy between Maxwell's equations and the equations relating the voltage and current in a transmission surface. Kirchoff's law of continuity of electrical current governs the boundary conditions at nodal points. This method has been discussed by Wright (1970), Swift (1971), Brewitt-Taylor and Johns (1980), and etc..

In the integral equation method, the two dimensional boundary value problem is reduced to a system of integral equations for the inhomogeneous region (Hohmann 1971, Patra and Mallick 1980). This is known to be less expensive in the computational sense and its main advantage is in dealing with simple inhomogeneities.

Finally there is the finite difference method, which is probably the most widely used, perhaps due to the early publication of a software package (Jones and Pascoe 1971). In this method, a set of finite difference equations is solved at each point on the grid mesh. The differential equations are then reduced to a system of linear algebraic equations for the field values at the grid points, with the substitution of derivatives by difference quotients. The original formulation by Jones and Price (1970) was later corrected - for variable grid spacings by Williamson et al (1974), for smooth transition in conductivity by Brewitt -Taylor and Weaver (1976) and by improving the boundary conditions by Weaver and Brewitt -Taylor (1978). Since the method as formulated by Brewitt-Taylor and Weaver (1976) has been used in the present study, a more detailed description now follows.

As discussed in Chapter 2, for a two dimensional situation, the fields and conductivities are assumed to vary only in the y and z directions. Thus Maxwell's equations de-couple into two distinct modes, the E- and B-

polarization modes as given in equations in 2.50 and 2.51. These two equations must be solved with appropriate boundary conditions in each region of the assumed conductivity model. In solving these equations, Jones and Pascoe (1971) have considered sharp conductivity boundaries. To find the correct finite difference representation, 'fictitious' field values must be introduced. Brewitt-Taylor and Weaver (1976) showed that this makes the solution overdetermined and they thus introduced the concept of 'transition zones'. They specified the conductivity values at the centres of grid element rather than at the nodal points. Hence, the value at any grid point is given by a weighted mean of the four actual assigned values of conductivity surrounding that point. With these modifications, the conductivity from one region to the other varies in a smooth linear manner. They have also referred to the errors arising in the application of boundary conditions from Jones and Pascoe's use of one sided differences. They preferred the application of central difference formulae to the diffusion equations in the determination of the finite difference representation.

The general boundary conditions in solving this problem are,

- at large distances from the model, i.e., as $y \to \pm\infty$, the conductivity 'σ' is a function of z alone,
- as $y \to \pm\infty$, the total magnetic field is constant above the surface of the earth,
- the magnetic field cannot penetrate beyond the bottom layer of the model and
- at the internal boundaries the tangential component of the fields and the normal component of magnetic field are continuous.

Apart from the above, there are additional boundary conditions to be satisfied. These are different for the two polarizations as described in Brewitt-Taylor and Weaver (1976).

In all the numerical procedures, it may be noted that continuous functions of electrical conductivity are represented by discrete points over a mesh of finite discontinuities, assuming a linear variation between two adjacent grid points. Thus successful utilization of the scheme depends mainly on the preparation of the grid for the assumed model. For proper grid design a few

'thumb rules' concerning the dimensions have been suggested by Muller and Losecke (1975), and by Wannamaker et al (1985).

7.2. The effect of near surface inhomogeneities and the edge effect

This study was initiated for the following two main reasons: Firstly, much of Northern England is covered by conducting Carboniferous sediments of the Northumberland and Stainmore Basins, which are separated by the resistive Weardale Granite batholith. Hence it is interesting to study the possible effect of the Stainmore Basin on observations made near the Northumberland Basin and the Weardale Granite. Secondly, since it is usual practice in numerical modelling to extend the grid mesh to large distances from the survey region and since the observations made in the present study covered only part of the Weardale Granite, it is useful to quantify the effect of assuming that this granite extends to infinity in the southward direction.

These structures- the Northumberland Basin, the Weardale Granite batholith and the Stainmore Basin - have been approximated in model 1 - Fig. 7.1 a. Model 2 (Fig 7.1 b) consists of the Northumberland Basin and the Weardale Granite and model 3 (Fig 7.1 c), is same as model 2 except that the Weardale Granite is assumed to extend to a large distance to the south. The resistivity and depth parameters assumed in the model are based on the 1-D results from the present study and from seismic and gravity studies (Bott et al 1984). A thickness of 2.5 and 8km. are assigned to the sedimentary Basins and the granite respectively. The resistivities for the sedimentary basins and granite are assumed to be 50 Ohm.m. and 2000 Ohm.m. respectively. 2D numerical modelling has been carried out for these models and for both E-pol and H-pol directions in the frequency range 0.01 to 100 Hz.. Discussion of the computed responses is restricted to the two locations A and B (see Fig. 7.1) although they were obtained at a series of locations along the traverse.

The results of the computations at A and B are presented in Figs. 7.2 and 7.3. Distortions of the response functions for each of models 2 and 3 with respect to model 1 are represented in these figures as percentage errors. In general, the errors are larger for the lower frequencies and the phase response function percentage errors are less than the apparent resistivities.

FIGURE 7.1

Models considered for forward computation of the effect of Weardale Granite and Stainmore Trough. a) Model 1- showing the Northumberland Basin, Weardale Granite and Stainmore Basin, b) model 2- showing Northumberland Basin and Weardale Granite and c) model 3- as for model 2 except that the Weardale Granite is assumed to extend to a large distance.

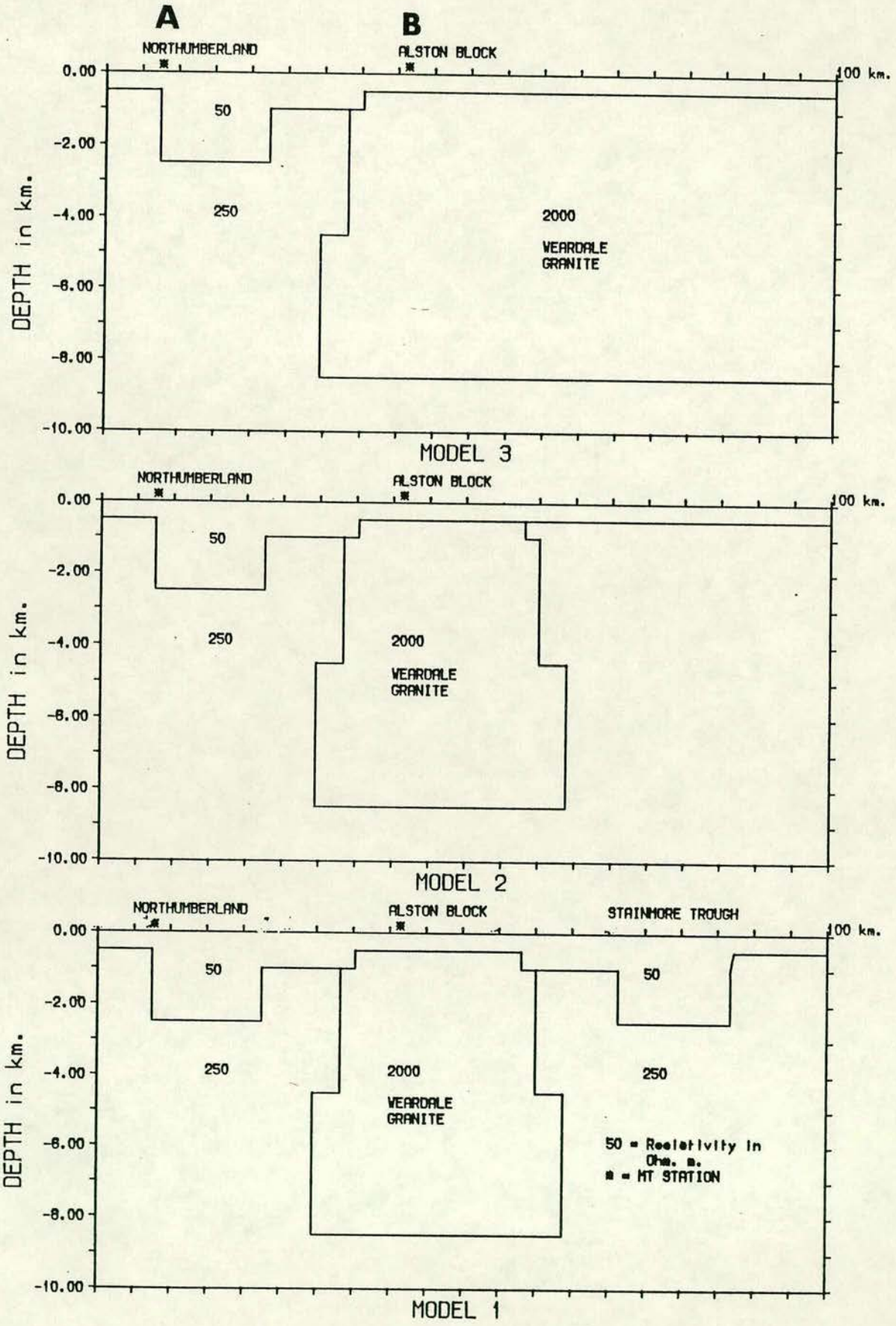
A
B
NORTHUMBERLAND
ALSTON BLOCK
0.00
-2.00
-4.00
-6.00
-8.00
-10.00
100 km.
DEPTH in km.
50
250
2000
WEARDALE
GRANITE
MODEL 3
NORTHUMBERLAND
ALSTON BLOCK
0.00
-2.00
-4.00
-6.00
-8.00
-10.00
100 km.
DEPTH in km.
50
250
2000
WEARDALE
GRANITE
MODEL 2
NORTHUMBERLAND
ALSTON BLOCK
STAINMORE TROUGH
0.00
-2.00
-4.00
-6.00
-8.00
-10.00
100 km.
DEPTH in km.
50
250
2000
WEARDALE
GRANITE
50
250
50 = Resistivity in Ohm. m.
* = MT STATION
MODEL 1

FIGURE 7.2

The percentage error in the response functions at Northumberland Basin sites- a) due to the presence of the Stainmore Basin and b) due to a large extension of the Weardale Granite.

b ERROR BETWEEN MODEL 1 AND 3 AT A

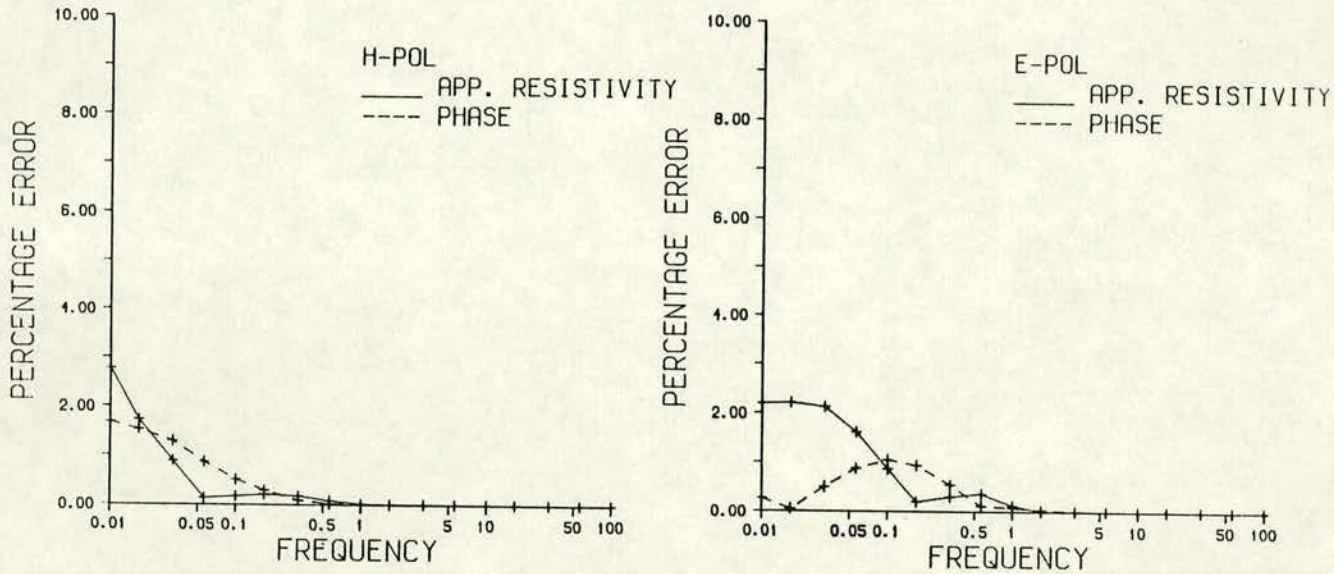

a ERROR BETWEEN MODEL 1 AND 2 AT A

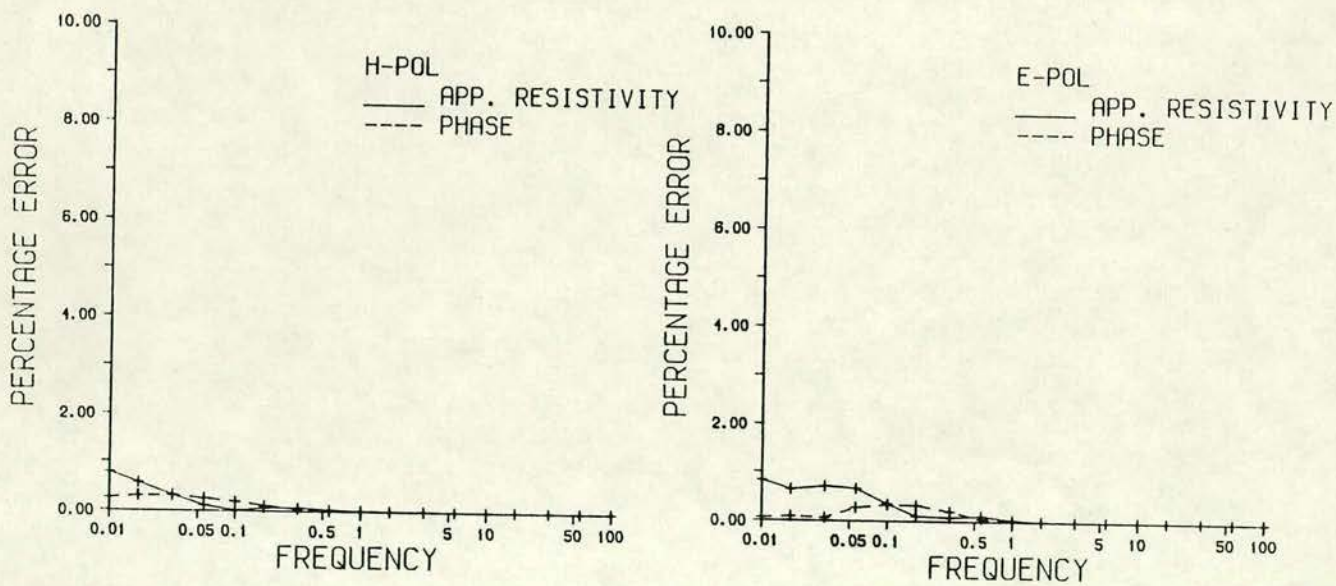

The results can be summarized as follows:

- Though the distortion effects are spatially variable and frequency dependent, it can be seen that, in general, the H-pol responses are more distorted than the E-pol response functions (Fig. 7.2a).

- For both the E-pol and the H-pol response functions, the maximum error observed near the Northumberland Basin (location A) due to the presence of Stainmore Basin is 1% for the apparent resistivities and less than 0.5% for the phase function Fig. 7.2b).

- Assuming the Weardale Granite extends to a large distance can distort the measurements over Northumberland (Location A) by about 3% for the apparent resistivity function and about 1.5% for the phase function.

- The presence of the Stainmore Basin can distort the measurements made near Weardale Granite (location B) by about 8% for the apparent resistivity function in the H-pol direction and about 3% in the E-pol direction. Phase responses are distorted by about 2.5% in the H-pol direction and about 1% in the E-pol direction (Fig. 7.3a).

- Assuming that the Weardale Granite extends to a large distance can cause distortions of the apparent resistivities (Location B) by as much as 24% in the H-pol direction and by about 8% in the E-pol direction. The phases are distorted by about 7% in the H-pol direction and by about 3% in the E-pol direction (Fig. 7.3b).

7.3. The effect of lateral inhomogeneities

As discussed earlier, the response functions obtained from the present study are dominantly one dimensional. However, at a few stations 2D effects become more prominent at long periods (See Fig. 4.3 J, m). Hence 2D modelling has been attempted to study the effect of lateral inhomogeneities along the traverse. The initial 2D model was formulated by compiling the 1D invariant modelling results. Since the effect of 1D structures is dominant it was expected that this 2D model would provide a satisfactory fit to the response functions in both E-pol and H-pol directions.

The 2D modelling was carried out in two stages. In the first stage, forward modelling was undertaken with variations in the resistivity and the position of the blocks of the initial model. For the second stage, a two dimensional inversion scheme (Hill 1987) was attempted. Resolution of the various block

FIGURE 7.3

The percentage error in the response functions at Weardale Granite sites – a) due to the presence of the Stainmore Basin and b) due to a large extension of the Weardale Granite.

b ERROR BETWEEN MODEL 1 AND 3 AT B

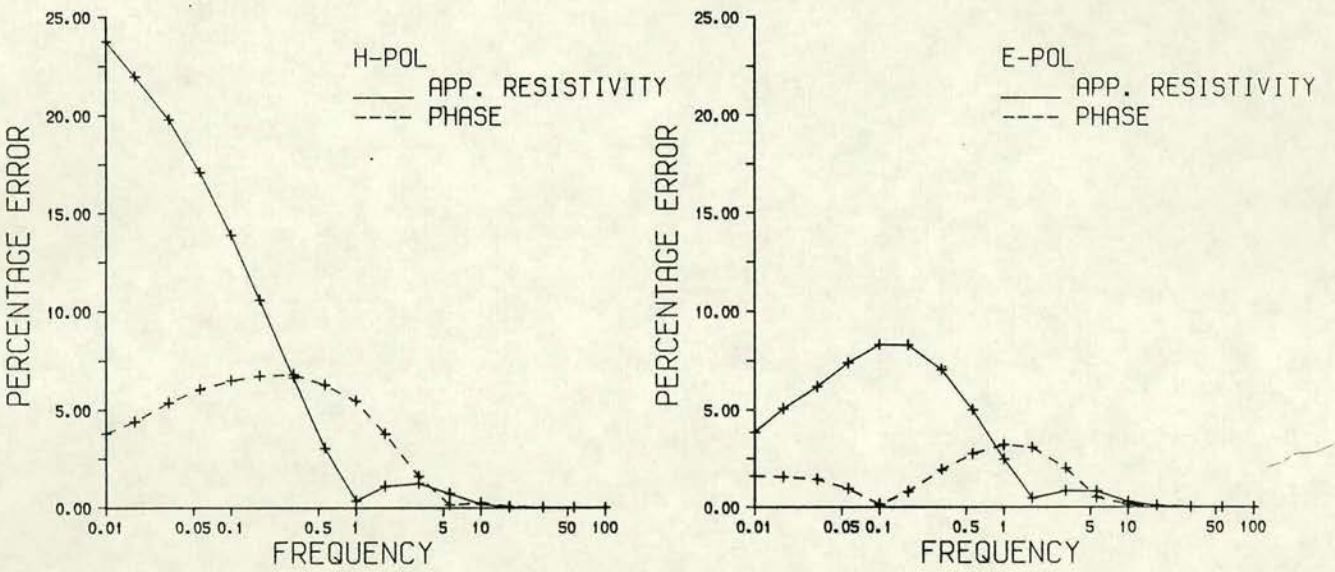

a ERROR BETWEEN MODEL 1 AND 2 AT B

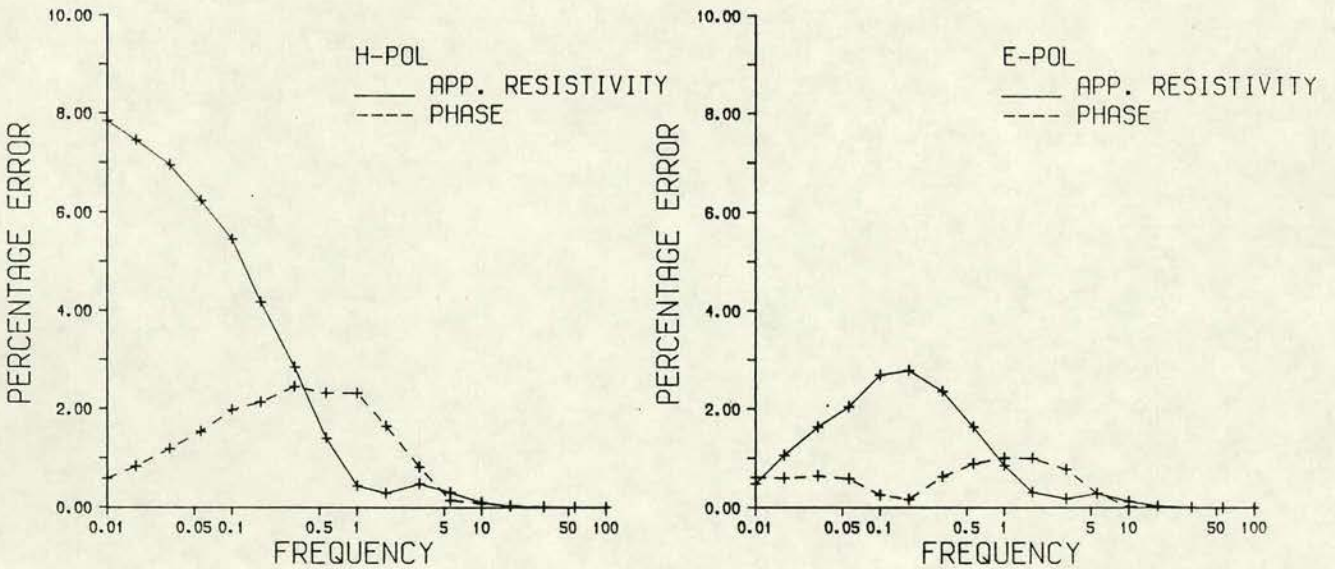

resistivities was also studied in the latter case.

7.3.1. Forward two dimensional modelling

As discussed earlier, to satisfy the assumptions made in the two dimensional modelling algorithm it is necessary to rotate the response functions such that in one direction the E-field is parallel (E-pol) to the dominant geological or tectonic structure. Alternately, the computed response functions in E-pol and orthogonal H-pol directions can be rotated to the measuring directions before comparison of the observed and computed data (Rasmussen 1987). This technique is particularly useful when the diagonal elements are corrupted with noise. In the present study, the former approach was used.

It may be noted that the study region extends over two distinct geological zones with different regional strikes. This can be approximated to the N 60° E direction in Southern Scotland and to approximately EW in Northern England. Since a single model was constructed for the whole traverse an average strike direction was used in estimation of the rotation angle. Considering the declination in the area as 10°w, an angle of rotation of 85° east of north was adopted.

Many problems were encountered during the modelling exercise, mainly due to the following reasons: a) the traverse in the present study is long (nearly 140 km.), b) the range of frequencies extends from 100 Hz. to nearly 0.002 Hz. and c) the top layer resistivity in Northern England is very low, nearly 20-50 Ohm.m.. Consequently, a large and closely spaced grid is necessary to represent the approximately smooth lateral variation in conductivity. This requires considerable computer storage and CPU time. To overcome this problem the different grid sizes were used according to the frequency under consideration. As an example, the grids for .002 Hz and 100 Hz. are listed in Table 7.1a and b. The vertical grid sizes for all frequencies, however, were kept fixed at the values given in table 7.1a for 0.002 Hz. As already discussed in section 7.2 there is a considerable error if the Weardale Granite is assumed to extend to a large distance southward. Hence, only a finite extension has been assumed as shown in the figure 7.4b. The presence of the Stainmore Basin, however, could not be incorporated in the modelling grid due to the resulting increase in CPU time. The general strategy adopted

TABLE 7.1

An example of the grid sizes used in the 2D numerical modelling. for a) frequency =0.002 Hz. and for b) frequency= 100 Hz.

Table 7.1a

Frequency = 0.002 Hz.

Z-grid (depth) values in km.

No.	Value	No.	Value	No.	Value
1.	-500.	16.	1.7	31.	10.5
2.	-300.	17.	2.5	32.	18.
3.	-200.	18.	2.9	33.	33.
4.	-100.	19.	3.3	34.	34.
5.	-50.	20.	3.4	35.	38.
6.	-25.	21.	5.2	36.	43.
7.	-5.	22.	5.9	37.	58.
8.	-1.	23.	6.0	38.	130.
9.	0.	24.	6.5	39.	250.
10.	0.1	25.	7.2	40.	550.
11.	0.2	26.	7.9		
12.	0.3	27.	8.4		
13.	0.6	28.	9.1		
14.	0.8	29.	9.8		
15.	1.1	30.	10.1		

Y-grid (Width) values in km.

No.	Value	No.	Value	No.	Value
1.	500.0	16.	5.0	31.	5.0
2.	100.0	17.	5.0	32.	1.0
3.	50.0	18.	2.0	33.	9.0
4.	9.0	19.	0.5	34.	14.0
5.	0.9	20.	1.0	35.	5.0
6.	0.1	21.	1.3	36.	50.0
7.	1.8	22.	4.0	37.	500.0
8.	2.0	23.	1.5		
9.	0.1	24.	0.5		
10.	10.4	25.	9.5		
11.	9.0	26.	2.5		
12.	8.0	27.	0.5		
13.	5.0	28.	6.5		
14.	8.0	29.	5.0		
15.	3.0	30.	1.0		

Table 7.1b

Frequency = 100 Hz.

Y-grid (width) values in km.

No.	Value	No.	Value	No.	Value	No.	Value
1.	500.0	27.	0.85	53.	0.07	79	0.30
2.	100.0	28.	0.60	54.	0.08	80.	0.15
3.	50.0	29.	1.20	55.	0.13	81.	0.07
4.	5.6	30.	2.40	56.	0.20	82.	0.13
5.	0.9	31.	2.40	57.	0.50	83.	0.29
6.	4.7	32.	2.40	58.	0.50	84.	0.55
7.	2.8	33.	6.57	59.	1.30	85.	3.00
8.	0.7	34.	0.78	60.	2.00	86.	2.30
9.	0.6	35.	0.63	61.	0.96	87.	0.55
10.	0.9	36.	0.63	62.	0.55	88.	2.30
11.	0.05	37.	3.70	63.	0.27	89.	2.02
12.	0.05	38.	0.63	64.	0.13	90.	0.63
13.	0.12	39.	1.27	65.	0.07	91.	0.50
14.	0.21	40.	6.72	66.	0.15	92.	0.50
15.	0.52	41.	2.36	67.	0.30	93.	2.60
16.	0.92	42.	0.63	68.	0.50	94.	2.30
17.	1.00	43.	1.27	69.	0.51	95.	0.72
18.	0.75	44.	3.72	70.	0.36	96.	0.27
19.	0.25	45.	1.89	71.	0.13	97.	1.80
20.	0.10	46.	1.89	72.	0.30	98.	7.10
21.	0.63	47.	0.60	73.	0.46	99.	14.00
22.	0.75	48.	0.60	74.	0.46	100.	3.10
23.	2.00	49.	0.63	75.	1.20	101.	1.80
24.	2.10	50.	0.53	76.	7.03	102.	1.10
25.	2.10	51.	0.53	77.	1.40	103.	2.30
26.	1.70	52.	0.30	78.	0.60	104.	46.50
						105.	500.00

in the modelling scheme was to start with simple shallow structures with only a few frequencies and then gradually to include deeper structures and consider more frequencies. All the complex structures of the Northumberland Basin, however, could not be included. For example, shallow structures such as the Great Whin sill and the Great Limestone which are known to be highly resistive formations were not considered. Thirteen frequencies were considered in the range 100-0.002Hz. After each run, apart from computing the misfit between observed and computed data, the data were plotted and a visual assessment was made before attempting to change the model. The final model consisted of 15 different resistivity blocks and they are listed in Table 7.3.

7.3.2. The two dimensional inversion scheme

After obtaining a reasonably good fit between the observed and computed response functions from the above forward modelling, an attempt was also made to use Hill's inversion scheme- this is described in a contemporary Ph.D. thesis. This scheme applies a biased linear estimation algorithm using singular value truncation and ridge regression techniques iteratively. The iteration procedure uses the Brewitt-Taylor and Weaver (1976) procedure for the forward calculation and reduction of the error between the observed and computed response functions. The inversion procedure is similar to that of Jupp and Vozoff (1977), but it has the advantage that both the position and the resistivity of the block can be considered as variables during iteration.

In this study to limit the CPU time the positions of the blocks, however, were fixed and only the block resistivities allowed to vary during iteration. Nine out of 13 stations which are reasonably distributed along the traverse were considered and the stations are listed in table 7.2. The details of the grid size, number of frequencies in this scheme are the same as those described earlier for the forward modelling. A reasonably satisfactory model obtained from the forward modelling scheme was used as the starting model in this scheme. The final model was obtained after 4 iterations. The total CPU time for the scheme was nearly 7200 seconds. Using the most square approach, as described earlier in chapter 6 the resolution of the block resistivity parameters was also studied as discussed in the next section.

TABLE 7.2

List of stations considered for 2D modelling.

S.No.	Station Name	Station No.	Station Code
1.	Drumezlier	515	DZR
2.	Cappercleuch	514	CAP
3.	Craik	503	CRK
4.	Carewoodrig	502	CWR
5.	Lampert	506	LAM
6.	Edgesgreen	606	EDG
7.	Whitfield	508	WHI
8.	Sinderhope	604	SIN
9.	Rookhope	603	ROO

TABLE 7.3

List of block numbers and their corresponding resistivities.

Block No.	Block resistivities before inversion	After inversion
1	10.	20.
2	2000	9978.
3	300	370.
4	250	271.
5	40	58.
6	1000	1550.
7	15	10.
8	50	71.
9	20	3.
10	1500	1120.
11	450	600.
12	3	0.44
13	150	171.
14	125	82.
15	250	285.

7.3.3. Modelling results

The final model is shown in figures 7.4a and b with the shallow features being presented in 7.4 a, (with the vertical scale exaggerated) and the complete model to the actual scale in 7.4b. The numbers shown in the figures are the block resistivities. The station locations considered for the 2D inversion scheme are indicated by 'asterisks' in Figs. 7.4a and b. The fit of the observed and computed E- and H- polarization apparent resistivity and phase response functions are presented in figures 7.5 a-i. In general, it was found to be more difficult to obtain a good fit for the Northern England stations than for the Southern Upland stations, especially for the long period part of the curves. Owing to the lack of closely spaced stations, the detailed structure of the highly conducting region around CAP was not obtained. The apparent resistivity (ρ_{xy}) data at SML, nearest to CAP was distorted between 1-10 Hz. and hence was not used for 2D modelling. Similarly, due to lack of consistent long period (10-1000 sec.) data at most stations along the profile the deep (greater than about 20 km.) structure assumed in the 2D model is poorly resolved. It should also be noted that the computed response function from the geo-electric model does not fit well the highly anisotropic behaviour of the observed response functions at SIN and the long period anisotropic data at ROO. No definite reason is apparent for the anisotropy in the data sets. However,it could possibly be due to the effect of the 3D character of the resistive Weardale Granite. The salient features of the 2D model are summarized below considering each region- the Southern Uplands, the Northumberland and the Alston block - individually.

The Southern Uplands

The stations DZR, CAP, CRK and CWR belongs to this region. The resistivity structure below these stations is as follows.

* The surface layer (1-2km.) of much of the Southern Uplands is resistive- 1550 ohm.m.. below DZR, 600 Ohm.m. below CAP and 285 Ohm.m. below CRK and CWR - with the resistivity decreasing from NW towards SE along the traverse.

* The model shows a conducting (3 Ohm.m.) layer below CAP at a depth of about 3.5 km. below which

FIGURE 7.4

The final two-dimensional geo-electric model showing a) the details of the shallow structures, upto 5 km. depth, with an exaggerated vertical scale and b) the complete structure with actual scales. The different numbers plotted in the model represent the resistivities in ohm.m.. The locations of the stations considered are indicated by 'asterisks' and the station codes can be seen on top of the figure (a).

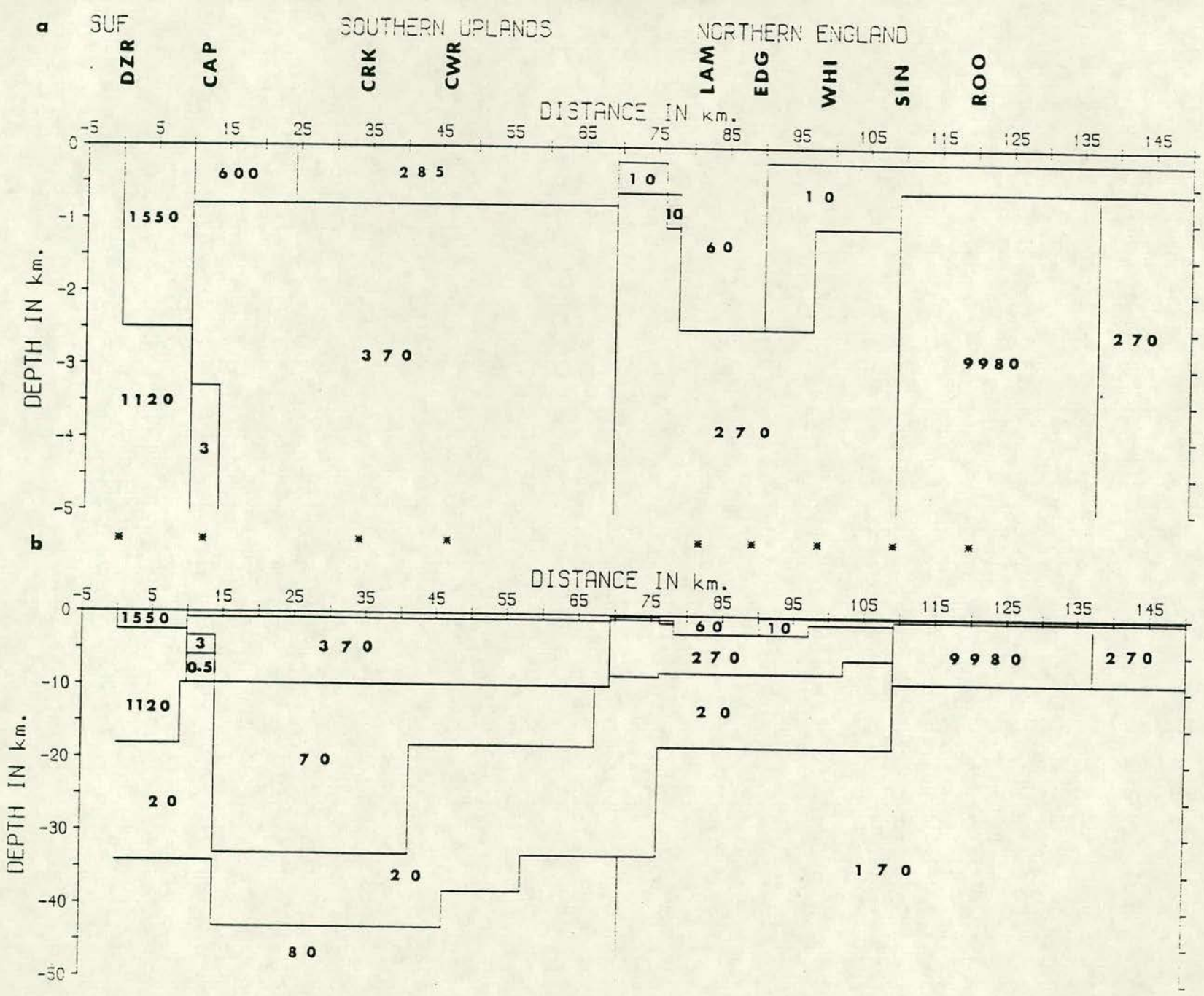
a
SUF
SOUTHERN UPLANDS
NORTHERN ENGLAND
DZR
CAP
CRK
CWR
LAM
EDG
WHI
SIN
ROO
DISTANCE IN km.
DEPTH IN km.
600
285
10
10
10
1550
10
60
370
270
9980
270
1120
3
270
b
DISTANCE IN km.
DEPTH IN km.
1550
3
0.5
370
60
10
270
9980
270
1120
20
70
20
20
170
80

FIGURE 7.5

a-i Observed (shown with error bars) and computed (continuous curve) E- and H- polarization response functions for different stations. Station codes can be seen at top of each figure.

a **DZR**
STATION 1

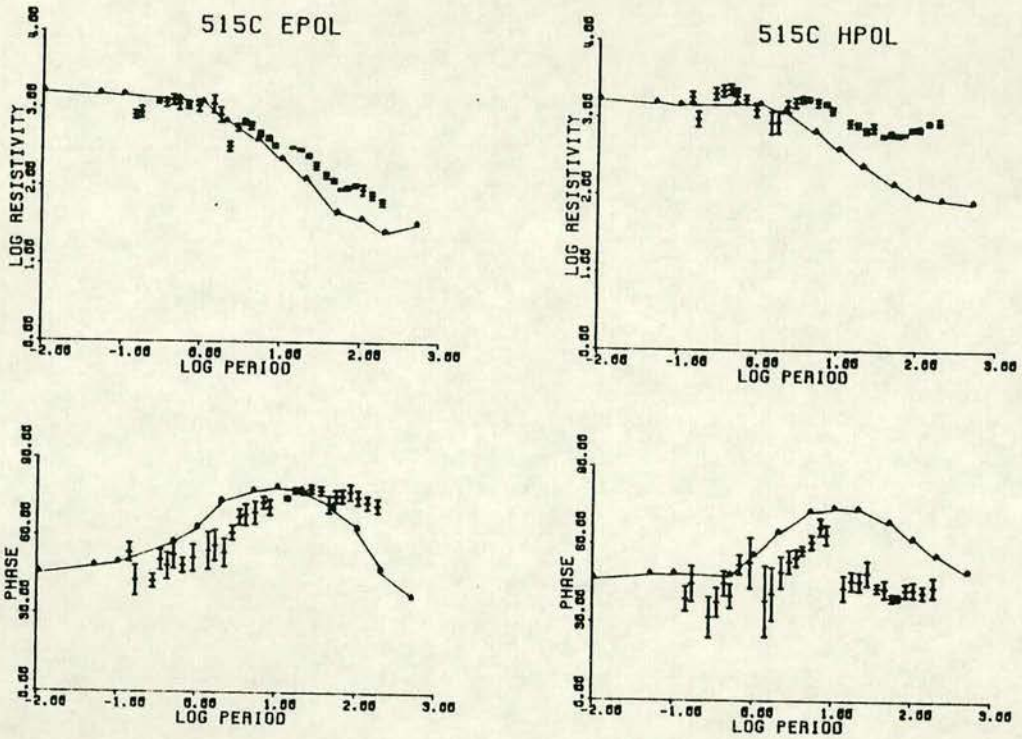

b **CAP**
STATION 2

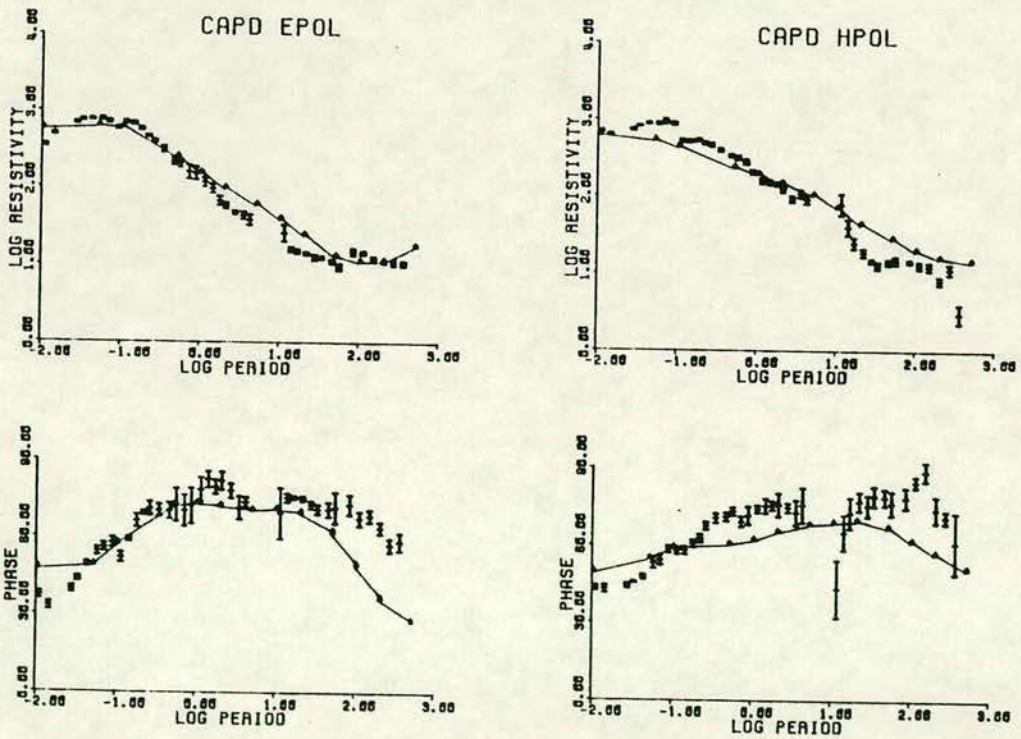

c

CRK
STATION 3

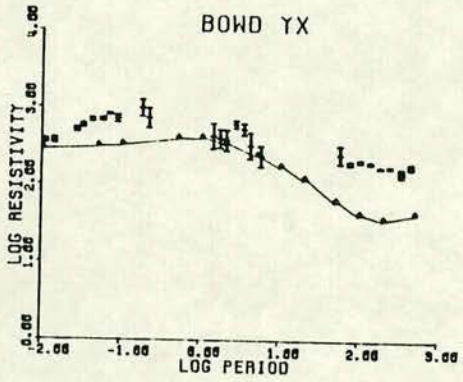

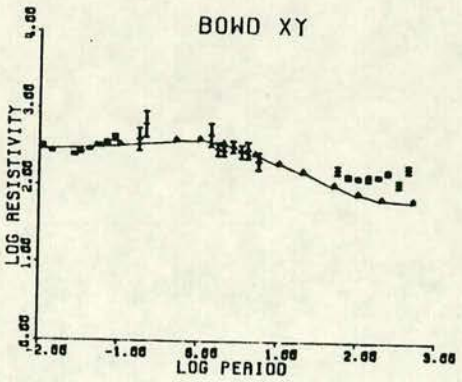

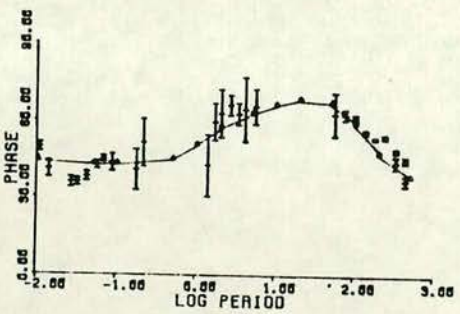

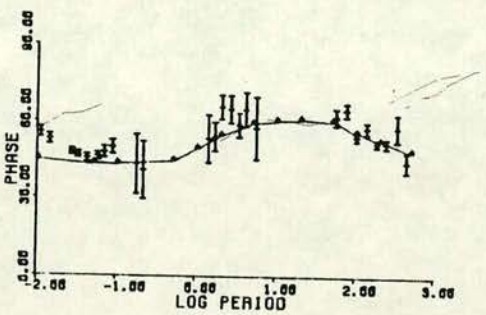

d

CWR
STATION 4

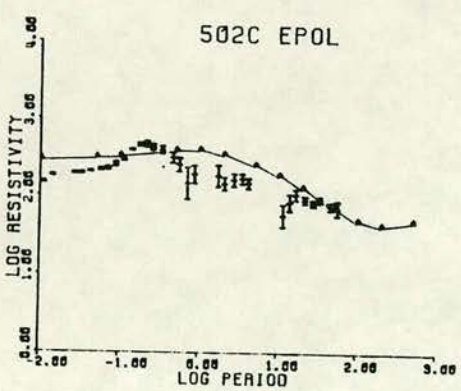

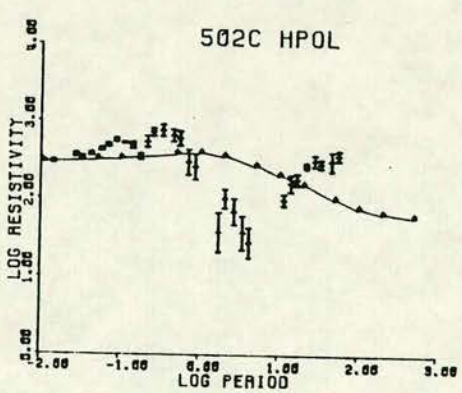

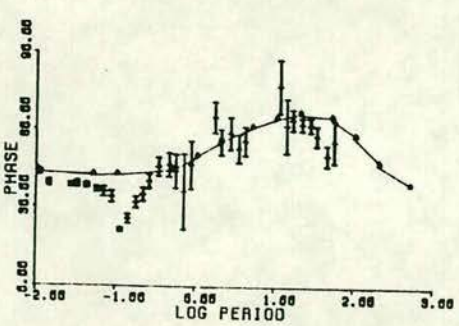

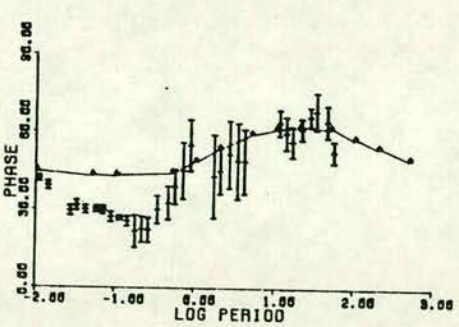

e

LAM

STATION 5

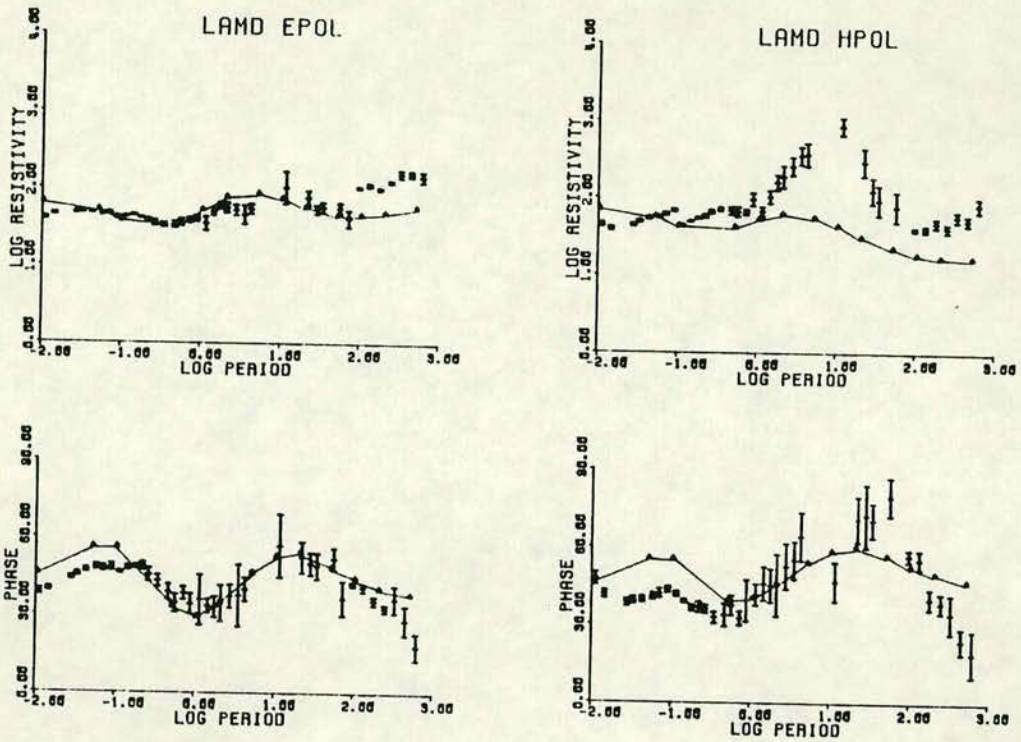

f

EDG

STATION 6

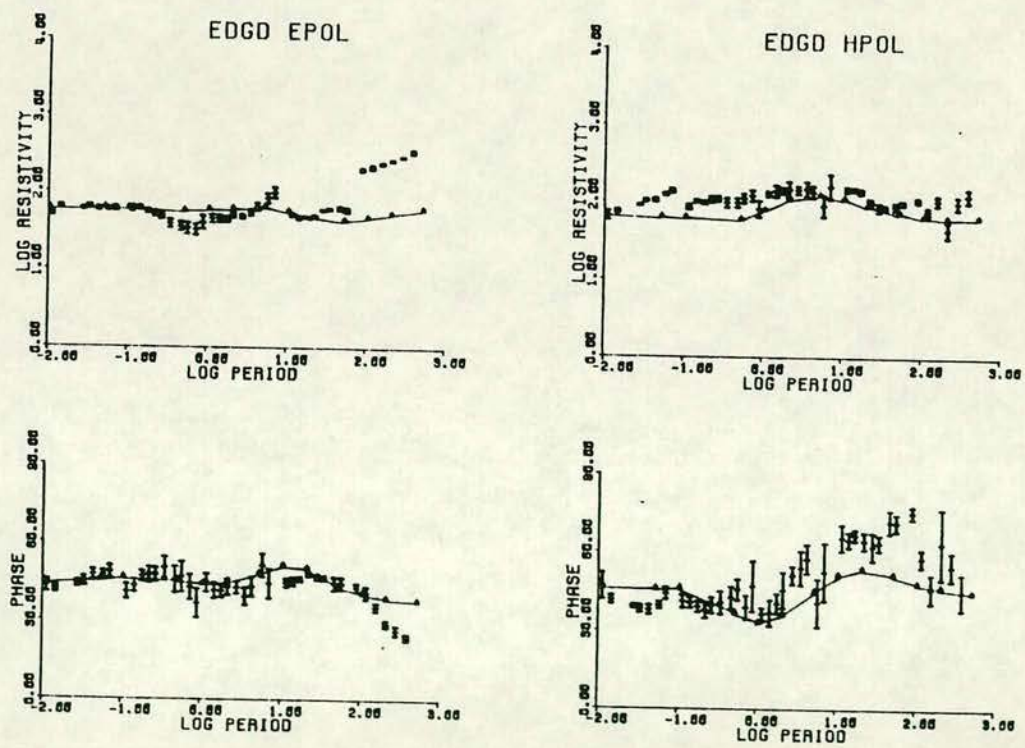

g

WHI
STATION 7

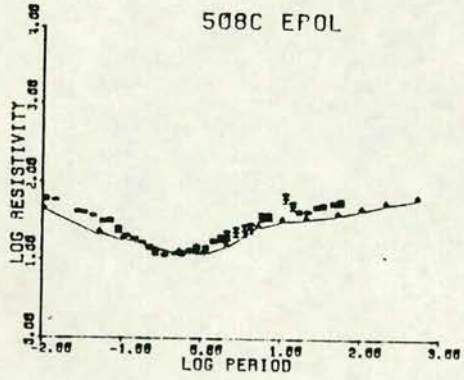

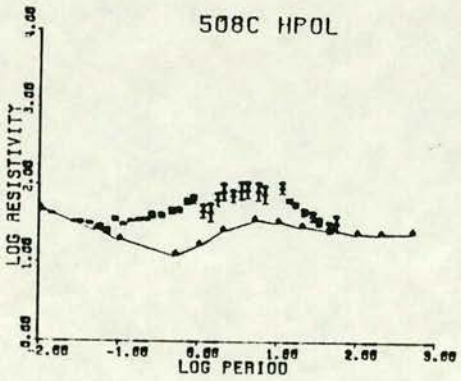

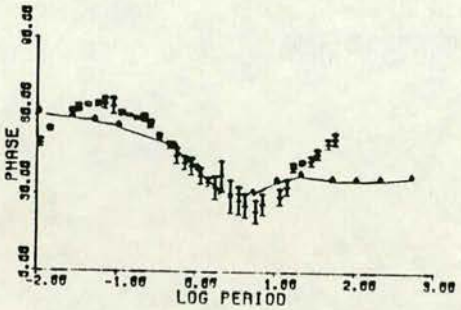

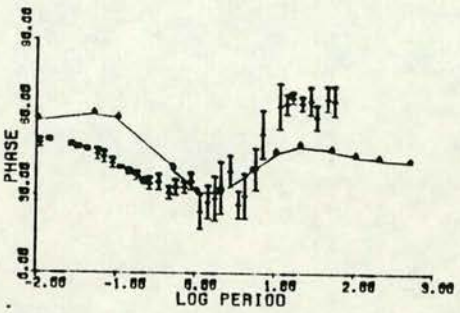

h

SIN
STATION 8

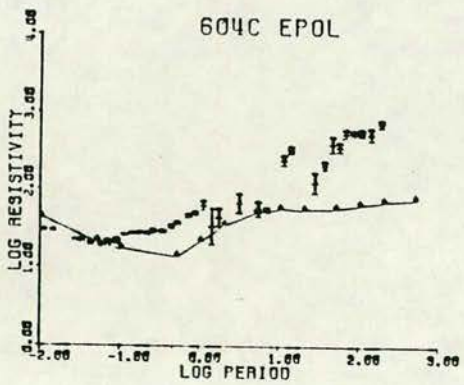

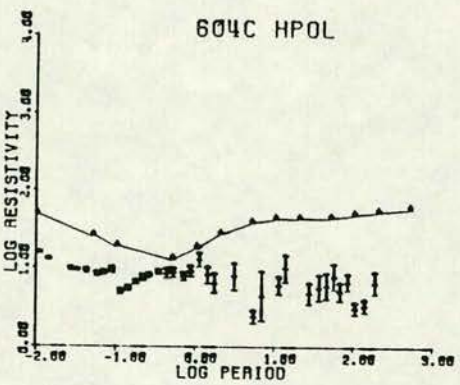

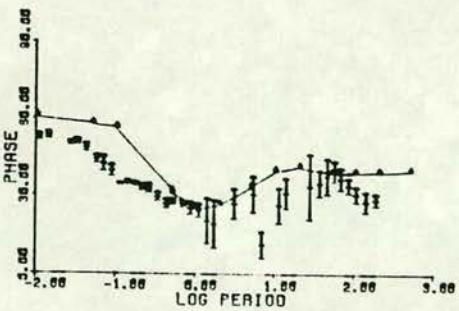

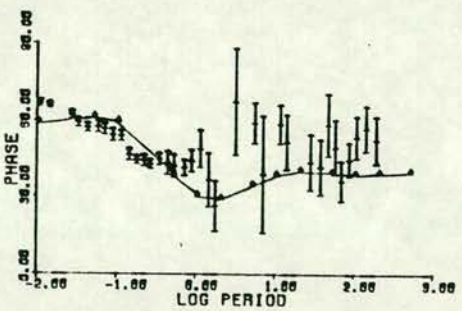

ROO
STATION 9

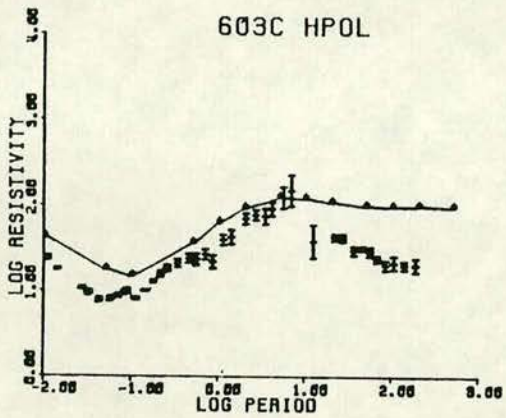

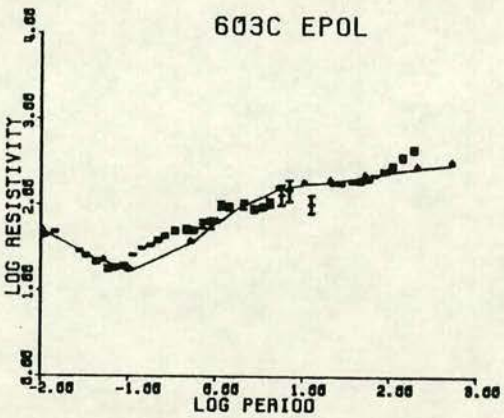

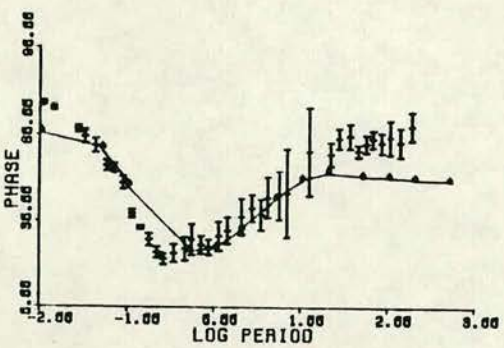

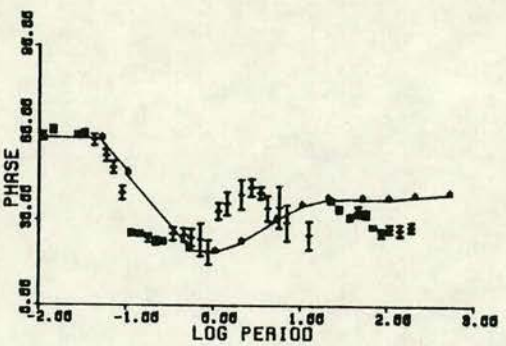

a more highly conducting layer (about 0.5 Ohm.m.) can be seen (Fig. 7.4b).

* Below CRK and CWR from about 1 km. to about 10 km. depth, the layer is moderately resistive (370 ohm.m.). This is underlain by a moderately conducting (71 Ohm.m.) layer to a depth of about 20km. (below CWR) and 30km. (below CRK).

* Below DZR, the model indicates a resistive (1120 Ohm.m.) layer from a depth of about 2.5 km. to a depth of about 18 km..

* All the stations are underlain by a conductor (20 Ohm.m.) whose thickness is about 10–15km. Its depth, however, varies. It is shallow (10km.) below CAP and 18km. deep below DZR and 33 and 20 km. deep below CRK and CWR respectively. This conductor together with the highly conducting layers (3 and 0.45 Ohm.m.) form a pillar-like structure below CAP. Below the conductor (20 Ohm.m.) a resistivity of 80 Ohm.m. is obtained at all the 4 stations.

The Northumberland Basin

The stations LAM, EDG AND WHI belong to this region. The prominent features of the model below the region are:

* The resistivity of the uppermost 0.5–2.5 km. is only 10–58 Ohm.m. is thus quite distinct from the region to and the north.

* The depth to the basement of this conducting layer vary- from about 0.5 km. below LAM, 2.5km. below EDG and about 1km. below WHI. The basement resistivity is 270 Ohm.m. to a depth of 8–9km..

* Below this layer there is a more conducting layer (20 Ohm.m.). This conductor has about 10 km. thickness and is at a depth of about 8–9 km. at all the stations. The resistivity of the lower crust is 170 Ohm.m. which also differs from the lower crust of the Southern Uplands.

The Alston block

The stations SIN and ROO belong to this region.

The distinct resistivity structure below these stations is-

- a thin (0.5 km.) conducting (10-30 Ohm.m.) layer underlain by a highly resistive layer (10000 Ohm.m.) of about 8.5 km. thickness and

- the resistivity of the crust below this highly resistive layer is same as the previous region (170 Ohm.m.).

The relation between this preliminary model of electrical resistivity structure and the regional geology and tectonics will be discussed in the next chapter.

Chapter 8

Discussion of the 1D and 2D modelling results

In this chapter, the 1-D and 2-D electrical resistivity models presented in 6 and 7 chapters are discussed. In section 8.1, the shallow electrical structure of the models is compared with structural geology. Comparison of the models derived in this study with those obtained in earlier induction studies of this region is considered in section 8.2. Earlier gravity, magnetic and seismic investigations are discussed in relation to the 2D electrical model in section 8.3, while in section 8.4, the interpretation of electrical resistivity values of the 1D and 2D models and its tectonic implications are discussed. Finally in section 8.5 the main conclusions of this thesis are presented followed by some suggestions for further work.

8.1. Comparison of the resistivity model with geology

The 2D geoelectrical structure for the traverse presented in chapter 7 is reproduced here as figure 8.1 for ease of discussion. From this figure it can be seen that there is a marked lateral variation of resistivity along the traverse. The resistivity towards NW part of the traverse is 1550 Ohm.m. decreasing to 600, 285 and 60 Ohm.m. respectively in the south eastward direction. This shallow (about 1-2.5 km.) resistivity variation can be compared with the surface geology.

As discussed earlier in chapter 1, the greater part of the study region is covered by Ordovician, Silurian and Carboniferous sedimentary rock formations. Correlating these sedimentary formations with the electrical model, it can be seen that the Ordovician sediments have a resistivity of 1550 Ohm.m. Silurian sediments 285-600 Ohm.m. and the Carboniferous sediments 58 Ohm.m.. From the geological time scale it is clear that the younger Carboniferous sediments are less resistive than the older Ordovician sediments. This is in good agreement with Haak and Hutton,s compilation (Fig.1 1986) of resistivity values of sedimentary rocks.

It is known that the boundary between the Ordovician and Silurian

FIGURE 8.1

The 2-D electrical model- a) to a depth of 5 km. and b) to a depth of 50 km.. There is vertical exaggeration of 10 in figure a). (Reproduced from chapter 7).

SUF= SOUTHERN UPLANDS FAULT

OBF= ORLOCK BRIDGE FAULT

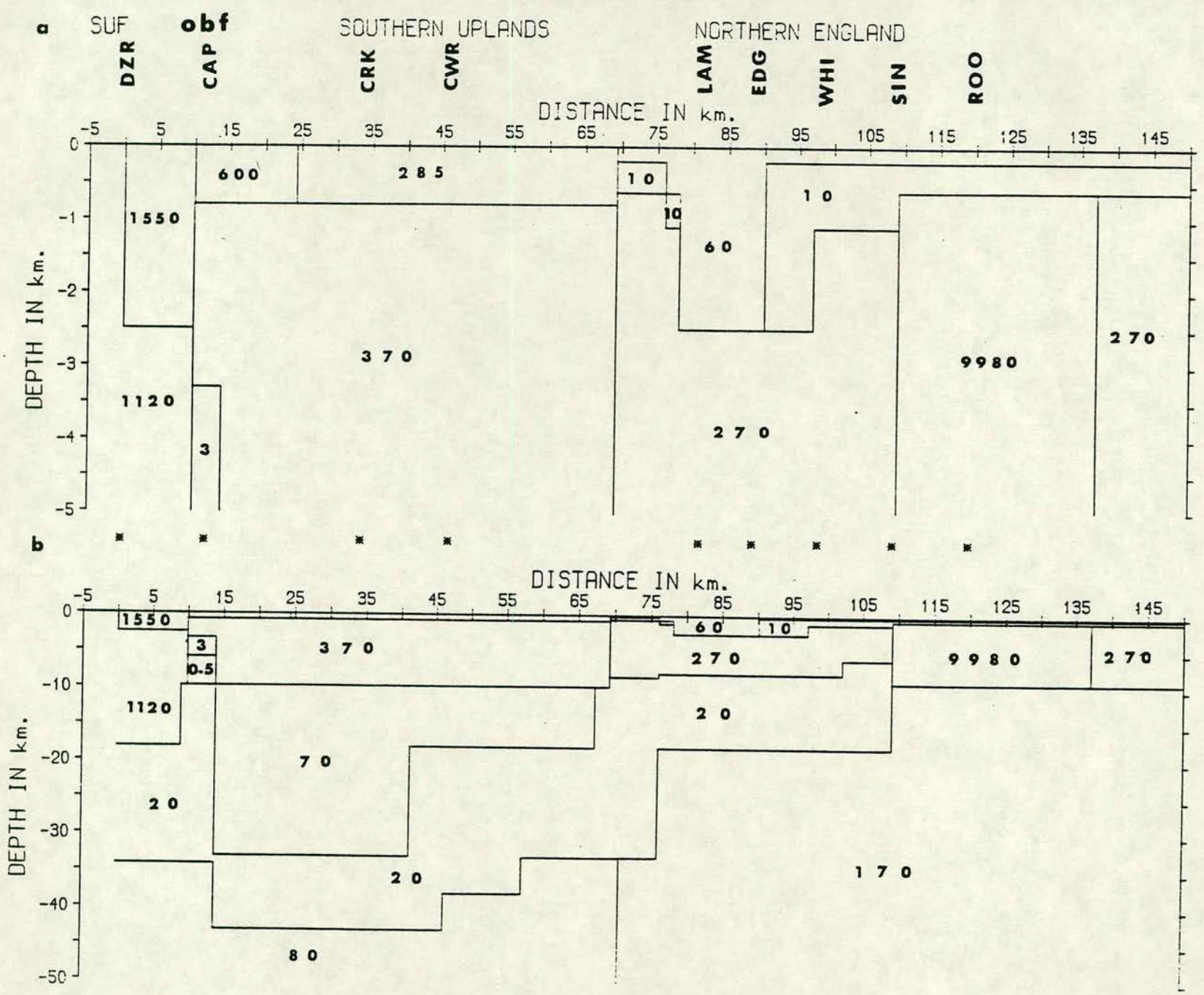
a
SUF
obf
SOUTHERN UPLANDS
NORTHERN ENGLAND
DZR
CAP
CRK
CWR
LAM
EDG
WHI
SIN
ROO
DISTANCE IN km.
DEPTH IN km.
1550
600
285
10
10
10
60
370
1120
3
270
9980
270
b
DISTANCE IN km.
DEPTH IN km.
1550
3
0.5
370
60
10
270
9980
270
1120
20
70
20
20
170
80

sediments is clearly demarcated by the major Orlock Bridge Fault, while that between the Silurian and Carboniferous sediments is not clearly defined being concealed below other sedimentary formations, for example, in the south of the Southern Uplands by Permian sediments (Greig 1971, Johnson 1984). Thus, it can be argued that since there is a considerable resistivity variation between the three distinct sedimentary formations the electrical methods, can be utilized in demarcating surface or even subsurface lateral boundaries.

The shallow electrical structure derived from the 1-D model results for the Northumberland is summarized in Fig. 8.2. These 1D results were obtained considering the invariant response functions using two inversion schemes as discussed in chapter-6. For BEW and EDG stations, E-pol response functions are considered, since these results are more comparable with the results of the adjacent stations. From the figure it can be seen that there is a distinct electrical boundary between sediments above and basement below. The resistivity of the sediments is about 10-60 Ohm.m. and that of the basement about 100-270 Ohm.m., however, the basement resistivity at ROO and HIL is as great as 500-1000 Ohm.m.. The basement depth is as shallow as about 0.2km. towards the NW but increases to about 2.5 - 3 km. near EDG and again becomes shallow near ROO and HIL, where the depth is about 0.5 km.. The seismic refraction basement determined by Bott et al (1984) using quarry blasts has been projected on to the present traverse and plotted for comparison on the same figure. Though there is a general agreement between the refraction and electrical basement depths, they differ at EDG by about 1km. The reasons for the discrepancy is not very clear, however, if the two different physical parameters represent the same structure, then the possible reasons for the discrepancy can be attributed either to the assumption of the seismic refraction velocity of sediments of Northumberland basin or an error in the assumption of MT 1D/2D modelling or to errors in both the methods.

The more resistive (500-1000 Ohm.m.) layer below the Alston block from a depth of about 0.5 km. at ROO and HIL stations corresponds to the Weardale Granite Batholith. It can be observed that the basement resistivity in the Northumberland basin ranges from 100-270 Ohm.m., which is quite distinct from that of the overlying sediments. By comparison with the resistivity of the Silurian sediments of Southern Scotland region it appears that these

FIGURE 8.2

A schematic diagram showing the shallow resistivity structure in Northumberland. This was prepared from a compilation of 1-D models.

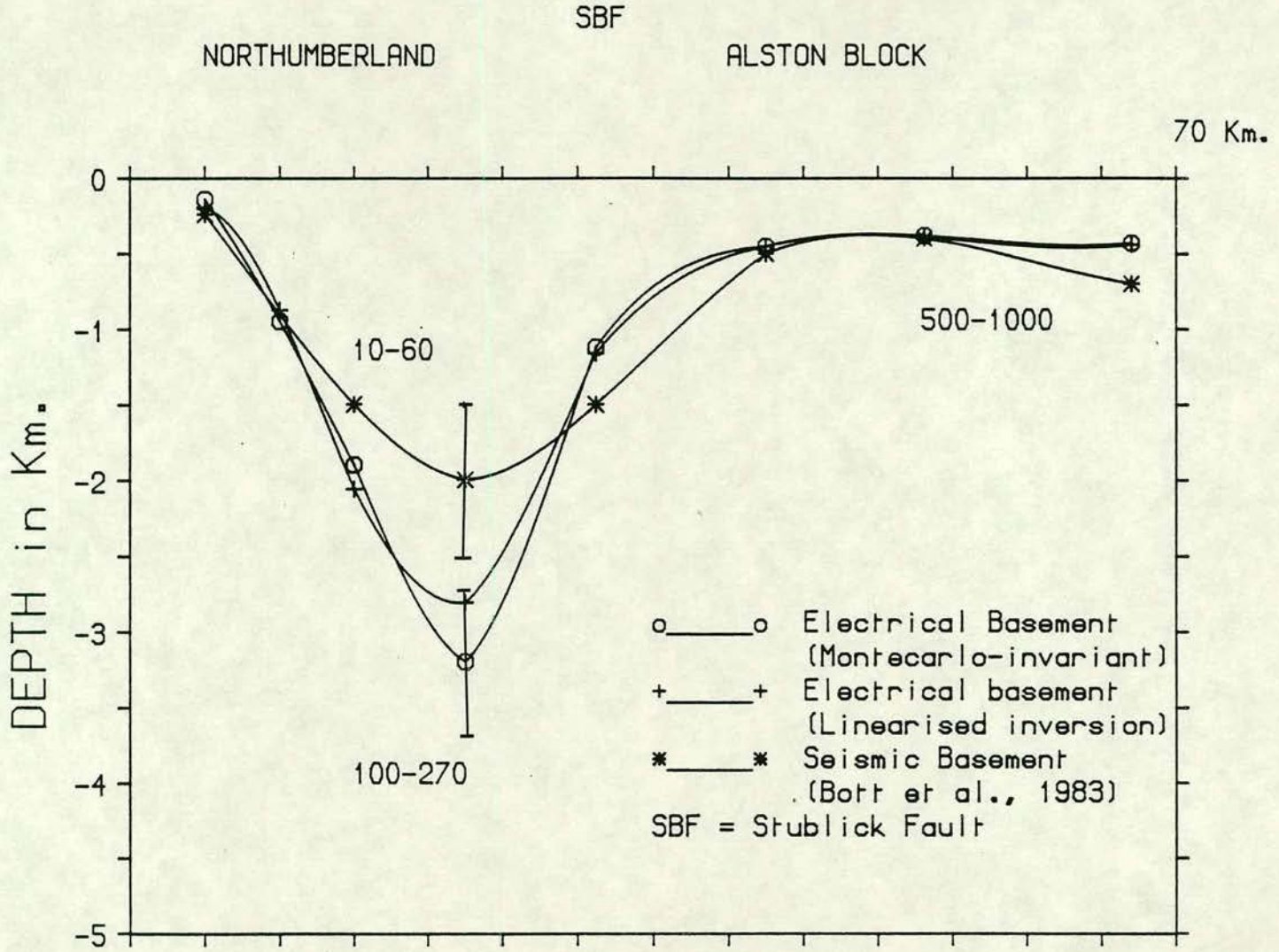
SBF
NORTHUMBERLAND
ALSTON BLOCK
70 Km.
DEPTH in Km.
0
-1
-2
-3
-4
-5
10-60
100-270
500-1000
o_____o Electrical Basement (Montecarlo-invariant)
+_____+ Electrical basement (Linearised inversion)
_____ Seismic Basement (Bott et al., 1983)
SBF = Stublick Fault

sediments probably formed the Northumberland basement. This deduction is supported by the results of the Caledonian suture seismic experiment (Bott et al 1985), which obtained a basement velocity of 5.5–5.7 km/sec indicating the presence of the Lower Palaeozoic rocks below the Northumberland basin. Thus it can be argued again that electrical methods in general and MT method in particular can be utilized in determining the basement elsewhere in Northumberland basin.

8.2. Comparison of the 2–D resistivity model with models derived from earlier induction studies

The details of the 2–D model of the present study have been described in chapter 7, but two features are considered again here. Firstly, the depth to the mid–lower crustal conductor obtained from this model varies from about 6.5 km. near the northern edge of the Weardale granite to about 30 km. under the Southern Uplands and then to a shallow 3.5 km. near CAP (Fig. 8.1b) which is located near the 'Orlock Bridge Fault'. Secondly, the crustal structure of the Southern Uplands shows a marked resistivity–depth variation –a) 370 Ohm.m. between 1–10km. b) 70 Ohm.m. from 10 to 30 km. and c) 20 Ohm.m. from 30 to 40 km. These two features can be directly compared with those of previous induction studies of the region.

Prior to this work, five main MT investigations had been undertaken in the study region (Jones and Hutton 1979, Ingham 1981, Novak 1981, Beamish 1986 and Sule and Hutton 1986), with results as summarized in Fig. 8.3. The 1–D modelling results obtained by Jones and Hutton using their Montecarlo inversion scheme are presented in Fig. 8.3a. This shows a conductor (25–90 Ohm.m.) below Southern Scotland and Northern England, with its depth being less than 5 km. below TOW in Northern England and as much as 24–42 km. below BOR and PRE in Southern Scotland. The 2–D model of Ingham and Hutton (1982) for a Southern Scotland traverse is presented in fig. 8.3b. This model includes a conductor (30–100 Ohm.m.) dipping from Northern England to Southern Scotland thickening in the latter region and then rising to shallow depths near the SUF and b) a resistivity of 3000–10000 Ohm.m. for the upper crust. Novak (1981) from his 1D modelling studies of broad band MT traverse (BB′ in fig. 1.2) suggested a conductor below the Northumberland basin.

FIGURE 8.3

Results of earlier induction studies. a) A schematic geoelectric section of the Southern Uplands. A fixed basement resistivity of 750 Ohm.m. is assumed. SUF= Southern Uplands Fault. BOR, NEW etc., are the station names and their locations can be seen in the Fig. 1.2 (from Jones and Hutton 1979).

b) A 2-D resistivity model across the Southern Uplands and the Midland valley. PEN, EAR etc., are the MT stations- their locations can be seen in the Fig. 1.2 along AA'. (from Ingham and Hutton 1982).

c) The simplified tectonic model proposed by Leggett et al (1983) is shown on the left hand side in zone a) of the figure and zone (b) of the figure represents the depth profile of the highly conducting layer from three MT stations. The MT station locations can be seen in Fig. 8.5a. Numbers shown in the figure represent the seismic p_wave velocities in km./sec. Note the vertical exaggeration X2 (from Beamish 1986).

d) A simplified 2D geoelectrical model for SE Scotland with a horizontal exaggeration of 3 (from Sule 1985).The location of this profile can be seen as CC' in figure 1.2.

e) A contour map showing the in-phase part of the vertical magnetic field, when the horizontal field is directed to the magnetic north. Solid circles represent the GDS station locations (from Banks et al 1983). The thick solid line -0 contour line- represents the axis of the magnetic variation anomaly.

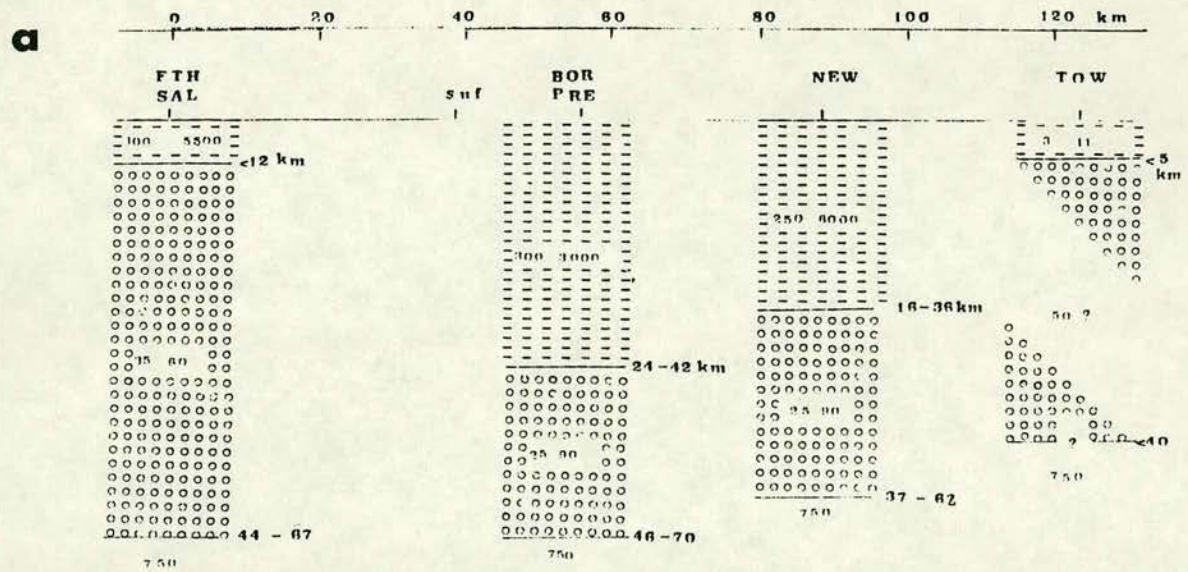
a
0
20
40
60
80
100
120 km
FTH
SAL
suf
BOR
PRE
NEW
TOW
100 5500
<12 km
44 - 67
750
300 3000
24-42 km
46-70
750
250 6000
16-36km
37 - 62
750
3 11
<5
km
50 ?
<40
750

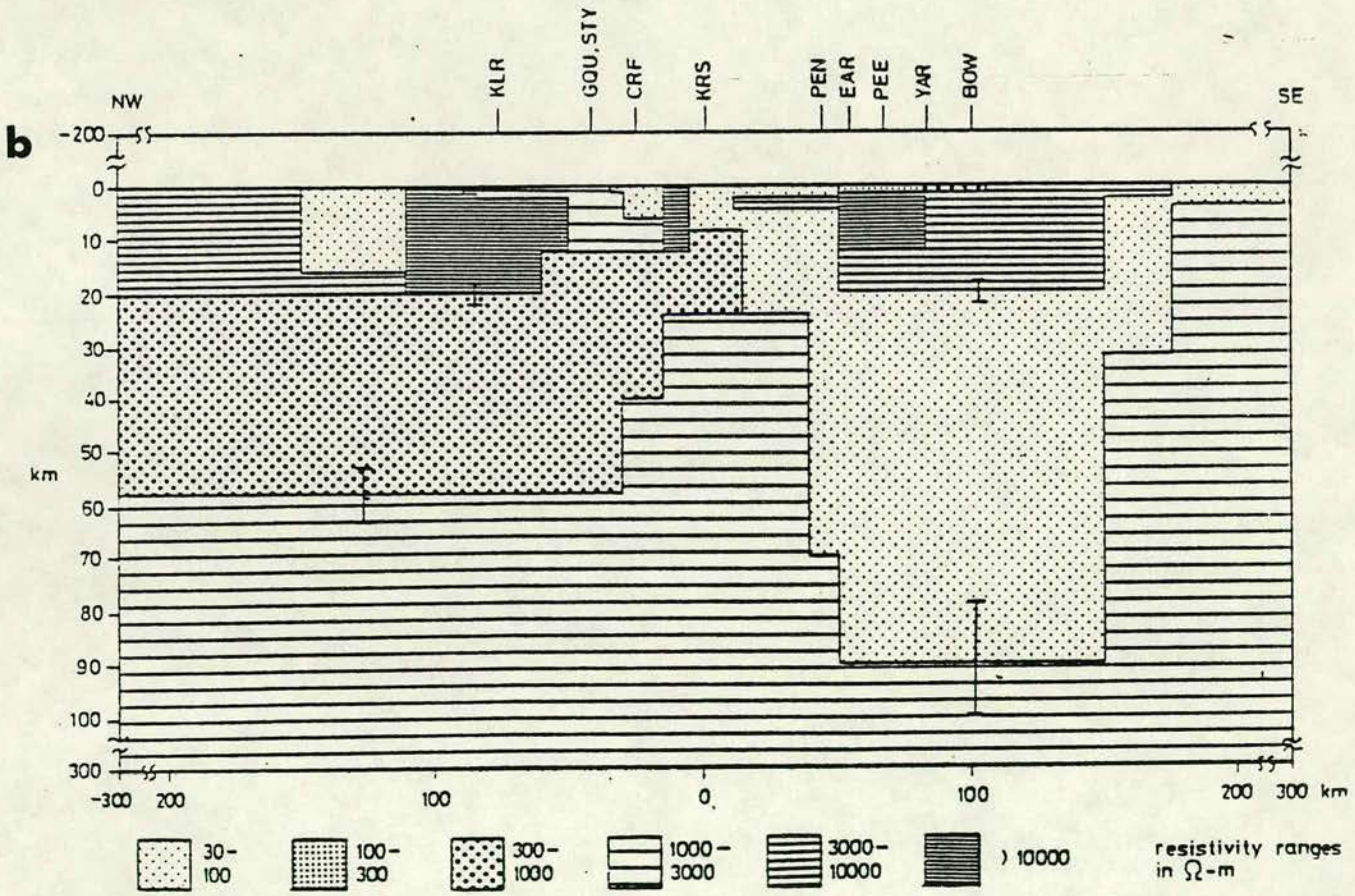
b
NW
SE
KLR
GQU,STY
CRF
KRS
PEN
EAR
PEE
YAR
BOW
-200
0
10
20
30
40
50
60
70
80
90
100
300
km
-300
200
100
0
100
200
300 km
30-
100
100-
300
300-
1000
1000-
3000
3000-
10000
) 10000
resistivity ranges
in Ω-m

c

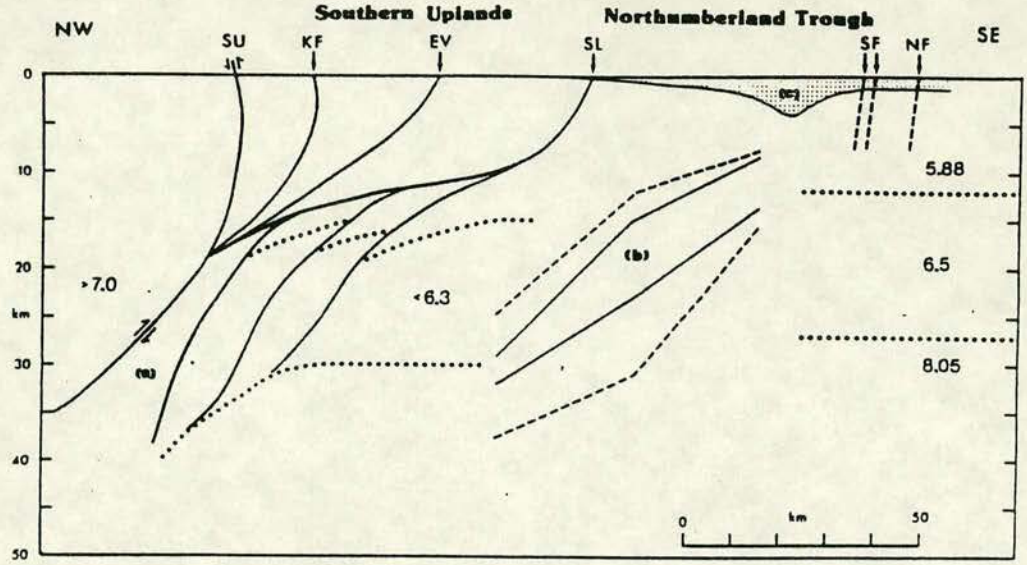
NW
Southern Uplands
Northumberland Trough
SE
SU
KF
EV
SL
SF
NF
0
10
20
km
30
40
50
>7.0
<6.3
(a)
(b)
(c)
5.88
6.5
8.05
0
km
50

d

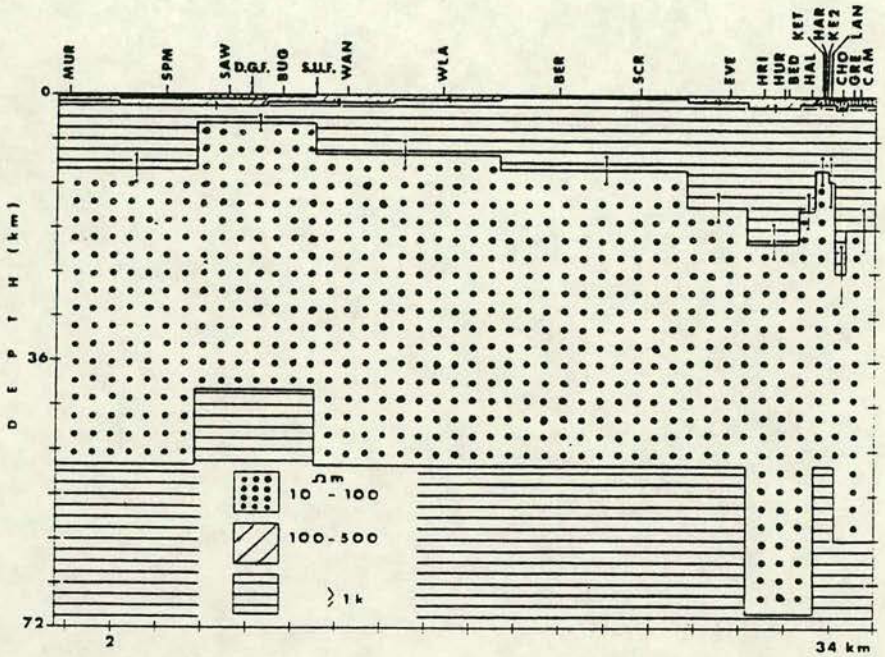
MUR
SPM
SAW
D.G.F.
BUG
S.U.F.
WAN
WLA
BER
SCR
EVE
HRI
HUR
BED
HAL
KET
HAR
KE2
CHO
ORE
LAN
0
DEPTH (km)
36
72
2
34 km
Ωm
10 - 100
100-500
≥ 1 k

e

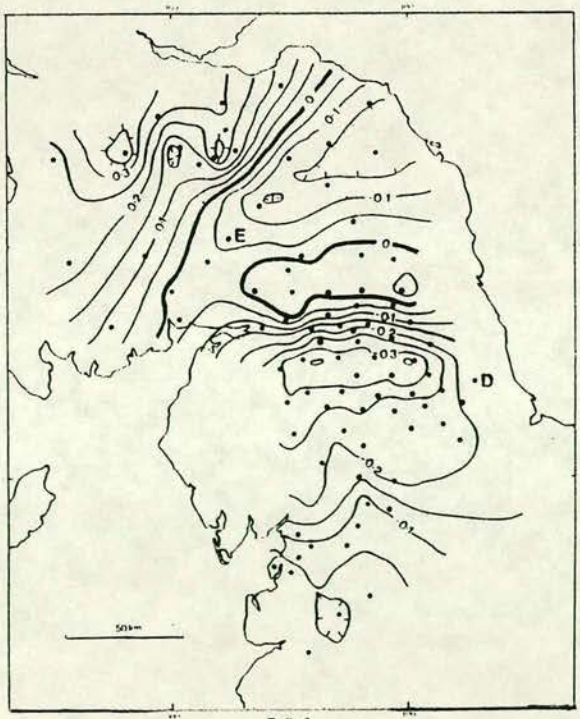
E
D
50km

Beamish's (1986) model derived from three long period (15-10000 sec.) MT soundings is presented in Fig. 8.3c superposed on Leggett et al (1983) tectonic model. The seismic refraction velocities can be seen to the right of this figure representing 5.88km./sec, 6.5 km./sec for the upper and lower crust respectively and 8.05 km./sec for the upper mantle. The electrical model includes a 5-10 km. thick conductor (10 Ohm.m.) dipping towards NW from the Northumberland basin. The upper crustal resistivity assumed in modelling these results 1 dimensionally, varies from 1000 Ohm.m. in the Northumberland basin to 1,00,000 Ohm.m. in Southern Scotland.

The 2-D model from a broad band MT investigation along a shorter parallel traverse about 55 km. east of the present traverse is presented in Fig. 8.3d (Sule and Hutton 1986). Due to the closer station spacing in this investigation and use of both AMT and MT frequencies a detailed electrical structure was obtained. From their model it can be seen that a shallow (at about 4 km. depth) conductor (10-100 Ohm.m.) exists near the Southern Uplands Fault (SUF in the figure). It dips to both north and south.

Comparing these previous models with that of the present study this study has yielded some new information and resolved in greater detail the structures indicated by the earlier studies. The new results are -a) the detection of the shallow conductor about 20 km. south of Southern Uplands Fault near CAP, b) the indication of a significant electrical resistivity variation at a depth of about 10 km. below the Southern Uplands, with a resistivity contrast of about 5 and c) a conductor, at a depth of about 8-10 km. from below the Northumberland basin to the Northern edge of the Weardale granite.

The present model has confirmed the results of the previous induction studies of a conductor dipping northward from Northumberland (about 10 km.) towards Southern Uplands (about 35km.). As the shallow conductor near CAP appears to correspond with the shallow conductor detected by Sule (1985) to the east, it is probable that these two shallow conductors belong to a single unit (Sule and Hutton 1986). Apart from MT results, results of several GDS investigations in the study region have been published (Bailey and Edwards 1976, Hutton and Jones 1980). From these studies, a major magnetic variation anomaly, named the 'Eskdalemuir anomaly', was detected. Its axis is approximately parallel to and south of the SUF. With the addition of results

from a dense array in Northern England, Banks et al (1983) located an additional anomaly around the Northumberland basin as shown in Fig. 8.4e. From the 2-D modelling of GDS data, Banks (1986) has proposed the existence of a deep conductive body below the Northumberland basin.

Recent MT measurements in a traverse across the Irish Midlands, (Whelan and Hill 1987) and that of Sule (1985) both of which are parallel to the present traverse have indicated the presence of a shallow (at about 3 km.) conductor near the Virginia line and the SUF respectively. It is interesting to speculate that this shallow conductor is related to the shallow conductor near CAP and that it may be considered a signature of major tectonic processes.

For the region mapped in Fig. 8.4e, a 3D thin sheet model study has also been carried out (Jowiak and Beamish 1986). The anomalous vertical magnetic field at 750s period was considered for modelling. In the model, considering 0.2 S/m conductivity and 2.5km. thickness, 500 S was assumed for the sediments of Northumberland basin. From the present study, however, lower conductance values are observed for the basin. Considering an optimum resistivity value of 30 Ohm.m., a thickness of 3 km. for the sediments (Fig. 8.2), and neglecting the presence of bulk resistive formations such as Great Limestone and Great Whin sill, a conductance of 100 S should be assigned to the Northumberland basin. It can be argued, however, that such a high conductance (500 S) is possible in this region if the parameters of the deep (8-10 km.) conductor below the basin are also considered.

8.3. Comparison of the electrical resistivity model with other geophysical models

8.3.1. Seismic investigations:

Results of various on-shore and off-shore seismic studies are available from the region in and around that of this study. The main on-shore seismic investigations include - LISPB (Bamford et al 1978), seismological array studies by Hall et al (1983) and the CSSP profile (Bott et al 1985). The off-shore seismic investigations of interest to the present study are the - WINCH-2E (Brewer et al (1983) and NEC (Klemperer and Matthews 1987) profiles.

LISPB, the first seismic refraction profile across Britain revealed a contrast

FIGURE 8.4

a) The location of NEC and WINCH (Brewer et al 1983, Hall et al 1984) seismic profiles; 'Stars' represent the MT stations of Beamish (1986); Structural contours for the Iapetus suture can also be seen.

b) Line drawings of unmigrated and migrated time sections along NEC and WINCH profiles; IS= Iapetus suture (from Klemperer and Mathews 1987).

a

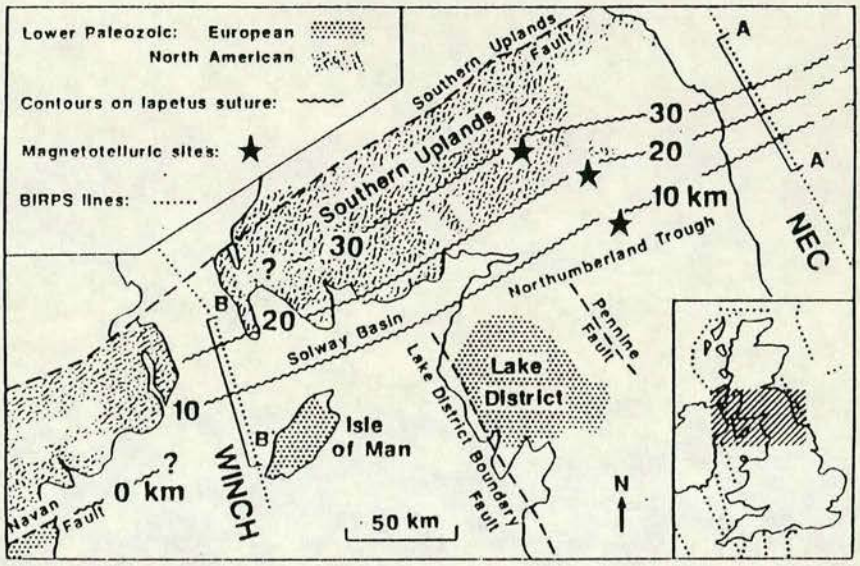
Lower Paleozoic: European
North American
Contours on Iapetus suture:
Magnetotelluric sites:
BIRPS lines:
Southern Uplands Fault
Southern Uplands
30
20
10 km
A
A'
NEC
Northumberland Trough
Pennine Fault
Solway Basin
Lake District
Lake District Boundary Fault
Isle of Man
WINCH
B
B'
10
0 km
Navan Fault
50 km
N

b

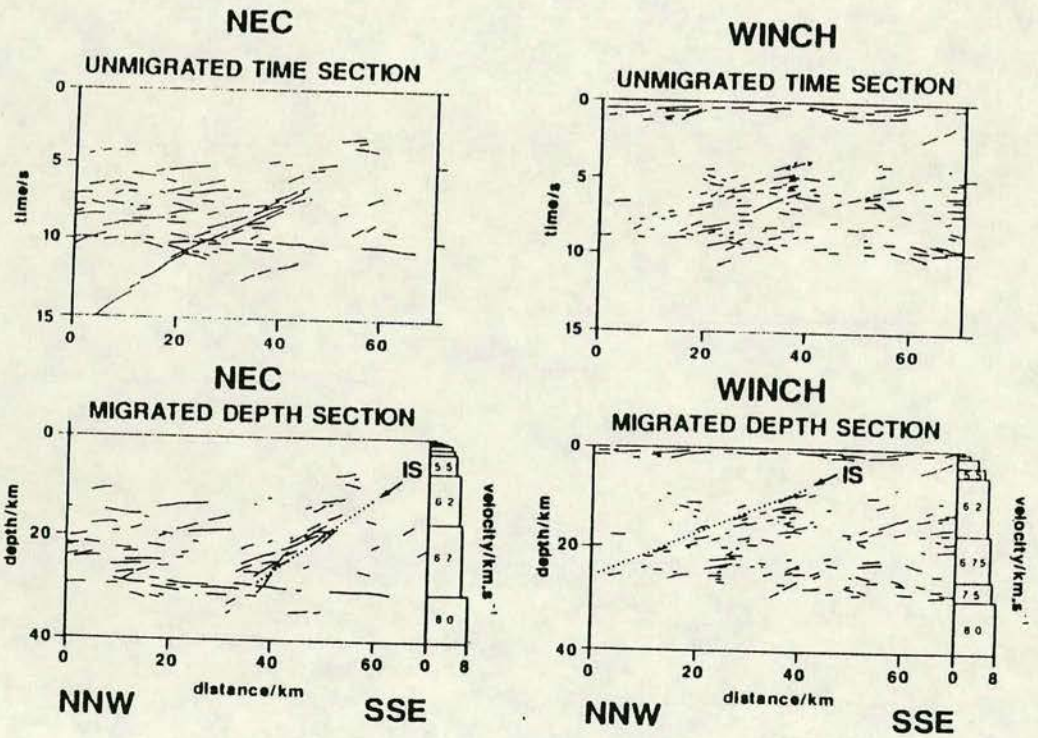
NEC
UNMIGRATED TIME SECTION
time/s
WINCH
UNMIGRATED TIME SECTION
time/s
NEC
MIGRATED DEPTH SECTION
depth/km
IS
velocity/km.s⁻¹
distance/km
NNW
SSE
WINCH
MIGRATED DEPTH SECTION
depth/km
IS
velocity/km.s⁻¹
distance/km
NNW
SSE

in velocities of the pre-Caledonian crustal layers on either side of the Southern Uplands Fault and in the Southern Uplands two seismically 'undetermined' regions observed at depths of about 15 - 20 km. respectively (see Fig. 2 of Bamford et al. 1978). From observations of quarry blasts and seismic array studies, Hall et al (1983) proposed that crystalline rocks of continental affinity exist at a depth of 1-5 km. below the Southern Uplands and that the Midland valley crust continues for 15-20 km. southwards into the Southern Uplands. The CSSP profile (Bott et al 1985), crossing Northern England has been has been interpreted as indicating the presence of continental basement below the Lower Palaeozoic layer of the Northumberland basin.

Comparing these results with the electrical model of Fig. 8.1b it can be observed that near the seismically 'undetermined' region, south of the SUF, a highly conducting zone has ben detected. The electrical boundary at a depth of about 10 km. below the Southern Uplands corresponds to the seismic refraction basement at a depth of about 15km. It can also be noted that the lower crust under the Northumberland basin has a resistivity of about 170 Ohm.m. and a seismic velocity of 6.6 km/sec. as observed from CSSP study, both are considered to be the 'normal' values for the lower continental crust.

From the results of the deep seismic reflection surveys, a NW dipping reflector has been observed off-shore along the WINCH-2E profile. This has been interpreted as a signature of the Iapetus suture by Brewer et al (1983). In the parallel NEC profile in the North sea this feature has also been observed, dipping more steeply than on the WINCH section (fig. 8.4). The NW dipping conductor detected by previous studies appears to be compatible with the present data and to correspond more with the WINCH-2E reflectors than those of the NEC profile.

Thus the model derived from the present study has features which in some respects have some correspondence with the models from other geophysical studies. In the following section the possible causes of high conducting zone and the tectonic setting of the region are discussed.

8.4. Reasons for high electrical conductivity and tectonic implications

8.4.1. Reasons for high electrical conductivity

The causes of high electrical conductivity in the crust and mantle layers have been extensively discussed by Shankland and Ander (1983), Etheridge et al (1983), Schwarz et al (1984), Gough (1986), Haak and Hutton (1986) and Campbell (1987). The conductivity of rocks near the earth's surface is mostly electrolytic and depends mainly on the amount of water content, its salinity etc.. The electrical conductivity of crustal rocks can be due to the presence of free water, free carbon, hydrated minerals (eg. Serpentine), aqueous fluids with high ionic content, magnetic oxides, sulphur etc.. Thus the presence of high electrical conductivity in a region can be due to either one or combination of these factors. Any factor assigned to the high conductivity is generally based on considering the indirect evidence from several other factors, for example, high heat flow, the presence of hot springs and from laboratory analysis of rock samples etc.. In recent years, however, the most favoured factor for high electrical conductivity of crustal rocks is the presence of aqueous fluids with high ionic content (Shankland and Ander 1983).

Only a few heat flow observations are available for the present study region (Gale et al. 1984, Oxburgh et al 1980). A high heat flow (about 100 mW. m^{-2}) has been reported near the Weardale granite and a broad heat flow value of 50 mW m^{-2} has been deduced for most of the Southern Uplands and Northumberland basin (Gale et al. 1984). If the same conducting mechanism is assigned to the deep conductor obtained below Northern England and Southern Scotland and the assumed heat flow value for the Southern Uplands is valid an increased fluid concentration as argued by Shankland and Ander (1983) is probably the most preferable cause for the highly conducting zone.

8.4.2. Tectonic implications:

As discussed earlier in Chapter 1, various complex tectonic models have been proposed for Southern Scotland since the hypothesis for the existence of a 'proto-Atlantic' or 'Iapetus' ocean between Scotland and England during Ordovician and Silurian times was proposed by Wilson (1966). All these models have been compiled and discussed by Holland et al (1979) and are shown in Fig. 8.5. It can be seen that the models are quite complex and

FIGURE 8.8

Summary of the tectonic models proposed for the British islands. (from Holland et al 1979)

a) after Dewey (1969)

b) after Fitton and Hughes(1970)

c) after Jeans (1973) and Gunn(1973)

d) after Church and Geyer (1973)

e) after Lambert and Mckerrow (1976)

f) after Wright (1976)

and g) after Phillips, Stillman and Murphy (1976).

HBF= Highland Boundary Fault

SUF= Southern Uplands Fault

LD= Lake district

MT= Moine thrust

TD= Tweedale

C= continental crust

o= oceanic crust

r= spreading ridge

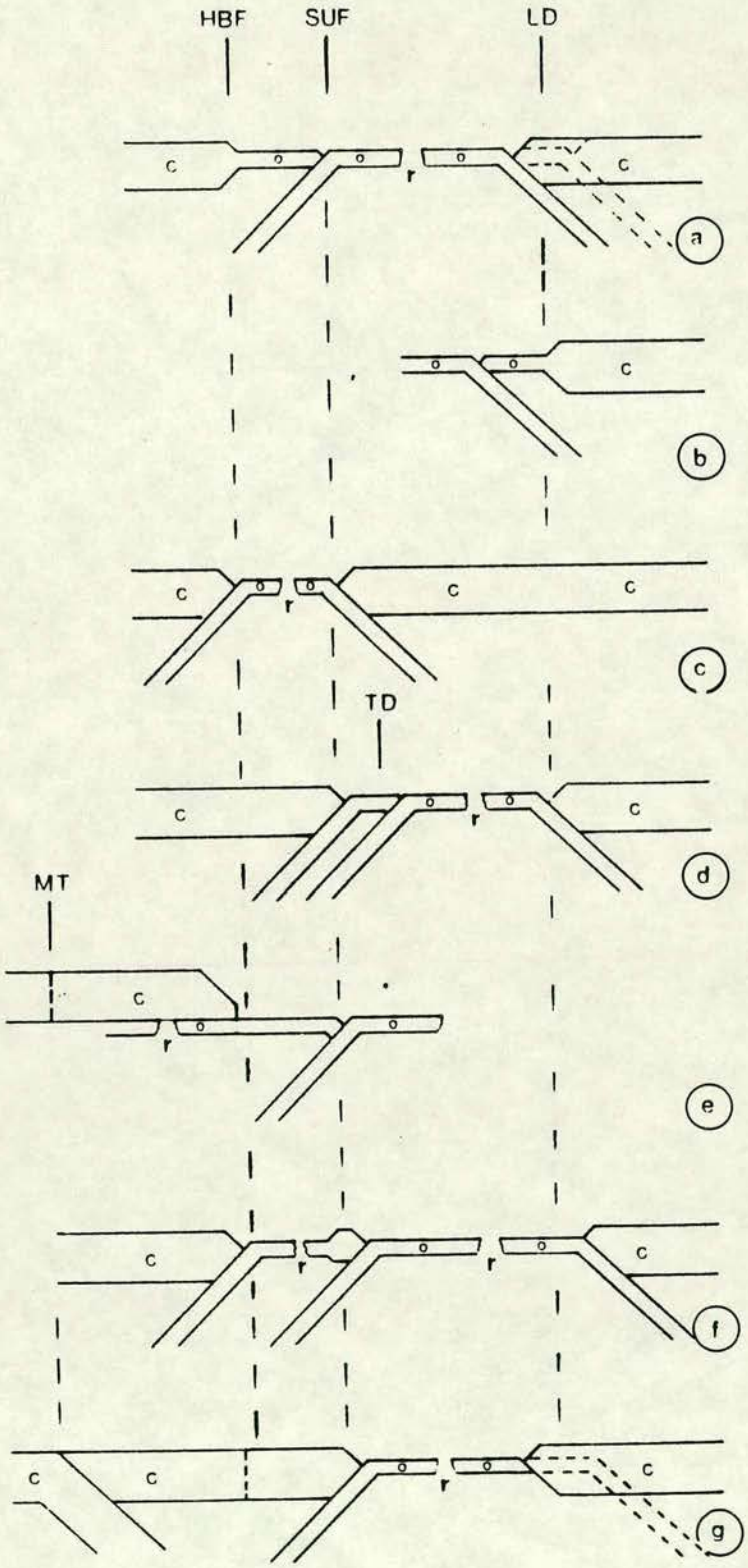
HBF
SUF
LD
TD
MT
c
r
a
b
c
d
e
f
g

contain between one and three subduction zones. Unfortunately, no single model has yet been accepted as illustrated by the continued controversy at a recent Geological Society of London meeting (Mckerrow 1987). Perhaps more geological and geophysical investigations may help resolve the diverse views.

An attempt is made here to speculate on a tectonic model on the basis of the present study and to compare it with other tectonic regions. Based on the 2D-model of the present study, a simplified electrical model is presented in Fig. 8.6a and for comparison the geoelectric models derived from Vancouver island and Japan, are presented in Fig 8.6b and c (Kurtz et al 1986 and Rikitake 1975 respectively).

From study of the short period geomagnetic variations, a model comprising a thin conducting layer, 'triangular' in shape (see Fig. 8.6c), has been proposed for the structure under Japan (Rikitake 1975). It can be seen from this figure that the highly conducting mantle drops to a depth of about 200 km. from a depth of about 40-50 km. beneath the Pacific coast. This depression gradually becomes shallower towards the Japan sea. From magnetotelluric and geomagnetic depth sounding measurements across Vancouver island, a highly conducting zone has been detected at the top of the subducting Juan de Fuca plate dipping gradually from Pacific Ocean (Kurtz et al 1986). From the two dimensional model shown in fig 8.6b, it can be seen that this conductor is shallow near the Georgia Strait. A 30 Ohm.m. resistivity has been assigned to the dipping conductor which is surrounded by highly resistive (5000 Ohm.m.) medium. Comparing the three models (Fig. 8.6a, b and c) some similarities can be observed. These are- a) a dipping highly conducting layer is present and b) all the three models contain an approximately similar 'triangular' resistive block. If such a 'triangular' model is acceptable as a signature for subducting plates in an island-arc environment, it is of great interest that such a model exists in the Southern Uplands. It may be worth mentioning here again that- a) the northward dipping structure has been detected not only from the present study but also from the earlier induction and seismic reflection studies. b) the shallow conductor south of the SUF has been observed in 2 parallel MT traverses and from GDS studies. It is also of interest to note that this conductor is near the major Orlock Bridge Fault. c) It is generally accepted that the final closure of the Iapetus is along the Solway Firth line.

FIGURE 8.9

a) A speculative model based on the 2-D model of the present study. The dotted area represent the conducting regions.

b) A 2-D resistivity model which represents the subduction of the Juan de Fuca plate. The location of the area is shown in a rectangular box at the top side of the figure. (from Kurtz et al 1986)

c) A triangular model resulting from GDS studies. The dashed curve is the smoothed distribution of actual observations for 30 min. period (after Rikitake 1975)

a

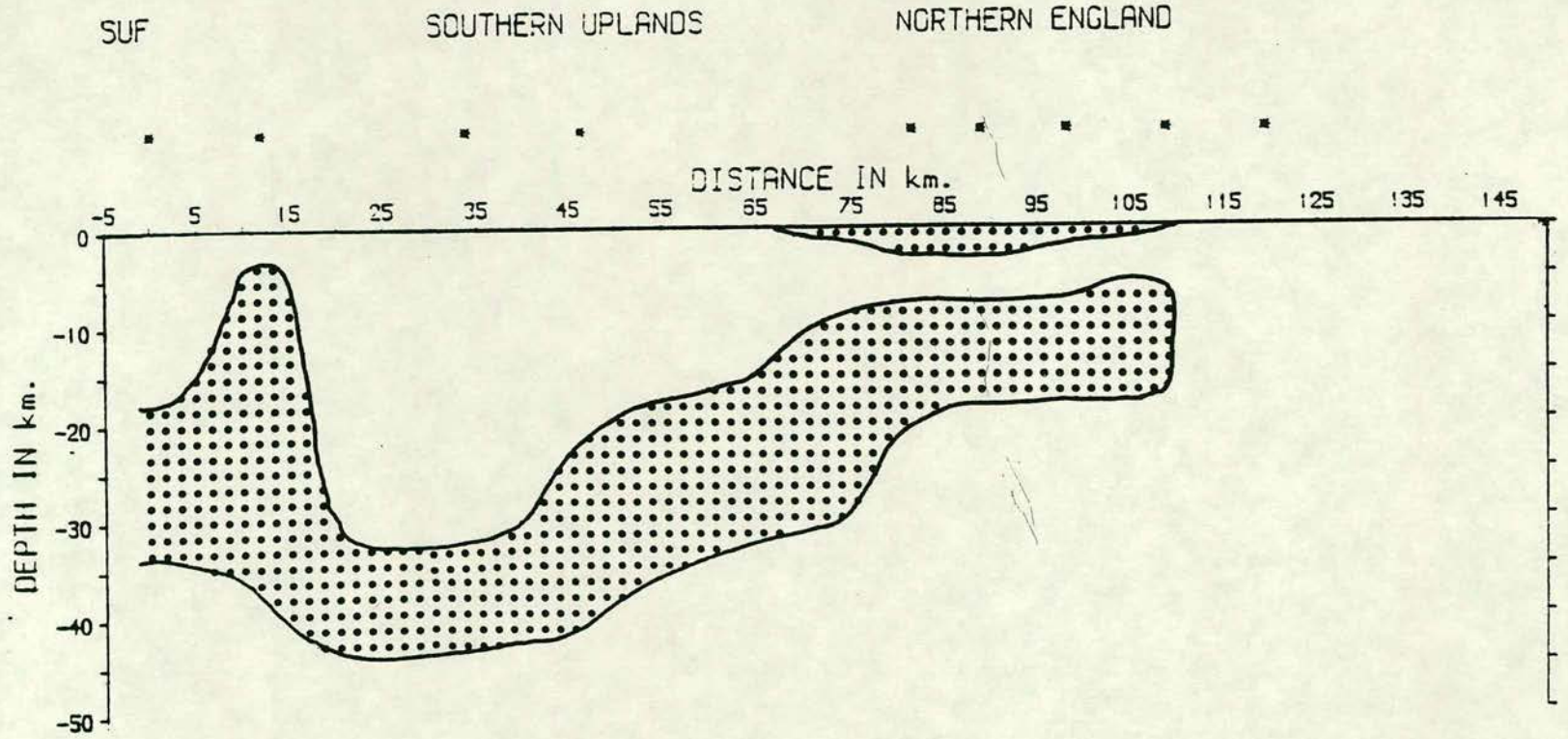
SUF
SOUTHERN UPLANDS
NORTHERN ENGLAND
DISTANCE IN km.
-5
5
15
25
35
45
55
65
75
85
95
105
115
125
135
145
0
-10
-20
-30
-40
-50
DEPTH IN km.

b

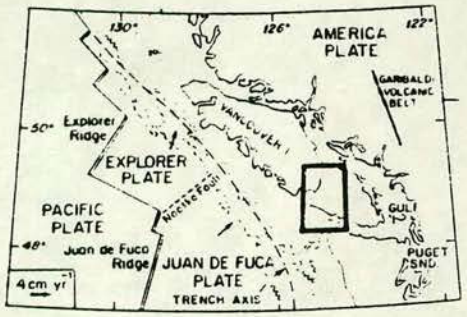
130°
126°
122°
AMERICA PLATE
GARIBALDI VOLCANIC BELT
50°
Explorer Ridge
EXPLORER PLATE
VANCOUVER I.
Nootka Fault
PACIFIC PLATE
GULF
48°
Juan de Fuca Ridge
JUAN DE FUCA PLATE
PUGET SND.
4 cm yr⁻¹
TRENCH AXIS

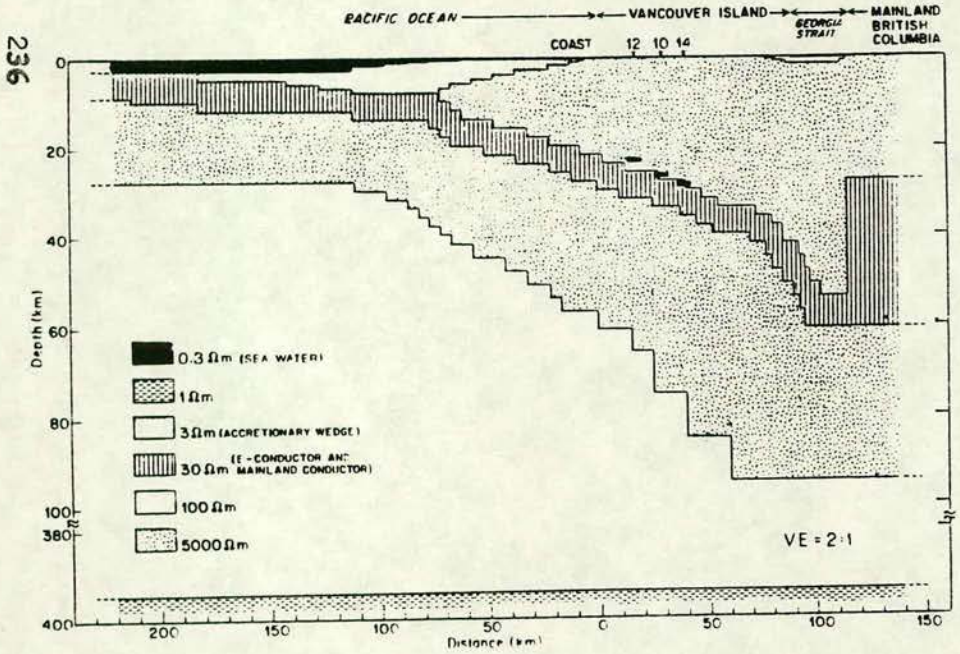
PACIFIC OCEAN
VANCOUVER ISLAND
GEORGIA STRAIT
MAINLAND BRITISH COLUMBIA
COAST
12 10 14
0.3 Ωm (SEA WATER)
1 Ωm
3 Ωm (ACCRETIONARY WEDGE)
30 Ωm (E-CONDUCTOR AND MAINLAND CONDUCTOR)
100 Ωm
5000 Ωm
VE = 2:1
Depth (km)
Distance (km)

c

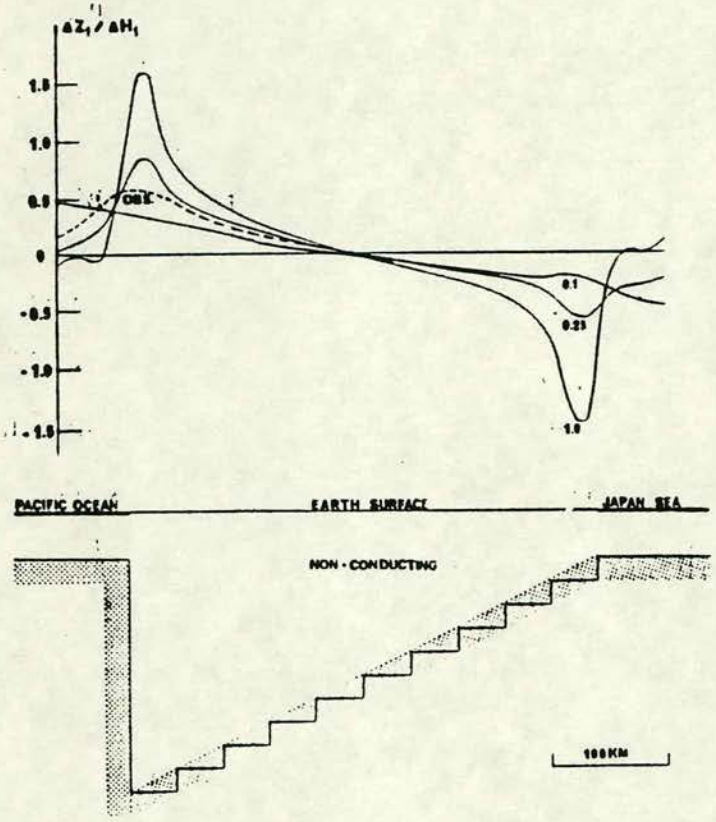
ΔZ₁ / ΔH₁
1.5
1.0
0.5
0
-0.5
-1.0
-1.5
OBS
0.1
0.25
1.0
PACIFIC OCEAN
EARTH SURFACE
JAPAN SEA
NON-CONDUCTING
100 KM

Thus considering these results for the U.K. and by analogy with those from Japan and Vancouver it is possible to reach the speculative conclusion that the Southern Uplands region from the Orlock Bridge Fault to the Solway Firth was part of an island. However, before accepting such a conclusion all the available geological and geochemical data require examination to assess whether or not they support this hypothesis.

8.5. Conclusions and suggestions for further work

8.5.1. Conclusions

The conclusions which can be drawn from the studies associated with this thesis are now presented separately for field and computational aspects.

Field investigations:

The present field study has not only confirmed the results of the earlier studies but the resistivity structure along the traverse has been better resolved, especially for the upper crust, as discussed below:

- A shallow (at about 3.5 km.) conductor (about 0.4-5 Ohm.m.) has been detected near CAP in the Southern Uplands. Interestingly, this shallow conductor exists near the major 'Orlock Bridge Fault' and also corresponds to the Eskdalemuir magnetic variational anomaly.

- The complex upper crustal resistivity structure below the Southern Uplands has been resolved. The top layer resistivity is about 250-600 Ohm.m. below which there is a moderately conducting layer.

- The marked lateral variation of the surface resistivity obtained from the present study corresponds to the three distinct geological formations- Ordovician, Silurian and Carboniferous sediments. The older sediments are more resistive than younger sediments.

- The present study provides information about the electrical basement of the Northumberland basin and shows a distinct resistivity contrast between the sediments and basement. The depth to the electrical basement compares well with seismic refraction results.

- Joint inversion of MT and DC data has resolved a thin shallow high resistivity structure at ROO in the Alston block. This structure can be identified as the Great Limestone layer.

- A speculative tectonic model is proposed following comparison of the results of the present study with those of other tectonic areas. The hypothetical model proposed implies that the Southern Uplands region from Orlock Bridge Fault to the Solway Firth was part of an island arc.

Computational analysis:

- The Maximum entropy and delay line filtering techniques have been applied both to synthetic and field data and found to be useful in eliminating persistent noise such as regular coherent noise and spike noise.

- A conducting hill in a sedimentary environment can distort the telluric measurements with the distortion depending strongly on the inclination, the height of the hill and the basement depth. It is shown that the apparent resistivity values of MT soundings near hills may be overestimated.

- From 2D forward modelling studies of the Northumberland basin, Weardale granite and Stainmore basin, observations made over the Weardale granite have been shown to be distorted by about 10% by the sediments of the basins.

8.5.2. Suggestions for further work

The results of the present study indicate that further investigation is required in the study region as described below:

- It would be interesting to study further the areal extent of the shallow conductor, detected south of the SUF in the present study. For this purpose an MT traverse along a traverse parallel to and west of the present study traverse is suggested.

- Since much of the southern part of the Southern Uplands seems to be affected by cultural electrical noise, careful selection of sites is crucial in getting good data. Some times, it is not possible to find a good site within a radius of even 5–10km. since (eg. near ESK) there may be a 5 km. or more length of electrical fences. In such noise areas, a controlled source technique is suggested. If a remote site not affected by local noise can be located, then the remote

reference technique may be used to reduce the noise at the survey site.

- Since the data sets from SIN and ROO are highly anisotropic, a detailed MT investigation with closer spacing (about 1 km.) would help provide better resolution of the crustal structure in this region. A full 3D modelling study may be necessary to understand the anisotropic behaviour of the response functions in this complex area and also to study the effect of the adjacent shallow seas.

- Since the present study has been carried out on a regional basis, an increase in station density would certainly help to resolve the crustal structure proposed by this study.

I. APPENDIX-A

I.I. Adaptive processing

The use of adaptive processors and filters is popular in engineering applications, especially for telecommunications and data transmission systems. For example, the concept of adaptive noise cancelling and the use of adaptive filters and their application in various noise environments, have been extensively discussed by Widrow et al (1975) and Cowan and Grant (1985). Generally, in data processing, the method employed for estimating a signal corrupted by additive noise involves passing it through a filter which tries to suppress the noise while leaving the signal relatively unchanged. The advantages of adaptive filters are their ability to adjust their own parameters automatically and the fact that their design requires little or no a priori knowledge of the signal or noise characteristics.

The problem considered first in this study was the estimation of impulse response function of the earth from a single-input and single-output system. This was considered as a system identification problem and its solution was approached using the adaptive least mean square algorithm. The necessary software for LMS algorithm was provided by Mc Kerrow (1987, per. comm.). The adaptive approach to this problem is described in fig. A.1.

Assume that X,Y are the input and output repectively of a linear system whose impulse response W is required. Consider,

$$\overline{x_j} = [\, x(j),\, x(j-1) \ldots\ldots,\, x(j-n+1) \,]^T$$

$$\overline{w(j)} = [\, w_0(j) ,\, w_1(j) \ldots\ldots,\, w_{n-1}(j) \,]^T$$

.....A.1

$\overline{w}(j)$ is the estimate of the actual impulse response $\overline{w}$ at time j. d(j) is the actual system output. The estimated output y(j) can be written as,

$$y(j) = \overline{w}^T(j) \,.\, \overline{x}\,(j)$$

FIGURE A1

The block diagram showing the application of adaptive filters to a single-input and single-output system.

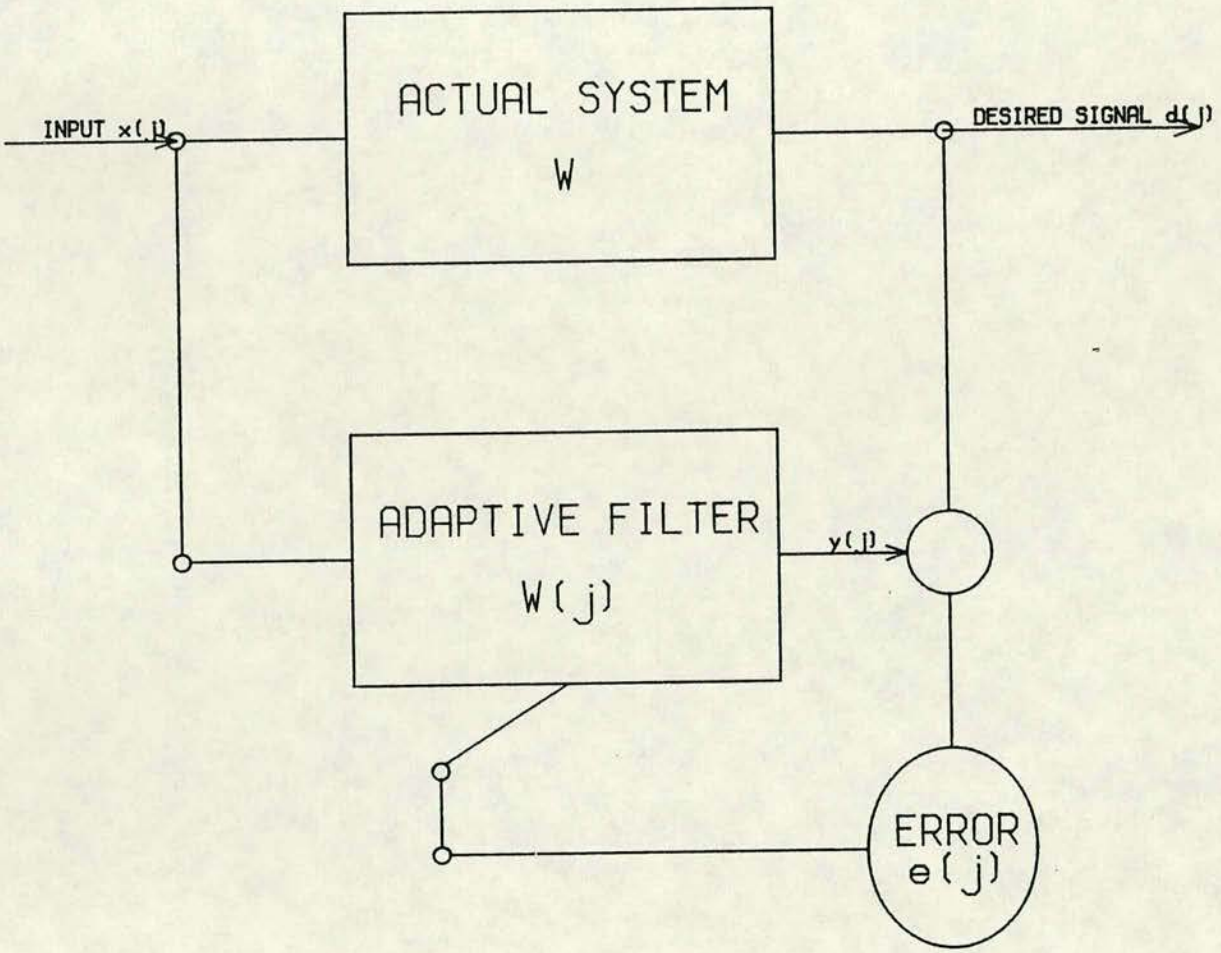
ACTUAL SYSTEM
W
INPUT x(j)
DESIRED SIGNAL d(j)
ADAPTIVE FILTER
W(j)
y(j)
ERROR
e(j)

The error e(j), becomes

$$e(j) = d(j) - y(j)$$

.....A.3

and the impulse response function w(j+1) can be written as

$$\bar{w}(j+1) = \bar{w}(j) + 2\ \bar{x}(j)\ e(j)$$

I.II. Applications

This method was first applied to synthetic data from a single-input single-output system as follows: Firstly, an input sequence x(j) and an impulse response function w(j) were assumed and an output sequence y(j) was computed using equation A2. Thus all the parameters- input, output and the impulse response function- of the system were known. Given these input and output sequence the LMS algorithm estimated the impulse response function. Its performance could be tested by comparing the computed and actual impulse response functions. The processes involved in the algorithm can be explained in the following simple terms. a) For each input sequence value an output sequence value was computed assuming the impulse response function. It may be noted that initially all the values of the impulse response function were zero. b) The computed sequence output by the system was compared with the given output sequence and an error estimated. c) Since the input sequence was a continuous series, this can be continued as an iteration process. At each iteration the error was reduced such that the system impulse response function was updated. d) When the error between these computed and actual output sequences reduced to about -40DB it could be assumed that the system impulse response function matched well with the actual impulse response function.

The input data considered in the present study were a random number series (NAG library routine- G05CAF). Results of two examples considering arbitrary impulse response functions are shown in figures A.2a and b. In the

FIGURE A2.

The error power between the assumed and computed output sequences for the single input system. The impulse response function assumed for the results shown in a) was exp (−0.5j), b) sin (−2.5j), where j is the sample number.

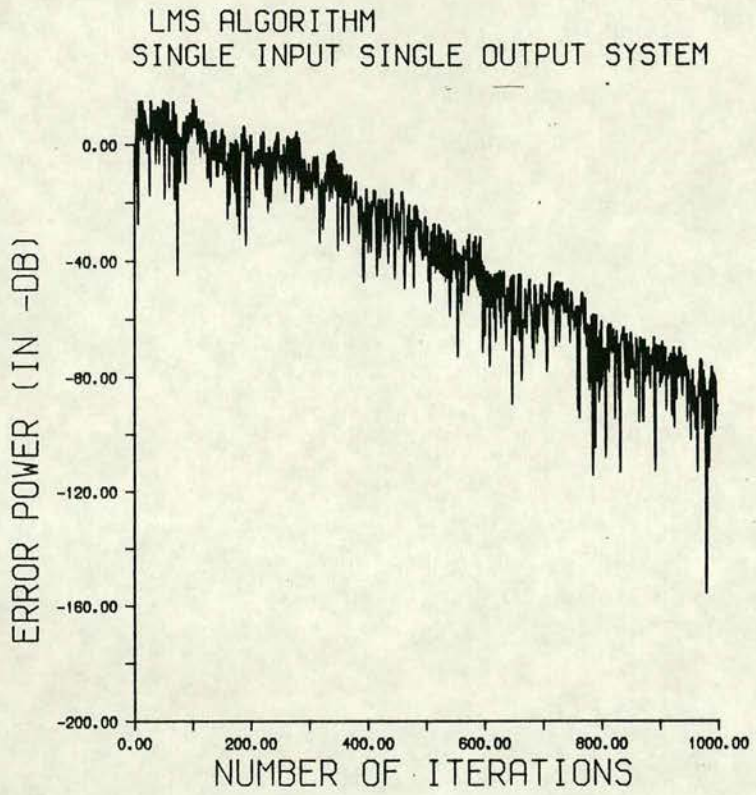
LMS ALGORITHM
SINGLE INPUT SINGLE OUTPUT SYSTEM
ERROR POWER (IN -DB)
0.00
-40.00
-80.00
-120.00
-160.00
-200.00
0.00
200.00
400.00
600.00
800.00
1000.00
NUMBER OF ITERATIONS

b

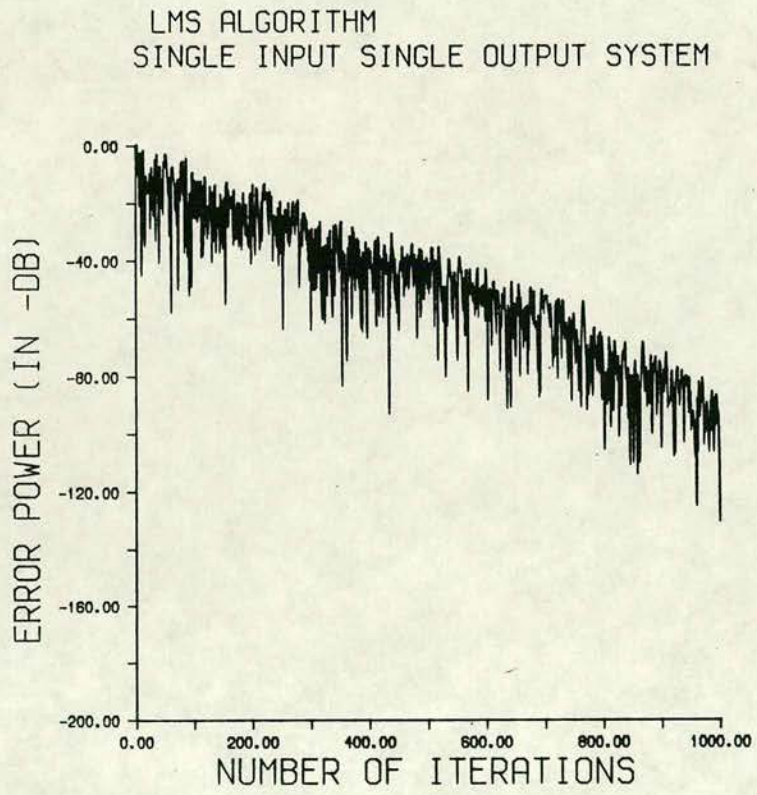
LMS ALGORITHM
SINGLE INPUT SINGLE OUTPUT SYSTEM
ERROR POWER (IN -DB)
0.00
-40.00
-80.00
-120.00
-160.00
-200.00
0.00
200.00
400.00
600.00
800.00
1000.00
NUMBER OF ITERATIONS

a

first example, the impulse response function was assumed as 'exp(−0.5j)' and in the second example, sin(−2.5j) was considered, where j varies from 1 to 32. The error power between the desired and computed output as a function of number of iterations for the first example can be seen in fig. A.2a and for the second example in fig. A.2b. It can be seen that for both the response functions the error level falls below about −90 DB after 1000 iterations.

The results for two input and single output system are shown in figures A.3a and b. The two impulsive response functions considered in the example 1 (Fig. A.3a) were exp(−2.5j) and exp(−0.4j) and for the example 2 (Fig.A.3b) sin (−2.5j) and sin(−0.4j) .

It can be seen from the above figures that the convergence rate for the two input system is slower than the single−input system. It can also be observed that when impulse response functions are considered as exponential functions the convergence is faster compared to sine−impulse response functions. In all the examples shown, however, the error level after 1000 iterations is below −40DB. In fig. A.4 a and b the assumed and estimated impulse response functions (exp) for the two−input system are illustrated after 100 and 500 iterations and in Fig. A.5 a and b sin functions are considered as impulse response functions.

. It can be seen from the figures that after 500 iterations, the estimated functions are closely matched with the assumed functions. It may be noted that this study has been made considering synthetic data without the addition of any noise. The performance of the proposed technique should be assessed using input data sequences which are non− white (i.e., correlated from sample to sample) and taken from a continuous distribution (eg. Gaussian) before application to field data.

FIGURE A3

The error power between the assumed and computed output sequences for the two-input and single outut system. The impulse response functions assumed to obtain the results shown in a) are exp (−0.4j), exp (−2.5j) and in b) are sin(−0.4j) and sin(−2.5j).

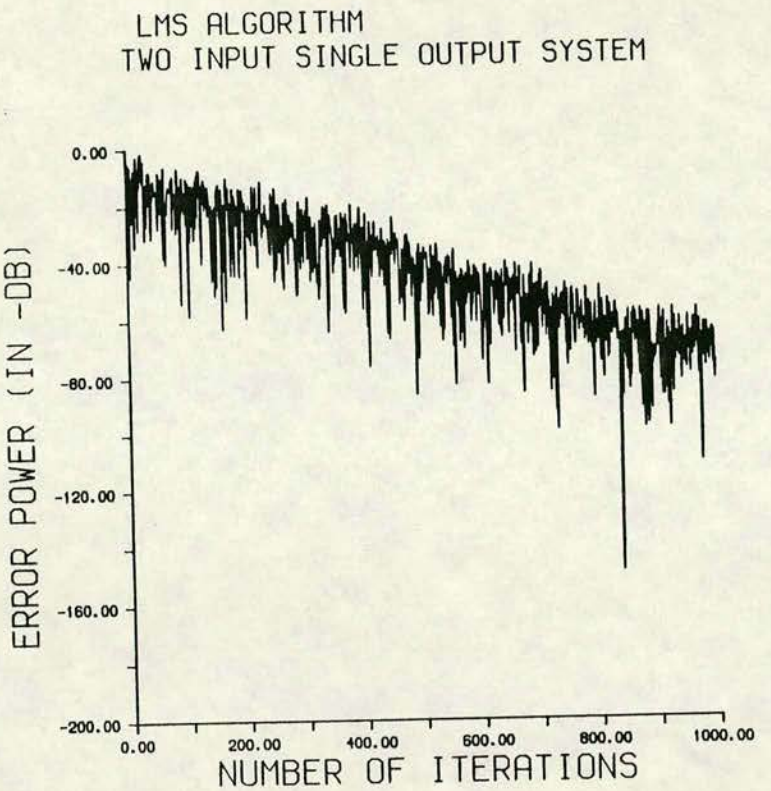
LMS ALGORITHM
TWO INPUT SINGLE OUTPUT SYSTEM
a
ERROR POWER (IN -DB)
0.00
-40.00
-80.00
-120.00
-160.00
-200.00
0.00
200.00
400.00
600.00
800.00
1000.00
NUMBER OF ITERATIONS

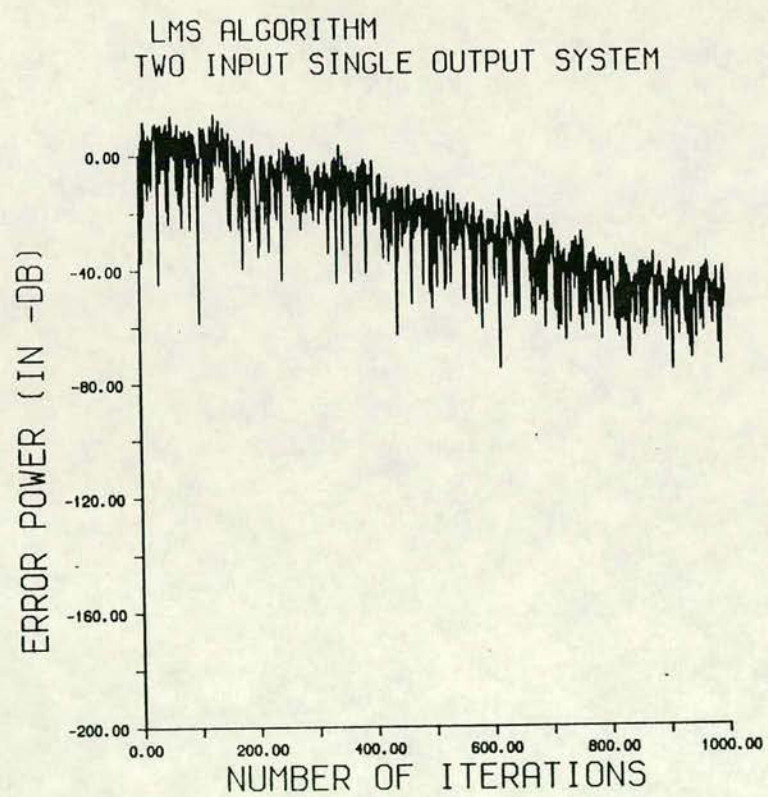
LMS ALGORITHM
TWO INPUT SINGLE OUTPUT SYSTEM
b
ERROR POWER (IN -DB)
0.00
-40.00
-80.00
-120.00
-160.00
-200.00
0.00
200.00
400.00
600.00
800.00
1000.00
NUMBER OF ITERATIONS

FIGURE A4.

Comparision of assumed and computed impulse response functions for two input system after a) 100 iterations b) 500 iterations. The curves shown with 'o' symbols are assumed functions and the curves shown with '+' symbols are computed functions.

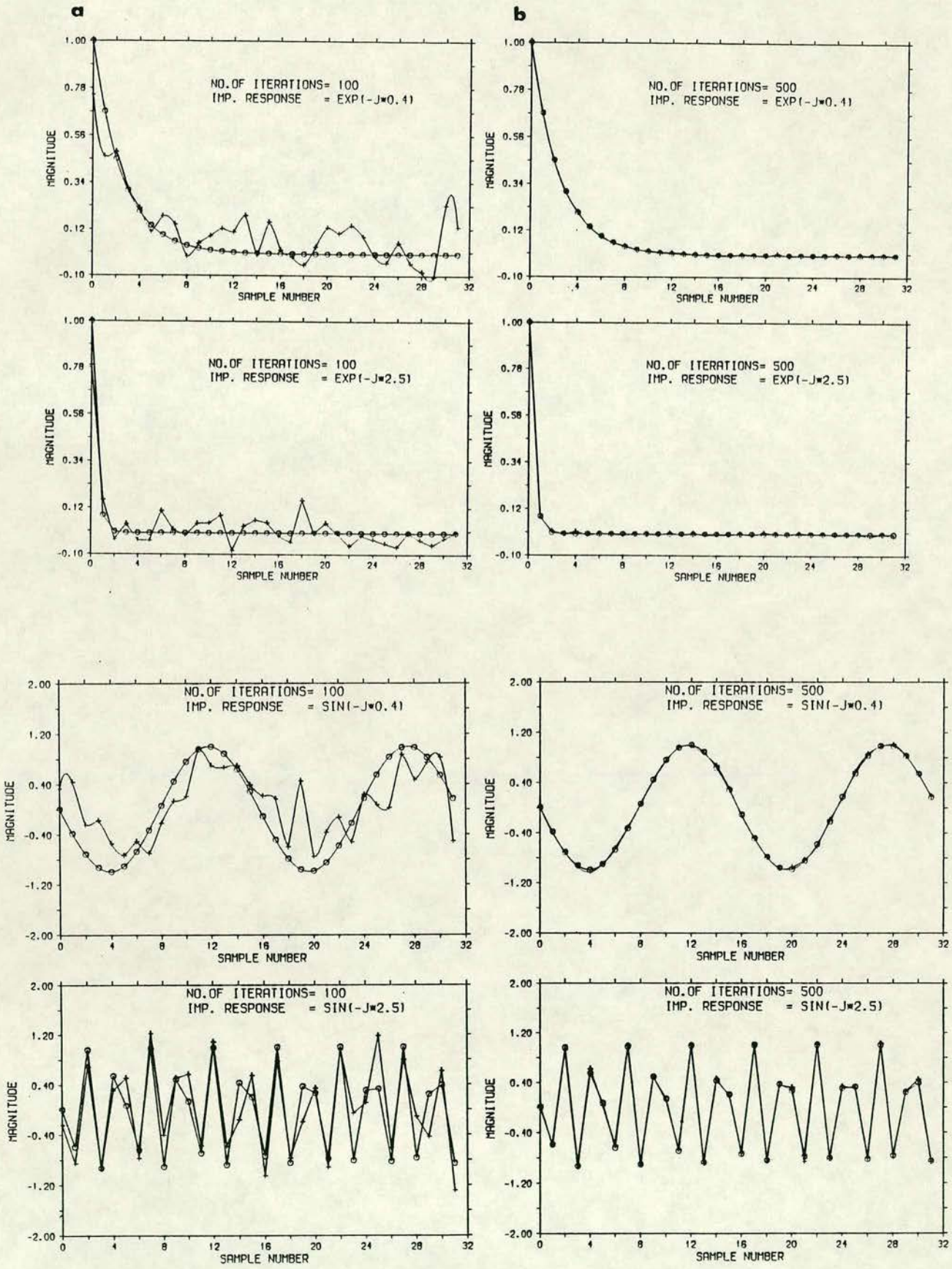
a
b
NO.OF ITERATIONS= 100
IMP. RESPONSE = EXP(-J*0.4)
NO.OF ITERATIONS= 500
IMP. RESPONSE = EXP(-J*0.4)
NO.OF ITERATIONS= 100
IMP. RESPONSE = EXP(-J*2.5)
NO.OF ITERATIONS= 500
IMP. RESPONSE = EXP(-J*2.5)
NO.OF ITERATIONS= 100
IMP. RESPONSE = SIN(-J*0.4)
NO.OF ITERATIONS= 500
IMP. RESPONSE = SIN(-J*0.4)
NO.OF ITERATIONS= 100
IMP. RESPONSE = SIN(-J*2.5)
NO.OF ITERATIONS= 500
IMP. RESPONSE = SIN(-J*2.5)
MAGNITUDE
SAMPLE NUMBER

APPENDIX-B

PROCESSING OF NOISY MAGNETOTELLURIC DATA USING DIGITAL FILTERS AND ADDITIONAL DATA SELECTION CRITERIA*

S.L.FONTES+, T.HARINARAYANA++, G.J.K.DAWES AND V.R.S.HUTTON

Department of Geophysics, University of Edinburgh

James Clerk Maxwell Building

Mayfield Road

Edinburgh EH9 3JZ

* - Paper presented at the 8th Workshop on Electromagnetic Induction in the Earth and Moon, 1986, Neuchatel - Switzerland.

+ - Permanent address: Observatorio Nacional, Rio de Janeiro, Brasil.

++ - Permanent address: NGRI, Hyderabad, India.

ABSTRACT

Although the magnetotelluric (MT) method is known to be effective and fast in probing the electrical conductivity structure of the earth at crustal depths, the results are often degraded by industrial and cultural noise. To obtain reliable processed results for modelling, it is first necessary to extract or select the natural signals from the contaminated time series.

Various noise-reduction techniques based on digital filters are discussed with special reference to persistent noise signals, e.g. from power lines, DC operated railways, and electrical fences. Both previously suggested techniques (delay-line and notch filtering) and two other procedures (maximum entropy extension and deconvolution filtering) are applied to both synthetic data and to field observations from S. Scotland and the Italian Alps. Better quality data sets and more geophysically acceptable earth models are shown to result.

Noise of a more intermittent nature has recently been observed in MT observations near the development site of the geothermal power station on Milos, Greece. Large highly coherent electromagnetic field signals were observed to coincide with the opening and closure of the valves on the test wells. In this case, meaningful apparent resistivity curves could be obtained from an undisturbed sub-set of the previously accepted data, which had been selected mainly on the basis of signal power.

Delay-line filtering is shown to be superior to notch filtering in eliminating non-sinusoidal noise , while both the MEM extension and the window deconvolution techniques are found to be useful in spike removal.

These studies illustrate that use of automatic data selection procedure should only be undertaken with great care in areas where the cultural noise is high. In such cases, continuous time-domain monitoring of the MT signals is recommended. The appropriate techniques of noise reduction can then be applied.

1.Introduction

Man-made noise in certain regions can be a major obstacle to the effective application of the MT method in studies of the electrical structure of the Earth's crust. Noise is that portion of the measured electric and magnetic data which is neither induced nor homogeneously induced, and which thus does not fulfil the plane wave assumption required by the magnetotelluric method. The non-induced part exists in the recordings of both magnetic and electric fields, the noise in the magnetic field being independent of that in the electric field, i.e. incoherent or random MT noise. Noise due to inhomogeneous induction is essentially that of a nearby source (i.e. < 3 skin-depths away) and therefore the electric and magnetic fields are related to each other, i.e. coherent noise. Both categories of noise may occur either singly or in combination, exhibiting variable amplitude and frequency of occurrence, and they may be generated by a great number of sources.

Incoherent noise may sometimes have its origin in the data acquisition system itself, may be caused by moving vehicles which produce magnetic disturbance or arise from natural disturbances such as wind or microseismic activity. Several workers have assessed the biasing of the transfer function estimations introduced by incoherent noise (Sims et al,1971; Goubau et al,1978; Pedersen and Svennekjaer,1984). If severe surface distortions are not present, and some care is exercised during acquisition and processing of data contaminated only by random noise in a single site study, one can generally get an interpretable set of resistivity and phase curves.

Coherent noise in MT signals is due to various sources and the literature concerned with the problems caused by these noise sources is considerable. The noise signatures of various man-made disturbances have been reviewed by Herman (1979). The stray currents observable in the vicinity of DC operated railways and their influence in masking the natural electromagnetic signals have

been discussed by Kovaleskiy et al (1961), Jones and Geldart(1967), Chaize and Lavergne(1970), Linington (1974), Yanagihara(1977) ,etc. Besides the railway noise problem, Adam et al(1986) have reported on their experience of various other noisy signals in magnetotelluric data recorded in the highly resistive and mountainous Eastern Alps. These include signals from an umbalanced power network and from pipeline anticorrosion currents. A recent comprehensive review of man-made electromagnetic noise sources has been given by Szarka (1986).

Processing of MT signals degraded by coherent noise poses a formidable task as the natural and man-made signals are indistinguishable. With the advent of more sophisticated acquisition systems possessing comprehensive real-time analysis capabilities, a clear indication of the presence of coherent noise may only be noticed after data processing, e.g. the apparent resistivity and phase curves may exhibit unrealistic slopes or provide unreasonable Earth's models. Nevertheless, on scrutiny of the original time series the noisy segments or spikes may be located on amplitude considerations, if the noise amplitude is considerably higher than the natural signals. The discussion which follows is restricted to this situation. It is useful to distinguish between two types of coherent noise according to whether it occurs regularly or irregularly.

The general objective of the present study is the assessment of the effectiveness of various digital filtering techniques to remove regular and irregular coherent noise from the recorded magnetotelluric signals. The analysis is performed both on synthetic data and on noisy field data recorded in three different regions: Asiago in Northern-Italy, Craik in Southern- Scotland and Milos in Greece. The results of the analysis are presented in three following sections. Firstly, the reduction of regular coherent noise by the application of notch or delay-line filters are compared. Secondly, coherent 'spike' noise signals of regular or irregular character are detected on amplitude grounds and reduced by two distinct approaches. In one, the data set is divided into 'contaminated' and

'uncontaminated' segments and the uncontaminated segments are extended to replace the contaminated segments, by means of the maximum entropy method. The second approach assumes that the data set is convolved with a combination of retangular windows such that the contamination by 'spike' noise is reduced. The resulting spectral distortion is attenuated by a deconvolution operation. These procedures are applied to data recorded in Asiago, N. Italy and Craik in S. Scotland.

Finally, MT data recorded in 1985 at a few stations on Milos, Greece exhibited such a high disturbance level that only careful selection of sub-sets of data has provided meaningful impedance values.

2. Regular coherent noise

Usually, MT field data acquisition systems incorporate notch filters which remove with varying level of success the 50Hz (or 60Hz) noise and its harmonics from power-lines. The main concern here is with the regular coherent noise which has not been eliminated during acquisition time. Such noise is highly coherent and since in-field data selection is generally based on minimum coherency levels (Pedersen, 1986), apparently excellent MT responses result as shown in examples observed in data sets recorded in Scotland and Italy. In the Scottish example, shown in Fig.1(a)-(c), a source with repeat frequency of 0.8Hz observed in three different frequency bands covering the range 128Hz-0.125Hz has been later attributed to electrified cattle fences. In this latter case the current pulse has produced, as a result of the bandpass filters (6 pole Butterworth low pass and 2 pole Butterworth high pass filters) of the MT instrumentation, a random character in band 0 (cut- off frequencies 128Hz- 16Hz)-Fig.1(a) and a remarkably periodic signal in bands 1 (16Hz- 2Hz)-Fig.1(b) and 2 (2Hz- 0.125Hz)-Fig.1(c). Note the correspondence between Fig.1(b) and a hypothetical spike source- Fig.1(d). In Italy, a predominantly 100Hz noise appears to be rectified mains frequency. No

hardware provision had been made for removal of 50Hz even harmonics in this study. This example is discussed later.

To reduce such regular coherent noise, two digital filtering techniques have been used- the notch and delay-line filters.

2.1 The notch filter

The notch filter is well known to geophysicists involved in acquisition and processing of data. The outline which follows is based on the discussion by Kanasewich (1981, pp.248-252). The description of its digital formulation may easily be given in the z domain. Let

$$z = e^{-iw} \qquad (1)$$

Each point on the unit circle $|z|=1$ represents an infinitely long sinusoidal oscillation with frequency $f=w/2\pi$, w being the angular frequency. The z transform of the notch filter impulse response can be written as

$$W(z) = G\ (z-z_z)(z-z_z^*)/\ (z-z_p)(z-z_p^*) \qquad (2)$$

where z_z is the point on the unitary circle associated with the frequency to be rejected, z_z^* is its complex conjugate. z_z and z_z^* are the 'zeros' of equation (2).

z_p is a point of radius r_p located just outside the unitary circle and z_p^* is its complex conjugate. z_p and z_p^* are the 'poles' of equation (2).

G is a constant for normalizing the filter response gain to unity for a particular frequency, usually the Nyquist frequency.

The value chosen for r_p gives a compromise between sharpness of the filter and length of the impulse response. Thus if r_p is very close to 1 (say $r_p=1.001$) the filter produces a very sharp cut-off response but it requires a signal of long duration for the filter to become effective.

2.2 The delay-line filter

The delay-line filter (or Comb filter) was first applied to MT data by Schnegg et al (1980). Its impulse response in the Z domain is

$$W(z) = 1 - z^n \qquad (3)$$

which has n zeros equally spaced on the unitary circle at locations given by

$$Z_z = e^{i2\pi z/n} \qquad ,z=0,1,2,\ldots,(n-1) \qquad (4)$$

Z_0 corresponds to the fundamental frequency to be filtered, e.g. 50 Hz , and $Z_1,\ldots,Z_n$ are all the higher harmonics up to the Nyquist frequency. The corresponding linear difference equation for this filter is

$$y(t)=x(t)-x(t-n) \qquad (5)$$

where x(t) is the sampled signal at the time t.

It is easily verified that W(z) in equation (3) has variable amplitude with its maximum value reaching 2 at all the frequencies midway between two harmonics (or zeros of W(z)). Fortunately, this undesirable behaviour does not lead to a serious problem when this filter is applied to MT data as both magnetic and electric signals (or their spectra) are equally affected.

2.3 Applications

A comparison of notch and delay-line filtering techniques applied to a synthetic sinusoidal signal sampled at 1/1600s and composed by four unitary amplitude sinusoids of frequencies 100Hz, 219Hz, 375Hz and 563Hz is presented in Fig.2(a)-(c) and Fig.3(a)-(b). The signal and its FFT spectrum are given in Fig.2(a). In Fig.2(b) the same signal corrupted by a 50Hz sinusoidal noise of amplitude 4 times that of each individual sinusoid, and its respective spectrum are shown. The same synthetic signal as before but 'corrupted' by non-sinusoidal noise and its spectrum are shown in Fig.2(c). It is shown that unlike the 50Hz sinusoidal noise, the 50Hz non- sinusoidal noise resulted in a spectrum presenting several 50Hz odd harmonics. The spectra resulting from the application of both the notch and the delay- line filters to the 50Hz sinusoidal noise added signal are shown in Fig.3(a). From these examples, it is clear that the notch filter is more effective in removing pure sinusoidal noise from the data (in this case a 50Hz signal with no harmonics),

while the delay-line filter may remove 'good' components of signal along with the noise, e.g. the 100Hz sinusoid has been removed in this particular example. In Fig.3(b) the spectra resulting from the application of both the notch and the delay-line filters to the signal 'corrupted' by non- sinusoidal noise are presented. In this situation the delay-line filter appears to be more effective than the notch filter in removing the non-sinusoidal noise. Note however that the 100Hz is again absent and that the spectral components have their amplitudes changed as a result of the variable gain response for the delay- line filter mentioned earlier in section 2.2.

The application of the delay-line filter to real data is shown in Fig.4(a)-(b). A dominant regular 100Hz coherent noise signal of amplitude greater than 100 mV/Km in the electric channels completely masks the natural signal in data recorded in Asiago, Northern Italy (Fig.4(a)). The delay-line filtered data window (256 samples per channel) corresponding to Fig.4(a) is shown in Fig.4(b). The respective rotationally invariant apparent resistivity and phase curves obtained after processing 60 data windows are shown in Fig.4(c). The effect of filtering in the (1/512- 1/64s) band results in continuity of the MT response with the values found for the undisturbed adjacent frequency band.

3. Irregular coherent noise

Irregularly occurring coherent noise in recorded MT signals is only recognizable if its amplitude exceeds the natural signal. The primary difficulty in this situation is the establishment of a discrimination level between good signal and noise. Therefore, whatever criterion is adopted, the detection of noise-contaminated segments of a data window must be based on amplitude levels. In the present study, each data window has been sub-divided in such way that 16 partial variances have been estimated and highly coherent segments with unexpectedly high variance values have been disregarded. As gaps result in some data windows, two approaches have been examined for processing these particular

data windows- use of the maximum entropy method for extending good data to the rejected segments and use of a window deconvolution scheme.

3.1 The maximum entropy extension

The maximum entropy method (MEM) was proposed by Burg(1967) and since then has been utilized as an important tool in spectral analysis. Its improved spectral resolution compared to most traditional methods is well known, more especially when periods of interest are comparable to data sample lengths. In the present study, the potentiality of MEM as a predictive technique is explored. In fact, the potentiality of this technique has already been investigated on synthetic data by Ulrych and Clayton (1976). Wiggins and Miller (1972) have successfully employed a predictive noise reduction technique derived from Burg's method ,to seismological data. The scheme proposed differs in some aspects from the Wiggins and Miller technique and the steps necessary for its implementation are outlined here. Consider a non-deterministic time series

$$s_t \qquad , t=1,\ldots,n$$

Then

$$s_t = \sum_{k=0}^{\infty} a_k e_{t-k} \tag{6}$$

is its infinite moving average (MA) representation, where $a_0=1$ and e_t is a white noise process.

Whether or not a_t is a minimum delay wavelet , it is always possible to convert a MA process to an autoregressive process (AR) (Robinson,1964,1967)

$$s_t = \sum_{k=0}^{\infty} p_k s_{t-k} + e_t \tag{7}$$

the main advantage being that AR parameters are easier to estimate (Ulrych and Clayton,1976). For practical applications the number of parameters to be estimated must be finite and the forward prediction error (EF) may be written as

$$EF_t = \sum_{k=0}^{M} a_k s_{t-k}, \qquad a_0=1$$

$$a_i=-p_i \ ,i=1,\ldots,M \tag{8}$$

and the backward prediction error (EB) as

$$EB_t = \sum_{k=0}^{M} a_k s_{t+k} \quad (9)$$

The noise reduction scheme based on the MEM extension of good segments of a data window is undertaken through the following steps:

(i)- Noise-contaminated segments are rejected, the criterion being a partial variance exceeding 3-4 times the average variance for the particular site;

(ii)- EF_t and EB_t are estimated for the non-contaminated subsets of a data window using the Burg algorithm and the Akaike final prediction error criterion (Akaike,1969) for controlling the order of the process M;

(iii)- The gaps in the data window are filled with values obtained by averaged forward and backward predictions;

(iv)- Transfer functions of 'cleaned' data windows are estimated in the frequency domain in the conventional way.

3.2 The window deconvolution technique

In this scheme the gaps created by the deletion of the noisy segments are not filled, i.e. zero signal level is assumed. It implies that the signal s_t is multiplied by a window W_t

$$W_t = 1, \quad \text{noise-free data}$$

$$W_t = 0, \quad \text{noise-contaminated data} \quad (10)$$

or in the frequency domain

$$S_w(w) = S(w) * W(w)$$

with power spectra representation

$$PS_w(w) = PS(w) * PW(w) \quad (11)$$

The distortion introduced by the W_t can be attenuated by deconvolving $PS_w(w)$ with $PW^{-1}(w)$

$$PS_w(w) * PW^{-1}(w) \quad (12)$$

The inverse $PW^{-1}(w)$ can be calculated by means of a spiking filter operation as

described by Robinson (1967). Spiking filter computer routines are available in Silvia and Robinson (1979).

3.3 Applications

In Fig.5(a)-(b), application of both the MEM extension and the window deconvolution techniques are demonstrated for the same synthetic data used in the examples of section 2.3, considering two distinct levels of contamination by spike noise. The FFT spectrum for the series in which 25% of its length is contaminated by irregularly occurring spike noise is given in Fig.5(a). This figure also shows the FFT spectrum estimated for the time series with spike segments replaced by zeros (the 'zeroed' series) and the spectra obtained after spike removal by the MEM extension and the window deconvolution techniques. Similarly, the results for the 35% contaminated signals are given in Fig. 5(b). From comparison of spectra given in Fig.5, one can see that the MEM extension technique recovers the FFT amplitudes of the original series (Fig.2(a)) for both levels of contamination. While the window deconvolution technique can recover the peaks amplitudes when compared to the 'zeroed' series spectrum, it does not remove completely the additional noise in other portions of the spectrum.

An application of these techniques to field observations recorded in Craik, S. Scotland are illustrated in Fig.6(a). Rotationally invariant apparent resistivity and phase curves before and after application of the MEM extension technique (1/128- 1s) and delay-line filtering (1/2- 8s) are presented.The improvement achieved, especially in the frequency range 1/16-1s, in which nearly 30% of each data window is corrupted by noise, is clearly demonstrated. In Fig.7, the MEM extension and the window deconvolution techniques are compared for a field data from Asiago, Northern Italy. The noise source was found to be leakage currents to ground from the DC electric railway system. This affect a large area of the very resistive Alps (Schnegg et al,1986). The comparison of results for the two techniques when applied to field data shows that they are equally efficient.

4. Data selection

The noise-reducing techniques discussed above are not effective when severe conditions of irregular coherent noise are present. This statement is well exemplified by the AMT data recorded in Milos- Greece. Indeed, large highly coherent magnetic and electric signals were observed in measurements surrounding the development site of the Milos geothermal power station. From inspection of data windows from the most disturbed site (Fig.8(b)), it is obvious that the signals are not natural, but the actual waveform of the noise source required examination of the signals prior to filtering by the real-time MT system used in this study. For this purpose, simultaneous chart recording of the sensor outputs (Fig. 8(a)) made the identification of the stepwise character of the noise possible. Correspondence between the opening and closure of the valves of the test wells and the recorded noise had also been noted during the fieldwork itself.

Fortunately, due to the intermittent character of this noise source, it was possible in this case to scrutinize all recorded data windows and to perform a window by window analysis in order to attempt the separation of good and corrupted data. The invariant apparent resistivity and phase curves derived from both 'noisy' and 'good' data windows for the most disturbed site are presented in Fig.9. They show a significant difference between the responses of the 2 data sets. The same process was repeated for three other sites, where the same noise problem existed to a lesser extent. These yielded data sets and 1D models which are in agreement with available borehole information (Dawes,1985).

5. Discussion

When man-made noise reaches high levels, as observed in data sets from S.Scotland, N.Italy and Greece, the notch filters normally incorporated in MT data acquisition systems are inadequate since large amplitude non-sinusoidal noise sources can produce very high order harmonics in the data. Additional notch filters could be included either in the acquisition systems or alternatively, be

applied to the data during processing. The latter option should only be considered when hardware limitations didn't enable adequate notch filtering as the data resolution may be considerably reduced due to the limited dynamic range of the recording device.

The delay-line filter has been shown to be more effective than the notch filter since the main noise source frequency and all its harmonics (odd and even) are completely eliminated. Unlike the notch filter, which is applied either to analog or digital signals, the delay- line filtering is more generally applicable to digital signals. It thus appears advantageous to incorporate an optional delay-line filter in real time data analysis.

In frequency domain processing of MT data, the presence of a single spike noise can contaminate the whole spectra. Simply deleting the spikes can cause leakage from this portion to the uncontaminated portion of the data set. The maximum entropy method used as a predictive technique has been applied to this problem. When applied to field data which > 30% have been contaminated by spike noise, the technique has proved effective in producing acceptable resistivity and phase curves.

The window deconvolution technique presented in this study attenuates the noise effects simply by deleting the noise-contaminated segments of a data window. The application of this technique to synthetic and field data showed that it was in good agreement with the MEM extension technique, although it does not represent a significant improvement when compared to the simple replacement of the spike segments by zero. The only advantage is its easiness of implementation in the data processing.

For MT data, acquired by a real-time system which uses coherency as one of the data acceptance criteria and badly contaminated by coherent noise of an intermittent nature, the selection of sub-sets of data windows is essential. As an example of this situation, data recorded on Milos has shown to yield earth models

compatible with borehole data.

No claim is made that all man-made noise can be eliminated by the techniques discussed, nor is it guaranteed that all the superposed noise has been removed from the field examples presented in this study. Filtering itself may introduce noise and should thus always be applied with great care. The case studies discussed in this study show that automatic data acquisition alone is not advisable in areas affected by high cultural electric noise as it can yield misleading results. In such cases, continuous time-domain monitoring of the unfiltered MT signals, e.g. using a chart recorder is also necessary. The appropriate noise-reduction technique can then be applied.

Acknowledgments

One of the authors (S.L.F.) wishes to thank the Brazilian Research Council (CNPq) and another (T.H.) the Association of Commonwealth Universities for providing financial assistance in the form of scholarships. The authors are thankful to Dr. A.G. Jones, Ottawa for useful discussions during his visit to Edinburgh University in July, 1986.

References

- Adam,A., Szarka,L., Vero,J., Wallner,A. and Gutdeutsch,R.,1986. Magnetotellurics (MT) in mountains: noise, topographic and crustal inhomogeneities effects. Phys.Earth Planet.Inter., 42: 165-177.
- Akaike,H., 1969. Power spectrum estimation through autoregressive model fitting. Ann. Inst. Stat. Math., 21: 407-419.
- Burg,J.P., 1967. Maximum entropy spectral analysis. 37th Ann. Int. Meet., Soc. Explor. Geophys., Oklahoma City, Okla, Oct. 31
- Chaize,L. and Lavergne,M., 1970. Signal et bruit en magnetotellurique. Geophys. Prosp., 18: 64-87

-Dawes,G.J.K., 1985. Magnetotelluric feasibility study, Island of Milos- Greece. External report contr.number EN-3G 0008-UK (H) , 3rd EEC Geothermal Programme.

-Goubau,W.M., Gamble,T.D. and Clarke,J., 1978. Magnetotelluric data analysis: removal of bias. Geophysics 43: 1157-1166.

-Herman,J.R. 1979. Electromagnetic ambients and man- made noise. Multi- volume EMC encyclopedia series, vol. 3, Don White Consultants, Inc., Virginia.

-Jones,F.W. and Geldart, L.P., 1967. Vertical telluric currents. Planet.Sci. Lett., 2: 69-74.

-Kanasewich,E.R., 1981. Time sequence analysis in geophysics. University of Alberta Press, third edition, Alberta, 480pp.

Kovaleskiy,I.V., Mikerina,N.V., Novysh,V.V. and Gorodnicheva,O.P., 1961. Distribution of the earth currents from an electrified railroad in the Southern Urals. Geomag. Aeron. 1, 5: 723-726.

-Linington, R.E., 1974. The magnetic field disturbances caused by dc electric railways. Prospezioni Archeolog., 9: 9-20.

-Pedersen,L.B. and Svennekjaer,M., 1984. Extremal bias coupling in magnetotellurics. Geophysics 49: 1968-1978.

-Pedersen,L.B., 1986. Some aspects of magnetotelluric field procedures. 8th Workshop on Electromagnetic Induction in the Earth and Moon. Neuchatel.

-Robinson,E.R., 1964. Recursive decomposition of stochastic processes. In: H.O. Wold (editor), Econometric Model Building, North- Holland, Amsterdam, pp. 111-168.

-Robinson,E.R., 1967. Statistical communication and detection. Hafner, New York, N.Y., 362pp.

Schnegg,P.-A., Le Quang,B. and Fischer, G., 1980. Management and processing of MT data in the field with a microprocessor. 5th Workshop on Electromagnetic Induction in the Earth and Moon. Istanbul.

Schnegg,P.-A., Fischer,G., Fontes,S.L., Hutton,V.R.S. and Finzi,E. 1986. The effect of dc railways on MT measurements in northern Italy. 8th Workshop on Electromagnetic Induction in the Earth and Moon. Neuchatel.

Silvia,M.T. and Robinson,E.R., 1979. Deconvolution of geophysical time series in the exploration for oil and natural gas . Elsevier, Amsterdam, 251pp.

Sims,W.E., Bostick,F.X. and Smith,H.W., 1971. The estimation of magnetotelluric impedance tensor elements from measured data. Geophysics 36: 938-942.

Szarka,L. 1986. Distortions of electromagnetic field: man- made noise in Geophysics. 8th Workshop on Electromagnetic Induction in the Earth and Moon. Neuchatel.

Ulrych,T.J. and Clayton,R.W., 1976. Time series modelling and maximum entropy. Phys. Earth Planet. Int., 12: 188-200.

Wiggins,R.A. and Miller,S.P., 1972. New noise-reduction technique applied to long-period oscillations from the Alaskan earthquake. Bull. Seismol. Soc. Am., 62: 471-479.

Yanagihara, K., 1979. Magnetic field disturbance produced by electric railway. Mem. Kakioka Magnetic Observatory, 38: 17-36.

Figure captions

Fig.1- Field example of regular noise recorded in Craik, S. Scotland for three consecutive frequency bands. Magnetic (nT) and electric (mV/Km) signals are bandpass filtered (6 pole Butterworth low pass and 2 pole Butterworth high pass) and are shown in data windows consisting of 256 samples per channel.

(a)- Data window for band0 (128Hz- 16Hz).

(c)- Data window for band1 (16Hz- 2Hz).

(c)- Data window for band2 (2Hz- 0.125Hz).

(d)-Hypothetical spike source signal of 0.8Hz repeat frequency which emulates the noise waveforms observed at the three bands .

Fig.2-

(a) Synthetic example of 'pure' signal (time series and FFT spectrum) sampled at 1600Hz and composed by four unitary amplitude (arbitrary units) sinusoids of frequencies 100Hz, 219Hz, 375Hz and 563Hz.

(b)- Same signal of (a) superposed by a 50Hz sinusoidal 'noise' of amplitude 4 times that of each individual sinusoid.

(c)- Same signal of (a) superposed by a 50Hz square pulse 'noise' of amplitude 4 times that of each individual sinusoid.

Fig.3- Comparison of digital filtering for 50Hz noise by notch and delay-line.

(a)- FFT spectra of 50Hz sinusoidal 'noise' filtered by notch and delay- line.

(b)- FFT spectra of 50Hz square pulse 'noise' filtered by notch and delay- line.

Fig.4 Field example of regular coherent noise on MT data recorded in Asiago, N. Italy.

(a)- Magnetic (nT) and electric (mV/Km) signals for a recorded data window.

(b)- Same data window after delay- line filtering. Note the different amplitude

scales used for the electric and magnetic signals.

(c)- MT response curves (averaging of 60 data windows) for the invariant before and after application of delay-line filtering (.005s-.01s).

Fig.5- Application of MEM extension and window deconvolution techniques to the same synthetic signal of Fig.2(a) in which 25% and 35% of its length is contaminated by spike 'noise' signals of irregular occurrence.

(a)- FFT spectrum of spike added time series (25% case), and the FFT spectra after spike removal by 'zeroed' series, MEM extension and window deconvolution techniques.

(b)- Same as (a) for 35% spike noise added.

Fig.6- Field results recorded in Craik, S. Scotland before and after the application of the MEM extension technique (0.01s - 1s) and delay- line filtering (1s - 10s): MT response curves and 1D model for the filtered response.

Fig.7- Field results recorded in Asiago, N. Italy before and after the application of the MEM extension and window deconvolution techniques (0.2s - 10s): MT response curves and 1D model for the filtered response.

Fig.8- Field data recorded on Milos, Greece showing the effect of opening and closure of the geothermal power station test wells.

(a)- Chart recording of the magnetic signal in the magnetic north direction (Hx) at two stages prior to filtering of the MT acquisition system. (b)- Simultaneously recorded noisy data window (orthogonal magnetic and electric signals overlapped) in the frequency range 0.1- 0.125Hz.

Fig.9- Field results recorded on Milos, Greece, before and after data selection: MT response curves and 1D model for the selected data.

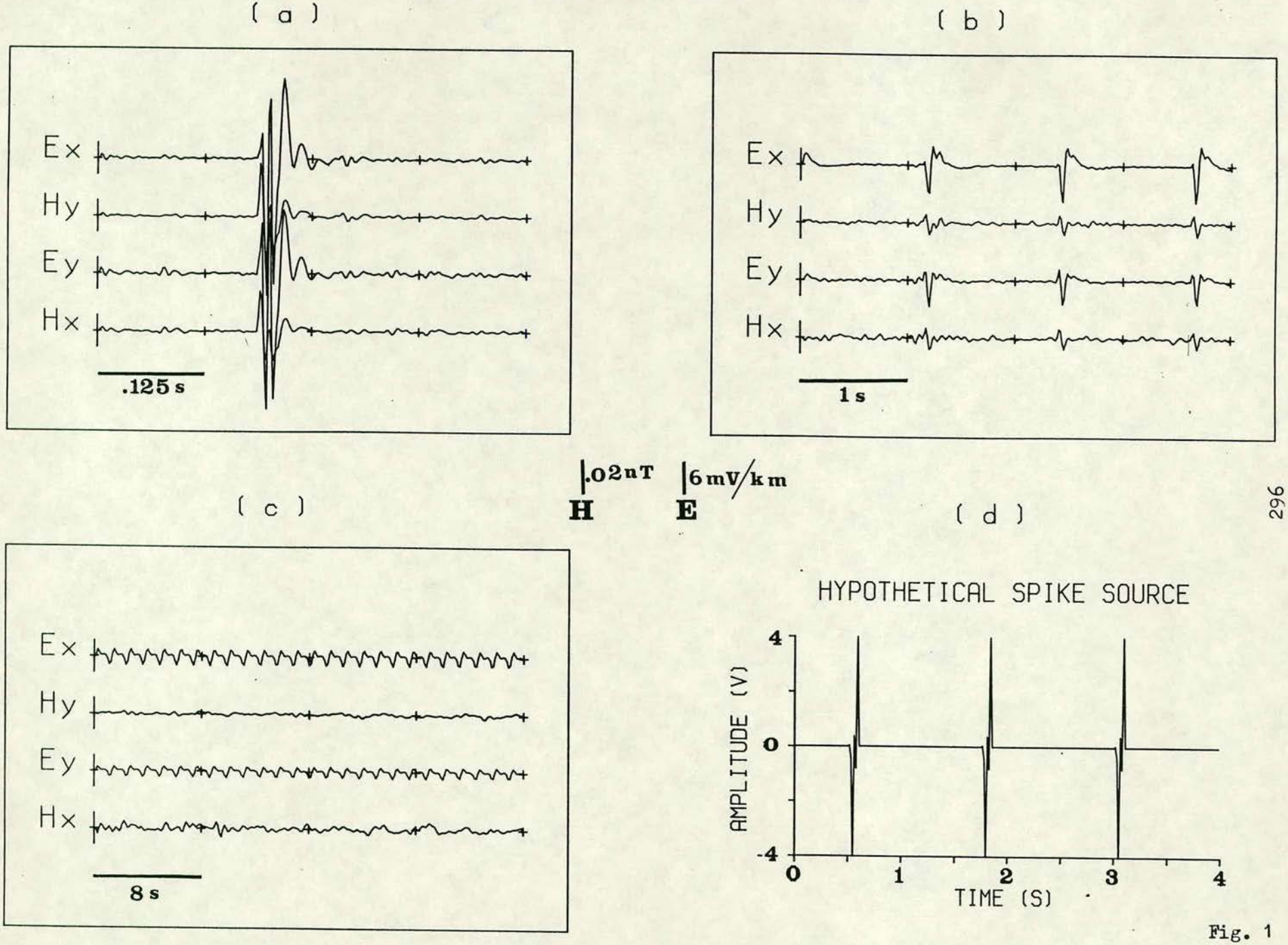
(a)
Ex
Hy
Ey
Hx
.125 s
(b)
Ex
Hy
Ey
Hx
1 s
.02nT
6mV/km
H
E
(c)
Ex
Hy
Ey
Hx
8 s
(d)
HYPOTHETICAL SPIKE SOURCE
AMPLITUDE (V)
4
0
-4
0
1
2
3
4
TIME (S)

Fig. 1

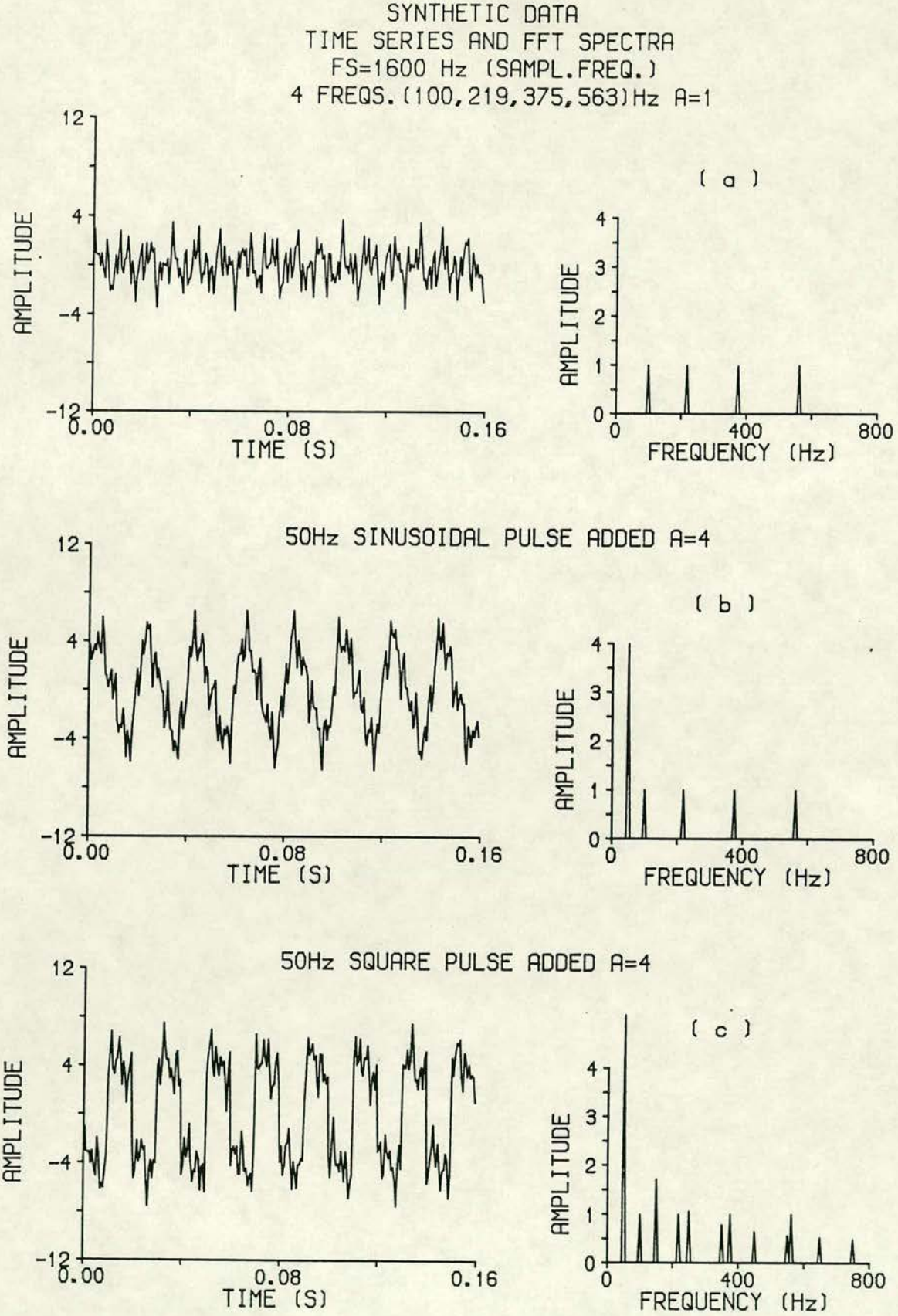
SYNTHETIC DATA
TIME SERIES AND FFT SPECTRA
FS=1600 Hz (SAMPL.FREQ.)
4 FREQS.(100,219,375,563)Hz A=1
(a)
AMPLITUDE
TIME (S)
FREQUENCY (Hz)
50Hz SINUSOIDAL PULSE ADDED A=4
(b)
50Hz SQUARE PULSE ADDED A=4
(c)

Fig. 2

FFT SPECTRA OF FILTERED DATA

50Hz SINUSOIDAL PULSE

(a)

NOTCH FILTERED

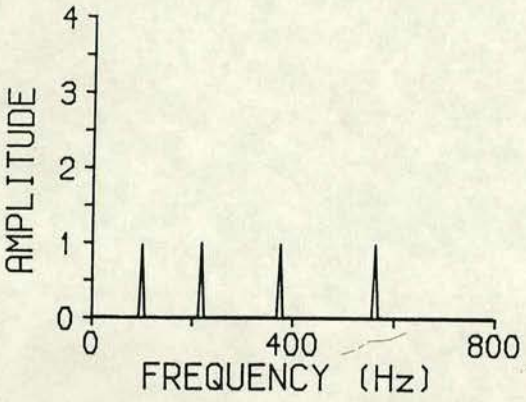

DELAY-LINE FILTERED

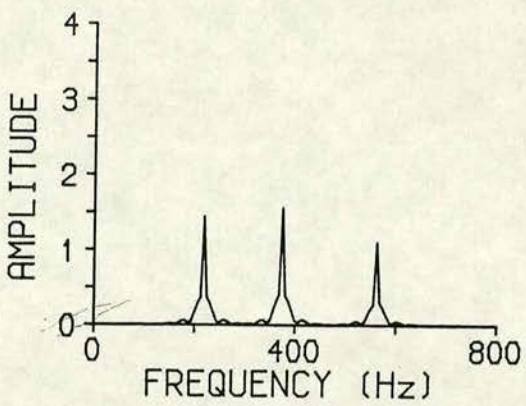

50Hz SQUARE PULSE

(b)

NOTCH FILTERED

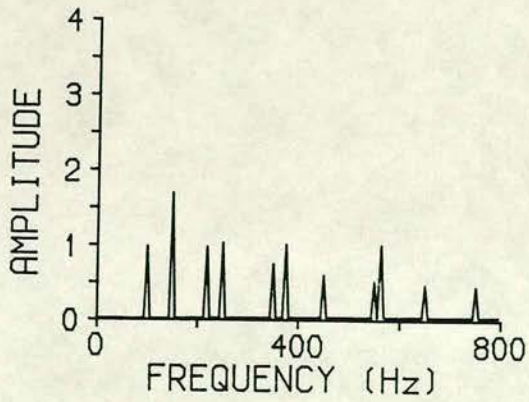

DELAY-LINE FILTERED

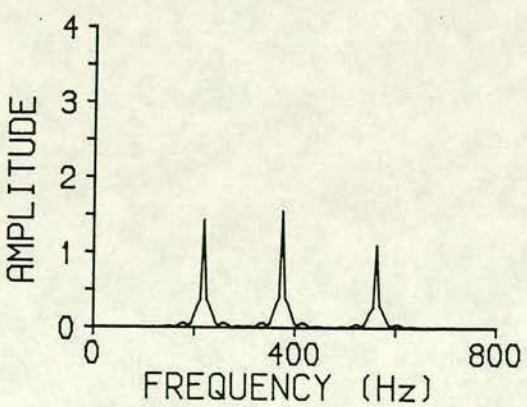

Fig. 3

FIELD EXAMPLE ASIAGO- N. ITALY

(a) DATA WINDOWS (b)

BEFORE FILTERING AFTER DELAY-LINE FILTERING

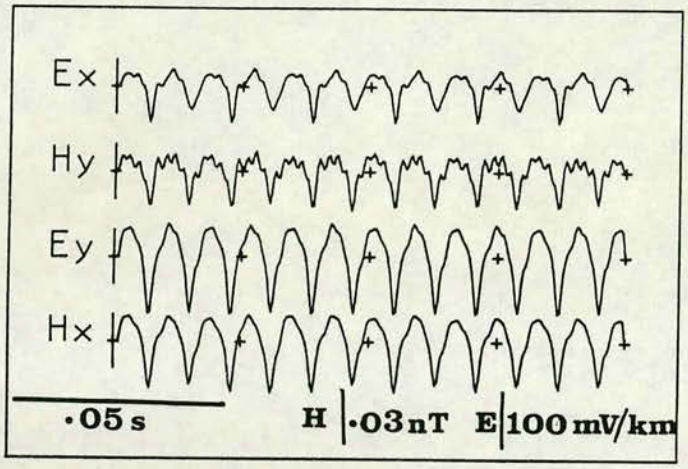

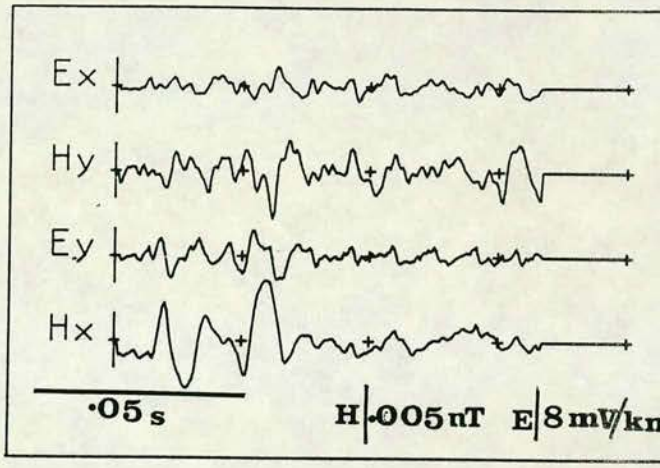

(c): MT RESPONSE CURVES

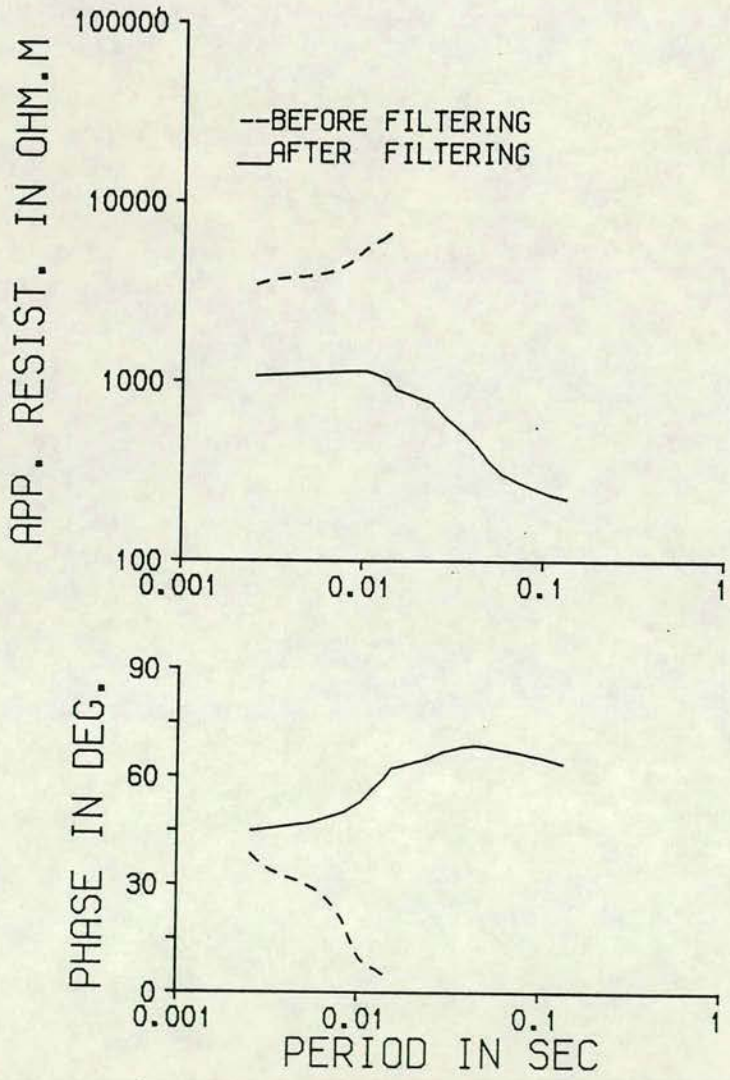

Fig. 4

SPIKE CONTAMINATED TIME SERIES- SPECTRA BEFORE AND AFTER SPIKE REMOVAL

(a) 25% OF SERIES CONTAMINATED WITH SPIKES

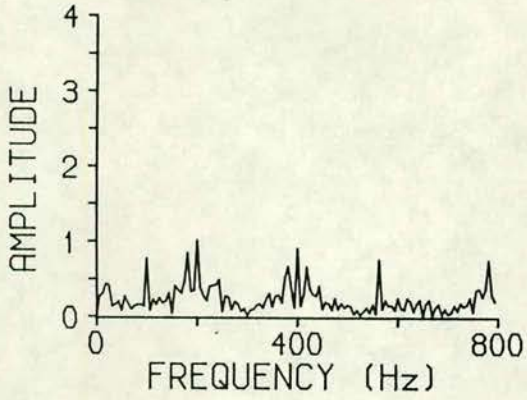

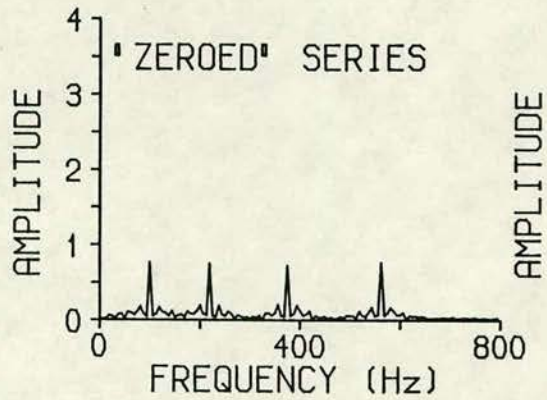

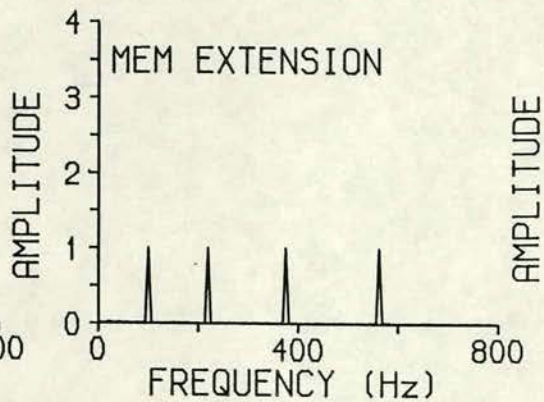

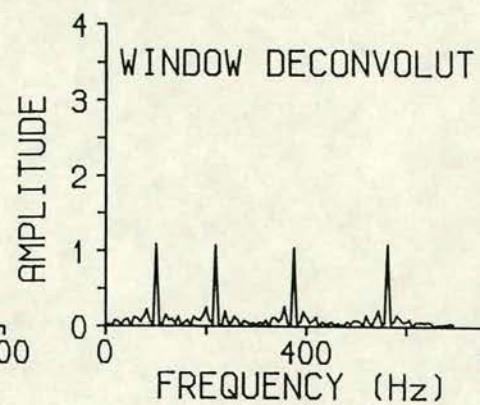

(b) 35% OF SERIES CONTAMINATED WITH SPIKES

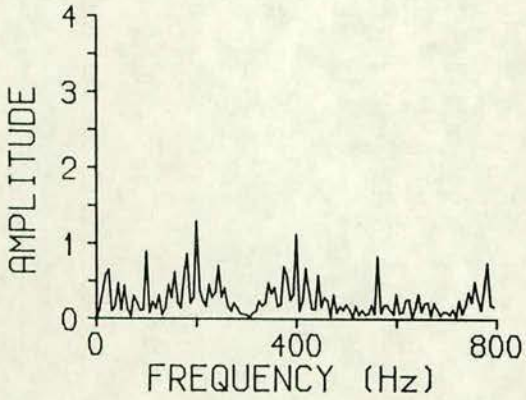

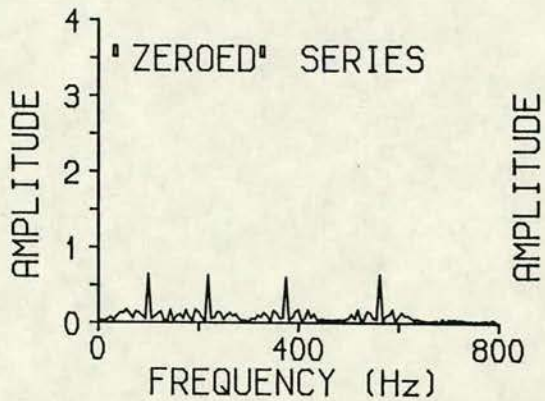

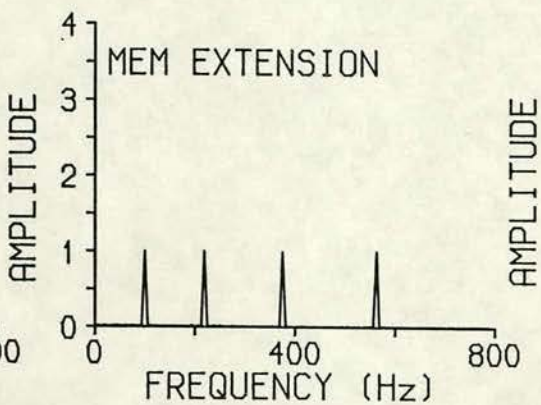

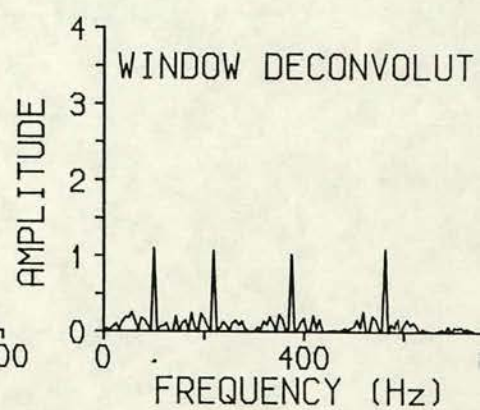

Fig.

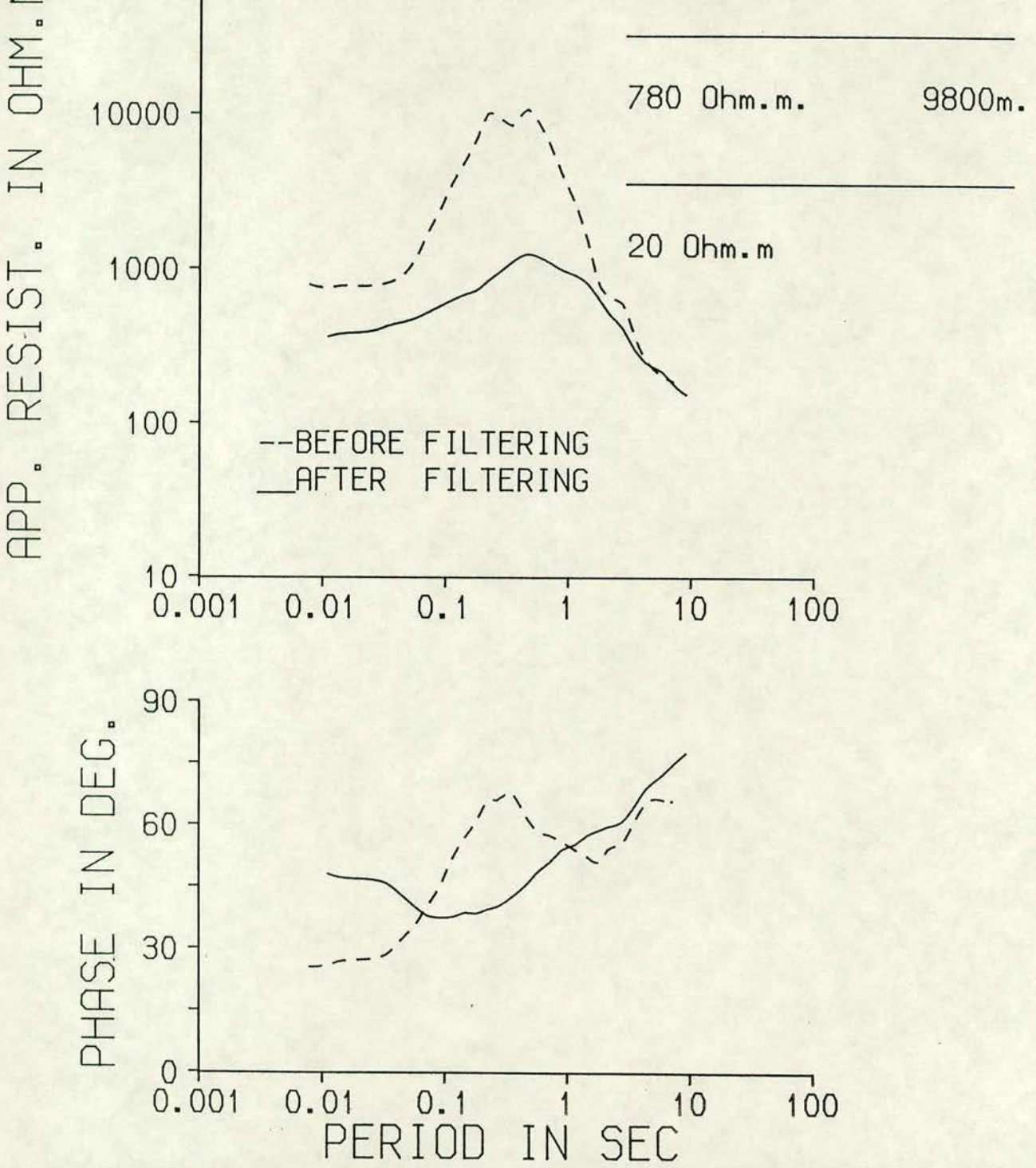
APP. RESIST. IN OHM.M
10000
1000
100
10
780 Ohm.m.
9800m.
20 Ohm.m
--BEFORE FILTERING
__AFTER FILTERING
0.001
0.01
0.1
1
10
100
PHASE IN DEG.
90
60
30
0
PERIOD IN SEC

Fig. 6

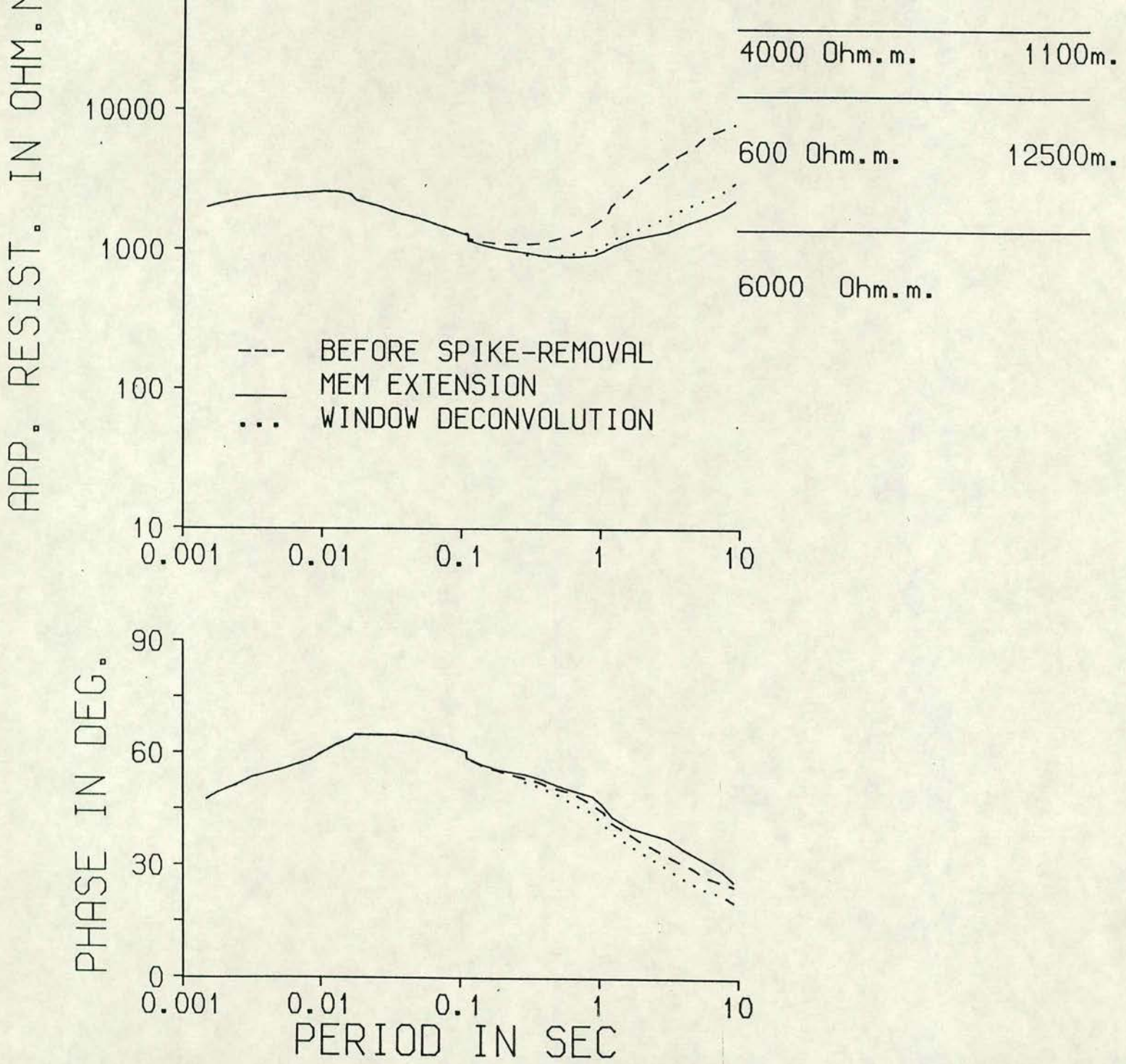
APP. RESIST. IN OHM.M
10000
1000
100
10
0.001
0.01
0.1
1
10
--- BEFORE SPIKE-REMOVAL
MEM EXTENSION
... WINDOW DECONVOLUTION
4000 Ohm.m. 1100m.
600 Ohm.m. 12500m.
6000 Ohm.m.
PHASE IN DEG.
90
60
30
0
PERIOD IN SEC

Fig. 7

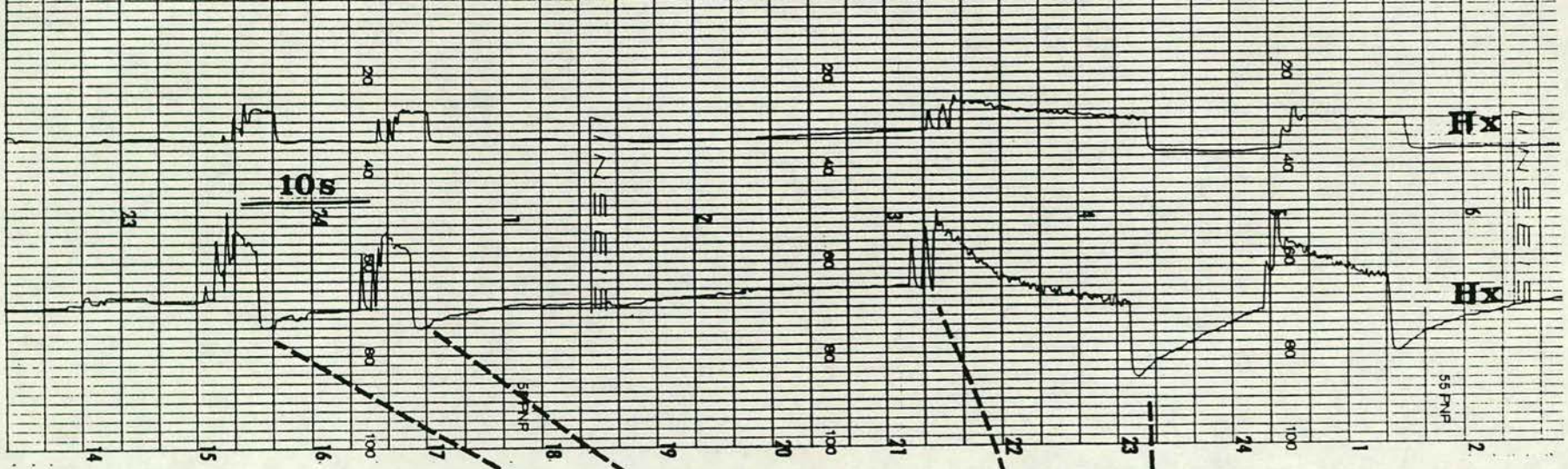

[a]

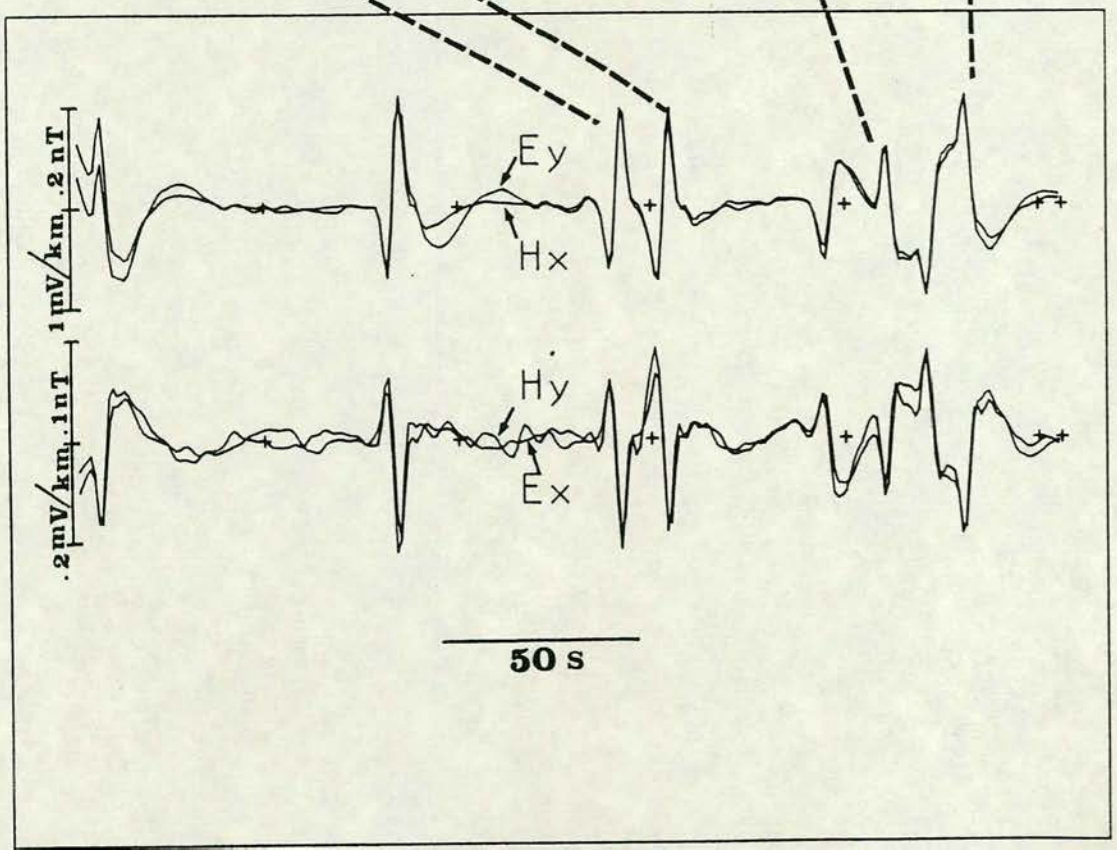

[b]

Fig. 8

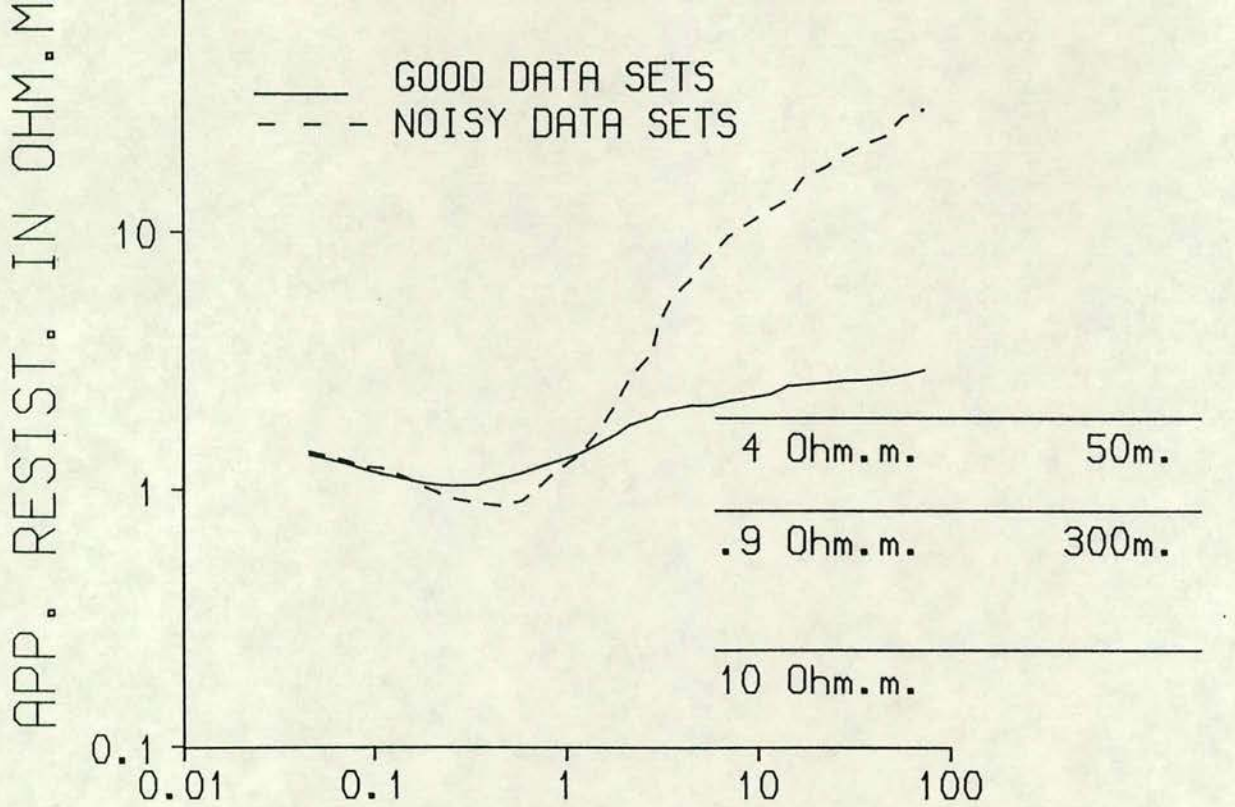
APP. RESIST. IN OHM.M
GOOD DATA SETS
NOISY DATA SETS
4 Ohm.m.
50m.
.9 Ohm.m.
300m.
10 Ohm.m.
10
1
0.1
0.01
0.1
1
10
100

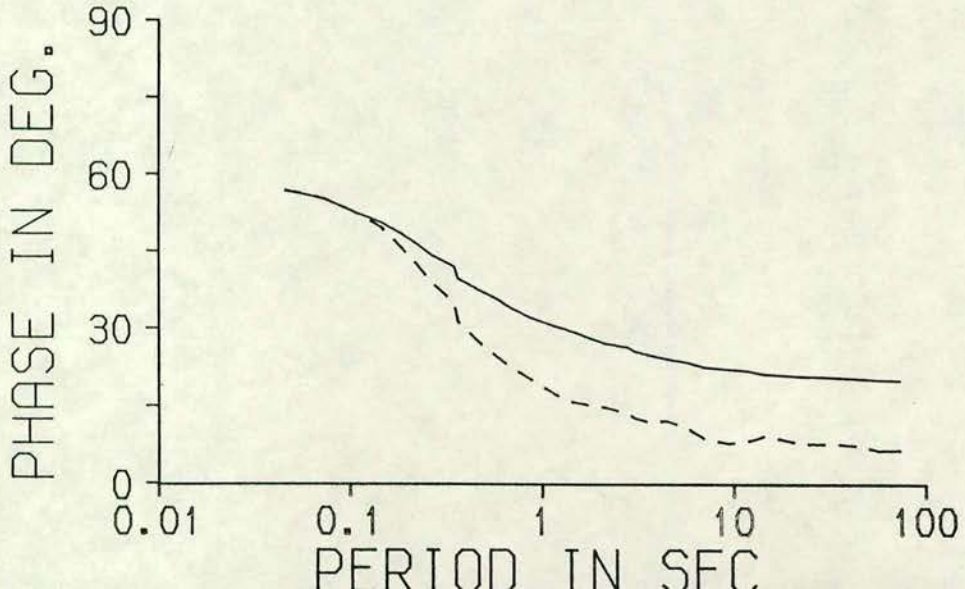
PHASE IN DEG.
90
60
30
0
0.01
0.1
1
10
100
PERIOD IN SEC

Fig. 9

II. APPENDIX - C

II. APPENDIX-C

DISTORTION OF TELLURIC FIELD MEASUREMENTS NEAR HILLS USING A CONFORMAL MAPPING METHOD

T.HARINARAYANA *
Department of Geophysics
University of Edinburgh
Mayfield Road
EDINBURGH-EH93JZ.

Permanent address:

* National Geophysical Research Institute, Hyderabad-500 007. INDIA.

ABSTRACT

The effect of a two dimensional conducting hill on the telluric fields measured along the perpendicular direction has been studied near a horizontal surface using the Schwarz-Christoffel conformal transformation technique. Though the solution presented here is valid for various model parameters of the hill, this paper is restricted to consideration of symmetric surfaces. The effect has been analysed by varying the normalized height from the surface and its inclination (α) with respect to the horizontal surface. The results indicate that both the height of the hill and its inclination affect telluric field measurements significantly. For the same hill height, distortion of the telluric field is observed to a greater distance from the offset for the less inclined hills compared to steep hills. For example, to obtain telluric field measurements within 10 percent of their undisturbed values, it is observed that if the resistive basement is at 1 Km. depth and the hill is 500 m. high, the stations must be located more than 60m. from an 80° inclined surface and more than 150m. for a 20° inclined surface. Distortion of apparent resistivity values computed from magnetotelluric field measurements is also discussed.

1. INTRODUCTION

Most geophysical data collected during field observations require correction before interpretation. The type of correction depends on the nature of the errors involved associated with the observation. Field geophysicists in general attempt to minimise errors involved during observations. However, sometimes the data may need to be accepted with errors. It is important to correct for these errors to fulfill the necessary assumptions for modelling.

Telluric and magnetotelluric methods have an advantage over other geeoelectrical methods because of their deeper level of investigation at low cost, This arises from the utilization of natural fields as a source. But this natural source field is of extremely low amplitude and thus the data often suffer from local industrial and cultural electrical noise. Apart from artificial electrical noise, topography distorts telluric fields. To avoid topographic effects, the station locations should ideally be located in relatively flat areas.

Topographic undulations are a commonly occurring feature and in some studies it may be necessary to collect data near them. Modelling algorithms in general assume that the earth is a plane surface; however, if the earth's surface becomes non-horizontal the data should be corrected so that the assumption is valid. In recent years with the advent of fast computers, numerical modelling algorithms which can accommodate non-horizontal topographic earth surfaces (Reddig and Jiracek 1984, Wannamaker 1985) have been developed. Apart from these numerical studies, topographic problems have been examined using analog models (Wescott and Hessler 1962, Faradzhev et. al., 1972 etc.,) and using conformal mapping techniques (Kunetz and de Gery 1972, Thayer 1975, Harinarayana and Sarma 1982, etc.). Analytical methods have an advantage over numerical methods because of their capability of analysing the variation of different parameters of the model with a minimum of computation.

In the present paper a two dimensional topographic hill model is considered and the distortion effects on telluric field measurements perpendicular to the model are determined using the conformal mapping technique. This technique is based on the principle that an area in one plane can be mapped onto another plane conformally, provided there exists a continuous and one to one correspondence of points and angles between the two planes. Among the conformal techniques, the Schwarz-Christoffel transformation technique is probably the most convenient for solving problems relating to two dimensional potential distribution. The model assumed in the present study is bounded by the air above and a very highly resistive basement below. Thus the electrical currents are constrained to flow in the conducting surface layer. This assumption is not unreasonable. For example, the electrical basement is usually several orders of magnitude more resistive than overlying sedimentary rocks.

To solve the problem of the hill geometry, the assumed model (Fig.1) in the z-plane is transferred to another, w-plane, using the transformation. The telluric field is computed in the w-plane and then transferred back to the z-plane. The solution of the present problem can be treated as semi-analytical in the sense that the relevant differential equation is solved with numerical integration using the Runge-Kutta method. The solution presented here is closely related to Naidu(1965), where details can seen,

however, a brief description of the theory is given here.

2. THEORY

2.1 Formulation of the problem

The period of telluric field signals considered is assumed to be sufficiently long to be approximated by a D.C. field for which the potential satisfies Laplace's equation.

Along the boundary EDCBAA'E' in Fig.1 the normal gradient vanishes, i.e.,

$$\partial V / \partial n = 0$$

By conformal transformation, the complex geometry in the z-plane can be mapped into the w-plane to form a simple geometry with the same boundary conditions, the potential still satisfying Laplace's equation. The Schwarz-Christoffel transformation of the geometry of the structure can be written in differential form as

$$dz/dw = p\, w^{\alpha/\pi} (w-k)^{-(\alpha+\beta)/\pi} (w-l)^{\beta/\pi} (w-1)^{-1} \qquad \text{.....(1)}$$

where, α and β are the angles of the inclined surface of the hill. The constants p, k and l can be determined by integrating along EE' and AA'.

Therefore,

$$p = H_1/\pi \qquad \text{.....(2)}$$

where, H_1 is the depth to the basement from the horizontal surface

and

$$k=1-[\,(1-l)^{\beta/\pi}]^{\pi/(\alpha+\beta)}$$

.....(3)

From the above equation it is clear that the values k and l cannot be obtained uniquely. However, the value of l can be assumed arbitrarily such that $0< l <1$. As the object of this study is to estimate the effect of topography at points on the horizontal surface, it is necessary to map the x-axis in the z-plane onto the u-axis in w-plane. To solve this the procedure used in Roy and Naidu (1972) can be adopted as follows.

Equation 2 can be written in real and imaginary parts, as

$$\partial u/\partial x = \text{Real}[1/p\; w^{-\alpha/\pi}(w-k)^{(\alpha+\beta)/\pi}(w-l)^{-\beta/\pi}\,(w-1)]$$

.....(4)

$$\partial v/\partial x = \text{Imag}[1/p\; w^{-\alpha/\pi}(w-k)^{(\alpha+\beta)/\pi}(w-l)^{-\beta/\pi}\,(w-1)]$$

.....(5)

Since equations 4 and 5 are nonlinear differential equations, they can be solved numerically, integrating simultaneously along D to B keeping y=0 in z-plane. However, to start the integration one requires initial conditions. At the point D the above equations become singular, because, at x=0, u=v=0. This difficulty can be overcome by considering the asymptotic solution of equation 2 (for details see Naidu 1965). Therefore,

$$v/u = \tan\,[\,\alpha/(1+\alpha/\pi)]$$ .....(6)

Either v or u may be assumed << 1. Suppose u << 1, then the initial

conditions can be written as,

.....(6)

$$v_o = u_o \tan [\ \alpha/(1+\alpha\ /\pi)],$$

.....(7)

and

$$x_o = [\{ -p\ k^{-(\alpha+\beta)/\pi}\ l^{\beta/\pi}\} / (1+\alpha/\pi)]\ (u^2+v^2)^{(1+\alpha/\pi)/2}.$$

.....(8)

Using these initial conditions it is now possible to integrate equations 4 and 5.

After integration, u approaches l at the point B, v approaches 0 and x assumes a certain value which in turn depends on the assumed value of l. Knowing the values of x, α and β, the height of the hill H_2 can be determined.

Since v=0 along BA, the equation required for mapping x-axis on the u-axis can be written as,

$$\partial u/\partial x = 1/p\ u^{-\alpha/\pi}\ (u-k)^{(\alpha+\beta)/\pi} (u-l)^{-\beta/\pi} (u-1)$$

.....(9)

This may be considered as a non-linear differential equation relating u and x and can be solved again numerically. The initial values to initiate the integration can be obtained by solving equations 4 and 5.

After transforming the complex geometry and finding the solution for mapping x-axis onto the u-axis, the remaining problem is the computation of

the telluric field.

2.2 Computation of the telluric field:

The telluric field in the z-plane can be considered as if produced from a line source and a sink placed at + respectively. The potential distribution in the w-plane for such a situation is given by

$$V = (I/\pi) \; / \; \log(w-1)$$

.....(10)

where, I is the current strength.

Differentiation of this potential will give the telluric field E in the w-plane in the form,

$$E = -dV/dw = (I/\pi)\; 1/(w-1).$$

.....(11)

Therefore,

transforming this field to the z-plane, we have,

$$E = -\, dV/dz = (I/H_1)\; w^{-\alpha/\pi}(w-k)^{(\alpha+\beta)/\pi}\; (w-l)^{-\beta/\pi}.$$

.....(12)

Since, along BA v=0 we have,

$$E = -\, dV/dx = I/H_1\; u^{-\alpha/\pi}(u-k)^{(\alpha+\beta)/\pi}\; (u-l)^{-\beta/\pi}$$

.....(13)

3. DISCUSSION

The results derived from the hill model can be studied by varying six parameters: the angles α and β of the hill surface, the elevation H_2, the depth to the basement H_1, the distance x from the offset (i.e., from point B in Figure 1) and the distortion of telluric field. In such a study one can have many families of computed curves. However, in the present study it is assumed that $\alpha=\beta$, i.e., restriction to a symmetric model and that the parameters H_1, H_2 and x are normalized. The distortion of the telluric field is represented as a percentage error computed with respect to the value observed at a large distance x. As a result, the number of variables reduces to four– for example, inclination, normalized distance, normalized elevation and percentage error– making the analysis of the results of the study more tractable. Among the four parameters, each one is assumed invariant in turn, two of the parameters are specified on the x and y axes and curves representing the fourth parameter are plotted as shown in Figures 2 to 5. It should be noted that for convenience, the origin shown in these figures is assumed to be at point B, instead of point D as shown in Figure 1.

With the above convention, the distortion of telluric field measurements due to topography is studied first with the inclination ($\alpha=\beta$) assumed invariant and varying the normalized depth parameter H_1/H_2 (Figure 2) and secondly with the inclination again constant and varying the normalized height parameter H_2/H_1 (Figure 3). It is observed from these Figures that the error increases as the values of H_1/H_2 and H_2/H_1 increases. In other words, for the same height of the hill, the deeper the electrical basement the larger is the distortion on telluric field measurements (Figure 2). Similarly, for the same basement depth model it can be seen that a more elevated hill distorts the measurements to a larger distance compared with the less elevated hill. From these figures (2 and 3) it can also be verified that for any given model the distortion effect decreases as the distance from the inclined surface increases.

The effect of the inclination observed at a constant distance from the offset is shown in Figure 4. From this figure one can observe that for any value of α, as the H_2/H_1 value increases the error also increases with all

curves exhibiting an asymptotic behaviour i.e., the error remains constant for larger values of H_2/H_1. It can also be observed that for lower values of H_2/H_1 the error increases as α decreases. This can be understood well by considering the following example. At a normalized distance ($x/H_1=-0.1$) if $H_2/H_1=1.0$, the error due to topography is about 10% for $\alpha=80^\circ$ and it is nearly 25% for $\alpha=50^\circ$. This is not unreasonable, because for the same height of the hill, a small α value model has a large area of hill surface compared with a model with a large value of α.

Figure 5 shows the normalized distance necessary in order to limit the distortion of telluric field measurements to within 10% of their undistorted value. The curves are plotted in the figure for different α values. It can be seen that as the H_2/H_1 value increases, the normalized distance (x/H_1) necessary to limit the error within 10% also increases. The curves, however, show an asymptotic trend to a value of x/H_1 for larger H_2/H_1 values. Again for the same reason as discussed earlier for the results presented in Figure 4, it can be verified that for a lower value of H_2/H_1, a model with smaller α parameter (i.e., less inclined topography) distorts the measurements to larger distances than does a model with larger α values (i.e., more inclined topography).

Though the solution presented here is strictly valid for D.C. fields, the study is extended to demonstrate the topographic effect on magnetotelluric apparent resistivity versus period curve considering the simple two layer earth model as shown in figure 6. The resistivity of top layer is 200 Ohm.m., its thickness is 2 Km. and it overlies an electrical basement of resistivity 50,000 Ohm.m.. The model considered here is consistent with the previously assumed model in that the conducting layer is several orders of magnitude less resistive than the basement. A magnetotelluric sounding curve (the 'normal' curve in Fig. 6) is computed for this model for the period range of 0.01 to 10 sec. using a forward modelling scheme (eg. see Keller and Frischknecht 1970 p.224). To apply the results of the present study the following assumptions were made.

- The longest period considered can be approximated to D.C.– this can be justified as skin depth for 10 sec. period is over 10 times the thickness of the conducting layer.

- The short period signals are less distorted due to the topography than the long period signals and the distortion decreases linearly on a logarithmic scale in the period range 0.1 to 10 sec.

- Since the telluric field computed in the present study is along the direction perpendicular to the strike of the topographic model it is assumed that the effect of the topography on the magnetic field is negligible compared to the telluric field distortion.

With these assumptions for the study of the distortion of the magnetotelluric apparent resistivity, it is now possible to apply the results to the M.T. curve. For example, the magnetotelluric apparent resistivity curves shown in the figure are for telluric field measurements distorted by 10%, 20%, and 30% error due to topography. It can be seen that the apparent resistivity values computed are overestimated near the topography with the curves showing an unrealistic slope compared to the horizontal surface model.

4. CONCLUSIONS

The topographic effect of a hill on telluric field measurements is studied by varying different parameters of the model. From the models considered in the present study it is observed that the topographic effect is observed to increase with the height of the hill surface and with the basement depth. For a particular distance from the hill it is observed that as the height of the hill surface increases the distortion effect due to topography also increases but it soon reaches a maximum and remains constant irrespective of height of the topography. In certain cases, for the same elevation a hill with less inclination distorts the telluric field to larger distances than one with greater inclination. For example, if the basement depth (H_1) is 1 km. and the hill is 500 m. high, for measurements within 10% error the station location must be more than about 150 m. distant for a 20° inclined hill surface, and 60 m. for an 80° inclined hill surface. The magnetotelluric apparent resistivity values are overestimated near such a topographic feature.

ACKNOWLEDGEMENTS

I am indebted to Dr.V.R.S.Hutton for her continuous encouragement and critically going through this paper. Many thanks to Dr.B.A.Hobbs for comments made on the manuscript. Financial support in the form of a scholarship by the Association of Commonwealth Universities is gratefully acknowledged.

REFERENCES

Faradzhev, A.S., Kakhramanov, K.K., Sarkisov, G.A., and Khalilova, N.E., 1972. On effect of terrain on results of Magnetotelluric sounding (MTS) and profiling (MTP). Izvest. Earth Phys., 5: 329–330.

Harinarayana, T., and Sarma, S.V.S., 1982. Topographic effects on telluric field measurements. Pageoph, 120: 778–783.

Keller, G.V. and Frischknecht, F.C., 1970. Electrical methods in Geophysical prospecting, Pergamon, Oxford, 519pp.

Kunetz, G., and de Gery, C.J., 1956. Examples d'application de la representation conform a l'interpretation du champ tellurique. Revue del' Inst. Francais du Petrole, 11: 1179–1192.

Naidu, P.S., 1965. Telluric field and Apparent resistivity over an inclined normal fault. Can. J. Earth Sci., 2: 351–360.

Reddig, R.P., and Jiracek,G.R., 1984. Topographic modelling and correction in magnetotellurics. Presented at 54th Annual meeting SEG, Atlanta, Expanded abstracts: 44–47.

Roy, K.K., and Naidu, P.S., 1972. Computation of telluric field and apparent resistivity over an anticline. Pageoph, 80: 205–217.

Thayer, R.E., 1975. Topographic distortion of telluric currents, A simple calculation. Geophysics, 40: 91–95.

Wannamaker, P.E., 1985. Finite element program for solutions of magnetotelluric responses of two dimensional earth resistivity structure, user documentation: 1–72.

Wescott, E.M. and Hessler, V.P., 1962. The effect of topography and geology on telluric currents. J. Geophy. Res., 67: 4813–4823.

FIGURE CAPTIONS

FIG.1 (a) Geometry of the hill surface model in z-plane. The shaded region represents the conducting region of the earth. Air and electrical basement resistivities are assumed to be infinite. The surface BCD represents the hill surface and A'E' is the electrical basement surface. (b) Schwarz-Christoffel transformation of the surface shown in (a).

FIG.2 Distortion of telluric field measurements shown as percentage error near a hill surface varying the normalized basement depth. Percentage computed with respect to the undisturbed value observed far away from the hill surface. Distance 'x' is normalized with the height of the hill 'H_2'. The inclination ($\alpha=\beta$) is 80° assumed to be invariant.

FIG.3 Distortion of telluric field measurements near a hill varying the normalized height (H_2/H_1) parameter. The inclination is assumed as 20°. Distance 'x' is normalized with H_1

FIG.4 Effect of topographic hill surface observed at a distance, $x/H_1=-0.1$. The curves shown are for different values of inclination.

FIG.5 Nomogram showing normalized distance (x/H_1) as a function of normalized height (H_2/H_1). The percentage error is assumed to be invariant and the curves shown are for different values of 'λ' parameter.

FIG.6 Distortion of magnetotelluric apparent resistivity curve near the hill surface. The normal curve computed for the model shown on the left hand top corner. The distorted curves shown are for the 10, 20, 30 percent error in the observed telluric field measurements due to topography.

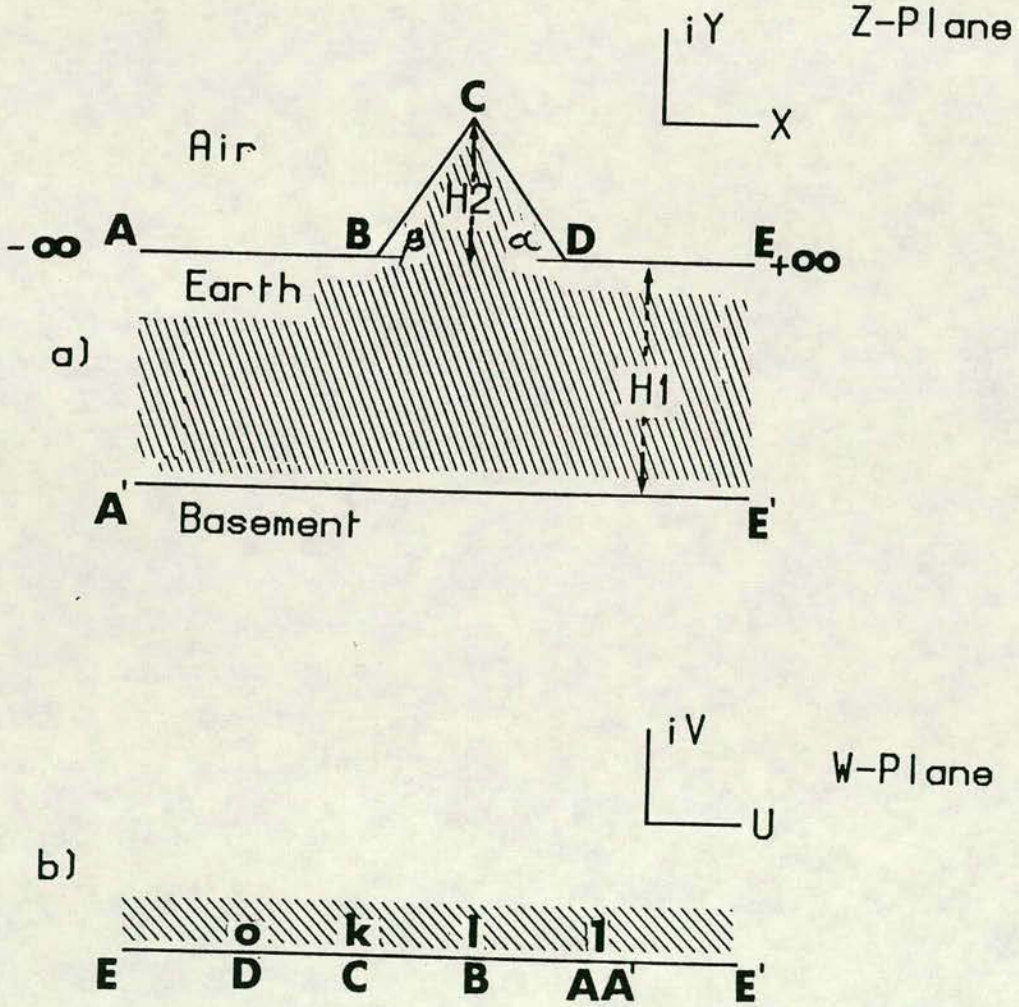
iY
Z-Plane
X
C
Air
H2
-∞
A
B
β
α
D
E
+∞
Earth
a)
H1
A'
Basement
E'
iV
W-Plane
U
b)
o
k
l
l
E
D
C
B
AA'
E'

Fig. 1

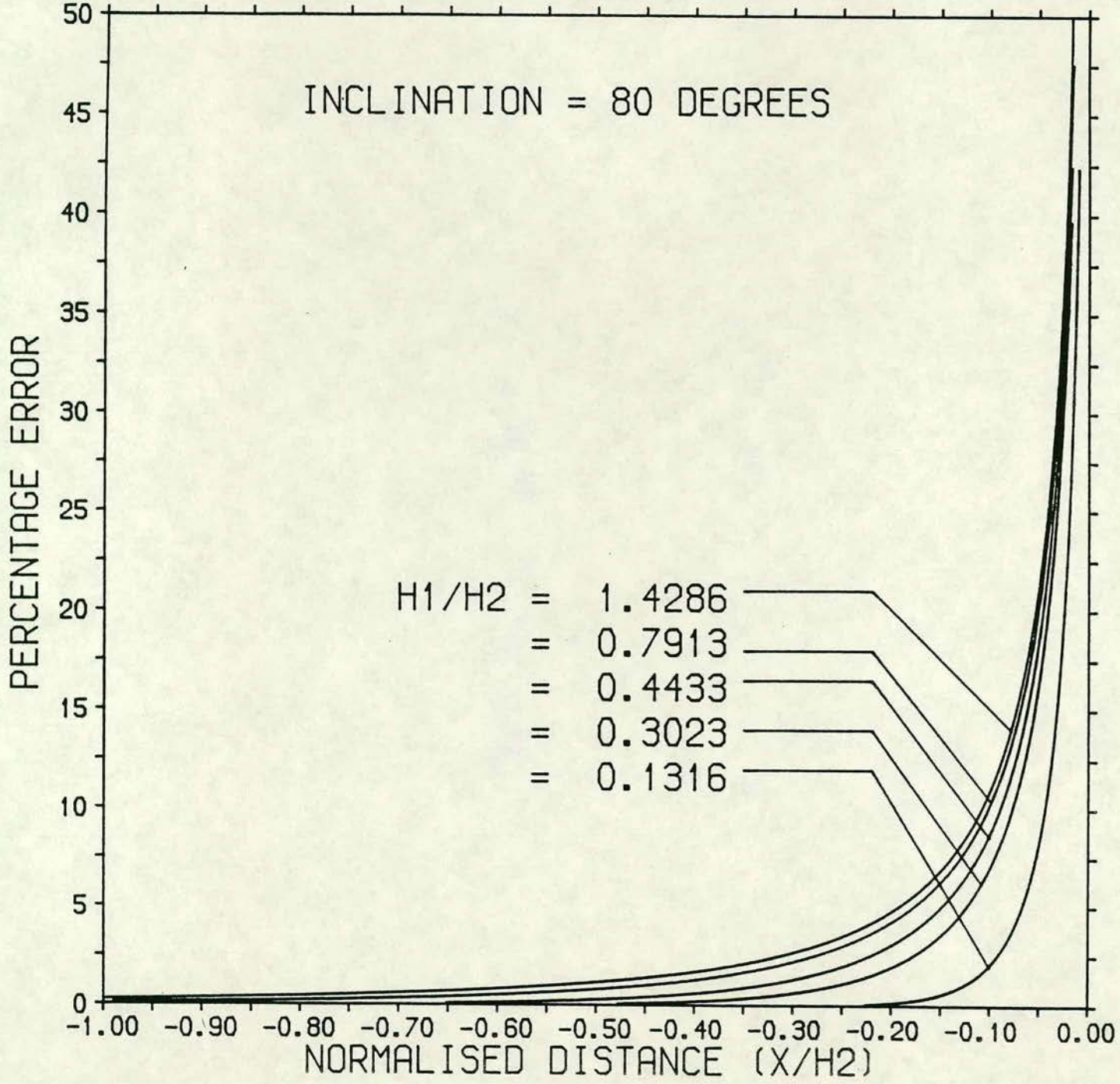
INCLINATION = 80 DEGREES
PERCENTAGE ERROR
NORMALISED DISTANCE (X/H2)
H1/H2 = 1.4286
= 0.7913
= 0.4433
= 0.3023
= 0.1316
50
45
40
35
30
25
20
15
10
5
0
-1.00
-0.90
-0.80
-0.70
-0.60
-0.50
-0.40
-0.30
-0.20
-0.10
0.00

Fig. 2

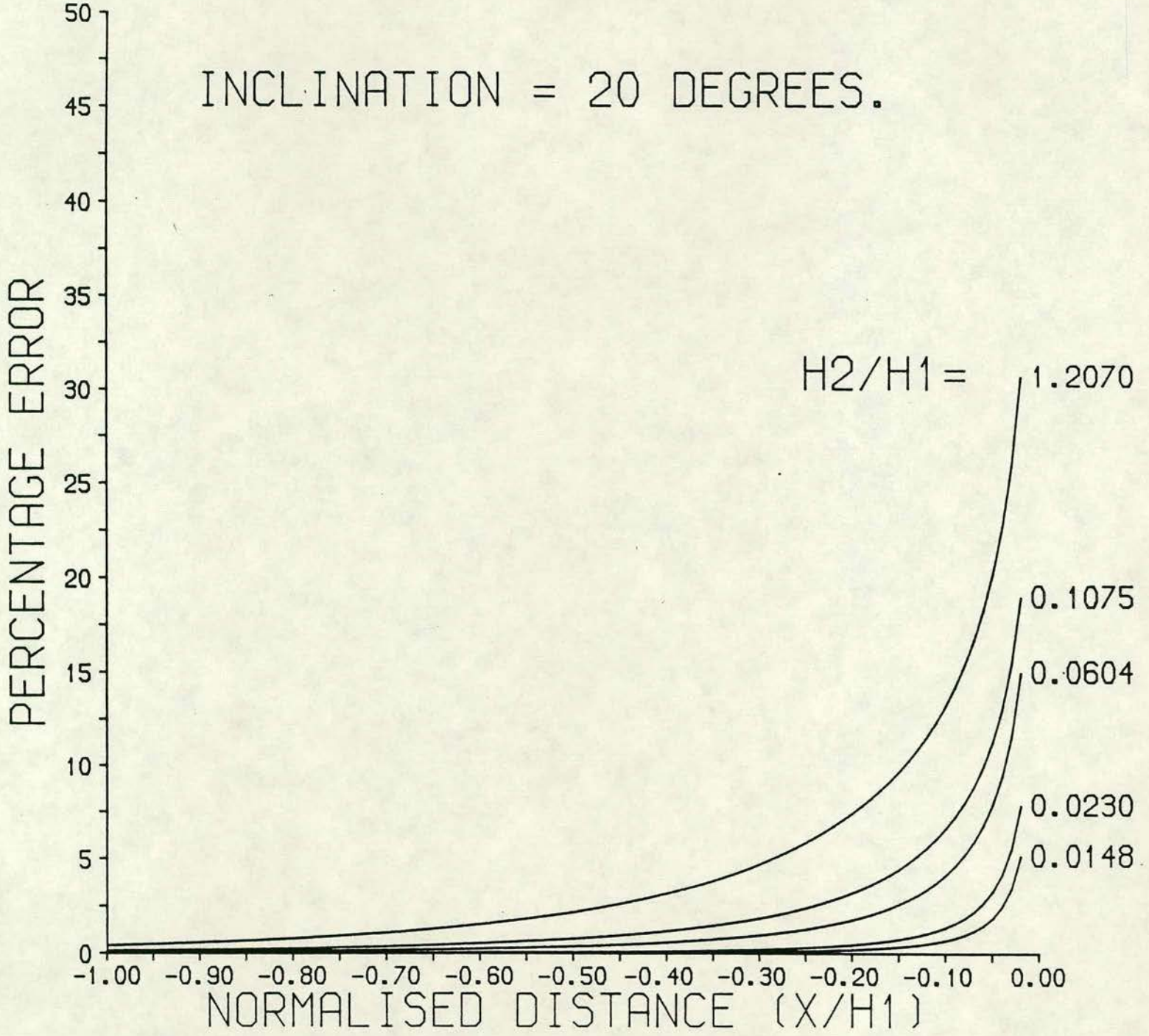
INCLINATION = 20 DEGREES.
PERCENTAGE ERROR
NORMALISED DISTANCE (X/H1)
H2/H1 =
1.2070
0.1075
0.0604
0.0230
0.0148
50
45
40
35
30
25
20
15
10
5
0
-1.00
-0.90
-0.80
-0.70
-0.60
-0.50
-0.40
-0.30
-0.20
-0.10
0.00

Fig. 3

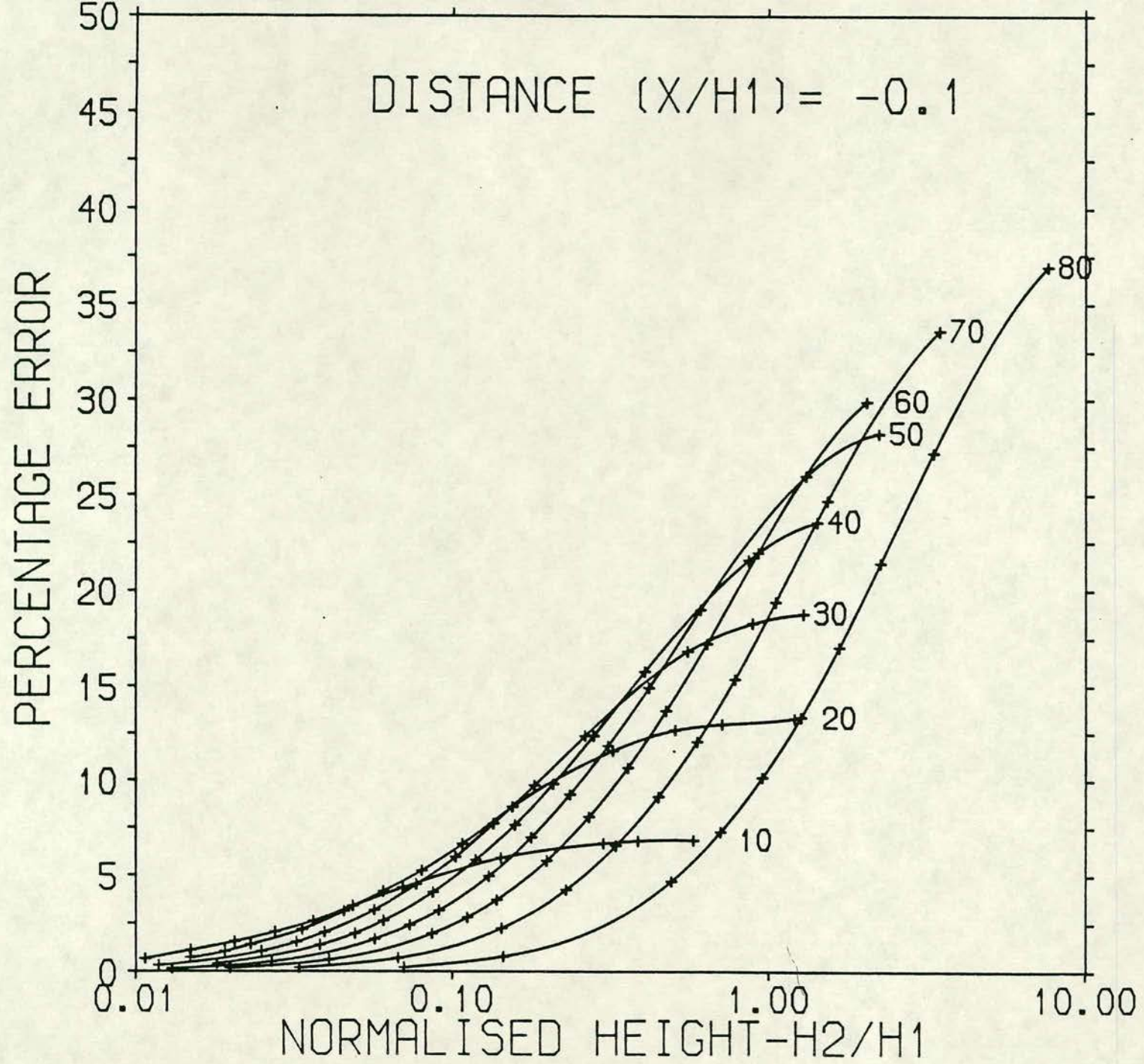
DISTANCE (X/H1)= -0.1
PERCENTAGE ERROR
NORMALISED HEIGHT-H2/H1
0
5
10
15
20
25
30
35
40
45
50
0.01
0.10
1.00
10.00
10
20
30
40
50
60
70
80

Fig. 4

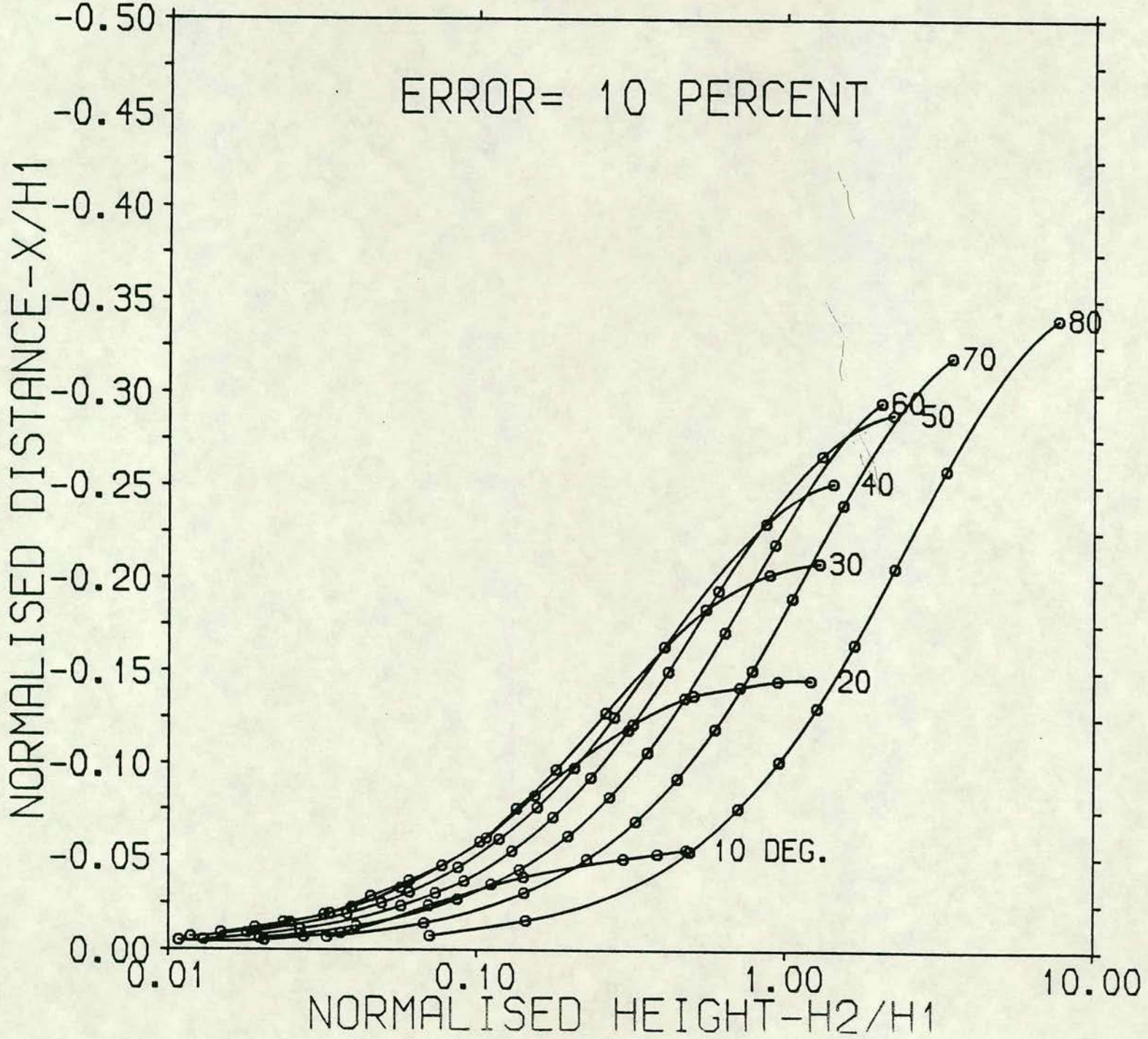
ERROR= 10 PERCENT
NORMALISED DISTANCE-X/H1
NORMALISED HEIGHT-H2/H1
-0.50
-0.45
-0.40
-0.35
-0.30
-0.25
-0.20
-0.15
-0.10
-0.05
0.00
0.01
0.10
1.00
10.00
80
70
60
50
40
30
20
10 DEG.

Fig. 5

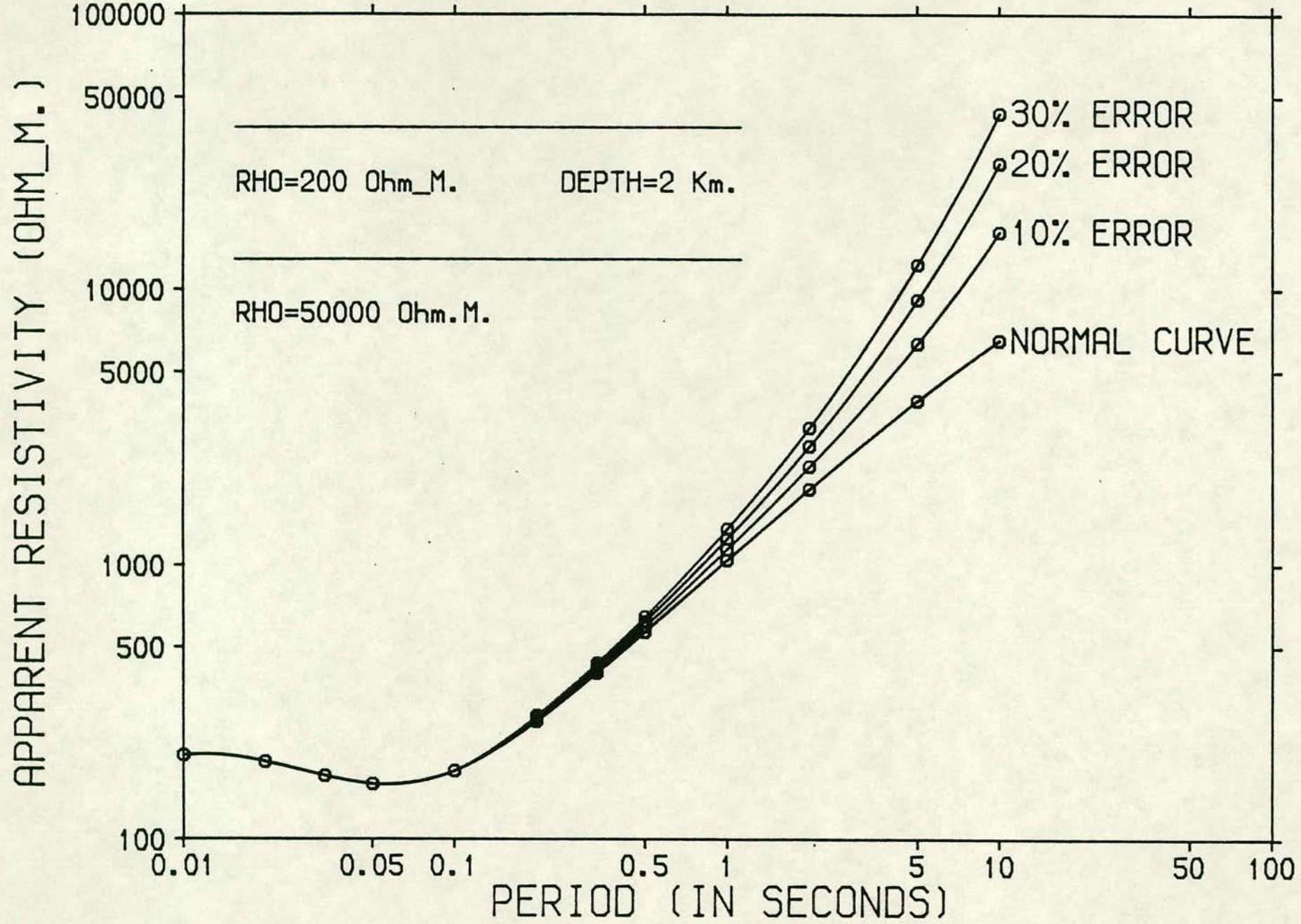
100000
50000
10000
5000
1000
500
100
APPARENT RESISTIVITY (OHM_M.)
RHO=200 Ohm_M.
DEPTH=2 Km.
RHO=50000 Ohm.M.
30% ERROR
20% ERROR
10% ERROR
NORMAL CURVE
0.01
0.05
0.1
0.5
1
5
10
50
100
PERIOD (IN SECONDS)

Fig. 6

REFERENCES

Abramovici, F. and Shoham, Y., 1977. Inversion of anisotropic magnetotelluric data. Geophy. J. Roy. astr. Soc., 50, 55–74.

Airy, G.B., 1868. Comparison of magnetic disturbances recorded by the self-registering magnetometers at the Royal Observatory, Greenwich with magnetic disturbances deduced from the corresponding terres trial galvanic currents recorded by the self-registering galvanometer of the Royal Observatory. Phil. Trans. Roy. Soc., 158, 465.

Anderson, T.B. and Oliver, G.J.H., 1986. The Orlock Bridge Fault: a major late Caledonian sinistral Fault in the Southern Uplands terrane, British Isles. Trans. R. Soc. Edin. Earth Sci., 77, 203–222.

Backus, G. and Gilbert, F., 1967. Numerical application of a formalism for geophysical inverse problems, Geophys. J. Roy. astr. Soc., 13, 247–276.

Bailey, R.C. and Edwards, R.N., 1976. The effect of source field polarisation on geomagnetic anomalies in the British Isles, Geophys. J. Roy. astr. Soc., 45, 97–104.

Bailey, R.C., Edwards, R.N., Garland, G.D., Kurtz, R. and Pitcher, D.H., 1974. Electrical conductivity studies over a tectonically active area in Eastern Canada. J. Geomag. Geoelectr., 26, 125–146.

Bamford, D., Nunn, K., Prodehl, C. and Jacob, B., 1977. LISPB-III. Upper crustal structure of northern Britain. J. Geol. Soc. Lond., 133, 481–488.

Bamford, D., Nunn, K., Prodehl, C. and Jacob, B., 1978. LISPB-IV: Crustal structure of northern Britain. Geophy. J. Roy. Astr. Soc. 54, 43–60.

Banks, R.J., 1986. The interpretation of the Northumberland trough geomagnetic variation anomaly using two dimensional current models. Geophy. J. Roy. Soc., 87, 744–766.

Banks, R.J., Beamish, D. and Geake, M.J., 1983. Magnetic variation anomalies in Northern England and Southern Scotland. Nature, 303, 516–518.

Banks, R.J. and Beamish, D., 1984. Local and regional induction in the British Isles. Geophy. J. Roy. astr. Soc., 79, 539-553.

Beamish, D., 1986a. Deep crustal geoelectric structure beneath the Nothumberland Basin. Geophys. J. Roy. astr. Soc., 84: 619-640.

Beamish, D., 1986b. Geoelectric structural dimensions from magnetotelluric data: methods of estimation, old and new. Geophys., 51, 6: 1298-1309.

Beamish, D., Smythe, D.K. 1986. Geophysical images of deep crust: the Iapetus suture. J. Geol. Soc., London, 143: 489-497.

Beamish, D. and Banks, R.J., 1983. Geomagnetic variation anomalies in Northern England: Processing and presentation of data from a non-simultaneous array. Geophy. J. Roy. astr. Soc., 75, 513-539.

Beamish, D., 1986. Deep crustal geoelectric structure beneath the Northumberland basin. Geophy. J. Roy. astr. Soc., 79, 539-553.

Bentley, C.R., 1973. Error estimation in two-dimensional magnetotelluric analysis. Phys. Earth Planet. Int., 7, 423.

Berdichevsky, M.N., 1960. Principles of magneto-telluric profiling theory, Applied Geophys., (Prikl. Geofiz.), 28.

Berdichevsky, M.N., 1963. Linear relationships in the magnetotelluric field, Applied Geophys., (Prikl. Geofiz.), 38.

Berdichevsky, M.N. and Dmitriev, V.I., 1976. Distortion of magnetic and electrical methods by surface lateral inhomogeneities. Acta. Geod. Geophys. Mont. Acad. Sci. Hungary, 11, 447-483.

Berdichevsky, M.N., Vanyan, L.L., Kuznetsov, V.A., Levadney, V.T., Mandelvavm M.M., Nechaeva G.P., Okulesky B.A., Shilovsky P.P. and Shpak, I.P., 1980. Geoelectric model of the Baikal region. Phys. Earth Planet. Intr., 22, 1-11.

Blaxland, A.B., Aftalion, M. and Van Breeman, O., 1979. Pb isotopic composition of feldspar from Scottish Caledonian granites and the nature of the underlying crust. Scott. J. Geol., 15, 139-151.

Bostick, F.X. (Jr.), 1977. A simple and almost exact method of MT analysis. in "workshop on electrical methods in geothermal exploration", U.S. Geol. Surv., contract No. 14080001-8-359.

Bott, M.H.P. and Masson-Smith, D., 1957a. A geological interpretation of a gravity survey of the Alston block and the Durham coal field. Q. J. Geol. Soc. Lond.,. 113, 93-117.

Bott, M.H.P. and Masson-Smith., D., 1957b. Interpretation of vertical magnetic field in north-east England. Q. J. Geol. Soc., 113, 119-129.

Bott, M.H.P., Swinburn, P.M. and Long, R.E., 1984. Deep structure and origin of the Northumberland and Stainmore troughs, Proc. Yorks. Geol. Soc., 44, 479-495.

Bott, M.H.P., 1967. Geophysical investigations of the northern Pennine basement rocks. Proc. Yorks. Geol. Soc., 35, 139-168.

Bott, M.H.P., Long, R.E., Green, A.S.P. Lewis, A.H.J., Sinha, M.C. and Stevenson, D.L., 1985. Crustal structure south of the Iapetus suture beneath Northern England. Nature, 314, 724-727.

Bott, M.H.P., 1961. A gravity survey of the coast of north east England. Proc. Yorks. Geol. Soc.. 33, 1-20.

Brewer, J.A., Matthews, D.W., Warner, M.R., Hall, J., Smythe, D.K. and Whittington, R.J., 1983. BIRPS deep seismic reflection studies of British Caledonides- the WINCH profile. Nature, 305, 206-210.

Brewitt-Taylor, C.R. and J.T. Weaver, 1976. On the finite difference solution of two-dimensional induction problems. Geophys. J. Roy. astr. Soc., 47: 375-396.

Brewitt-Taylor, C.R. and Johns, P.B., 1980. Diakoptic solution of induction problems. J. Geomag. Geoelectr., 32, Suppl. I: SI73-SI78.

Briden, J.C., Turnell, H.B. and Watts, D.R., 1984. British Palaeomagnetism, Iapetus oceans and the Great Glen Fault. Geology, 12, 428-431.

Bullerwell, W., 1968. Aeromagnetic map of part of Great Britain and Northern Ireland. Sheet 11, Inst. Geol. Soc. London.

Burg. J.P., 1972. The relationship between maximum entropy spectra and maximum likelihood spectra. Geophysics, 37, 375-

Cagniard, L., 1953. Basic theory of the magnetotelluric method of geophysical prospecting, Geophys., 18, 605-635.

Campbell, W.H., 1987. Introduction to Electrical properties of the Earth's Mantle. PAGEOPH, 125, 193-204.

Cantwell, T., 1960. Detection and analysis of low frequency magnetotelluric signals, Ph.D. Thesis, Dept. Geology & Geophysics, M.I.T. Cambridge, Massachusetts.

Chave, A.D., Thomson, D.J. and Ander, M.E., 1987. On the Robust estimation of power spectra, Coherences and transfer functions., J. Geophys. Res., 92, B1, 633-648.

Christie, P.A.F., 1978. A report on the Cambridge North sea experiment (abstract) Geophys. J. Roy. Soc. 53, 140.

Church, W.R. and Gayer, R.A., 1973. The Ballantrae ophiolite, Geol. Mag., 110, 497-510.

Coggon, J.H., 1971. Electromagnetic and electrical modeling by the finite element method, Geophysics, 36, 132-155.

Constable, S.C., Parker, R.L. and Constable, C.G., 1987. Occam's inversion: A practical algorithm for generating smooth models from electromagnetic sounding data. Geophys., 52, 289-300.

COPROD, 1977, Comparative study of methods of deriving the conductivity profile within the earth from one-dimensional magnetotelluric data- organised by A.G.Jones. (personal communication)

Cowan, C.F.N., and Grant, P.M., 1985. Adaptive Filters. Prentice-Hall, Signal processing series.

Craig, G.Y. and Walton, E.K., 1959. Sequence and structure in the Silurian rocks of Kirkcudbrightshire. Geol. Mag., 96, 209-220.

D'Erceville, I. and Kunetz, E., 1962. The effect of a fault on the earth's natural electromagnetic field, Geophysics, 27, 651-665.

Das, U.C. and Verma, S.K., 1982. Electromagnetic response of an arbitrary shaped three dimensional conductor in a layered earth-numerical results. Geophy. J. Roy. astr. Soc., 69, 55-66.

Dawes, G.J.K., 1980. Computer program library. Internal publication, Dept., of Geophysics, Univ. of Edinburgh. U.K.

Dawes, G.J.K., 1984. Short period automatic magnetotelluric (SPAM) system in A broadband tensorial magnetotelluric study in Travave-Radiocondili geothermal Field. Final report, by V.R.S. Hutton et al. EEC Report Series. EUR A2-031-UK.

Dawes G.J.K., 1985. Magnetotelluric feasibility study Island of Milos - Greece., Final report, EN-3G-0008-UK (H).

Dewey, J.F., 1969. Evolution of the Appalachian /Caledonian Orogen. Nature, 222, 124-129.

Dewey, J.F., 1971. A model for the Lower Palaozoic evolution of the southern margin of the early Caledonides of Scotland and Ireland. Scott. J. Geol., 7, 219-240.

Dosso, H.W., W. Nienaber, 1986. A laboratory electromagnetic model study of the Juan de Fuca Plate region. Phys. Earth Planet. Int., 43: 34-46.

Dowling, R.A. and Gray, D.A., 1986. Geothermal resources of the United Kingdom. Jour. of the Geol. Soc. Lond., 143, 409-507.

Dunham, K.C., Dunham, A.C., Hodge, B.C. and Johnson, G.A.L., 1965. Granite beneath visean sediments with mineralisation at Rookhope, Northern Pennines. Q.J. Geol. Soc. Lond., 121, 383-417.

Eastwood, T., 1971. Northern England. British Regional hand book, 4th edition. Her Majesy's stationary office., 125pp.

Edwards, R.N., Law, L.K. and White, A., 1971. Geomagnetic variations in the British Isles and their relation to electrical currents in the ocean and shallow

seas, Phil. Trans. Roy. Soc. Lond., No. 1204, 270, 289-323.

El-Isa, Z.H.M., 1977. Seismic studies of local events received at three arrays in southern central Scotland. Ph. D., thesis, University of Glasgow.

Ernst, T., 1981. A comparison of two methods of the transfer function calculation using the least-square criterion in time and frequency domain. Publ. Inst. Geophys. Pol. Acad. Sci., G-2(143), 13-24.

Etheridge, M.A., V.J. Wall, R.H. Vernon, 1983. The role of the fluid phase during regional metamorphism and deformation. J. metamorphic Geol., 1: 205-226.

Everett, J.E. and Hyndman, R.D., 1967a. Geomagnetic variations and electrical conductivity structure in S.W. Australia, Phys. Earth. Planet. Int., 1, 24-34.

Everett, J.E. and Hyndman, R.D., 1967b. Magneto-telluric investigations in South-Western Australia, Phys. Earth. Planet. Int., 1, 49-54.

Faradzhev, A.S., Kakhramanov, K.K., Sarkisov, G.A., Khalilova, N.E., 1972. On effect of terrain on results of magnetotelluric soundings (MTS) and profiling (MTP). Izv., Earth Phys., 5: 92-94.

Fischer, G. and Le Quang, B.V., 1982. Parameter trade off in one-dimensional magnetotelluric modelling. J. Geophys., 51, 206-215.

Fischer, G. and Le Quang, B.V., 1981. An analytic one dimensional magnetotelluric inversion scheme. Geophys. J. Roy. astr. Soc., 67, 257-278.

Fitton, J.G. and Hughes, D.J., 1970. Volcanism and plate tectonics in the British Ordovician, Earth. Plan. Sci. Lett., 8, 223-228.

Fontes, S.F., Harinarayana, T., Dawes, G.W.K. and Hutton, V.R.S., 1987. Processing of noisy magnetotelluric data using digital filters and additional data selection criteria (P.E.P.I., in press).

Gale, I.N., Rollin, K.E., Downing, R.A., Allen, D.J. and Burgess, W.G. 1984. An assessment of the geothermal resources of the United Kingdom. Investigations of the Geothermal potential of the UK, British Geological Survey.

Gamble, T.D., Goubau, W.M.,. Clarke, J. 1979. Magnetotellurics with a remote

reference. Geophys., 44, 1: 53-68.

Goldberg, S. and Rotstein, Y., 1982. A simple form of presentation of magnetotelluric data using the Bostick transform. Geophys. pros., 30, 211-216.

Golub, G.H. and van Loan,C.F., 1983. Matrix Computations, North Oxford Academic, Oxford.

Goubau, W.M., Maxton, P.M., Koch, R.H. and Clarke, J., 1984. Noise correlation lengths in remote reference magnetotellurics. Geophys., 49, 4: 433-438.

Gough, D.I., 1986. Seismic reflectors, conductivity, water, and stress in the continental crust. Nature, 323: 143-144.

Grant, A.L., 1972. The continental margin off Labrador and Eastern Newfoundland - morphology and geology, Can. J. Earth. Sci., 9, 1394-1440.

Grant, F.S. and West, G.F., 1965. Interpretation theory in applied geophysics. McGraw-Hill New York.

Green, C.A., 1975. An induction study at micropulsation periods in the British Isles, Geophys. J. R. astr. Soc., 40, 225-240.

Greig, D.C., 1971. The South of Scotland. British Regional Geology Handbook - 3rd edition. Her Majesty's Stationery Office.

Gunn, P.J., 1973. Location of the proto-Atlantic suture in the British Isles, Nature, 242, 111-112.

Haak V. and Hutton R., 1986. Electrical resistivity of continental lower crust; The nature of the lower continental crust, Geological Society special publication no. 24, 35-49.

Habberjam, G.M. and Thanassoulas, C., 1979. A deep resistivity sounding at Rookhope, Northern England. Trans. Roy. Soc., 70, 171-179.

Hall, J., Powell, D.W., Warner, M.R., El-Isa, Z.H.M., Adesanya, O. and Bluck, B.J., 1983. Seismological evidence for the shallow crystalline basement in the Southern Uplands of Scotland. Nature, 305, 418-420.

Hall, D.H. and Dagley, P., 1970. Regional magnetic anomalies. An analysis of

the smoothed aeromagnetic map of Great Britain and Northern Ireland. Inst. Geol. Sci. report, 70/110, 1-7.

Harinarayana, T. and S.V.S. Sarma, 1982. Topographic effects on telluric field measurements. PAGEOPH, 120: 778-783.

Harinarayana, T. and Hutton, V.R.S. 1987. Lateral variations of conductivity structure across the S.Scotland and N.England. (abstract) Geophys. J. Roy. astr. Soc. 89, 485.

Harland, W.B. and Gayer, R.A., 1972. The Arctic Caledonides and earlier oceans. Geol. Mag., 109, 284-314.

Harris, A.L., Holland, C.H. and Leake, B.E., 1979. The Caledonides of the British Isles. Reviewed. Scottish Academic Press.

Hermance, J.F., 1973. Processing of magnetotelluric data. Phys. Earth Plan. Int., 7: 349-364.

Hermance, J.F., 1982. The assymptotic response of three dimensional basin offsets to magnetotelluric fields at long periods: The effect of current channeling. Geophysics, 47, 1562-1573.

Hill, E.R.G., 1987. A magnetotelluric study in the Moine Thrust region of Northern Scotland. Ph.D. thesis, submitted Univ. of Edinburgh, 197pp.

Hipkin, R.G. and Hussain, A., 1983. Regional gravity anomalies. 1. Northern Britain., Institute of Geological Sciences, Report 82/10, 45pp.

Hobbs, B.A., 1982. Automatic model for finding one-dimensional magnetotelluric problem. Geophys. J. Roy. astr. Soc. 68, 253-266.

Hobbs, B.A., 1975. Analytical solutions to global and local problems of electromagnetic induction in the Earth. Phys. Earth Planet. Int., 10, 250-261.

Hohmann, G.W., 1973. Three dimensional EM modelling. Geophy. surveys, 6, 27-54.

Hohmann, G.W., 1971. Electromagnetic scattering by conductors in the earth near a line source of current. Geophys., 36, 101-131.

Holland, C.H., Kelling, G. and Walton, S.E., 1979. O. T. Jones and after: A multitude of models. in The Caledonides of the British Isles. reviewd, Geol. Soc. London special publication N0. 8 (edited by Harris et al.,) 469–481.

Hutton, V.R.S., Sik, J., Jones, A.G. and Rooney, D., 1977. The inter pretation of geomagnetic variation observations in Scotland using the hypothetical event technique: abstract Geophys. J. R. astr. Soc., 49, 275.

Hutton, V.R.S., Sik., J. and Gough, D.I., 1977. Electrical conductivity and tectonics of Scotland. Nature. 266, 617–620.

Hutton, V.R.S. and Jones, A.G. 1980. Magnetovariational and magnetotelluric investigations in Scotland. J. Geomag. Geoelec., 32, Supl.1, 141–150.

Hutton, V.R.S., Harinarayana, T., Novak M. and Sule P., 1985. Electromagnetic induction studies in the region of the lapetus suture–an update. Presented at general assembly of IAGA, Prague, August.

Ingham, M.R., 1981. Lateral variation of the eletrical conductivity structure across south Scotland. Ph. D. thesis. Univ. of Edinburgh. U.K., 219pp.

Ingham, M.R. and Hutton, V.R.S., 1982. Crustal and upper mantle electrical conductivity structure in Southern Scotland. Geophy. J. Roy. astr. Soc., 69, 579–594.

Jackson, D.D., 1973. Marginal solutions to quasi–linear inverse problems in geophysics: The Edgehog Method. Geophys. J. Roy. astr. Soc., 35, 121–136.

Jackson, D.D., 1976. Most squares inversion. J. Geophy. Res., 81, 1027–1029.

Jacobs, J.A., 1970. Geomagnetic micropulsations, Springer–Verlag, New York.

Jacob, A.W.B., 1969. Crustal phase velocities observed at the Eskdalemuir seismic array. Geophy. J. Roy. Soc., 18, 189–197.

Jain, S., 1964. Electrical conductivity of the crust and upper mantle at Eskdalemuir, S. Scotland, Nature, 203, 631–632.

Jain, S. and Wilson, C.D.V., 1967. Magnetotelluric investigations in the Irish Sea and Southern Scotland, Geophys. J. R. astr. Soc., 12, 165–180.

Jeans, P.F.J., 1973. Plate tectonic reconstruction of the Southern Caledonides of Great Britain. Nature Phy. Sci., 245, 120–122.

Jodicke, H., Untiedt, J., Oglemann, W., Schulte, L. and Wagenitz, V., 1983. Electrical conductivity structure of the crust and upper mantle beneath the Rhenish Massif, Plateaus uplift (edited by K. Fuchs et al), Springer–Verlag, Berlin, 288–302.

Johnson, G.A.L., 1982. Geographical change in Britain during the Carboniferous period. Proc. Yorks. Geol. Soc., 44, 181–203.

Johnson, G.A.L., 1984. Subsidence and sedimentation in the Northumberland trough. Proc. Yorks. Geol. Soc., 45, 71–83.

Jones, A.G., 1977. Geomagnetic induction studies in Southern Scotland. PhD Dissertation, University of Edinburgh.

Jones, F.W. and Pascoe, L.J., 1971. A general computer programme to determine the perturbation of alternating electric currents in a two–dimensional model of a region of uniform conductivity with an embedded inhomogeneity, Geophys. J. Roy. astr. Soc., 24, 3–30.

Jones, F.W. and Price, A.T., 1970. The perturbations of alternating geomagnetic fields by conductivity anomalies, Geophys. J. R. astr. Soc., 20, 317–334.

Jones, A.G., 1987a. MT and Reflection: an essential combination. Geophy. J. Roy. astr. Soc., 89, 7–18.

Jones, A.G. and Hutton, V.R.S., 1979. A multi–station magnetotelluric study in Southern Scotland. II– Monte Carlo inversion of the data and its geophysical and tectonic implications. Geophy. J. Roy. astr. Soc., 56, 351–368.

Jones, A.G., 1983. The problem of current channelling: a critical review. Geophys. surv., 6, 79–122.

Jones, A.G., 1983. On the equivalence of the Niblett and Bostick transformations in the magnetotelluric method. J. Geophys., 53, 72–73.

Jones, A.G. and Garland, G.D., 1986. Preliminary interpretation of the upper crustal structure beneath Prince Edward Island. Ann. Geophysicae, 4B, 157–164.

Jones, F.W. and Pascoe, L.j., 1972. The perturbation of alternating geomagnetic fields by three dimensional conductivity inhomogeneities. Geophy. J. Roy. astr. Soc., 27, 479-485.

Jowiak, W. and Beamish, D., 1986. A thin sheet model of electromagnetic induction in Northern England and Southern Scotland. Geophys. J. Roy. astr. Soc., 85, 629-643

Jupp, D.L.B. and K. Vozoff, 1977. Two-dimensional magnetotelluric inversion. Geophys. J. R. astr. Soc., 50: 333-352.

Jupp, D.L.B. and K. Vozoff, 1975. Stable iterative methods for the inversion of geophysical data. Geophys. J. Roy. astr. Soc., 42: 957-976.

Kaikkonen, P., 1977. A finite element program package for eletromagnetic modeling. J. Geophys., 43: 179-192.

Kao, D.W. and Rankin, D., 1977. Enhancement of signal-to-noise ratio in magnetotelluric data. Geophys., 42, 1: 103-110.

Kao, D. and Orr, D., 1982. Magnetotelluric studies in the Market Weighton area of eastern England. Geophys. J. Roy. astr. Soc., 70: 323-327.

Klemperer, S.L. and Matthews, D.H., 1987. Iapetus suture located beneath the North Sea by BIRPS deep seismic reflection profiling. Geology, 15, 195-198.

Kurtz, R.D., DeLaurier, J.M. and Gupta, J.C., 1986. A magnetotelluric sounding across Vancouver Island detects the subducting Juan de Fuca plate. Nature, 321: 596-599

Lagios, E. and Hipkin, R.G., 1982. A geophysical approach to the granite batholith under the Eastern Southern Uplands. PAGEOPH. 120, 375-388.

Lagios, E. and Hipkin, R.G., 1979. The Tweedale Granite - a newly discovered batholith in the Southern Uplands. Nature, 280, 672-675.

Lagios, E. 1984. A geophysical study of the East Lothian volcanics, south east Scotland, Earth and Planet. Sci. Lett., 67, 205-210.

Lambert, R.St.J. and McKerrow W.S., 1976. The Grampian Orogeny. Scott.

J. Geol., 12, 271–292.

Lanczos, C., 1964. Linear differential operators. pp 124. D. Van Nostrand, Princeton, N.J.

Larsen, J.C., 1977. Removal of local surface conductivity effects from low frequency mantle response curves. Acta Geod., Geophys. Mont. Acad. Sci. Hung., 12(1–3): 183–186.

Larsen, J.C., 1981. A new technique for layered earth magnetotelluric inversion. Geophys., 46, 9: 1247–1257.

Lee, M.K., Wheildon, J., Webb, P.C., Brown, G.C., Rollin, K.E., Crook, C.N., Smith, I.F., King, G. and Thomas-Betts, A., 1984. Dry rock prospects in Caledonian granites. Investigations of the geothermal potential of the U.K., British Geological Survey.

Leeder, M.R., 1976. Sedimentary facies and the orgins of basin subsidence along the northern margin of the supposed Hercynian ocean. Tectonophysics, 36, 167–179.

Leeder, M.R., 1982. Upper Palaeozoic basin of the British Isles. Caledonide inheritance versus Hercynian plate margin process. J. Geol. Soc. London, 139, 479–491.

Leggett, J.K., McKerrow W.S. and Soper, N.J., 1983. A model for the crustal evolution of the Southern Scotland. Tectonics, 2, 187–210.

Lilley, F.E.M., 1976. Diagrams of magnetotelluric data. Geophys., 41, 766–770.

Lineart, B.R., 1980. The effect of source field polarisation on estimates of the magnetotelluric impedance tensor. Geophys., 45, 1803–1812.

Lines, L.R. and Jones, F.W., 1973. The perturbation of alternating geomagnetic fields by three-dimensional island structures, Geophys. J.Roy. astr. Soc., 32, 133–154.

Marquardt, D.W., 1963. An algorithm for least squares estimation of non-linear parameters, J. Geophys. Res., 67, 1907–1918.

Mbipom, E.W. and Hutton, V.R.S., 1983. Geoelectromagnetic measurements across the Moine Thrust and the Great Glen in Northern Scotland. Geophys. J. Roy. astr. Soc., 74, 507-524.

McKerrow, W.S., 1987. The Southern Uplands Controversy. J. Geol. Soc. London, 144, 735-736.

McMechan, G.A. and Barrodale I., 1985. Processing of electromagnetic data in the time domain. Geophys. J. Roy. astr. Soc., 81, 277-293.

Mckerrow, W.S., Leggett, J.K. and Eales, M.H. 1977. Imbricate thrust model of the Southern Uplands of Scotland. Nature, 267,237-239.

Mckirdy, D.McA., Weaver, J.T. and Dawson, T.J. 1985. Induction in a thin sheet of variable conductance at the surface of a stratified earth-II. Three dimensional theory. Geophys. J. Roy. astr. Soc., 80, 177-194.

Mitchell, A.H.G. and McKerrow, W.S., 1975. Analogous evolution of the Burma orogen and the Scottish caledonites, Bull. geol. Soc. Am., 86, 305-315.

Moroz, Yu. F., 1985. A layer of increased electrical conductivity in the crust and upper mantle under Kamchatka. Izvestia, Earth Physics, 21, 693-699.

Moseley, F., 1977. Caledonian plate tectonics and the place of the English Lake district. Geo. Soc. Am. Bull., 88, 764-768.

Muller W. and Losecke W., 1975. Accelerating convergence techniques and grid spacing problems in two dimensional magnetotelluric modelling. Geophys. J. Roy. astr. Soc., 41, 185-191.

Nabetani S. and Rankin D., 1969. An inverse method of magnetotelluric analysis for a multilayered Earth. Geophys. 34, 75-86.

Niblett, E.R. and Sayn-Wittgenstein, C., 1960. Variations in electrical conductivity with depth by the magneto-telluric method, Geophys., 25, 998-1008.

Nienaber, W., Dosso, H.W. and Hutton, V.R.S., 1981. Electromagnetic induction in the British Isles Region: analogue model and field station results. Phys. Earth Planet. Int. 27, 122-132.

Novak, M., 1981. A broad band magnetotelluric study in the north England high heat flow region. Ph. D. thesis., Univ. of Edinburgh. U.K., 162pp.

Oldenburgh, D.W., 1979. One-dimensional inversion of natural source magnetotelluric observations. Geophys., 44, 7: 1218-1244.

Oldenburgh, D.W., Whittall, K.P. and Parker R.L., 1984. Inversion of ocean bottom magnetotelluric data revisited. J. Geophy. Res., 89, 1829-1833.

Osemeikhian, J.E.A. and Everett, 1968. Anomalous magnetic variations in S.W. Scotland, Geophys. J. Roy. astr. Soc., 15, 361-366.

Oxburgh, E.R., Richardson, S.W., Wright, S.M., Jones, M.Q.W., Penney, S.R., Watson, S.A. and Bloomer, J.R., 1980. Heat flow pattern of the United Kingdom, Second international seminar on the results of E.E.C. Geothermal Energy Research, Strasbourg, 149-152.

Park, S.K., 1985. Distortion of magnetotelluric sounding curves by three dimensional structures. Geophys. 50, 785-797.

Park, J. and A.D. Chave, 1984. On the estimation of magnetotelluric response functions using the singular value decomposition. Geophys. J. Roy. astr. Soc., 77: 683-709.

Parker, R.L., 1983. The magnetotelluric inverse problem. Geophys. Surv., 6: 5-25.

Parker, R.L., 1977. Understanding inverse theory. Ann. Rev. Earth Planet. Sci., 5: 35-64.

Parker, R.L., 1970. The inverse problem of electrical conductivity in the mantle, Geophys. J. Roy. astr. Soc., 22, 121-138.

Parkinson, W.D., 1962. The influence of continents and oceans on geomagnetic variations, Geophys. J. Roy. astr. Soc., 6, 441-449.

Parley, J.R., 1969. Integral equation formulations of scattering from two-dimensional inhomogeneities in a conductive earth. Ph.D thesis, Univ. of California, Berkeley, 340pp.

Patella, D., 1976. Interpretation of Magneto-telluric resistivity and Phase soundings over horizontal layers, Geophys., 41, 96-105.

Patra, H.P. and Mallick, K. 1980. Geosounding principles; Vol.2. Time varying geoelectric soundings. Elsevier Scientific Publishing company, 419pp.

Peach, B.N. and Horne, J., 1899. The Silurian rocks of Britain, Scotland. 1, Mem. Geo. Surv. 749pp.

Pedersen, L.B. and Svennekjaer, M., 1984. Extremal bias coupling in magnetotellurics. Geophys., 49, 11: 1968-1978.

Pedersen, L.B., 1982. The magnetotelluric impedance tensor - its random and bias errors. Geophys. Prosp., 30: 188-210.

Phillips, W.E.A., Stillman, C.J. and Murphy, T., 1976. A Caledonian plate tectonic model, J. Geol. Soc. Lond., 132, 576-609.

Porstendorfer, G., 1975. Principles of Magneto-Telluric Prospecting. Bontraeger, Berlin, 118pp.

Powell, D.W., 1971. Comment on "A model for the Lower Palaeozoic evolution of the southern margin of the early Caledonides of Scotland and Ireland" by Dewey (1971), Scott. J. Geol., 7, 369-372.

Price, A.T., 1950. Electromagnetic induction in a semi-infinite conductor with a plane boundary, Quart. J. Mech. Appl. Maths., 3, 385-410.

Price, A.T., 1962. The theory of magnetotelluric fields when the source field is considered, J. Geophys. Res., 67, 1907.

Price, A.J., 1963. A note on the interpretation of the magnetic variations and magnetotelluric data. J. Geomag. Geoelec., 15, 4, 241-248.

Pridmore, D.F., Hohmann, G.W., Ward, S.H. and Sill, W.R., 1981. Investigation of finite element modelling for electrical and electromagnetic data in three dimensions. Geophys., 44, 1009-1024.

Raiche, A.P., 1974. An integral equation approach to three dimensional modelling. Geophy. J. Roy. astr. Soc., 36, 363-376.

Rankin, D., 1962. The magnetotelluric effect of a dike. Geophys., 27: 666-676.

Ranganayaki, R.P., 1984. An interpretive analysis of magnetotelluric data. Geophys., 49, 1730-1748.

Rao, C. and Mitra, S., 1971. Generalized inverses of matrices. pp.50, John Wiley, New York.

Rasmussen, T.M., 1987. Magnetotelluric investigation of the Baltic shield in Sweden. Techniques and geophysical implications. Ph.D. thesis. university of Sweden.

Reddy, I.K. and Rankin, D., 1972. On the interpretation of magnetotelluric data in the plains of Alberta. Can. J. Earth Sci., 9, 514-527.

Reddy, I.K. and Rankin, D., 1973. Magnetotelluric response of a two-dimensional sloping contact by finite element method, Pure Appl. Geophys., 105, 847.

Rikitake, T. 1975, A model of the Geoelectric structure beneath Japan, J.G.G., 27, 233-244.

Rokityansky, I.I., 1982. Geoelectromagnetic investigation of the Earth's crust and mantle. Springer-Verlag, Berlin, 381pp.

Rooney, D. and Hutton, V.R.S., 1977. A magnetotelluric and magnetovariational study of the Gregory Rift Valley, Kenya, Geophys. J. Roy. astr. Soc, 51, 91-119.

Rooney, D., 1976. Magnetotelluric measurements across the Kenyan Rift Valley. Ph. D. thesis, Univ. of Edinburgh, U.K., 206pp.

Roxis, N., 1984. The development of deep sounding technique using resistivity methods and an investigation of the associated interpretation problems. Ph. D. thesis, University of Leeds, U.K., 531pp.

Schmucker, U., 1970. Anomalies of geomagnetic variations in the southwestern United States, J. Geomag. Geoelec., 15, 193-221.

Schwarz, G., Haak, V., Martinez, E. and Bannister, J., 1984. The electrical conductivity of the Andean crust in northern Chile and Southern Bolivia as

inferred from magnetotelluric measurements. J. Geophys., 55: 169–178.

Shankland, T.J. and Ander, M.E., 1983. Electrical conductivity, temperatures, and fluids in the lower crust. J. Geophys. Res., 88, B11: 9475–9484.

Shankland, T.J., 1969 Transport properties of olivine, in The Application of Modern Physics to the Earth and Planetary Interiors, ed. S.K. Runcorn. Interscience, New York.

Silvester P. and Haslam C.R.S., 1972. Magnetotelluric modelling by the finite element method. Geophys. Pros. 20, 872–891.

Sims, W.E. and Bostick, F.X. Jr., 1969. Methods of magnetotelluric analysis. Tech. Rep. 58, Univ. of Texas at Austin.

Sims, W.E., Bostick, F.X. Jr., and Smith, H.W., 1971. The estimation of magnetotelluric impedance tensor elements from measured data. Geophys., 36, 5: 938–942.

Smith B.D. and Ward S.H., 1974. On the computation of polarisation ellipse parameters. Geophys., 36, 938–942.

Srivastava, S.P., 1965. Method of interpretation of magneto-telluric data when the source field is considered, J. Geophys. Res., 70, 945–954.

Strangway, D.W., Swift, C.M.(Jr.) and Holmer, R.C., 1973. The application of audiofrequency magnetotellurics (AMT) to mineral exploration. Geophysics, 38, 1159–1175.

Sule P.O., 1985. A broad band magnetotelluric investigation in Southeast Scotland. Ph.D. thesis, University of Edinburgh, 302pp.

Sule, P.O. and Hutton, V.R.S., 1986. A broad band magnetotelluric study in southeastern Scotland. Data acquisition, analysis and one dimensional modelling. Annales. Geophysicae, 4, B2, 145–156.

Swift, C.M., 1967. A magneto-telluric investigation of an electrical conductivity anomaly in the south-western United States, Ph.D. Thesis, Department of Geology & Geophysics, M.I.T., Cambridge, Massachusetts.

Swift, C.M., 1971. Theoretical magnetotelluric and Turan response from two-dimensional inhomogeneities, Geophys., 36, 38-52.

Talwani, M., Worzel, J.L., Landisman, M., 1959. Rapid gravity computations for two-dimensional bodies with application to the Mendocino submarine fracture zone. J. Geophys. Res., 64, 49-59.

Thayer, R.E., 1975. Topographic distortion of telluric currents: a simple calculation. Geophys., 40, 1: 91-95.

Tikhonov, A.N., 1950. On investigation of electrical characteristics of deep strata of Earth's crust (in Russian). Dokl. Akad. Nauk. SSSR, 73: 295-297 (cited by Rokityansky, 1982).

Tikhonov, A.N. and Berdichevskii, M.N., 1966. Experience in the use of magneto-telluric methods to study the geological structures of sedimentary basins, Izv. Phys., 2, 34-41.

Ting, S.C. and G.W. Hohmann, 1981. Integral equation of the three-dimensional magnetotelluric response. Geophys., 46, 2: 182-197.

Travassos, J.M., 1987. Investigations of the Analysis and Modelling of Magnetotelluric data. Ph.D. thesis, University of Ediburgh, pp219.

Valiant, M.J., 1976. N.E.R.C. (Natural Environmental Research Council) geologger technical handbook, IGS magnetic observatory, Hartland.

Vasseur, G. and Weidelt, P., 1977. Bimodel electromagnetic induction in non-uniform thin sheets with an application to the northern Pyrenean induction anomaly. Geophy. J. Roy. astr. Soc. 51, 669-690.

Vozoff, K., 1972. The magnetotelluric method in the exploration of sedimentary basins. Geophys., 37, 1: 98-141.

Vozoff, K. and Jupp, D.L.B., 1975. Joint inversion of geophysical data, Geophys. J. Roy. astr. Soc., 42, 977-999.

Wait, J.R., 1954. On the relationship between telluric currents and the earth's magnetic field, Geophys., 19, 281-289.

Wannamaker, P.E., J.A. Stodt and L. Rijo, 1986. Two-dimensional topographic responses in magnetotellurics modelled using finite elements. Geophys., 51, 11: 2131-2144.

Wannamaker, P.E., Hohmann, G.W., San Filipo, W.A., 1984. Electromagnetic modelling of three dimensional bodies in layered earths using integral equations. Geophys, 49, 60-74.

Wannamaker, P.E., Stodt, J.A. and Rijo, L., 1985. Finite element program for solution of magnetotelluric responses of two dimensional earth resistivity structure, User documentation, Univ. of Utah.

Warner, M.R., Hipkin, R.G. and Brewitt, C.W.A., 1982. Southern Uplands seismic refraction profile- preliminary results (abstract). Geophy. J. Roy. astr. Soc., 69, 279.

Weaver, J.T. and C.R. Brewitt-Taylor, 1978. Improved boundary conditions for the numerical solution of E-polarization problems in geomagnetic induction. Geophys. J. Roy. astr. Soc., 54: 309-317.

Weaver, J.T., 1973. Induction in a layered plane earth by uniform and non-uniform source fields. Phys. Earth Planet. Int., 7, 266-281.

Weidelt, P., 1975. Eletromagnetic induction in three-dimensional structures. J. Geophys., 41: 85-109.

Weidelt, P., 1972. The inversion problem of Geomagnetic induction, Zeitschrift fur Geophysik, 38, 257-289.

Weidelt, P., Muller W., Losecke W. and Knodel K., 1980. Die Bostik transformation in Protokoll uber das kolloquium "Elektromagnetische Tiefenforschung", edited by V. Haak and J. Homilius, 227-230, Berlin- Hannover.

Weidelt P., 1986. Discrete frequency inequalities for magnetotelluric impedances of one-dimensional conductors. J. Geophys., 59, 171-176.

Whelan, J.P. and Hill, E.R.G., 1987. An audio magnetotelluric profile across the Irish Midlands. (abstract) Geophys. J. Roy. astr. Soc., 89, 485

Widrow, B., Glover, J.R., McCool, J.M., Kaunitz, J., Williams, C.S., Hearn, R.H.,

Zeidler, J.R., Dong, E. JR. and Goodlin, R.C., 1975. Adaptive noise cancelling: Principles and Applications. Proc. IEEE, 63, 1692–1716.

Wieladek, R. and Ernst, T., 1977. Application of method of least squares to determining impulse reponses and transfer functions. Publ. Inst. Geophys. Pol. Acad. Sci., G–1(110), 3–12.

Williamson, K., Hewlett, C. and Tammemagi, H.Y., 1974. Computer modeling of electrical conductivity structures. Geophys. J.R. astr. Soc., 37, 533–536

Wilson, J.T., 1966. Did the Atlantic close and then re–open Nature, 211, 676–681.

Wright, A.E., 1976. Alternating subduction directions and the evolution of the Atlantic Caledonides. Nature. 264, 156–160.

Wright, J.A., 1970. Anisotropic apparent resistivities arising from non–homogeneous two–dimensional structures, Can. J. Earth. Sci., 7, 527–531.

Wu, F.T., 1968. The inverse problem of magnetotelluric sounding. Geophys., 33: 972–979.